Funtionalized gold nanoparticles for retinoblastoma cancer diagnosis and therapy

AUTHOR(S)

Jeanne Boyer

PUBLICATION DATE

01-04-2015

HANDLE

10536/DRO/DU:30079110

FUNCTIONALIZED GOLD NANOPARTICLES FOR RETINOBLASTOMA CANCER DIAGNOSIS AND THERAPY

By

Sushma Kalmodia (M.Sc)

Submitted in fulfillment of the requirements for the degree of

Doctor of Philosophy

School of Life and Environmental Sciences

Faculty of Chemistry and Biotechnology

Deakin University, Australia

[April 2015]

DEAKIN UNIVERSITY

ACCESS TO THESIS- A

I am the author of the thesis entitled" **Functionalized Gold Nanoparticles for Retinoblastoma Cancer Diagnosis and Therapy'** submitted for the degree of Doctor of Philosophy.

This thesis may be made available for consultation, loan and limited copying in accordance with the Copyright Act 1968.

'I certify that I am the student named below and that the information provided in the form is correct'

Full Name: **Sushma Kalmodia**

Signed: Signature Redacted by Library

Date: **April 2015**

DEAKIN UNIVERSITY CANDIDATE DECLARATION

I certified the following for the thesis entitled "**Functionalized Gold Nanoparticles for Retinoblastoma Cancer Diagnosis and Therapy"** submitted for the degree of Doctor of philosophy.

I The content of the thesis is research work carried out by me at Deakin University under the supervision of the thesis supervisor (s)

II The thesis guideline has been closely followed and the reference has been made to the research findings of others and due acknowledgment has been given.

III The thesis content (s) is not in any way a violation or infringement of any copyright, patent and all sources used have been cited appropriately.

I certify that the work has not been submitted else ware for a degree and the information give is correct to the best of my knowledge.

Full Name: **Sushma Kalmodia**

Signed: Signature Redacted by Library

Date: **April 2015**

INDEX

LIST OF FIGURES

LIST OF TABLES

ACKNOWLEDGEMENTS

Foremost, I thank almighty **GOD** for perseverance and strength that he has bestowed upon me for completing my ph.d dissertation successfully. It has been a long journey for me with lots of ups and downs, which I can overcome by grace of the God, family, friends and colleagues. I am grateful for all of them.

I would like to thank to my venerated supervisors, **Prof. Colin J. Barrow**, **Dr. Subramanian Krishnkumar** and **Dr. Wenrong Yang** for their help and support during my dissertation. They gave me plenty of room to grow as an independent researcher, on the same token always provide guidance to me and supervised to take the right path. There, in-depth understanding of chemistry, nanomaterial and cancer biology, improve my understanding in the field of translational research. I learned from them how to plan independently and handle stressful situations, as well as how to maintain a balanced in graduate study. I enjoyed working with them, they inspire and encourage me right from the beginning of my research work.I would like to thank, **Dr. S. Badrinath** to give me an opportunity to work at **Sankara Nethralaya**, a best place to work and understand the clinical significance of the beach work for the bedside application. Also, I would express my sincere thanks to **Dr. J Biswas** for his help during my research activity in the department.I would like to thank, **Prof. David Morgan** (Chancellor), **Prof. Jane Den Hollander** (Deputy vice chancellor**) Prof. Lee Astheimer** (Deputy Vice Chancellor-research), **Prof. Guang Shi** (head of school of life and environmental sciences), **Prof. David Chill** (associate dean, research, life and environmental sciences), **Prof. Tess Toop**, **Ms. Helen Woddall** and **Ms. Gyathri Vedanarayan** for their help to provide me an opportunity to conduct research and help in all academic and administrative help

complete my work useful. Though my research topic is very much interdisciplinary in nature, I am able to complete because of research experience and knowledge I gain from my study at the Indian Institute of Technology Kanpur under the supervision of **Prof. Bikramjit Basu** (IIK & IISc) and **Prof. Ashutosh Sharma** (IITK). Their wide knowledge, ideas and concepts have remarkably improved my understanding in the field of biomaterials, nanomaterials, and engineering. I feel very much blessed and proud to be their student. I take this opportunity to convey my heartfelt gratitude to them. I am very much thankful for the encouragement and help I receive from **Prof. Kantesh Balani** (IITK) Prof. **Alok Dhawan** (ITRC, CSIR) and **Prof. K Biswas** at (IITK) **Prof. Thomas J. Webster** (Northeastern University, USA). I would like to thank to **Prof. T. Pradeep** and **Prof. Ram Prabhu,** (IITM) **Dr.Pimm and Prof. Jagat Kanwar** (Deakin University, Australia) to extend their support and allow me to conduct the experiment under their esteem supervision. I would express my thanks to **Dr. Sailaja, Dr. Navodita, Dr. Sowmya, Dr. Narayan** for their day to day help and discussion of my research work. I am very much thankful to **Ms. Kalavani** (Junior Scientist) for her extend support in the last phase of my study to conduct histopathology studies.My sincere thanks to all of my senior, friends and colleague from IITK who help me in all the possible to complete my work successfully. Thank to **Dr.Shekar Nath, Dr. Raju, Dr. Manoj , Dr. Shilpee Jain, Dr. Neelima Mahato, , Dr. Ashutosh Dubey, Dr. Amit S. Sharma, Dr. Yousuf Khan, Dr. Sumanta Samal, Dr. Naresh Saha, Dr. K. Madhav Reddy, Dr. Abhishek Tiwari Dr. Neha Gupta, Ms. Sharmistha Dhara, Dr. Indu Bajpai,** and all lab members from IITK.

Dr. Priti Roy, Dr.Binapani Mahaling, Dr. Alok Kumar, Ayan Roy, Ravi Verma, who never stop believing in my ability and their role in my professional and

personal life is priceless. I would like to thank all my lab members **from Sankara Nethralaya, Dr. Jaisy Samuel, Ms. Srilatha Jasty, Mr. Job, Ms. Sangetha, Mr Gopinath, Ms. Vinitha, Ms. Jayshree, Mr. Prasana, Mr. Ravi**kant**, Mr. Madhu,** Ms. Abhirami. **Ms. Chitra, Ms. Rajeswari, Dr. Seetha, Dr.Vandan**, **Ms. Vidhya, Ms. Aparna, Ms. Deepa, Dr. Nalini, Dr. Nithya, Ms. Meena, Ms. Shyama, Ms. Charanya** working in my department who had been a constant support me and encouragement during the research. I would like to thank all the lab members from Deakin University. **Mr. Moti, who** helped me during my stay at Deakin University. I would like to thank **Mr. Mahesh, Mr. Yuancho Zhang, Mr. Ranjith, Mr. Zhen Liu, Ms. Tejaswani.** I am grateful to my grandparents, parents (**Miss Pushpa Verma, and Mr.Lakshmicahnd Verma**), and in-laws **(Miss Ramshree Verma and Mr. Badriprasad Verma)** and **(Miss Sarita and Miss Sangeeta, (Mr. Pramod Verma and Mr. Sanjay Choudhary)** my whole family, whose utmost support and love gave me endless support without complaint to complete this work successfully. Their enormous support gave me untiring strength during my difficult moments. I have no words to thank my friend and soulmate **Dr. Ghanshyam Verma**, who allows me to fulfill my dream of doing research without his support and confidence in my ability, it would impossible for me to complete my degree. I need to mention my kids **Darsh**, **Shriyanshi,** and their siblings Bala, Naksh, Vikas, Tapan, Swati and Sachin they gave me immense happiness in my difficult situation. At last I would like to pay my sincere thanks to all of those who have contributed to this work directly or indirectly. I dedicate this thesis to my loving brother late "**Suresh Kalmodia**"

Sushma Kalomodia

April, 2015

LIST OF ABBREVIATIONS

Abbreviation	Expansion
ANOVA	Analysis of Variance
Pep-A	Antioxidant Peptide-A
BAX	Bcl-2-associated X protein
BBI	British Biocell International
Bcl-2	B-cell lymphoma 2
BSA	Bovine Serum Albumin
CAT	Catalase
CTAB	Cetyl trimethylammonium bromide
DAPI	4',6-diamidino-2-phenylindole
DCF	2', 7' Dichlorodihydrofluorescein
DCFH-DA	2', 7'-Dichlorodihydrofluorescin diacetate
DH	(β-hydroxy acyl dehydratase)
DLS	Dynamic Light Scattering
DMSO	Dimethyl sulfoxide
ELISA	Enzyme Linked Immuno Sorbent Assay
EPR	Enhanced permeability and retention
FACS	Fluorescence Activated Cell Sorting

FBS	Fetal Bovine Serum
FITC	(Fluorescein isothiocyanate)
FTIR	Fourier-Transform Infrared Spectroscopy
GNPs	Gold nanoparticle
GOI	Gene of Interest
GPX	Glutathione peroxidase
HDM-2	Human Double Minute -2
IARC	The International Agency for Research on Cancer
ICDDC	International Committee for Diffraction Data
ICMR	Indian Council of Medical Research
ICRB	International Classification of Retinoblastoma
MIO-M1	Mullar glial cell line
MTT	3-(4, 5-dimethylthiazol-2-yl)-2, 5-diphenyltetrazolium bromide
PBS	Phosphate Buffered Saline
PEG	Polyethylene glycol
qRT-PCR	Quantitative Real-Time Polymer chain Reaction
RB	Retinoblastoma
R6G	Rodamine 6 G
ROS	Reactive Oxygen Species
RPMI 1640	Roswell Park Memorial Institute 1640

RT	Room Temperature
SOD	Superoxide dismutase
SERs	Surface Enhanced Raman scattering
SPR	Surface Plasmon Resonance
SPSS	Statistical Package for the Social Sciences
TEM	Transmission Electron Microscopy
UV Vis	Ultraviolet-Visible

Symbol	**Expansion**
Au	Gold
A	Alpha
B	Beta
Λ	Gamma
Δ	Delta
μ	Micro
Nm	Nano

LIST OF PUBLICATIONS

1) Sushma Kalmodia et al., Synthesis and characterization of surface-enhanced Raman-scattered gold nanoparticles, International Journal of Nanomedicine, 2013; 8: 4327–4338.

Manuscript under Preparation

2) Sushma Kalmodia et al., Bio conjugation of antioxidant peptide on surface modified Gold nanoparticles: A novel approach to enhance the radical scavenging property in the cancer cell

3) Sushma Kalmodia et al., Curcumin loaded GNPs for targeted cancer therapy

4) Sushma Kalmodia et al., FTIR, A new paradigm to understand the GNPs mediated targeted therapy in Cancer

5) Sushma Kalmodia et al*., ln vitro* and *in vivo* preclinical evaluation of tumor growth inhibition by HDM2 peptide functionalized GNPs

List of conference poster presentation

1. Sushma Kalmodia et al., "**Gold Nanoparticles Theranostic for Retinoblastoma**" presented in Deakin India Research Initiative Symposium, Frontiers in Science 21/11/2011-23/11/2011, TERI, New Delhi, India

2. Sushma Kalmodia et al., '**Raman Active Biocompatible Gold Nanoparticles for Diagnostic and imaging application**' presented in the Gordon research conference on

Noble Metal Nanoparticles" 17/05/2012-22/05/2012, Mount Holyoke College, South Hadely, USA

3. Sushma Kalmodia et al., '**Targeted Delivery of Antioxidant Peptide Through Gold Nanoparticles for Retinoblastoma Therapy'** presented in Asia ARVO, 28/10/2013-31/10/2013, New Delhi, India

4. Sushma Kalmodia, **Theranostic peptide conjugated gold nanoparticles in Retinoblastoma Therapy'** presented in 6th Bangalore, India nano, 04/12/2013-06/12/2014, Banglore, India

5. Sushma Kalmodia et al., "**Delivery of antitumor peptide using multifunctional gold nanoparticles for theronostic application in Retinoblastoma**" presented in Cancer con 30/01/2014- 01/02/2014, Indian Institute of Technology Madras, Chennai, India

6. Sushma Kalmodia et al., "**Fabrication of Hdm2 peptide conjugated Gold Nanoparticles for targeted therapy of Retinoblastoma**" presented in Nano India, Tanjore, 29/01/2014- 30/01/2014, India.

Travel Grant Received

Selected for Gordon Research Conference in Nobel Metal Nanoparticles -2012 and Recipient of "International Travel Support (ITS)" from Science and Engineering Research Board (A Statutory body under Department of Science & Technology, Government of India

ABSTRACT

Cancer is a multifactor disease with an uncontrolled cell division. The cellular signaling process that controls the cell proliferation, differentiation and apoptosis are deregulated during the disease progression. Early stage detection and specific targeting of cancer are a challenging in many types of cancers including Retinoblastoma (RB). RB being one of the many pediatric eye cancer is encountered as a childhood malignancy below five years of age. Although, different treatment modalities have been available, targeted therapy is required to overcome the existing problems associated with the current treatment modalities. Nano-medicine can lead an effective approach to target the cancer. The dimensions similarity of gold nanoparticles (GNPs) with cellular component an added advantage in addition to biocompatibility and Physio-chemical properties that help in delivering and homing of the targeting moiety at the tumor site in cancer tissue.

Tumor progression includes multiple factors such as up-regulation of the oncogene, deregulation of signaling pathway and involvement of reactive oxygen species (ROS). ROS is a biochemical indicator and contribute to the pathogenesis and tumorogenesis. Apart from the ROS, several oncogenes have been identified, and one such gene is Human Double Minute 2 (HDM2). The up-regulation of HDM2 gene and oxidative stress in cancer encourage us to target these biological markers for effective targeted therapy in RB. Currently, there is a need to design the novel multifunctional therapeutic strategies that could attain more specific and effective response to the RB management.

In this perspective, self-therapeutic GNPs have been engineered for cancer theranostic which could help in homing of therapeutic molecules to the tumor site and

synergistically improve the therapeutic effect. The current research unveils the effect of reducing agent used in the synthesis of GNPs and highlight the significance of peptide in targeted therapy. A systematic approach for the synthesis of Surface Enhanced Raman (SERs) active GNPs and its application of as a nanocarrier, *in vitro* and *in vivo* for peptide mediated targeted therapy. The novel, conjugate GNPs-HDM2 and GNPs-Pep-A highlight the significance of targeted therapy in context with targeting HDM2 oncogene and ROS, respectively. In addition to this, vibrational spectroscopy was used to identify the molecular fingerprint in the xenograft RB tumor sample which can open a new path to delineate the interaction between the cellular biomolecule and targeted moiety.

GNPs for biological application has major concern due to size and intrinsic metal-dependent toxicity. Hence, it is imperative to develop a biocompatible, non-toxic nanomaterial. The green chemistry has paved a new opportunity for GNPs synthesis using less harmful, natural compounds which avoid chemical cytotoxicity. Therefore, a novel rapid method has been developed to synthesize the Surface Enhanced Raman scattered (SERs) GNPs using *Vitis vinifera L*. and *Curcuma longa L*. (Curcumin). Natural, compound play an important role to treat cancer due to its less cytotoxicity and less adverse effects. *Vitis vinifera L*. is a polyphenol known for anti-proliferative and antioxidant property, whereas, curcumin is a known an anticancer compound. The characterization of as-synthesized colloidal GNPs was confirmed the shape, size, and crystalline nature of GNPs. The characteristic Surface Plasmon Resonance (SPR) band between λmax at 528 ~540 NM is an indicative of the spherical shape of particles which is further confirmed by Transmittance Electron microscopy (TEM) analysis. The X-Ray Diffraction (XRD)

analysis showed the predominant (111) lowest-energy plane, which indicates the crystalline nature and purity of GNPs at the nano-scale.

To understand the biological application of novel synthesized GNPs, the in vitro stability and biocompatibility study was performed. The *in vitro* cytotoxicity was performed using various cancer cell lines, such as a breast cancer cell lines; MDA-MB 453 and MCF-7, Retinoblastoma (RB) cell lines;Y79 and WERI and non-cancerous Muller glial; MIO-M1 by MTT assay. The MTT data confirmed that cell viability is dependent on reducing agent, concentration of GNPs, time of treatment and type of cell line. The various time points such as 6, 12, and 24h and a range of concentration from 10-100 μM were selected to study non-cytotoxic concentration and time point using the different type of cancer cell line. 50% or more cell viability was observed at 6h of treatment with concentration ≤ 50μM. Cell viability was not dependent on the type of cancer cell line and reduced agents either *Vitis vinifera L.* or *Curcuma L.* were used for the GNPs synthesis. The cell viability was significantly decreased ($P<0.05$) in Y79 at 100 μM concentration. The maximum cell viability was 14.2 % at 24 h of treatment with GNPs synthesized with *Vitis vinifera L*. (V-GNPs) and the similar cytotoxicity trend was noticed with *Curcuma L.* GNPs (Cur-GNPs). The sensitivity of Y79 could be attributed to the self-therapeutic effect (anti-proliferative effects) of the reducing agent coating on GNPs. Whereas, MDA-MD-453 (Breast cancer) and MIO-M1 (Non-cancer) cell line showed, cell viability more than 70% post 24h treatment with the V-GNPs. The cell viability was more than 97.30 % at 100μM concentration post 24h treated in a normal cell (MIO-M1) compared to untreated cells. The therapeutic index that is a ratio of non-cancer to the cancer cell line was used to study the effect of GNPs. The *in vitro* cell viability of GNPs (V-GNPs and C-GNPs) shows

the dose- and time-dependent cytotoxic effects in Y79 cells. The therapeutic potential of V-GNPs confirmed that it can perform as a self-therapeutic SERs active nanomaterials. Whereas, the curcumin reduced GNPs showed 34.41 % cell viability in MIO-M1 cells at 100 µM concentration after 24h of post treatment. V-GNPs was found to be more effective in terms of colloidal stability, reproducibility and therapeutic index in vitro. To consider these properties, an attempt was made to conjugate the V-GNPs with anti- HDM2 peptide and antioxidant peptide (Pep-A) for targeted cancer therapy using the RB model.

The antioxidant peptide (Pro-His-Cys-Lys-Arg-Met (PHCKRM, Pep-A) functionalized GNPs is to attain a target specific delivery of the peptide for ROS scavenging in the cancer cell. The Pep-A showed antioxidant activity and reduced the ROS up to 40% at 100µM concentration relative to an untreated Y79 cell, *in vitro*. Whereas, ROS inhibition was 9% in GNPs, and 70 % in the case of GNPs-Pep-A treated condition compared to the untreated condition. The ROS reduction, 30 % in GNPs-Pep-A treated, confirmed the synergistic effect of GNPs-Pep-A. In addition to this, superoxide dismutase (SOD) enzyme activity was 81 % (% of inhibition) in Y79, RB after 24h of treatment with GNPs-Pep-A, whereas, GNPs shows 70%. A 11 % increase in SOD activity further confirmed the synergistic effect of GNPs on SOD activity. It has been found that modulation of the mRNA expression of antioxidant genes glutathione peroxidase (GPX), superoxide dismutase (SOD) and catalase was also observed by 2-3 fold (CAT). The effect of GNPs-Pep-A on SOD and ROS activity and regulation of antioxidant genes indicate that *Vitis vinifera L*. coated GNPs provide stability to the peptide and synergistically improve the antioxidant effect.

In continuation to this, further studied were performed, and therapeutic potential of anti-HDM2 peptide (QETFSDLWKLLP) functionalized GNPs was studied in detail. In normal tissues, HDM2 protein expression is very less, whereas in RB cancers it expression is very high. The higher expression of HDM2 in cancer can function as a promising clinical target. The up-regulation of HDM2 at mRNA and protein levels were observed at varying levels in RB tumor tissue. The *Vitis vinifera L*. (V-GNPs) and citrate is reduced GNPs (C-GNPs) were used for conjugation of HDM2 peptide and the in vitro knockdown of the HDM2 in Y79 was confirmed at mRNA and protein level. 5.8 and 4 fold down regulation of HDM2 was observed in V-GNPs-HDM2 and C-GNPs-HDM2, respectively ($P<0.05$). Interestingly, V-GNP, C-GNP, V-GNPs-HDM2 and C-GNPs-HDM2 showed differences with respect to regulation of p53. While, V-GNPs-HDM2 and V-GNPs showed 0.5 and 1.8 fold up-regulation of p53 ($P<0.05$) whereas, C-GNPs and C-GNPs-HDM2 do not up-regulate the p53 at both protein and mRNA level. Similarly, apoptotic cell death, 20% ($P<0.05$) was observed in the case of V-GNPs-HDM2 treated samples compared to the control sample. Also, C-GNPs-HDM2 shows 11% ($P<0.05$) necrosis cell death compared to C-GNPs. These results confirmed the knockdown of HDM2, *in vitro, in* RB cell line (Y79).

Further, we explore either the functionalized GNPs were effective *in vivo*. RB xenograft nude mouse model was established using the Y79 cells to mimic the in vitro experiment. The *in vivo* study were performed in 5-6 week old Hsd: Athymic Nude-Foxn1nu mice. The mice subcutaneously injected with the human Y79 (RB) cells and V-GNPs-HDM2 and C-GNPs-HDM2 (n=8) with a dose of 5µg/animal every day for a maximum of 24 days. The sterile water (100µl, n=10), was used for the vehicle (control

group). Tumor volume (TV) of V-GNPs-HDM2 and C-GNPs-HDM2 were 1755 ± 116 mm3, 1463 ± 109 mm3 and 1288 ± 210 mm3, respectively. The maximum tumor growth reduction attained by V-GNPs-HDM2 and C-GNPs-HDM2 was 17% and 28%, respectively. The results of in life phase response were more promising during the first ten days of treatment that showed 53.90 and 40.42 % tumor growth reduction moderate activity with of V-GNPs-HDM2 and C-GNPs-HDM2 treatment, respectively. The biochemical, hematological and histo-pathological analysis confirm that the selected dose was under the tolerable limit.

To understand *in vivo* therapeutic response the further study was performed by profiling the apoptosis and cytokine proteins in xenograft excised tumor and serum sample, respectively. Interestingly, apoptotic protein expression variation in C-GNPs-HDM2 and V-GNPs-HDM2 treated xenograft tumor samples. The important regulator of the HDM2-mediated apoptosis and cell cycle regulator protein, Cyclin-Dependent Kinase Inhibitor (CDKN1a) p21, significantly down-regulated in C-GNPs-HDM2 treated condition. The p53 released from the HDM2 upon the treatment with anti-HDM2 peptide conjugate promotes the degradation of the p21 confirmed that HDM2 mediated inhibition of p21 is a key switch between the apoptosis and cell cycle arrest. Within, the result confirmed that HDM2 induced cell death via down regulating, Bcl2 and the ration of Bcl-2 to Bcl-Xl is down-regulated more in case of C-GNPs-HDM2 compared to V-GNPs-HDM2. In addition to this, survivin is significant ($P<0.05$) up-regulated in both the conditions confirm the stress-induced responses after the treatment. Apart from Survivin, another stress-induced protein, Clusterin expression is also altered in the V-GNPs-HDM2 treatment condition. Similarly, cytokines/ chemokines study was performed to understanding the immune

responses during the treatment. It has been observed that a selective change in expression of cytokines/chemokines was noticed with respect to the V-GNPs-HDM2 and C-GNPs-HDM2. ICAM-1, IL-1a, GM-CSF and BLC ($P<0.05$) were significantly up-regulate in C-GNPs-HDM2 whereas V-GNPs-HDM2 showed an increased expression of Ca5 ($P<0.05$). The observed differences in the cytokine profile infer that the GNPs (C & V) reducing agent modulate the immune responses. To get an insight into the molecular difference observed in a xenograft mouse model in the antitumor responses the analytical techniques "Attenuated Total Reflectance/Fourier Transform Infrared" (ATR/FTIR) was used to study the spectral signature of the biomolecules.

ATR/FTIR mapping help to understand the in-life tumor growth reduction in RB xenograft tumor samples in combination with multivariate analysis. Principal component analysis (PCA) was used to analyze the FTIR image data after HCA analysis. PCA was performed on the spectral data of "biobands" through cross-validation at 7 PCs in the wavenumber range 3039.234-2811.677 and 1808.883-929.51. The PC-1, PC-2 and PC-3 that shows the difference in loading in the region 2847 2929 cm-1, a lipid-rich region. Apart from this the strong positive band observed at PC-1 (C-GNPs-HDM2) is 1092 cm-1 phosphodiester backbone of DNA/RNA, 2847 cm-1, CH2 group of lipids whereas the negative loading 1649 cm-1 indicates the Amide-1α helix. The PC-3 (V-GNPs-HDM2) loading showed the positive loading at 982, Ribose-2'-OH vibration of RNA, 1029 cm-1 CH2OH of polysaccharides, 1675 cm-1-(Amide-1β turn) and 1675 cm-1Amide-1β turn. Whereas, the negative loading observed in the 955 cm-1- Ribose-2'-OH vibration of RNA and 1649 cm-1 indicates the -Amide-1α helix.

Taken together the current study, showed for the first time a systemic approach from a synthesis of SERs active GNPs to its application for selective targeting of cancer marker *in vitro* and *in vivo* in RB model. The spectroscopic identification of the molecular fingerprint can pave a new path for understanding the therapeutic potential of the novel GNPs-HDM2 conjugate and the implication of the techniques for diagnostic application. The current data confirm that peptide is functional, and the nano-carrier based local delivery of peptide at tumor site could provide an effective approach for targeted therapy for the eye.

CHAPTER 1

1 Introduction

This chapter focus on the brief description of the nanotechnology with an emphasis on the biomedical nanotechnology for cancer theranostics. It describes the different applications and functionalization of gold nanoparticles (GNPs) for therapeutic applications. Further, it discusses the problems and limitations encountered in the current treatment modalities of cancer treatment with an emphasis on Retinoblastoma (RB). The chapter includes hypothesis, objectives and structure of the dissertation

1.1 Background

Nano-technology is filed of technology that deals with length scales below 100 nm [2]. “Nano” is the billionth of a meter (1 nm= 1x10-9 meter) whereas, an atom has a diameter of almost 1/3rd of a nanometer. The nano-size is a fundamental unit to tailor the properties of the material for specific applications in the field of supramolecular chemistry, biosensors, drug delivery and tissue engineering, etc.[3, 4]. Nanotechnology attained a major attention as because of unique size-dependent properties of nanomaterial and application of nanomaterial in various field such as electronics, energy generation, bio-sensing, imaging and therapy (Figure 1.1) [5].

Nano term was coined by “Richard Feynman” in his lecture entitled "There's Plenty of Room at the Bottom” in 1959 [6]. The alteration at atoms and molecular level can be possible using a set of precise principal for miniaturization, is necessary to obtain the specific function [7]. Nanotechnology is an emerging cross-disciplinary field of science and technology that involves disciplines in fields such as physics, chemistry, biology, engineering and material science[2, 8].

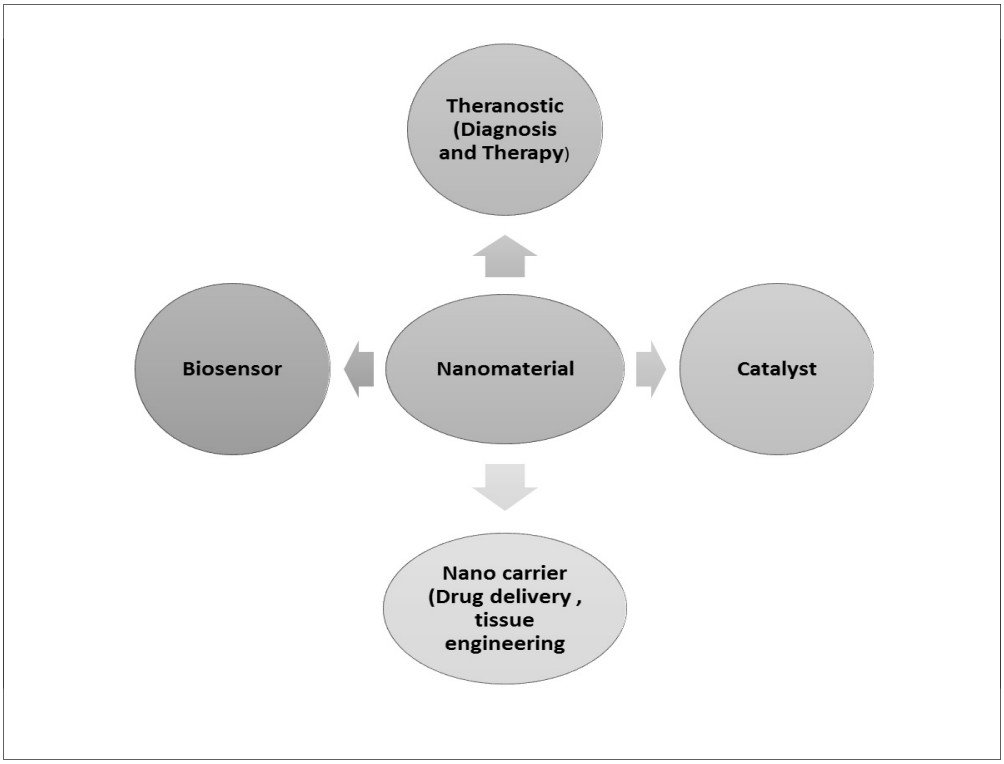

Figure 1.1 Bird's eye views; application of nanomaterial in various fields

The nanoparticles can be defined as anything less than 100 nm in size with novel functions/properties compared with the bulk material. Nanoparticles as such and a building block for the nanostructures such as " nanoclusters, nanowires, nanochains, and nano aggregates" shows novel functional properties. It contains a small number of atoms or molecules that possess different properties than the bulk material. The difference in the bulk and nanomaterial is due to surface effect as it has the highest number of electron density. The atoms in the nanomaterials are situated far apart and due to this lower coordinate and unsatisfied bond, the stability of the surface atom is less. The smaller a particle, the larger the fraction of atoms at the surface that increase the binding energy per atom. Moreover, the edge and corner atoms have even lower coordination compared to the central atoms which intern help in binding more foreign atoms and molecules more tightly [9].

The more surface to volume ratio of nanoparticles is one reason of having the different surface chemistry compared to its bulk form. In addition to this, the size of nanoparticles can be changed to synthesize the nanoparticles of different shape and size that help to develop a new effective nano-system. The size-dependent property provides an exceptional high possibility to probe the interaction at the cellular and molecular level with realistic clinical applications (Figure 1.2). Specific types of nanoparticles are being utilized as a drug delivery vehicle for targeted therapy cancer imaging agents. The ability of nanoparticles to deliver the high amount and specific delivery of molecules is the ultimate advantage of nanoparticles and its application to a carrier molecule. These properties make the nano-size material a suitable material for biomedical applications.

1.2 GNPs for biomedical application

The nanomaterial has greatly improved the nanomedicine through targeted, delivery, with specificity efficacy and less systemic toxicity [10]. The nanomaterials in biological applications is a growing field with an immense possibility in diagnosis, gene/drug delivery, imaging, biomolecular mapping and theranostics (Figure1.2). The nanoparticles (1-100 nm) are much smaller than the biological cell and cellular organelles. However, the cellular organelles and their cellular components such as protein and nucleic acid (DNA/RNA) are in the size of nano to sub-micron size (Figure 1.2). The size similarity of the cellular component with nanoparticles facilitates the development of nanoparticles based devices like nanosensors and nanocarriers to deliver the drug or therapeutic molecules to target specific manner for clinical applications. The nanomaterial and its interactions with biomolecules like DNA, RNA, protein and other cell organelles make nanoparticles as a suitable candidate with an ability to cross many biological barriers [11,

12]. The tunable size and shape opens a new way to interrogate the cellular and molecular process that helps in targeting cancer molecules and imaging. To target the specific molecules and organelles is the major concern and a need for sensitive detection, diagnosis and their treatment of diseases. The specific effect of a drug can be achieved if it reaches a desired site with an optimum amount through blood circulation and it should be effective only to tumor cells without causing any harmful effects on healthy tissues. Nanoparticles can be used to study the targeting the specific molecules of interest using active and passive targeting [13]. The passive targeted delivery is the use of nanocarriers for delivery or targeting of the molecules. Whereas the recent use of the nanoparticles has shown for the active targeting to interfere directly with the cellular pathways, and it involves a cell fate process such as cell cycle, apoptosis and cell proliferation [14].

The multiple functional GNPs has emerged as a new generation candidate material in the clinical application by merging of the size and surface chemistry of nanomaterial. Due to light scattering characteristics GNPs can function as contrasting agent in biomedical imaging whereas the inert nature of Au (Gold) offer a great opportunity for biological application such as drug/gene delivery. The site-specific delivery of the target molecules can be achieved using GNPs in systemic circulation and limit the access of target molecules at the target site [15]. Among all the different types of nanomaterials, metal nanoparticles have gained a major scientific attention for the biological applications due to biocompatibility and easy functionalization with the target molecules. The unique property of the GNPs apart from biocompatibility is contrasting agent due to a high atomic number

(atomic no.78, atomic mass 197). The higher atomic mass allows more absorption of X-rays to give better contrast than any other contrasting agents that are in use for the imaging.

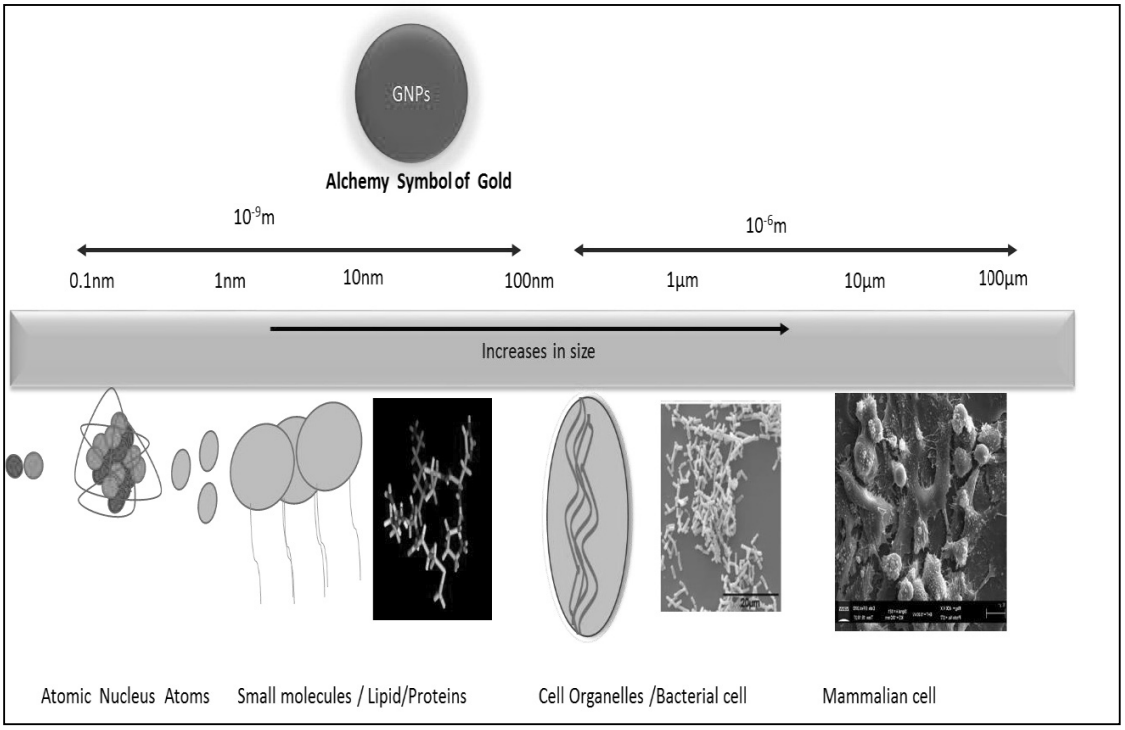

Figure 1.2 The length scale comparison of the biomolecules/organelles and cells [16].

1.3 GNPs in clinical application

Gold is a noble element, bring about lots of interest, particularly in the field of biomedical applications. Au is in use for cancer, HIV, bronchial asthma, and malaria for more than century[17]. NPs was introduced for biomedical application in 1890 by German Robert Koch for antibacterial application in Mycobacterium tuberculosis at very low concentration in the form of k[Au(CN)2] [18]. In the 1900s gold was used for the tuberculosis and rheumatoid arthritis [19, 20]. Au is approved by FDA (Food and Drug Administration) for the clinical application, and it is in use for treatment of rheumatoid arthritis more than 50 years. “Uni-Gold Recombigen (TM)” synthesized by Trinity Biotech

of Bray, Ireland, also got approved for the detection of HIV-1 in plasma, serum, and whole blood [21]. Recently, the “insulin coated ultra-thin GNPs” synthesized by the Meditech Ltd. in Oxford, U.K is in the first phase of clinical trial. The optoelectronic property such as, Surface Plasmon Resonance (SPR), Surface Enhanced Raman scattering (SERs) and biocompatibility which depends on the shape, size and coating on GNPs is discussed further in details [22].

1.3.1 Biocompatibility and colloidal stability

Au (Gold) salt-reduced and capped by plant-derived chemicals instead of chemicals such as hydrogen, sodium borohydride or Cetyl trimethylammonium bromide (CTAB), is the ultimate aim of the green nanotechnology .The phenolics phytochemicals and polysaccharides are frequently used natural plant derivatives for the GNPs synthesis. Some of the phytochemicals such “curcumin, isothiocyanate, genistein, epigallocatechin, Galatea, lycopene and Resveratrol” are used for the reduction of Au and also shows anticancer and antioxidant properties [17, 24]. The growing use of nano-materials in biomedical and medicine, it requires introducing a method that could minimize the application of synthetic toxic chemicals. Since, the green method used natural sources for the synthesis of nanomaterial, it can be presented as a sustainable method that produces self-therapeutics, biocompatible nanomaterials.

In addition to the biocompatibility, the colloidal stability of nanomaterial is one of the mandatory aspects to consider for the application of GNPs in biomedical application [25]. The GNPs are stable in the various buffers and ionic salts due to the presence of the biomolecules coated on its surface. The controlled assembly of biomolecules may increase

the stability in vitro at the various pH ranges in an ionic solution that could be an added advantage further to reduce the size and intrinsic metal-dependent toxicity.

1.3.2 Surface Plasmon Resonance (SPR)

Surface Plasmon Resonance (SPR) /localized surface plasmon resonance (LSPR), is a property of the metal nanoparticles due to presence of free electrons [26]. The localized plasmon resonance created by oscillation of free electrons in the presence of light. SPR property improves the application of GNPs in diagnosis and therapy (Figure 1.3) [27]. The absorption or scattering of light generate the SPR, the radiant light (Mie scattering) is useful for optical imaging, whereas, the absorbed light convert into heat that is more effective for cancer treatment. The scattering and absorption is competing process, and magnitude change depends on the size of the nanostructure whereas, the shift in SPR based on the distance between the GNP aggregates and biomolecules. The SPR enhancement of the nanoparticles size 10-100nm is 5 -7 times higher which can work as an optical probe. The added advantage of GNPs is sensitivity, thermal stability and resistant to photobleaching. The SPR shift generated due to conjugation of biomolecules depends on the distance between the GNPs dimers and biomolecules [28].

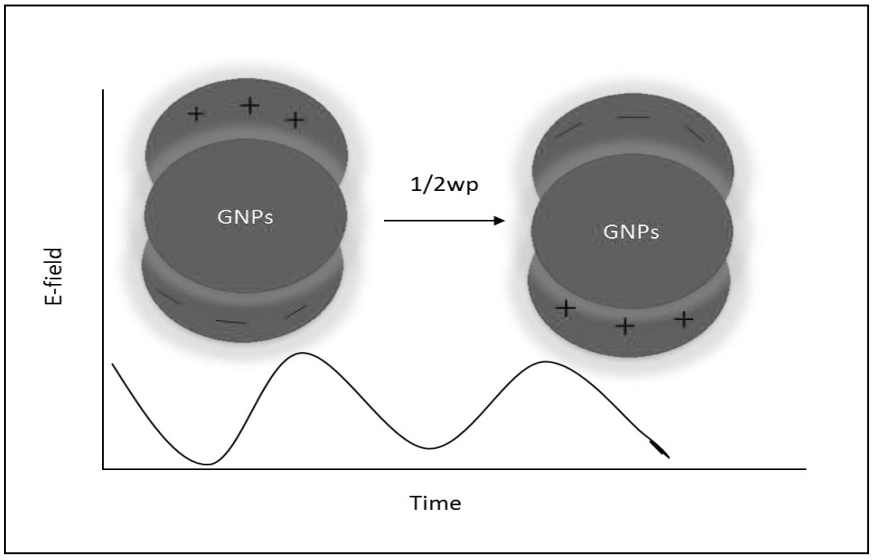

Figure 1.3 Schematic presentation of Surface Plasmon Resonance (SPR) of GNPs. The oscillation of the free electron in the presence of light gives huge optical field enhancements. The light scattering has application in bio imaging [29, 30].

1.3.3 Surface Enhanced Raman scattering (SERs)

Surface Enhanced Raman scattering (SERs) is another unique property of GNPs that has potential application in the field of theranostic. SERs was noticed for the first time was by studying the Raman spectroscopy of the electrode in 1974 [31]. In GNPs aggregated SERs intensity is more in intensity compared to the average particle size and the Raman scattering deviate from the fourth power of the normal Raman scatter range in SERs [32, 33]. In addition to the size and morphology of GNPs, SERs intensity also depends on the polarization of light from the nanoparticles which helps in determination of the orientation of molecules [34]. The SERs enhancement of the biomolecules achieves by trapped biomolecules between two gold nanoparticles that affected by the physical and chemical properties of the SERs substrate (Figure 1.4) [35, 36].

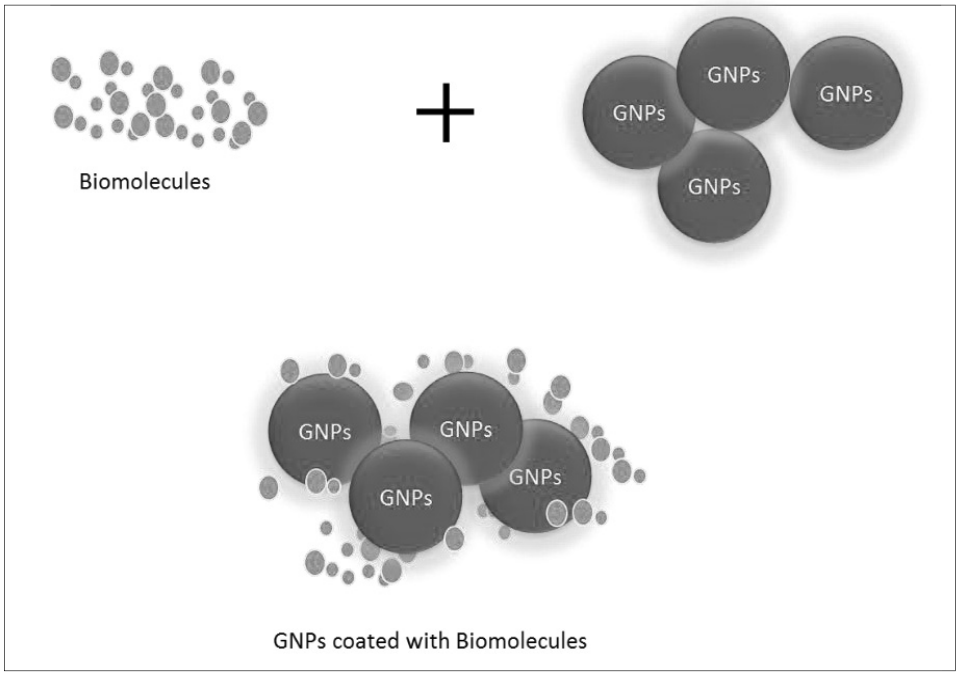

Figure 1.4 Schematic representation of SERs effect of GNPs [37]

1.3.4 Functionalization of GNPs with biomolecules

The bioconjugation is an important property of functional nanoparticles to attain the targeted delivery of the therapeutic molecules. Improvement of the clinical research and medicine by targeting the diseases in more efficient and specific manner is the long term aim of the Nanomedicine. Application of GNPs as a delivery vehicle for biomolecule and therapeutic molecules is an emerging area in the nanotechnology field. GNPs conjugated to appropriate tumor avid biomolecules with size ranging from 10-100 nm are ideal for targeting tumors, for imaging and therapy purposes [38]. The GNPs can be functionalized using different methods such as "covalent binding through metal sulfur bond (Au-S), electrostatic interaction, PEGylation and physical adsorption using surface chemistry [39-41]. The strong affinity of Au with thiol and amine functional group has been established with a variety of target agents, chemotherapeutics and drug molecules [42]. The functionalization of GNPs with antibodies, proteins, peptides DNA/RNA created

an expanding field of research for biomedical imaging, diagnosis, and therapy. The biomolecules through recognition of certain peptide sequences such as 'nuclear localization signaling, cell penetrating' and receptor targeted sequence [43-45]. The surface chemistry of the nanoparticles allows delivery of a wide range of chemicals, drugs, small molecules and biomolecules for cancer theranostic [13, 46, 47].

Thus, combined property of inorganic (GNPs) and organic (Peptide) molecules is possible to develop novel functional materials (Figure 1.5). The hybrid nanomaterial introduces a new functionality that help in specific interaction and reactivity with biological molecules [48-50].

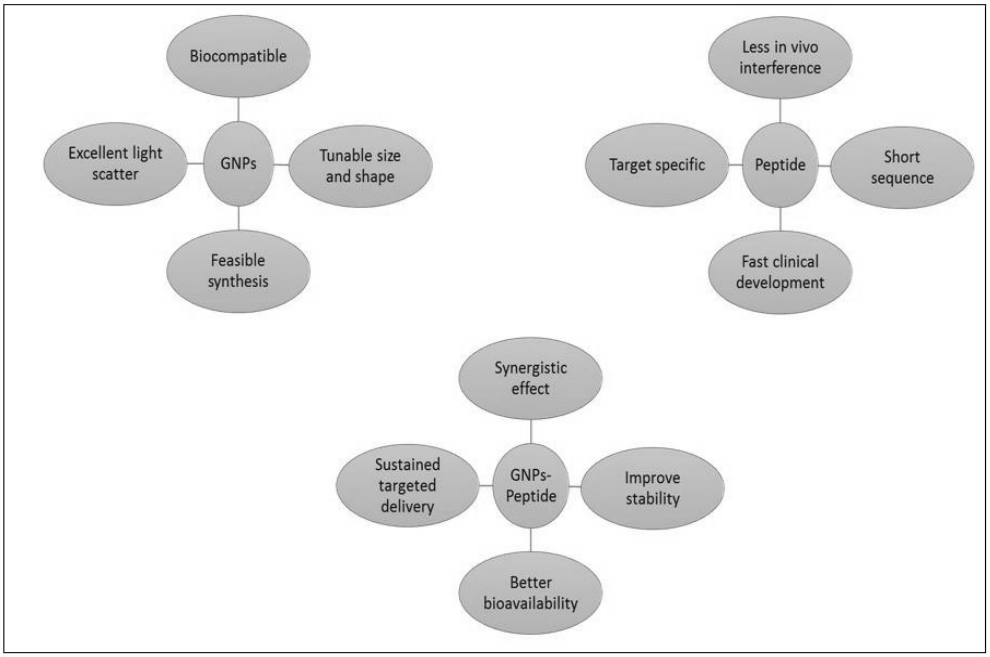

Figure 1.5Schematic representation of the important property of the GNPs, Peptide and GNPs-Peptide.

1.3.5 GNPs in cancer theranostic

The application of nanoparticles in biomedical is to achieve a long-term goal to revolutionize of health care. The current treatment modalities such as "chemotherapy, photo-thermal therapy and radiotherapy" are not very specific for the target and shows

many adverse effects that affect the normal tissues apart from the cancer tissue. The absence of specificity and bioavailability of a drug to the target tissue is the disadvantage of the current methods of cancer therapy. Therefore, conjugation of therapeutic molecules such as drug, peptide and antibody with nanocarrier is used for targeted delivery for cancer treatment [51-53].

The Cancer cell is different from the normal cell that possess many biochemical and morphological changes. The basic functional unit of living beings is a cell, which is a self-contained unit capable of undergoing self-replication if provided with the proper nutrients and ambient environment. In general, a eukaryotic cell is enclosed by a lipid bilayer and composed of nucleic acid, proteins, and other molecules. Whereas a cancer cell is defined as an uncontrolled division of cells, which spreads to the other parts of the body by local invasion, lymphatic and blood circulation. Any tissue in the body can turn into the cancerous tissue and the basic processes that induce cancer are quite similar in each type of cancer tough at the molecular level each type of cancer is different. At a molecular level cancer is known to have deregulation of the cellular signaling process that controls the cell proliferation, differentiation, and apoptosis. The discontinuous capillary walls with no basal lamina permitting particles less than 100 nm to penetrate easily into the cancer cell. The unique enhanced penetration and retention effect (EPR) of the solid tumor tissue allow the delivery of drug selectively to tumor tissue [54]. EPR is a unique property of solid tumors, which is indicated by extensive angiogenesis, hyper vasculature, absence of lymphatic drainage and imperfect vascular structure. The EPR effect can be utilized for the effective treatment for the delivery of the drug. EPR effect used in many cancer using “N-(2-hydroxypropyl) meth acrylamide” (HPMA) copolymer as a nanocarrier to deliver the

anticancer drug doxorubicin [53, 55]. The retention of the particles in the tumor tissue is an advantage in the delivery of the target molecule at the tumor site, which is known as homing. Similarly, the functionalized nanomaterials such as peptide functionalized GNPs also home at the tumor tissue and unable to eliminate, which interns increases the efficacy of the therapeutic molecules. Hence, once the nanoparticles penetrate to the tumor site, it increased the pharmacokinetics [56, 57].

1.4 Address the problem

Early stage detection and target specificity is a grand challenge in the cancer treatment from more than four decades. Cancer is a complex multifactor disease with uncontrolled cell division and deregulation of the cellular signaling process. It expresses different molecules as markers and shows the characteristic signals that are distinct, quantitative and qualitative compared to the normal cell. Tough expanded knowledge in molecular targets and pathways are being identified for the diagnostic and therapeutic of cancer. However, the drawbacks of the current method mainly chemotherapy to develop multidrug drug-resistant tumor less sensitive and more off-target effect. Therefore, till date cancer treatment/diagnosis is big challenges in biomedical science.

Retinoblastoma (RB) is a childhood eye cancer. It arises from all the layers of the retina. RB take in for 3% of childhood malignancies [58-60]. RB is the most common intraocular and life-threatening cancer of the eye in children [58]. RB originates from a multipotent stem cells and locally invasive tumor which developed because functional loss of both the alleles of the RB-1 gene (tumor suppressor gene) [59]. The loss of function of RB gene promote tumor progression and also induces cancer. Apart from the Rb-1 gene various other genes which express in RB play an important role in RB progression. One

such gene is HDM2 over amplified in RB, is a negative regulate for tumor suppress gene p53 [60, 61]. The selective inhibition of the HDM2 could be an effective therapy for eye cancer.

The RB-1 gene mutation and overexpression of the HDM2 are involved in the progression of the RB tumor [62, 63]. In addition to an oncogene, the redox state of a cell is an important factor which plays a critical function in cancer progression. ROS are oxidants and they have dual roles in promoting cell proliferation or cell death and also induced DNA damage. DNA damage is a critical factor to cause carcinogenesis. Oxidative stress is present more in the cancers compared to the normal cells is an indicator of the redox imbalance and can be used as a bio-indicator of the abnormal state of the cell. The oxidative stress, which is defined as an imbalance of the cell due to release of reactive oxygen species is also a major concern for cancer, which leads to cellular damage that ultimately causes cell death or uncontrolled cell proliferation [64, 65].

ROS in cancer have been studied extensively and most of the drugs act on cancer cells by increasing the ROS above its threshold levels thereby leading to apoptosis. However, this method has many disadvantages like an evolution of more aggressive tumors, the development of drug resistance, tumor invasion, and metastasis. The current treatment modalities for RB treatment are systemic chemotherapy, intravitreal injection and local therapy such as cryotherapy and brachytherapy [66, 67].

1.5 Hypothesis

The current cancer treatment methods have the limitation due to poor bioavailability and less specificity to the target site. Because of limitations associated with the current modalities for cancer treatment the novel method is of high demand that could

overcome the side effects and improve therapy and diagnosis. Targeted therapy could open a new path for the cancer treatment in combination with nano-medicine. Therefore, a nano-carrier based targeted therapy for delivery of molecules could be a new regime to combat the deadly disease such as cancer.

In view of the fact that, we proposed a systemic approach to the synthesis of multifunctional GNPs using a biological method and functionalization with peptides. HDM2is an oncogene which overexpressed in most of the cancers including retinoblastoma and a negative inhibitor of the p53 [68]. Thus, HDM2 is an important molecule for targeted therapy. The delivery of anti-HDM2 peptide with GNPs to obstruct the binding of HDM2 with p53 was the main idea of using HDM2 peptide for the RB therapy. On the other side, ROS in the cancer cell and the normal cell is known to increase the genetic instability and promote the cancer cell proliferation. Hence targeting the ROS would be an approach along with for therapeutic application. Oxidative stress is a complex process and the limitation has observed in use of antioxidant could be due to factors such as low bioavailability of antioxidants, non-specificity, stage of disease, factors other than oxidative stress that influence the disease. Apart from oncogene (HDM2), nano-carrier mediated ROS targeting would add an advantage to achieve the most effective therapy of the RB using *Vitis vinifera L.* reduced GNPs.

It was proposed that the novel synthesized nanoparticles would be a self-therapeutics and improve the therapeutic effect of targeted molecules. The hybrid organic-inorganic nanomaterial would be more effective and introduce new functional property that would be more effective in tumor regression in comparison with an individual component such as, peptide alone (Figure 1.5). It was also proposed that the reducing agents used for

the synthesis of the GNPs can differently regulate the apoptotic pathways that affect the tumor growth reduction along with the anti-HDM2 peptide. The nanocarrier based delivery of the peptide molecules will not only serve as a targeted therapy, but also, it can help in homing of the therapeutic molecules.

1.6 Objectives

1 To synthesize SERs active GNPs using different reducing agents *Vitis vinifera*, Curcumin

2 To characterize as synthesized GNPs using UV-Visible, DLS, XRD, MALDI, FT-IR and Raman spectroscopy.

3 To evaluate the biocompatibility of GNPs using different type of cancer cell line such as Breast cancer, Retinoblastoma and non-cancer.

4 Functionalization of GNPs with antioxidant (Peptide-A) and therapeutic (HDM2) peptide

5 To study the i*n vitro* functional property of the GNPs-Pep-A (Conjugate) by radicals scavenging and knockdown of HDM2 peptide.

6 To study the *in vivo* preclinical evaluation of antitumor efficacy of GNPs-HDM2 conjugate using retinoblastoma (RB) xenograft nude mouse model.

7 Xenograft nude mice tumor and serum sample to understand the apoptosis and cytokines

8 Spectroscopic studies to identify the molecular fingerprint in the treated xenograft tumor samples to identify the interaction between the C-GNPs-HDM2 and V-GNPs-HDM2 with bio molecules.

1.7 Structure of the thesis

This dissertation is divided into eight chapters

Chapter-1 was an introduction of nanotechnology in general and the subsequent discussion on the application of GNPs in nano-medicine. The chapter first ends with the problem, hypothesis and objectives of the desertion.

Chapter-2 provides an extensive literature review on GNPs for nano-medicine application. The chemical and biological method of nanoparticles synthesis and nanomaterial toxicity with an emphasis on the importance of different reducing agents. It summarizes the properties of different types of gold nanostructure and suitable application of each nanostructure for therapy and why and how the GNPs is the better choice than other available materials.

Chapter-3 This chapter discussed about the experimental procedures and methodologies adopted in synthesis, characterization, and bio-conjugation. The in vitro cell culture and in vivo xenograft nude mice model, methods were used for the functional study. It includes details of various characterization techniques adopted for detail, characterization of GNPs, UV- visible, FT-IR, XRD, MALDI, TEM and Raman spectroscopy, etc. It also includes the description about in vitro biocompatibility test for nanoparticles, FACS and microscopy analysis.

Chapter-4 discuss the first specific objective of the dissertation; synthesis of GNPs using green technology with the different reducing agent. An emphasis is given to the *Vitis vinifera L.* and *Curcuma L*. as a reducing agent for the GNPs synthesis and biocompatibility study using various types of cancer cell line.

Chapter-5 The antioxidant property of GNPs-Pep-A, highlighted using *Vitis vinifera* GNPs on reactive oxygen species scavenging in *in vitro* using Y79, the RB model.

Chapter-6 This study is the detailed study of the clinical significance of HDM2 functionalized GNPs in vitro and in vivo for anti-tumor effect. This chapter mainly discusses the biological significance of V-GNPs-HDM2 and C-GNPs-HDM2 with respect to the difference in the biological responses and its effect on HDM2 knockdown using RB as a tumor model.

Chapter -7 Discusses the analytical technique for the analysis of xenograft RB tumor sample by ATR/ FTIR spectroscopic analysis. The spectroscopic molecular signature helps to understand the interaction of the target molecules with different biomolecules.

Chapter-8 Summarizes the interpretation and conclusion based on the current experimental condition, data and results obtained in the dissertation. It also presents an understanding of the chemical interaction of the therapeutic molecules and identification of instruction through spectral fingerprint. This chapter also discusses the future scope of the current work in the light of results obtained in the dissertation

1.8 Outline of the thesis

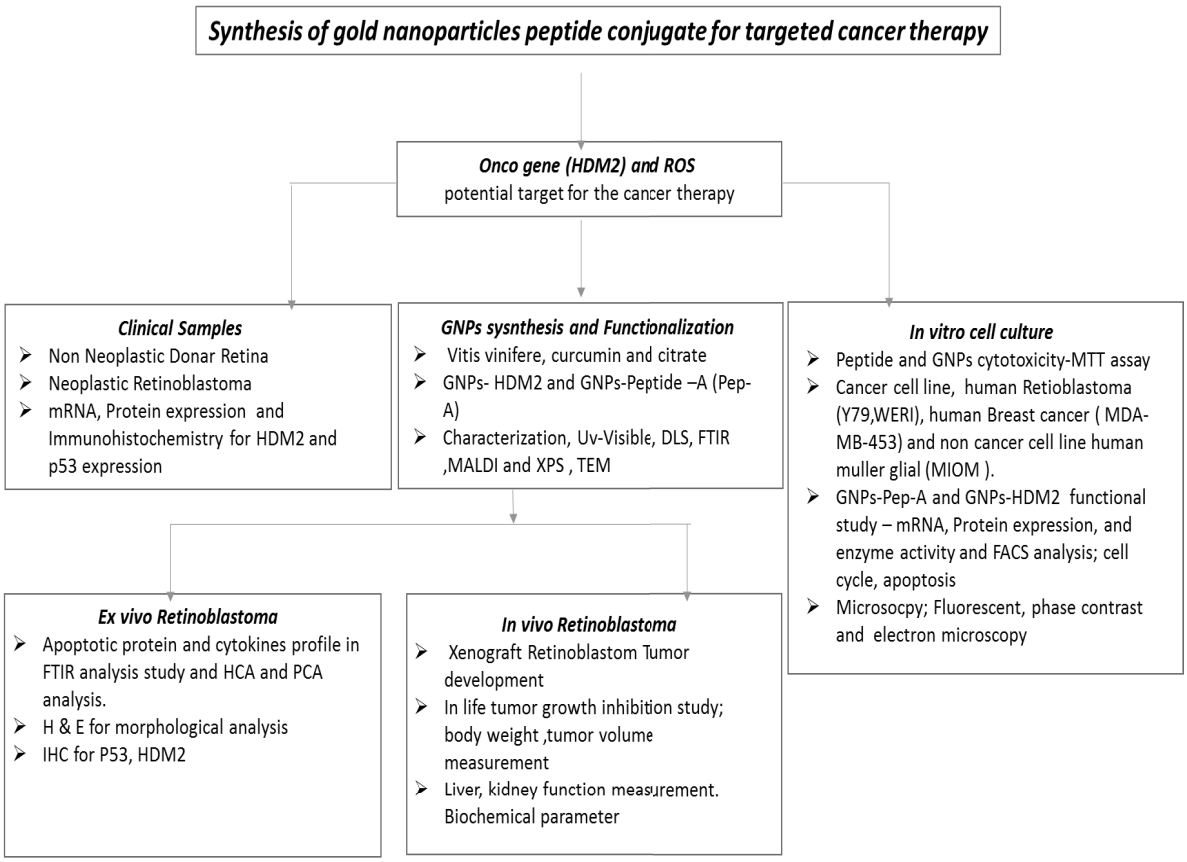

CHAPTER 2

2 Literature review

This chapter highlight on the literature review and summarizes the findings reported by other researchers working on the different aspects of the Gold Nanoparticles (GNPs). An emphasis will be given on advantages of biological reducing agents and functionalization with peptides for therapeutic application. It also includes the *in vitro* and *in vivo* preclinical application of functionalized nanomaterial in cancer theranostic. In particular, the literature review is useful to understand the need for the synthesis of GNPs using different reducing agents and applications of GNPs as nano-carrier to deliver the therapeutic molecules. It helps to interpret and understand the results of the current research reports in the dissertation. The extensive review of existing literature rationalizes the importance of targeted therapy for cancer theranostics.

2.1 Background

Nanomedicine is an emerging field, which utilize the advantages of size-dependent properties like high surface to volume ratio and quantum effects. Similarly, various mechanical and optical properties of nanomaterial have utilized to develop and design novel systems, which are effective in therapeutic applications [69, 70]. The use of nanomaterials (1-100 NM) for drug and small molecule delivery has vividly been altered the effect and can deliver the molecules to target specific manners, which can improve the specificity of therapeutic agents. The unique sizes and shapes with dependent properties of nanomaterial not only help in the delivery, but enhance the specificities for the target and reduces the side effect occur due to non-targeted therapy [71]. Due to its unique set of physio- bio-chemical, properties like, biocompatibility, colloidal stability, surface

chemistry, and optical properties of GNPs, which can have a variety of applications in theranostics [72-74]. The GNPs are more attractive due to loading efficacy of targeted which is in an order of 10^2-10^3 higher than the liposomal molecules or polymeric nanoparticles [75, 76]. In consideration of the unique property of GNPs, different nanostructures have been established and approved by the FDA for clinical use for disease one such example is rheumatoid arthritis. Some of the gold based drug are currently in use for the treatment of various diseases (Figure 2. 1) [21, 77].

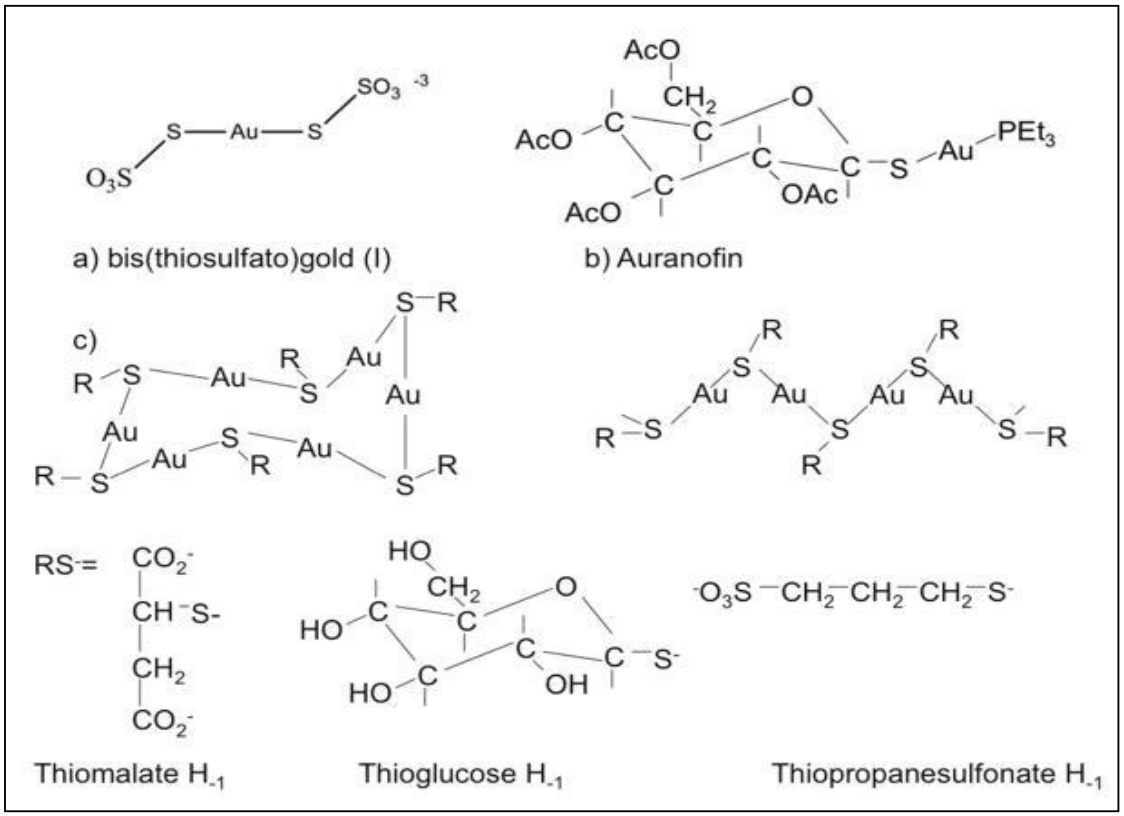

Figure 2.1 Chemical structure of the gold based drug approved for clinical trial [78].

2.2 Nanomaterial for biomedical applications

Early diagnosis and effective targeted therapy are needed for effective cancer therapy. The different kind of materials such as polymers, metals, carbon, and ceramic are in various applications for different tissue engineering and drug delivery. Since 1950s,

many polymeric nanostructure such as liposome and micellar have been developed to deliver the drug for targeted therapy [79-81]. Natural and synthetic polymers such as micelles, dendrimers, the nanosphere, and nanocapsule, gain much, attention among all types of approved materials in 1960-1970's for biomedical application. The polymer nanoparticles such as poly- L-glutamic acid are widely used for the delivery of various chemotherapeutics [82]. Albumin, heparin, chitosan, paclitaxel-loaded albumin are the natural polymers in use for lung cancer in various stage of clinical trial [83, 84]. Although polymers are good for the delivery application, it has limited application in imaging. Since, metal nanoparticles are effective in imaging due to its unique confinement effects, which arise from an optical property of GNPs, which is an added advantage over the polymeric material (Figure 2.2).

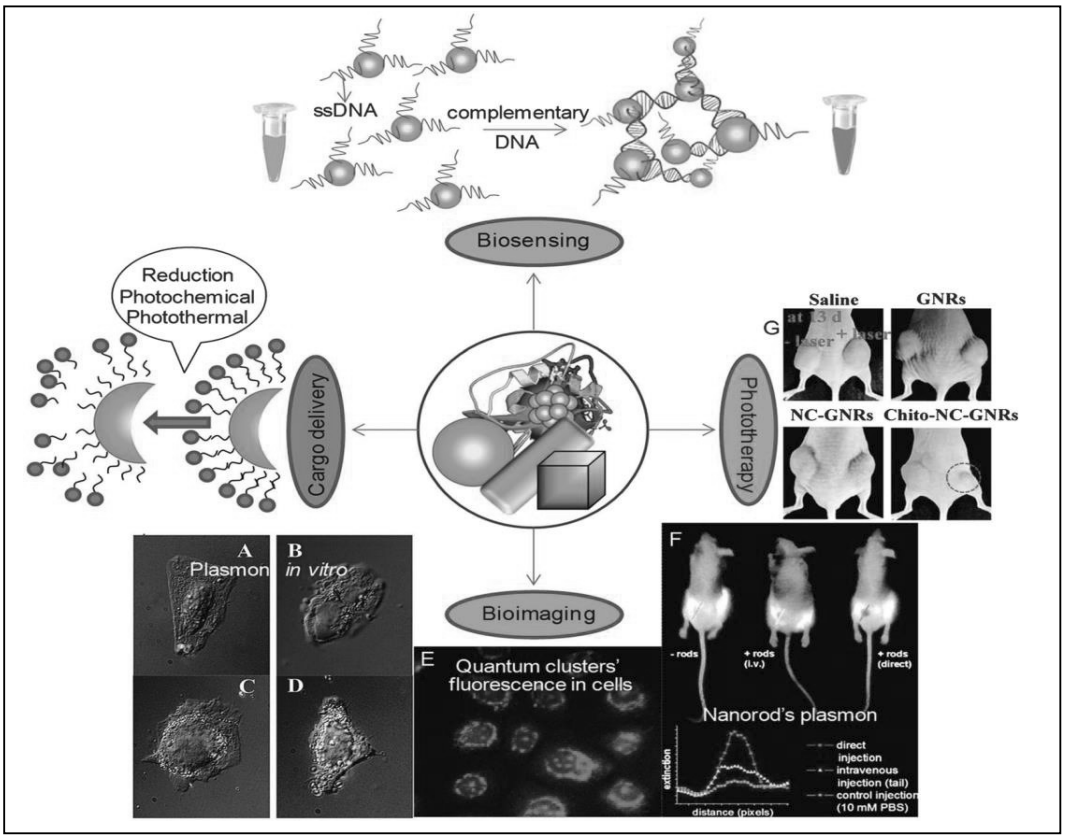

Figure 2.2 Represent the various applications of gold nanostructure for cancer theranostic

"(A–D) *In vitro* plasmonic images of HepG2 cells after treated with gold nanoparticle–peptide complexes and fluorescence image of H1650 cells incubated with bimodal nanoparticles composed of super paramagnetic iron oxide nanoparticles, fluorescent Au_{25}–BSA complexes and EGF (E) (F) *In vivo* NIR transmission image of tumor-bearing mice treated with or without PEG-ylated gold nanorods, (G) Photothermal thermal application in mice model after (A–D) [85] (E) E. S [86] (F) E. B. [87] and (G) W. I. [88, 89]".

2.3 Chemical method of GNPs synthesis

The unique metal-dependent property of the noble metal has a various application in cancer theranostic. Hence, the synthesis of the metal nanomaterial from different chemical and biological methods has been developed to obtain the nanoparticles [22, 90]. Turkevich method of GNPs synthesis use citrate for the reduce Au salt (HAuCl4). Whereas, in Brust's method two organic phases (water–toluene) and sodium borohydride was used for the GNPs synthesis (Figure 2.3) [91, 92]. The varying size and shape of colloidal GNPs can be synthesized by varying the concentration of the Au salt, reducing

agents temperature and pH, etc. The size ranges from 2-100 nm can be synthesized allowing optimizing the ratio of Au salt and reducing agent. Similarly, the shape of the particles can be controlled by using a different reducing agent. For example, Au salt reduced by sodium citrate predominantly, produce the spherical shape of GNPs [93]. CTAB (Cetyl trimethylammonium bromide) is the choice for the rods shape nanoparticles. The shape and size of the GNPs have a significant application in the various biological applications the most common are spherical and rod shape.

2.4 Different morphology of gold nanostructure

GNPs mainly categorized based on the shape, size and confinement of the particles. According to the confinement of atoms the shape of particles and its applications are defined. The colloidal gold is a nanoparticles suspension and the color of the suspension varies from intense red to blue which define the size of particles

2.4.1 Gold Nanoparticles (GNPs)

The commonly used shape as a nanocarrier is spherical with size in the range of 1-100nm synthesized predominantly by single phase method (Figure 2.4 A). The molar ratio of reducing agent and gold salt can affect the typical size of the nano-spheres. The size and shape of the GNPs can be easily controlled by varying the synthesis parameter such as temperature, concentration and type of reducing agent. The monodisperse gold nanospheres show the absorption peak (SPR) between 510-550 nm [94]. The increasing in the width of SPR band indicates a wide range of the size distribution. In the single phase synthesis of GNPs $AuCl_4^-$ was reduced and capped by Fe(II)-EDTA to form the different sizes of GNPs ranging from 6.7 to 50.9 nm[95].

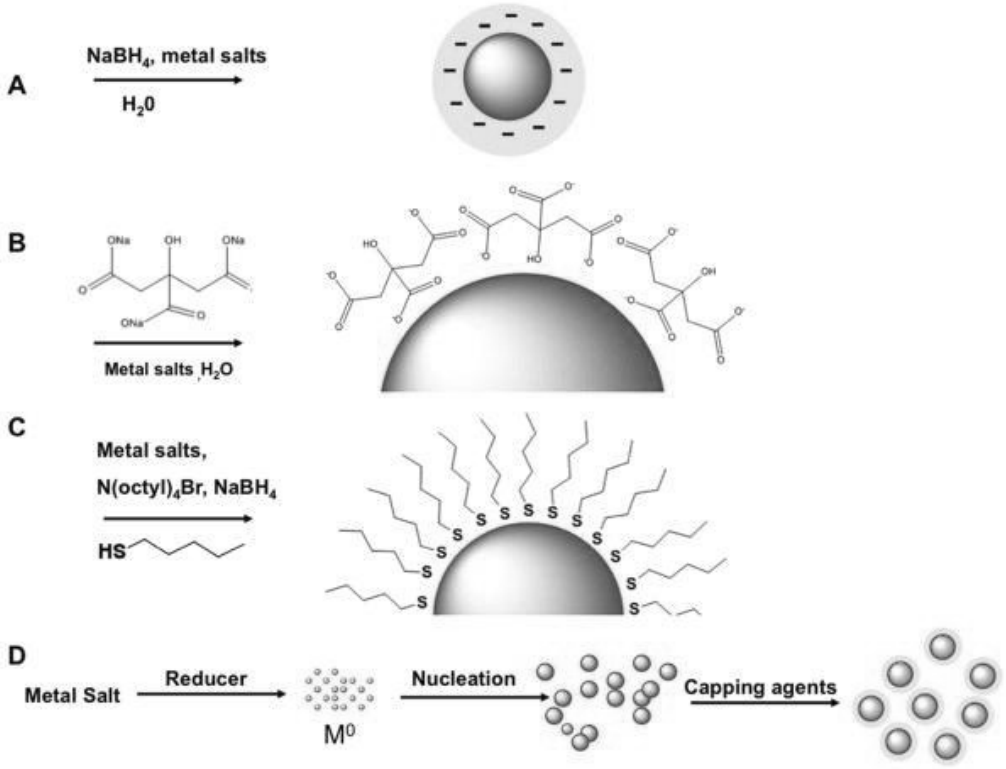

Figure 2.3 Schematics of representation of chemical method of GNPs synthesis.

(A-D) The reduction of the metal salt with standard reducing agent sodium citrate and sodium borohydrate with binding of nonpolar thiol. Nucleation and growth are the important phenomenon occur during the GNPs synthesis [78].

2.4.2 Gold Nanorods (GNRs)

The seed-mediated growth, using cetyltrimethylammonium bromide (CTAB) is the most common method to achieve rods in the range of 1-100nm. In the seed method, the citrate-capped gold nanospheres, work as seeds solution and HAuCl4 as a growth solution. The growth solution is prepared by the reduction of HAuCl4 with ascorbic acid and silver ions. The main advantage of gold nanorods is its SPR in the near infra-red (NIR) reason and biological tissue absorbed very less light in NIR reason. GNRs has an added advantage over other GNPs is the mainly photothermal application (Figure 2.4 B).

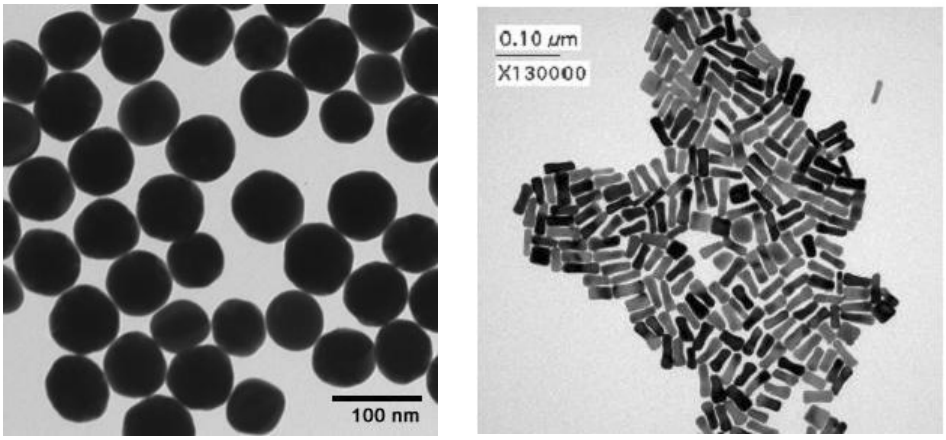

Figure 2.4 Representative gold nanostructure for predominantly useful in drug deliver, photo thermal and imaging application (GNPs and GNRs) [96].

2.4.3 Gold Nanostars (GNSs)

The Gold nanostar is another type of nanoparticles, which has a wide range of biomedical application such as drug delivery, geothermal, bio-imaging and sensor application. The most appropriate size is in the range of 45-116-nm with different in optical properties.The multiple pod with single crystalline tips nanostars can synthesize by Au seeding in presence of poly (vinylpyrrolidone) (PVP) in N,N-dimethylformamide (DMF) to using HAuCl(4) salt [97]. The nanostar morphology can controlled by controlling the nucleation and growth phenomenon during the synthesis process. The core size, number of branches, aspect ratio; with respect to the core size and branches are the important parameter which significantly altered the application of gold nanostars. The different sizes of the nanosars show long surface plasmon band shifts in the NIR region. The long NIR range plasmon shifts indicates the better application in the SERs application. The average EF was observed at 6333 nm is 5×10^3 [98, 99].

2.4.4 Biomedical application of different type of gold nanostructure

The different structure and shapes of the gold nanostructure has many applications.The different shape such as nano spheres, nanostars and nanorods absorb and scatter light in the visible to near-infrared region which gives the different SPR band. Gold nanoparticles (GNPs) absorb in the 520-540nm are widely in use for the targeted therapy using peptide, antibodies and aptamers. The functional blocking of the cancer biomarker suchas HDM2, HMG2 and EpCAM , MMPs has been targeted using gold nanoparticles[100]. In a study using RGD and myxoma peptide conjugated GNPs were used in a B16 melanoma allografts *in vivo* model. These findings confirm that peptides homes at the tumor site without cytotoxicity of melanoma tumor [100, 101].

Whereas, gold nanorods (GNRs) due to the anisotropic nature have more application in photo thermal, Raman signal enhancement, molecular detection and imaging application. The two absorption band of rods shows sensitivity and the local surrounded environment change the sensitivity which is more applicable for bio-sensing application [102, 103]. DNA functionalized gold nanorods are used for cancer cell imaging and also confirm the DNA binding on the surface of the rods. DNA functinalized gold nanorods are used for cancer cell imaging and also confirm the DNA binding on the surface of the rods. Similarly, other type of nano construct gold nanostars (GNS) also used for targeting the cancer molecules. In a study using nucleolin aptamer loaded GNS was used to target the ubiquitous protein. It has found that Apt-AuNS nano constructs internalized in cancer cell and down regulate Bcl-2, mRNA expression (anti-apoptotic protein) efficiently as compared to cells without the Apt-AuNS nano. Also, caspase 3/7 activity (apoptosis) which play important role in apoptosis also increased compared to cells which transfected with

free AS1411.The photothermal property of the gold nanostructure significantly enhanced the apoptosis in cancer cell [104]. The significance of the nanostructure clear indicates the importance of the different nanostructure in nano medicine

2.5 Effect of size and chemical agent used in GNPs synthesis

The application of nanoparticles in medicine is a rapidly growing area in the field of nano-medicine, hence, it is imperative to consider the cellular toxicity of nanoparticles to identify the dose-dependent effect of nanoparticles in the biological system. The internalization and cellular toxicity vary with the shape and size of nanoparticles. The GNPs internalized effectively compared to GNRs of similar size similarly the capping agents also affect the cellular toxicity [38, 105]. “Human lung cancer (A549)” shows toxicity by citrate capped GNPs. Whereas, same concentration is nontoxic to the “BHK21 (baby hamster kidney)” and “ HepG2 (humanhepatocellular liver carcinoma)” [106]. Apart from concentration, shape and size, diffusion and velocities, sedimentation of GNPs affect the cellular uptake process [107].

The size dependent cytotoxicity of 5 and 15 nm citrate stabilized GNPs was studied in vivo in Balb/3T3 mouse model. The colony forming efficiency (CFE) assay, results revealed that small size GNPs (5 nm) at concentration $\geq$ 50 μM size is cytotoxic compared to the big size (15 nm) [108]. The cellular behavior of GNPs treated cells gives an insight to understand the importance of size, shape and reducing agent. Similarly, cytotoxicity of triphenylphosphine derivative water-soluble GNPs was studied four different cell lines, such as epithelial, fibroblasts, macrophages, and melanoma cells. The data indicate that the most effective size of GNPs is 1.4 nm, which shows IC (50) concentration between 30-56 μM that variations in the different cell line. In contrast, GNPs of 15nm and Tauredon

(gold thiomalate) non-cytotoxic even at much higher concentrations, 60-fold and 100-fold respectively. The cell death necrosis or apoptosis is also dependent on the size and time of treatment in case of 1.4-nm GNPs cell death caused by necrosis whereas 1.2 nm GNPs predominantly follow programmed cell death [109]. The cell selective response of the Dihydrolipoic acid (DHLA) synthesized GNPs was studied in the normal human hepatic cell line (L02) and the human hepatoma cell line (HepG2). The cytotoxicity of these of GNPs at different time point and the concentration range from 10-125 μM till 72h showed no cellular cytotoxicity. The significant cell growth was observed in the HepG2 cells till 72h indicates that cell cycle growth was not hindered and cell enter from G1-S checkpoint. In an *in vivo* system GNPs induced the ROS formation, which cause oxidative stress and induced DNA damage and other cellular toxicity. Similarly, the accumulation of GNPs in various organs like spleen, liver, kidneys and lungs shows more toxicity due to the oxidative stress induced by the GNPs. Moreover, immunogenic responses such as thrombosis, hemolysis also reported *in vivo*, due to the presence of the GNPs [110]. In a study using "cationic shell-crosslinked knedel-like (cSCK) nanoparticles" for the delivery of the Peptide nucleic acids (PNAs) was constructed using bioreductively cleavable disulfide/ electrostatic interaction for the delivery of the PNAs. The Arg9-mediated method for PNA delivery in HeLa cells, showing lower toxicity and higher bioactivity [111, 112]. The unique characteristic of the cSCK is to reduce the cytotoxicity and increased the bioavailability than the into HeLa cells. [113-116].Also the different chemical modification such as binding of DOTA ,/ PEG maximized the application for imaging and *in vivo* at the same time minimized the detection by RES. The unique characteristic of the cSCK is to reduce the cytotoxicity and increased the bioavailability into HeLa cells. The

mechanism of the trapping of the cSCK into endosomal/lysosomal and release of PAN into cytoplasm is the important characteristics of these unique nanoconstruct to achieve the target specificity with minimal toxicity. The different chemical modification such as binding of DOTA / PEG maximized the application for imaging and *in vivo* at the same time minimized the detection by RES. The nanorods toxicity due to CTAB, can also altered by multi-coated GNRs. The GNRs coated with PSS, PAH, PSS/PAH and /PAH/PSS reduced the CTAB direct interaction with cell and reduce the cytotoxic effect of the CTAB. The GNRs coated with PSS, PAH, PSS/PAH and /PAH/PSS reduced the CTAB direct interaction with cell and reduce the cytotoxic effect of the CTAB [113, 114]. These findings confirm the effect of GNPs at various level, which predominately depending on size and various chemicals used in coating for nanoparticles. Table 2.1 briefly describe the effect of different parameters of GNPs on cellular behavior

Table 2.1 Cellular effect of GNPs, size, shape and concentration on different cell line

Cell line	**Size of GNPs**	**Concentration**	**Shape/Surface group**	**Cytotoxicity Assay**	**Cellular effect**	**Reference**
Human leukemia cells (K562)	4,8&12 nm	25-250mM	Citrate coated	MTT assay	Non toxic to K562 cells	[115]
Adipose derived stem cell	15-100nm	1μm	Spherical Citrate	Cell counting Kit (CCK-8) lives dead assay	Osteogenic differentiation, 30-50nm is the most effective size	
MG 63 Osteoblast like cell	10 nm	1-10ppm	Spherical Citrate	Annexin V-FITC assay	Apoptosis and necrosis	[116]
Human hepatocellular Carcinoma HepG2 cells	25±3.5 nm	1.0 nmol /L GNP, and 1.2_mol/L Paclitaxel (T)	Spherical particles	MTT, quartz crystal Microbalance (QCM) and flow cytometer assay	GNPs show low cytotocxicity more apoptosis in HepG2 cell. GNPs with Paclitaxel inhibits the	[117]

					growth than Paclitaxel alone	
Human skin cell line HaCaT keratinocytes	1.5 nm	10 µl	Spherically & nanorods CTAB coated	MTT assay	Spherical GNPs, non toxic. GNP, Nanorods were highly toxic due to the presence of CTAB	[118]
A549 cells, human alveolar epithelial-like cell	15 nm	200-2000 µg GNPs	Spherical GNPs	Real-time PCR, ELISA	Non toxicity, no oxidative stress markers and no inflammatory cytokines responses	[119]
Human prostate Carcinoma PC-3 cells	30-90 nm	1.5nM	Spherical GNPs	MTT and LDH assay	No LDH leakage observed up to 34nM., Spherical 50 & 90 nm diameter induced the proliferation of PC cells	[120]

2.6 Other types of inorganic nanomaterials

The current progress in the field of inorganic nanomaterials, which includes Au, Ag, Fe and I are in use for nanomedicine. Apart from Au, Ag nanoparticles are in use in the imaging and anti-microbial application. Similarly, Fe and Si also have myriad application in imaging and therapy [121]. The surface-functionalized nanoprobes are in use for the detection of the detect various biomolecules such proteins, lipids, nucleic acids and ions using different types of inorganic nanoparticles [122]. The application of Fe_3O_4 @ SiO_2 in nuclic acid research has shown in a study by covalent binding of biotinylated oligonucleotide on streptavidin coated Fe_3O_4 @ SiO_2 NP [123]. In an another study using Fe_3O_4 coated with silica coating significantly reduces the aggregation in solution and improved the chemical stability of the Fe_3O_4 @ SiO_2 and provided multiple functional site for functionalization with various molecules. Similarly, *N*-(rhodamine-6G) lactam–ethylenediamine functionalized Fe_3O_4@SiO_2 superparamagnetic NPs was prepared for the detection of Hg^{2+} and use as a fluorescent sensor[124, 125]. In addition to the conjugated with Fe nanoparticles, Si based mesoporous silica nanoparticles (MSN) were prepared for the delivery of the antibacterial ionic liquids against gram negative bacteria Escherichia coli K12. The organosiloxane function group conjugated with the fluorescein doped mesoporous silica nanoparticles (FITC-MSN) was used for the controlled-release of in mammalian cancer cell confirm that fluorescein was released due to reduction of disulfide bond reducing molecules [126].

2.7 Green nanotechnology for GNPs synthesis

GNPs potential application in Nanomedicine is largely contributed due to biocompatibility and gold (0) state, which is extremely inert in nature. The critical review

(Table 2.1) on GNPs synthesis by different reducing agents reveals the chemical of GNPs in biological systems, which depends on the type of cell, concentration and time of treatment [127]. An increasing application of nano-materials for various biological application, it is important to develop a method that reduces the use of toxic chemicals. The biological method of GNPs synthesis is entirely based on the biological safe chemicals, it will serve as an ecofriendly method for the GNPs synthesis.

The green nanotechnology could be an alternative and sustainable approach that can reduce the toxicity of reducing agents [128, 129]. The revolution has come with green nanotechnology for the synthesis of metal nanoparticles for biomedical application. The plant derivatives such as curcumin, isothiocyanate, genistein, epigallocatechin, gallate, lycopene and resveratrol are used in the synthesis of GNPs shows anticancer and antioxidant properties [130, 131]. The phytochemicals used in the synthesis process can interact with the biomolecules and altered the cellular signaling process, which could work as self-therapeutics molecules [132]. The application of phytochemicals in metal nanoparticles synthesis is an emerging area and gaining much attention, due to the less toxicity of metal nanoparticles. An active compound of the Memecylon edule, Macrotyloma uniflorum was used for the gold and silver nanoparticles synthesis of different shape and size [133]. In another study, Soy, Tea and Cumin was used for the synthesis of the GNPs [134, 135]. These reports suggest that phytochemicals show the unique kinetic propensity and can be used as an active reducing and capping agent. The antioxidant and anticancer property present in the plant phytochemicals can be used for the synthesis of self-therapeutic GNPs. The polyphenols such as flavonoids like

epigallocatechin gallate and catechins, curcumin have been used to the functionalized nanoparticles for anticancer and antioxidant effect in cancer cell [1, 136-138].

In addition to the plant phytochemicals biologically compatible buffers have been used for the reduction of the Au salts. The HEPES buffer reduced GNPs is more biocompatible over the sodium citrate at the dose of 500 μg/kg. The fibroblast cell (L929) viability shows that HEPES-reduced GNPs at 5.0- and 10.0-ug/ml concentrations are more biocompatible than citric reduced GNPs. In addition to this, more reactive oxygen species (ROS) were generated in the cell suspension when treated with citrate caped GNPs. The result confirmed that reducing agent is equally important to use GNPs in biological application [139].

2.7.1 Curcumin a reducing agent and an anti-cancer molecules

Natural polyphenol is known for anti-oxidative, anti-inflammatory, and modulator of pathological angiogenesis (Figure 2.5) [140, 141]. The poor water solubility of curcumin inhibits its application in vivo as an anticancer molecule. Curcumin is a known polyphenol it can used for the reduction of Au salt, which can help to improve its bioavailability and application in the field of cancer theranostic [142]. The previous study suggests that bioavailability and solubility of curcumin improved by conjugation with GNPs [143]. The solubility of poorly water-soluble curcumin has been improved by "anti-solvent precipitation with a syringe pump (APSP)" and "evaporative precipitation of nano suspension (EPN)" method of GNPs synthesis. 1, 3 diketone group of the curcumin chelate the metals during the GNPs [144]. The nucleation and growth process have been controlled, and minimum size was obtained in the range of 330 -150 nm. Overall, better solubility, dissolution rate, and antioxidant activity were obtained with GNPs synthesized by

curcumin compared to the curcumin alone [145]. In a study, GNPs has been synthesized by conjugating with hyaluronic acid (HA) to increase the solubility of curcumin [146]. HA-Cur-GNPs were used to target the folate receptors in cancer cell confirmed the hemocompatibility, cellular uptake and internalization of GNPs in HeLa cells, glioma cells and Caco-2 cancer cell line.

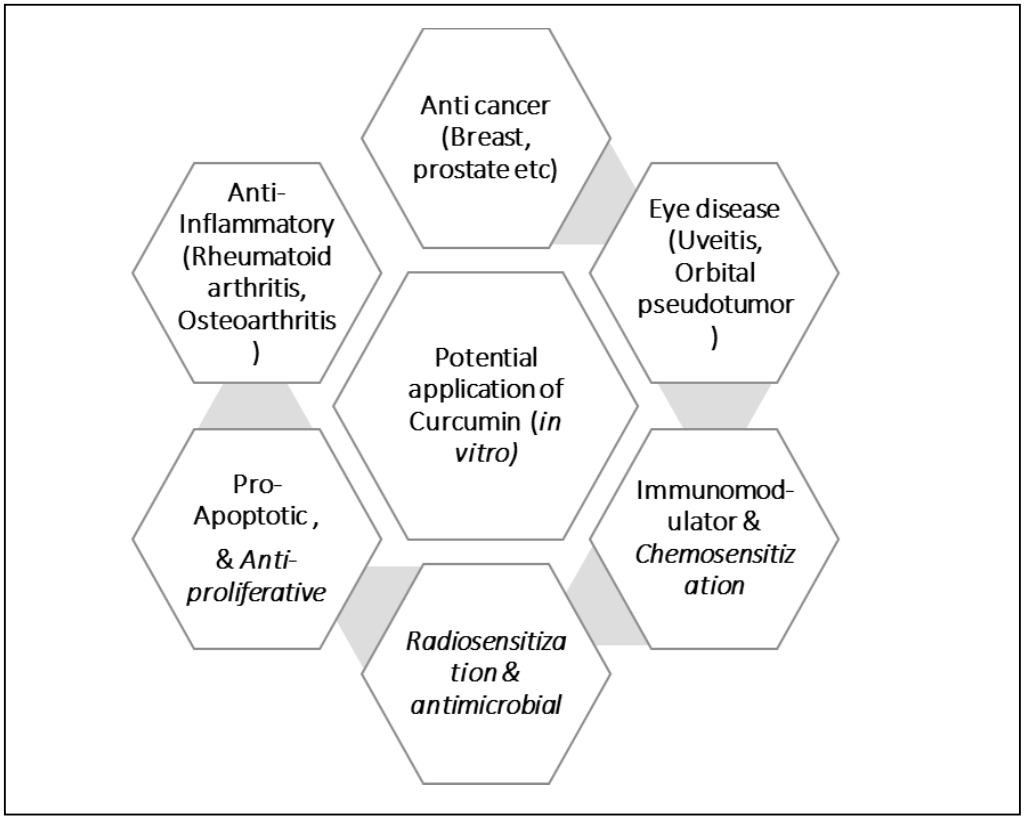

Figure 2.5 Curcumin and its various potential clinical application to treat the human disease [147].

2.7.2 Thiotic acid, an antioxidant molecules

Thiotic (TA) is a known antioxidant water insoluble molecule. Alpha-lipoic acid has been used to stabilize the GNPs and additionally improve the antioxidant effect of GNPs in cancer cell in vivo. The dihydrolipoate active form of the TA reacts with different ROS species that includes superoxide hydroxyl, peroxyl and hypochlorous acid. TA, can improve the metal chelating capacity, scavenge of ROS, improved the antioxidant effect

and repair the oxidative damage of the cell. It has been suggested that availability and compatibility of the colloidal GNPs were enhanced using covalently bound self-assembled monolayer (SAM) [148, 149]. The salt-mediated self-assembly of thioctic acid (TA) GNPs to improve its stability and application as an antioxidant molecule. It has explained using the hypothesis that collapsed-site defects and pinhole in the SAM were more accessible due to ionic strength and higher assembly of thiotic acid molecules [150]. The assembly of the molecules reduced the electrostatic interaction of molecules which increased the stability of functionalized GNPs by a factor two or more in comparison of GNPs functionalized without salts. This result would improve the backgrounds of reproducible functionalization of GNPs for various uses and could be further enhanced if studies were done to investigate the effect of GNP size, shape and radius on this assembly process.

2.7.3 *Vitis vinifera* a biological reducing agent with an anticancer and an antioxidant property

Vitis vinifera (European grapes) *Vitis labrusca* (North American grapes) and *Vitis rotundifolia* (French hybrid grapes) are the most common types of species available worldwide. The polyphenols of *Vitis vinifera* are phenolic anthocyanins, flavanols, flavonols, stilbenes (resveratrol) (Table 2.2). Flavonoids are the main component and widely present, which principally contain catechins, anepicatechin and procyanidin polymers. The active compound of *Vitis vinifera*, act as an anticancer molecules which is protective for cardiovascular diseases [151]. The kinetic potency of the active component can also reduce the Au salt and help in the stabilization of the GNPs.

The facile synthesis of GNPs from *Vitis vinifera* and its application for cancer has been demonstrated against HBL-100 cells. It showed potential to kill the cancer cell *in vitro*

[152]. Additionally, the functionalization of GNPs with peptides (GSH) and thiol-containing compounds (lipoic acid) showed significant anticancer property for the cancer cell [153]. In a study using epigallocatechin-3-gallate (EGCG), resveratrol (RSV), and fisetin (FS) confirm synthesis and stabilization of GNPs in a single step. The antioxidant and anti-proliferative activity of the nanosystems was confirmed on stable clones of neuroblastoma SH-SY5Y cells (Figure 2.6) [154, 155].

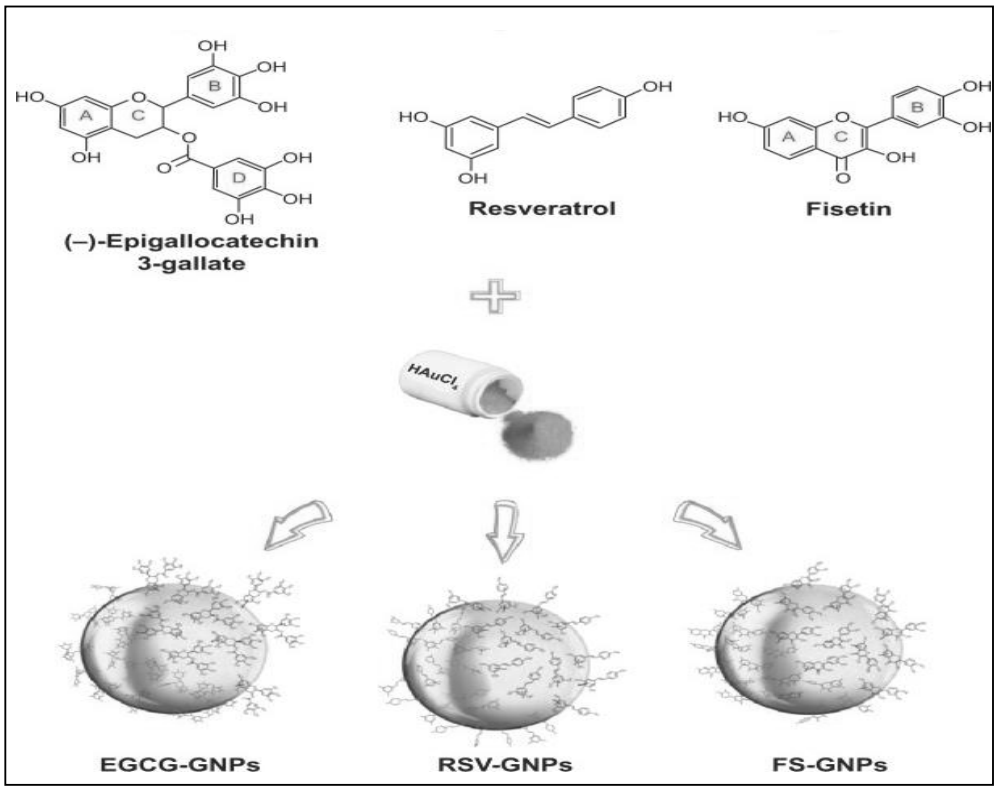

Table 2.1 Major component effect*Vitis vinifera* and its effect cellular behavior

Poly phenols	**Cell lines**	**Effect**	**Reference**
Proanthocyanidins	Mouse mammary carcinoma cell line	Inhibited breast cancer metastasis	[156]
Anthocyanin	Rat liver clone 9 cell line	Induces the antioxidant and activate the upstream of genes	[157]
Procyanidin, Catechin / Gallic acid	Mice spleen cells	Inhibit the H2O2 induced DNA damage	[158]
Catechin	Human breast cancer cell line	30 and 60 μg/mL is the optimum concentration to inhibit the cell proliferation and cell viability	[159]
Flavone	Human colon carcinoma HT-29 cells	54.8 ± 1.3 μmol/L, induced differentiation and apoptosis and decreased the cell proliferation	[160]
Flavonoid	HT-29 cells	Effectively induces apoptosis	[160]
Resveratrol	Prostate cancer cell lines	15 μmol/L or less effective for anti-proliferative effect	[158]

2.8 GNPs for targeted cancer therapy

The targeted therapy is effective if a target molecule or drug reaches the site of action with the minimal loss of activity in blood circulation. In addition to this the molecules should be targeting specific means it should target the tumor cells without affecting surrounding healthy tissue. It can be achieved by delivery of target molecules using nanocarriers, which selectively deliver the ligands molecules at the tumor site either passively or actively. Specificity and bioavailability to target tissue is the disadvantage of the non-targeted therapy, hence, the nanocarriers mediated targeted delivery of therapeutic molecules is required to overcome the disadvantages of the current method.

2.8.1 Enhanced Permeability and Retention (EPR) effect in targeted therapy

EPR is a unique characteristic of solid tumor, which indicates the higher angiogenesis, lymphatic drainage with acidic pH and with more of anaerobic metabolism [54, 161]. The EPR effect of the cancer cell enhanced the passive transport of the drug molecules with or without nanocarrier [162]. The presence of tumor-specific biomolecules and unique tumor microenvironment are an attractive means of targeted therapy through active and passive delivery, which support in transport and homing of the target molecule.

2.8.2 Passive targeting

Passive targeting is targeting of the tumor without using any ligand molecules to release the drug into the cells by exploiting the distinct pathophysiological property of tumor vessels. In addition to this disorganization, porosity and big gap junctions between endothelial cells allows the accumulation of the drugs in the tumor tissues. The passive targeting entirely depends on EPR. The hallmark of tumor micro-vasculatures, which allow the transport of macromolecules of submicron size into the surrounding tumor region

(Figure 2.7) [163]. Encapsulating potency drug inside nanocarrier to release the drug molecules to the target, enabling their use more efficiently patients when this might not be possible directly due to limitation solubility and availability in the in vivo system. Whereas, the passive target is attained by size, surface charge, which enhance the circulation time and also able to carry the targeted drug using the EPR effect of tumor cell [164]. Passive targeting offers a possibility for targeted therapy using the unique feature of the cancer cell, even though, some drawback of the method hinders its application as an effective mode of drug delivery. Because of the heterogeneity and vasculature the passive mode of delivery is not an effective mode of action.

2.8.3 Active targeting

The specific binding to tumor-associated biomarkers through ligand-receptor affinity is known as active targeting. For instance, legends like antibodies, peptides, or small molecules bind to specific receptors or molecular marker express by the cancer cells. The active targeting can overcome the multiple drug resistance (MDR). The nanoparticles can accumulate in the cells, which can the p-glycoproteins an effective protein in the MDR. The receptors that express homogenous and exclusively on cancer cell in higher amount (104-105/cell) can be targeted with peptide ligand for targeted therapy. The liposome-mediated delivery of cytotoxic platinum-based oxaliplatin and nanoparticles formulated cyclodextrin and siRNA were used for receptor-mediated targeting of the transferrin receptor. In addition to this polymeric nanoparticles was used for delivery of docetaxel for prostate-specific membrane antigen (PSMA) mediated cancer therapy. The target specific delivery of ligand moieties can facilitate and improve the more sensitive and effective

cancer detection with minimum concentration and no side or minimum side effect in the normal cell therapy.

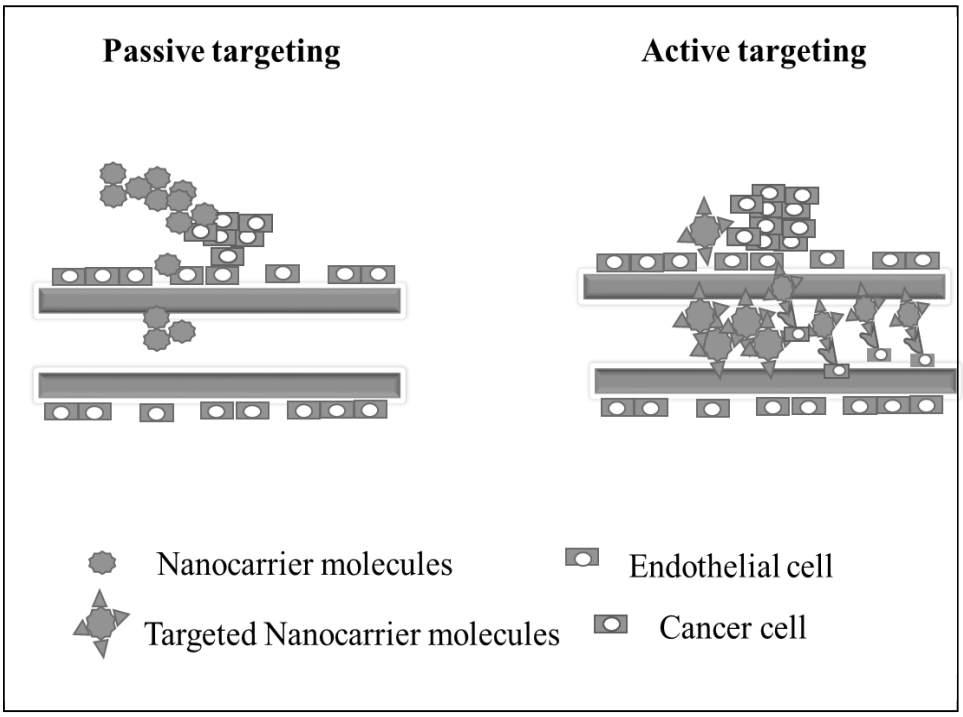

Figure 2.6 Schematic shows the active and passive targeting through nanocarrier.

In the passive targeting the nanocarrier get internalized by utilizing the cancer cell specific property (EPR effect) whereas, in case of the active targeting the nanoparticles are functionalized with target specific therapeutic molecules.

2.9 Functionalization strategies of GNPs for targeted cancer therapy

Multifunctional applications of GNPs are encompassing delivery diagnosis, monitoring and treatment of the disease in the hope of revolutionizing the current cancer treatment modalities [165]. The properties as mentioned earlier of GNPs leads dramatic electromagnetic scattering and absorption, which is useful for cancer theranostic [166].

2.9.1 GNPs functionalization with biomolecules

The bioconjugation is the functionalization of the GNPs with the biologically active molecules to synthesize the novel hybrid materials (Figure 2.8). The functionalization of

GNPs can be can be acquired by covalent binding through thiol molecules through electrostatic interaction by and physical adsorption through surface chemistry [39]. A study indicates that adsorbed of the peptide on inorganic substrate influenced by many factors such as the type of amino acid, the charge of the peptide or biomolecules. It also depends on the surface of the materials, peptide concentration, and stability of the colloidal molecules (Figure 2.8) [53, 167, 168].

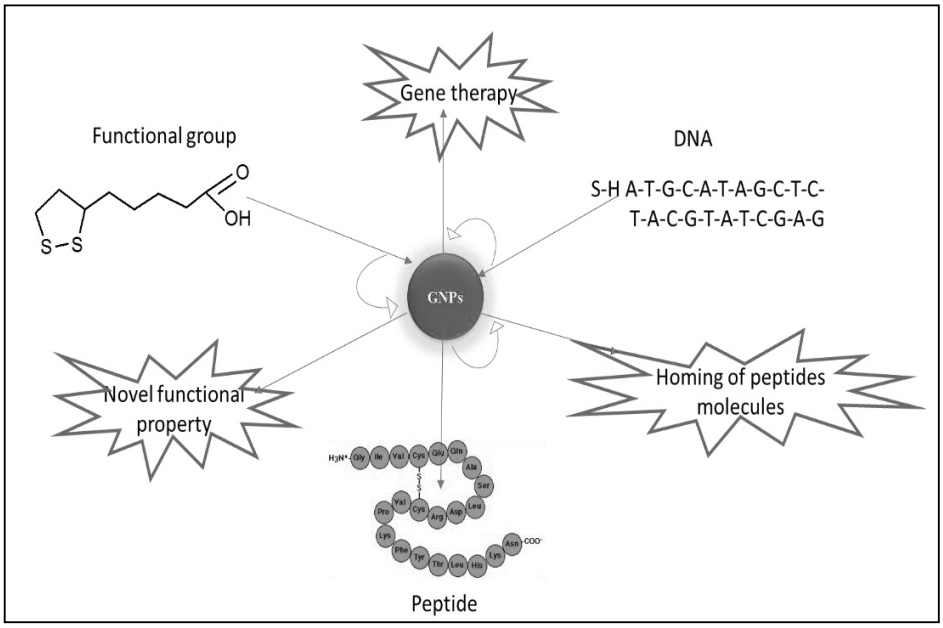

Figure 2.7 Represent the types of biomolecules conjugation with GNPs and its functional property [169].

2.9.2 GNPs, a carrier molecule for tarter therapy (*in vitro* and *in vivo)*

GNPs are a suitable carrier molecule to deliver therapeutic molecules not only due to inherent inert nature, but also due to compatibility in a cellular environment. GNPs functionalized with targeted specific protein, peptides, and nucleic acid can effectively

destroy cancer cells. Owing to the high surface to volume ratio of GNPs it enhances the loading capacity of the target molecules can easily cross cellular membranes owing to its interaction with the protein and lipid molecules present in the cell membrane. The active targeting of pancreatic cancer was achieved demonstrated by GNPs (5 nm) conjugated with cetuximab and gemcitabine. The increased intratumor concentrations of Au (4500 μg g−1) could be possible using cetuximab and gemcitabine targeting compared with untargeted GNPs (600 μg g−1) [170]. The significant tumor growth ~ 80% was observed in an orthotopic pancreatic tumor model *in vivo*. Apart from the drug, an antibody can also use as target molecules using GNPs as carrier molecules [171]. The epidermal growth factor receptor (HER) -2 in breast cancer cell SK-BR-3 was the target with multiple trastuzumab. The internalization of GNP–HER-2 to cytoplasm leads to a 40% reduction in surface HER-2 whereas trastuzumab alone not help in internalization of the receptor. This observation demonstrates that GNPs can influence cellular interactions and enhance therapeutic effects, in addition, to act as a carrier molecule [172]. The mode of injection of GNPs is very important parameter to consider for the effectiveness of the carrier-mediated therapy. The vital parameters, which could influence the efficacy and specificity of GNPs are the mode of administration, the size and shape of GNPs.

The important parameter that need to consider is the mode and dose of admiration. The gold complex Auranofin (trimethyl phosphine (2,3,4,6-tetra-O-acetyl-β-1-D-thiopyranosato-S) gold (I)) and gold sodium thiomalate is not approved for human application because the route of administration not yet optimized [173]. It has been observed that the mode of administration intramuscular and intravenous, intra tumor significantly affect the bioavailability of the therapeutic molecules apart from the

toxicological features of GNPs. The accumulation of the GNPs in the spleen and liver is the major concern which in addition to the mode of the administration [174]. An *in vivo* study was performed on citrate capped GNPs with the different size range from 15-200 nm [175, 176]. The results confirm that irrespective of size, the maximum amount of the gold is found in the liver, lung and spleen. The smallest nanoparticle (15nm) displayed the greatest bio-distribution throughout the mouse with maximum selectivity [177]. These findings confirmed that the application of GNPs as a carrier molecule for targeted therapy needs a significant consideration of many parameters.

2.9.3 GNPs, SERs substrate for multiplexing application in cancer biomarker detection.

The SERs effect was introduced in 1977 using the Ag electrodes [178]. SERs are an optical technique, which shows high sensitivity with no quenching of signal in the presence of laser and more effective for diagnosis in vitro and in vivo compared to fluorescence. Nanoparticles within the range of the 20-300nm show SERs spectra intensity almost 4 fold more compared to the normal range of the Raman scattering in the presence of a suitable substrate. Raman intensity of analysts increases in a closed proximity to a substrate which also varies due to the polarization of light from the nanoparticles. The SERs based multiplexing study was performed to target the anti-EGFR (Epidermal Growth Factor Receptor) and anti-HER2 in cancer cell [179-181]. In a similar kind of study important cancer cell biomarkers, EGFR, CD44, and TGFβRII were targeted using a breast cancer model with biocompatible SERs nanoparticles. The result confirms that until 6h the intensity from antibody was detectable due to nanotage whereas, in the absence of nanotage no signal was noticed [182].

2.10 Application of peptide in targeted cancer therapy

Peptides are a class of macromolecules which showed immense application in the field of cancer therapy. The current data shows that ~ 80 peptides are in the market for the application of different diseases, and total 600 are in different stage of clinical trial [183, 184]. The goserelin, leuprolide, and octreotide are in use for cancer the treatment directly or with other cancer drugs. The direct use of different type of peptides as therapeutic molecules is reached, by various kind mechanisms which control the tumor growth. The therapeutic function of peptide is various for the different class of peptides. Some of the important mechanisms controlled by peptides are angiogenesis, translation control through protein-protein interactions and transcription by gene expression. The antagonist's peptide function by binding to known receptor, whereas, "pro-apoptotic" peptides which induce the apoptosis (programmed cell death) in tumor cell [185].

The angiogenesis initiated by vascular endothelial growth factor (VEGF) by ligand-receptor binding in the cancer cell. The angiogenesis inhibition is a major mechanism of tumor growth inhibition. The proteins involved in the coagulation cascade, immunogenic responses such as chemokines/cytokines, type I thrombospondin proteins and serpins are in clinical use for targeting several diseases. Angiotensin-(1-7) [Ang-(1-7)], is a peptide hormone and a potent inhibitor of proliferation of lung tumor *in vivo* [186]. It reduces VEGF-A expression at the protein and mRNA level in the treated A549 human lung cancer xenograft mice model compared to untreated mouse. This result confirmed that tumor angiogenesis is attenuated by reducing vascular endothelial growth factor-A. Selective inhibition of αv integrins, an important membrane molecule involved in angiogenesis process is inhibited by "cilengitide" a salt of cyclized RGD pentapeptide (cyclo-[Arg-Gly-Asp-DPhe-(NMeVal)]). "Cilengitide" is approved for the treatment of glioblastoma and it

is under clinical trial phase II [187]. Another peptide, ATN-161 (Ac-PHSCN-NH2) inhibits (a51, av3, and av5) integrin involved in tumor progression without inhibiting adhesion which is a main mechanism of integrins inhibition by RGD sequence [188, 189]. Thymus gland normally shows the presence of L-glutamine and L-tryptophan (IM862) inhibit the angiogenesis in the cancer cell, is in advanced stage of cancer trial. It is in phase III trial for AIDS-Kaposi's sarcoma in 24-week (Table 2.3) [190].

Another class of protein molecules which involved in cancer malignancy is G-protein-coupled receptors that can selectively target by the bombesin/gastrin-releasing peptide (BN/GRP). It interferes with the growth stimulatory factor and knock down the EGFR receptor express in cancer cell [191]. The antagonists of the BN/GRP receptor such as RC-3095 (20 μg) or RC-3940-II (10 μg) were used in the breast cancer tumor model as a therapeutic approach (Table 2.4). The protein-protein interface is an important mechanism in DNA synthesis and can be targeted by thymidylate synthase (octapeptides), a homodimer enzyme has an inhibitory effect on drug-resistant cell lines. Similarly, KLAKLAK 2 and involved in apoptosis through mitochondrial membrane disruption [192]. On the other side the long peptides such as ecallantide-60-aa liraglutide -31 aa and icatibant-10 aa in length, contain both natural and non-natural amino acid and "Nutlin 3A" (cis-imidazoline) which inhibit the HDM2-p53 interaction are in clinical trial [46]. Amphiphilic poly (L-phenylalanine) -b-poly (L-serine) (PFS), polypeptides a novel hydrophilic peptide used for the cancer therapy using PFS micelles [193].

Table 2.2 FDA approved peptide during the period 2009-2011 [194, 195]

Generic/Trade name	**Disease /Target**	**Functional properties**
Ecallantide (Kalbitor®)	Hereditary angioedema	Plasma kallikrein inhibitor
Telavancin (Vibativ®)	Skin infection	Antibacterial agent
Romidepsin (Istodax®)	Cutaneous T-cell lymphoma	HDAC Inhibitor
Liraglutide (Victoza®	Type 2 diabetes	GLP-1 receptor agonist
Boceprevir (Victrelis™) Telaprevir (Incivek®	Hepatitis C Virus genotype 1	NS3/4A protease inhibitor
Brentuximab vedotin (Adcetris™)	Hodgkin's lymphoma	CD30 directed
Icatibant (Firazyr®)	Hereditary angioedema	Bradykinin B2 receptor antagonist

Table 2.3 “Important peptides and its application and cancer therapy and diagnosis” [185, 196-198].

Peptide receptors	**Receptor subtypes**	**Type of Tumor**	**Combinatorial therapeutic responsive**
Somatostatin	sst1-sst5	Pituitary adenoma, paraganglioma, nonfunctioning pituitary adenoma, pheochromocytomas	Radioisotopes, AN-201 (a potent cytotoxic radical 2-pyrrolinodoxorubicin), doxorubicin
Pituitary adenylate cyclase activating peptide (PACAP)	PAC1	Pheochromocytomas and Paragangliomas	Radioisotopes and doxorubicin
Vasoactive intestinal peptide (VIP/PACAP)	VPAC1 &VPAC2	Express on all major types of cancer, such as lung colon etc.	Radioisotopes and camptothecin
Cholecystokinin (CCK)	CCK1 (formerly CCK-A) and CCK2	Small cell lung cancers, Medullary Thyroid Carcinomas, Astrocytomas, & Ovarian cancers	Radioisotopes and cisplatin
Bombesin/gastrin-releasing peptide (GRP)	BB1, GRP receptor subtype (BB2), the BB3 and BB4	Renal cell, breast, and prostate carcinomas	Doxorubicin, 2-pyrrolinodoxorubicin

Neurotensin	NTR1, NTR2, NTR3	Small cell lung cancer, neuroblastoma, pancreatic and colonic cancer	Radioisotopes
Substance P	NK1 receptor	Glial tumors	Radioisotopes
Neuropeptide Y	Y1–Y6	Breast Cancer	Radioisotopes
LU-177 Octreotate with amino acid	Somatostatin receptors on cells	Neuroendocrine Cancer, neuroendocrine tumors including carcinoid, islet cell carcinoma of the pancreas, oat cell carcinoma of the lung, pheochromocytoma, gastro-entero-pancreatic neuroendocrine tumors (GEPNETS), and rare thyroid cancers	PRRT (Peptide Receptor Radionuclide Therapy
Multiple epitope peptide vaccine	TK protein kinase (TTK), up-regulated lung cancer 10 (URLC10), insulin-like growth factor–II mRNA binding protein 3 (KOC1), vascular endothelial growth factor receptor 1 (VEGFR1) and 2 (VEGFR2).	Esophageal cancer patients	Chemoradiation therapy (CRT)

2.11 Retinoblastoma (RB)

Cancer is defined as an abnormal cell division, is a major cause of deaths after cardiac failure worldwide. 'International Agency for Research on Cancer (IARC)' reports that more than 70 % of deaths happened due to cancer in developing countries whereas European countries showed a rate of 20%. Pediatric cancer accounts 1% among all types of cancer diagnosed every year, and the most common childhood cancers are Leukemia, Neuroblastomas, Osteosarcomas, and RB. According to "American Cancer Society-2012" RB accounts 3% out of all childhood cancers. The five years survival reports confirmed that the disease is more prevalent in the developing country with less than 50 % survival rate (Figure 2.9).

RB is intraocular malignancy of the retina in children with an incidence of 1/15,000 to 1/20,000 births [199, 200]. It can be bilateral or unilateral depends on whether both eyes and a single eye that can be hereditary or non- hereditary due to a mutation in the RB-1 gene and autosomal dominant gene, respectively. The 40 percentage RB is hereditary/germinal which can transfer to the next generation, whereas 60 percentage is non germinal cannot pass to the next generation[201]. It commonly detected in 2-5 years old child and the functional loss of RB-1 gene involved in initiation and progression of RB [202].

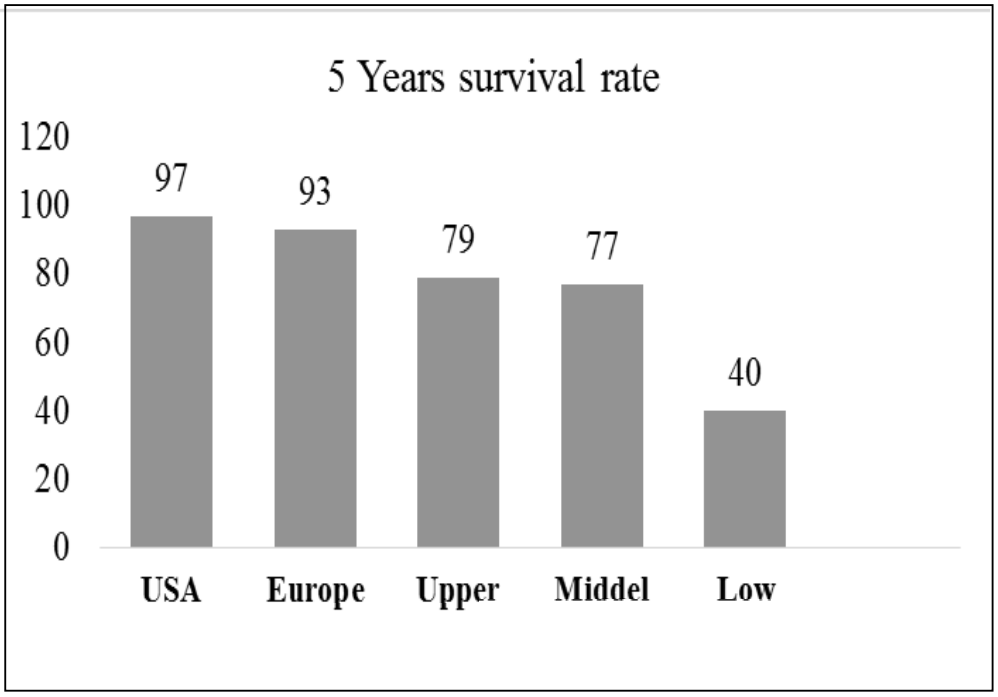

Figure 2.8 Represent the five years survival rate in different part of the world [185]

2.11.1 Clinical symptoms of the RB

RB appears with white, yellow mass or glows with poor vision in one or both eyes. As the tumor grows, it increased pressure in the eye with pain. In the earlier stage, of the disease, it appears as less than 2mm dimensions opthalmoscopically as a subtle, transparent or somewhat translucent lesion in the retina. In the late stage of tumor, it appears as foci of chalk like calcification that resemble cottage cheese and often present with leukocoria, is the most frequent symptoms revealing apart from strabismus (Figure 2.11). This white papillary reflex is a result of reflection of light from the white mass in the retrolental area [204].

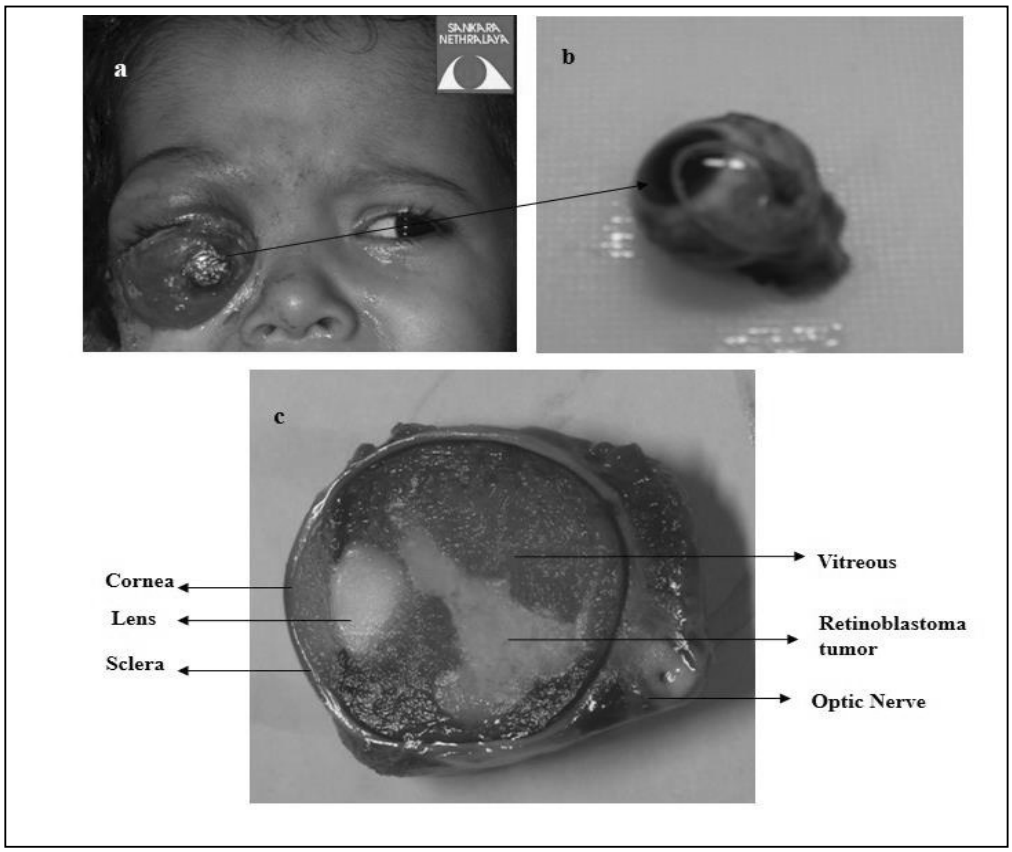

Figure 2.9 Retinoblastoma cancer

RB cancer. Advanced stage RB in the right eye has orbital RB with proptosis, chemosis and surface keratinisation. B) RB tumor, the enucleated globe (b) with large RB filling in the vitreous cavity. (Ocular Pathology Laboratory, Vision Research 3Foundation Sankara Nethralaya Chennai, India).

2.11.2 Genetics of RB

Retinoblastoma occurs due to the mutation in the Retinoblastoma1 (Rb1) gene, which is present on long (q) arm of chromosome 13 (13q14) (Figure 2.11). The Retinoblastoma protein (Rb protein) first discovers tumor suppressor gene apart from the p53. RB can be hereditary and non-hereditary depends on the mutation in the in Rb1. The inherited RB is an autosomal dominant trait, and hereditary RB children have a 1 in 2 chance of carrying a germ line mutation. The tumor protein pRB is encoded by Rb1 gene. It can originate from progenitor cell or nucleated layer of the retina.

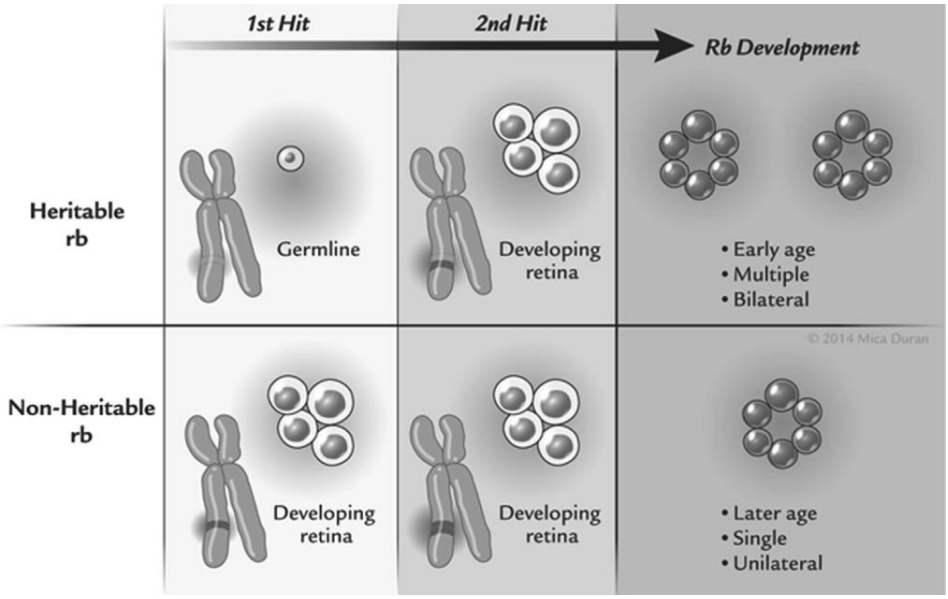

Figure 2.10 Schematic representation of RB inheritance. Heritable RB occur due to mutation in germline or developing retina in early stage of development of eye.

Non-heritable (acquired) occurr due to two mutations and both occur in developing retina usually single and unilateral at a later stage [203].

2.11.3 Role of RB1 and pRb in RB

Rb1 is a regulator of cell growth and prevents cells from uncontrolled proliferation thus inhibiting tumor growth. In a normal functioning cells, the active form of Rb proteins is dephosphorylating which has the role in cell survival, apoptosis and differentiation [205]. pRb interact with the transcription factor E2F1, which is required for the cell to enter into the synthesis (S phase) phase. E2F1 can control the cell cycle progression and it binds to active dephosphorylate form of pRb and stop the cell to enter the synthesis phase [206]. The cell enters into S phase from G1-S checkpoint through an inactive form of pRb [207]. The phosphorylation of pRb inhibits the binding of transcription factor E2F1, which allows the cell to progress. The activation and inactivation of the transcription factor are directed by a cascade of cyclins, which plays an important role in the cell cycle [208, 209].

2.11.4 Classification of RB

The RB has been classified according to the guideline of the RB International Staging Working Group (IRSWG). This report provides the guidelines for the classification of RB based on the enucleated eye. The classification of RB based on the presence or absence of vitreous seeds, invasion to the anterior chamber, choroids and optic nerve. The thickness of the tumor and involvement of other parts of an eye also consider for the classification.

1) If tumor measures < 3mm or more in any dimension, it reaches the inner fibers of the scleral whereas the tumor focus of > 3mm in any diameter and not involve the scare it reaches choroids

2) Differentiation of tumor; well differentiated, moderately differentiated or poorly differentiated

3) The optic nerve invasion includes classification as prelaminar, laminar, post laminar, or tumor at surgical margin

2.11.5 Pathology of RB

The type of cells observed in the RB is the typical shows difference with the stage of the RB. The RB tumor shows different pathological feature compared to the undifferentiated RB cells. A different stage of the RB can be classified by the pathological feature of the tumor cells. The "Homer-Wright rosettes and or Flexner Winterstrin rosettes" is highly specific cells indicates a well differentiated stage of RB [210]. Tumor cells are arranged around a clear central lumen indicates well-differentiated tumor as indicated in the Figure 2.12. The poorly differentiated RB cells arrange around blood vessels which invading the portion of the post laminar optic nerve (Figure 2.12).

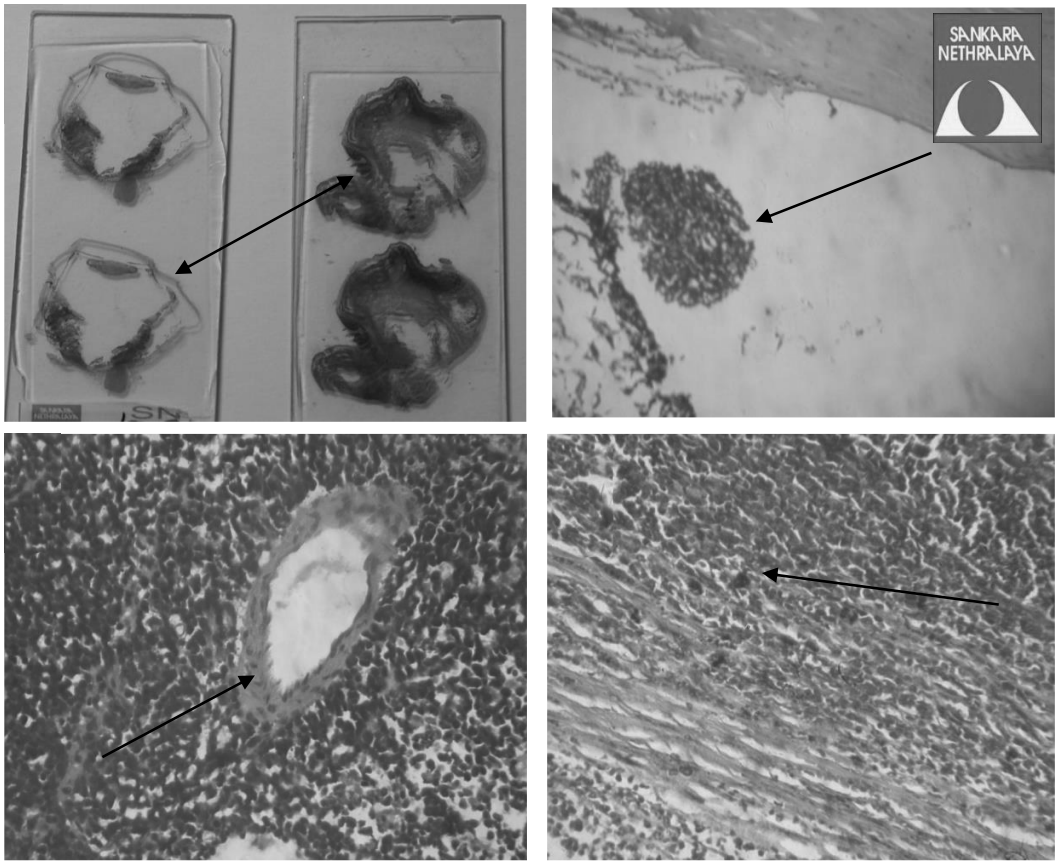

Figure 2.11 Photomicrograph of RB, showing histology section of the enucleated eye ball (a) H & E stain of the cross section of the enucleated eye (b) Thick lobs seen in front of the iris. (c) RB indicates the massive invasion of the choroid (20X). (c) RB cell arrange around the blood vessels. Tumor arises from all layers of retina with choroid invasion at outer margin of scalar (d) (Hematoxylineosin staining and picture were taken at sankarna Nethralaya, India by ocular pathologist).

2.11.6 Treatment modalities for RB

The treatment of the RB depends on the disease such as systemic status, unilateral or bilateral, size and localization. The risk associated for secondary cancers such as stage of tumor, malignant or benign, size, unilateral or bilateral. The treatment aims to cure patients with preservation of vision and also to reduce the long-term side effects of therapy. The current treatment modalities are “surgery, chemotherapy, focal and radiation” therapy

2.11.6.1 Enucliation (Surgery)

In the advanced stage of RB, the entire eye (s) removed surgically. In the advanced stage of disease, where the restoration of vision of the affected eye is, less likely and if the tumor has invaded choroid, optic nerve, and orbit. In case of unilateral enucleation is the preferred method, whereas if both eyes affected then one eye is enucleated to save the other eye. The necessity of enucleation procedure has reduced in number with adjuvant treatment, according to the histological risk factors.

2.11.6.2 External beam radiation therapy (EBRT)

This method involves radiation, using external radiation X-ray dose. The radiosensitive tumor (RB) presented with a diffuse vitreous seeding. This method improves the eye preservation. Since the method has the limitation, that involves the recurrence of the tumor within 1-4 years of treatment [211, 212]. The tumor recurrence depends on the stage and size of the tumor. Since, this method uses the radiation for the treatment there is a chance of the retina, lens, and optic nerve damage. It can also induce secondary cancer in the field of irradiation [213, 214]. It can be external radiation or internal radiation. In case of external radiation, the machine was used for delivery rays from outside the body. Whereas in internal case “needles, seeds, wires, or catheters (tubes)” used to introduce the radiation in the proximity of the tumor site.

2.11.6.3 Chemotherapy

It uses anticancer medicines to kill cancer cells and suppress the growth of the dividing cells. The drug can be administered in different ways, such as systemic, periocular and intra-arterial. In the systemic mode of the drug either injected intravenously or can be

given orally. In the advanced stage of the RB apart from the systemic the chemo drug such as carboplatin injected into the tissue around the eye that can diffuse to the eyeball. A new approach intra-arterial can also use in which the drug such as melphalan, topotecan directly injected into the ophthalmic artery under the anesthesia condition. Chemotherapy is often given to avoid enucleation and external beam radiation and to reduce the formation of second malignancies due to the radiation therapy. The chemo reduction is a protocol to shrink the tumor volume for the purpose of focal treatment procedures like laser, cryotherapy and brachytherapy.

2.11.6.4 Focal therapy

The treatment of the cancer with laser or cryotherapy under anesthesia is the main principal of the focal therapy. If the tumors are very tiny it is difficult to treat with focal therapy and patient may even receive drug continue after chemotherapy for the effective therapy. Advanced stage of RB can invade to other parts such as bone marrow, brain, etc. Therefore, the choice of the treatment includes increasing the number cycles with a high dose of chemo drug may save the patient and increase the life expectancy for few more years.

2.11.6.5 Molecular target for RB

It involves the identification of the molecule, which is expressed in RB, such as Fatty Acid Synthase (FAS) and Nm 23 and EpCAM [215]. The down-regulation of FASR correlates with aggressiveness in many tumors [216, 217]. Nm 23 Metastasis suppressor gene located on chromosome 17q21.3 strong expression of Nm 23 correlates with decreased aggressiveness in many tumors. EpCAM is a cancer stem cell marker, and it up-regulate in many cancers [218]. The EpCAM has been shown over-express in RB, and the

miR17-92 cluster is a potential target RB influence by EpCAM influences in RB [219]. The miR17-92 located in 13q31 locus has been shown a potential regulator of RB progression [220].

Oncogene, such as gene is HDM2, plays an important role in tumorigenesis. HDM2 is regulated by interaction with p53 by interacting with the N-terminal loop of the HDM2 protein domain. The RING finger motif of HDM2 protein has the ubiquitin protein ligase E3 activity, which to degrade the p53. The feedback inhibition between p53-HDM2 is a main mechanism to regulate the expression of this two important proteins at both transcription and translation level. F, W, L, amino acid of the p53 protein involves the binding with the HDM2 domain (Figure 2.13).

Thus, the knockdown of HDM2 with the anti-HDM2 peptide prevented the interaction HDM2 and p53 and enhanced the expression of p53. siRNA [221] against HDM2, silence knock down the HDM2 at mRNA level and induced apoptosis in breast cancer cells by altering the ratio of the Bcl-2/ Bax [222]. Similarly, transducible peptide (Tat-HDM2) is effective in uveal melanoma and RB cancer, which selective inhibition of the HDM2. Tat peptide, derived from conjugating Tat sequence with the anti-HDM2 peptide sequence (QETFSDLWKLLP) which can an effective for delivery of the peptide. The anti-HDM2 peptide inhibits the expression of the Bcl-2 and HDM2 in RB as well as in in vivo rabbit model[43].“MDM2 Inhibitory Peptide (MIP) (PRFWEYWLRLME) 12-mer peptide” bind with MDM2 and MDM4 [223]. He hydrophobic region of MIP from Phe3 to Met11 help in interactions and strong binding between the interfaces of the two molecules. The structural information and hydrophobic nature of the MIP peptide provides a new direction for the design of inhibitors against MDM2:p53 interaction. The molecule

targeting has an added advantage of the cancer due to the specificity, effectively and less side effects [224].

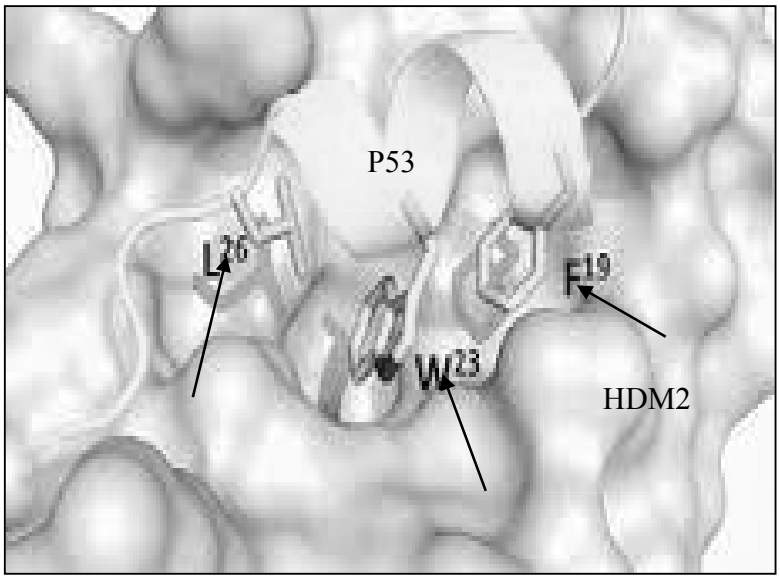

Figure 2.12 p53 inhibits by binding of HDM2 to p53 transactivation domain.

HDM2, the onco-protein HDM2 binds to tumor suppressor protein p53 and inhibits its anticancer activity. The amino acid Phe-19, Leu 26 and Trp 23 bind of p53 protein bind with the HDM2 [225].

2.12 GNPs for phthalmic applicationso

The nano-carrier mediated targeted therapy could be a new strategy for targeted RB therapy [226]. GNPs of ~20 nm cross the "blood-retinal barrier (BRB)" and nontoxic to the retina, which also help to deliver the drug intravenously administered in all layers of retina [227]. A study using mammalian retinal cell line confirmed that GNPs in the range of 67 -70 micromol/0.1 mL is nontoxic [228]. It has been suggested that retinal neovascularization and vascular permeability inhibited by targeting the VEGF-receptors in age-related macular degeneration (MDA) and retinopathy [229, 230]. Nevertheless, the systemic circulation and pharmacokinetics and systemic circulation of also increased to deliver the therapeutic molecules using nano-carrier [15, 231].

2.13 Summary

In this chapter, current applications of GNPs have been discussed with an emphasis on the existing methods of GNPs synthesis and advantage of green nanotechnology. Overall, the review of the literature clearly reveals that there is the lack of understanding of the importance of the reducing in GNPs synthesis. Apart from this the target therapy significance with respect to RB clearly indicate that HDM2 could be the effective molecular marker for RB and nano-carrier based delivery system can be utilized to target the cancer biomarkers. In this context, following chapters will present the findings of current research. It will discuss the synthesis of GNPs using a biological method and its application for the targeted therapy using RB as a tumor model at *in vitro* and *in vivo*. A significance of the FTIR techniques a tool for the diagnosis also highlighted at the end of the dissertation.

CHAPTER 3

3 Experimental

This chapter describes the materials and methods used in the dissertation followed by experimental detail for each experiment. It reports the gold nanoparticles (GNPs) synthesis and functionalization with HDM2 (Human Double Minute 2) and peptide A (Antioxidant peptide). It includes the techniques used for the characterization of GNPs and conjugate. This chapter has four sections, the first section describes the methods of GNPs synthesis and characterization, the second section about the *in vitro* stability and functional analysis. Third and fourth section for *in vivo* xenograft, RB nude mouse model study followed by apoptosis cytokine array analysis and spectroscopic study using xenograft samples.

3.1 Principal and kinetics of GNPs synthesis

The chemical reduction is the frequently used method of GNPs synthesis, the first documentation of the chemical synthesis was reported by Michael Faraday in 1857 [232]. The colloidal GNPs synthesis method was reported for the first time by J. Turkevich *et al.,* in 1951 and further developed by G. Frens in 1970s [91, 233]. The two types of methods were used for the synthesis of GNPs; a biological method (*Vitis vinifera L*. and *Curcuma L*.) and chemical method (Tri-Sodium-Citrate). The nanoparticles size depends on the nucleation and growth phenomenon. The atoms, which are stable at thermal fluctuation without any further dissolution is called nucleation whereas the growth process results in the increase in the size particles from the core nuclei atoms through an addition of atoms. The reaction kinetics and principal of GNPs are described below (Figure 3.1).

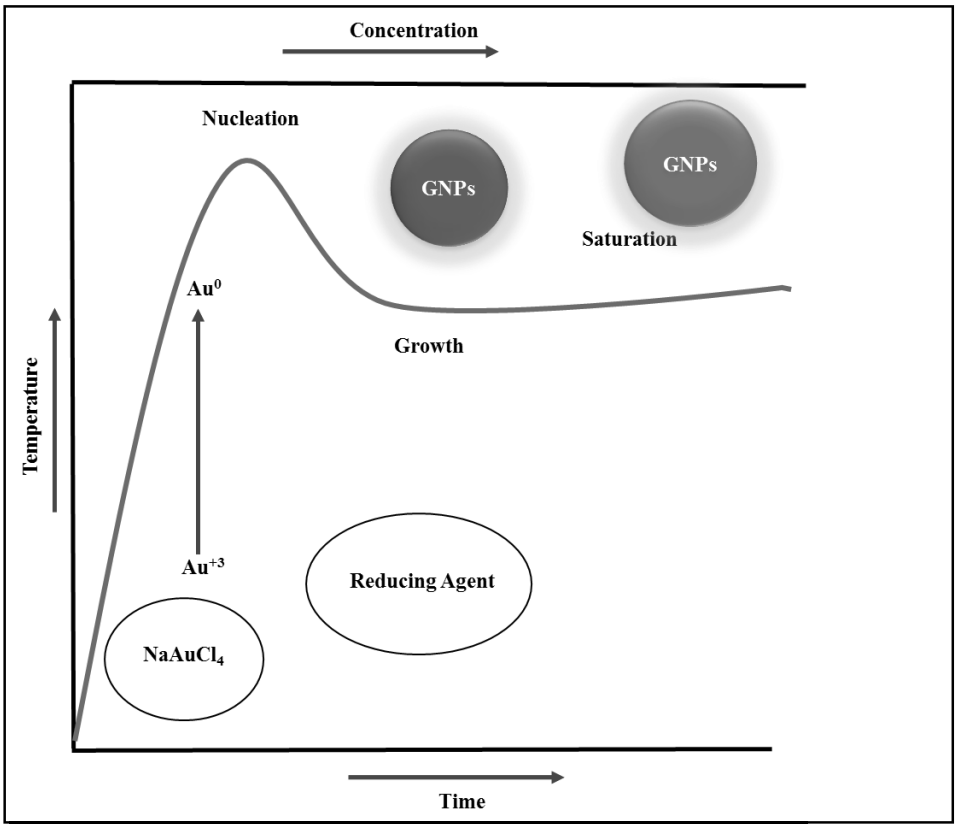

Figure 3.1 Represent reaction kinetics involved in the nanoparticles synthesis

3.1.1 Biological method of GNPs synthesis: $NaAuCl_4$ reduced by *Vitis vinifera L.*

Preparation of *Vitis vinifera* extract

Vitis vinifera was washed using Milli-Q water, and extract was prepared by grinding and centrifugation. The extract was centrifuged at 11,000 rpm for 5-10 minutes, followed by filtration with 0.2µm Millex-CV Syringe filter (MilliporeSLGV033RS). The filtered fresh sterile extract was used for the reduction of the NaAuCl4.

GNPs sysnthesis by *Vitis vinifera*

$NaAuCl_4$ (Sodium tetrachloroaurate (III) dihydrate (sodium;gold(3+);tetrachloride) 99%Sigma Cat.No.298174 . M.W.361.7683). was used for the GNPs synthesis. 18 ml of

deionized water heated till 80 ºC and 36 mg of Acacia Senegal (gum arabic, C26H34N2O13) and 300µl of the *Vitis vinifera extract* was added to a using pipette in a round bottom flask heated with constant stirring for 15minutes. 300µl of 0.1 M NaAuCl4 (36.17 mg/ml) was added to the solution. The observed color change from yellow to red is an indication of the Au salt reduction and change in the atomic state (Au+3) to Au0 (GNPs). The reaction was terminated by fast cooling of the solution on ice. After optimization of the synthesis protocol using *Vitis vinifera L.,* the optimized protocol was used for the synthesis of GNPs using other reducing agents (Figure 3.2).

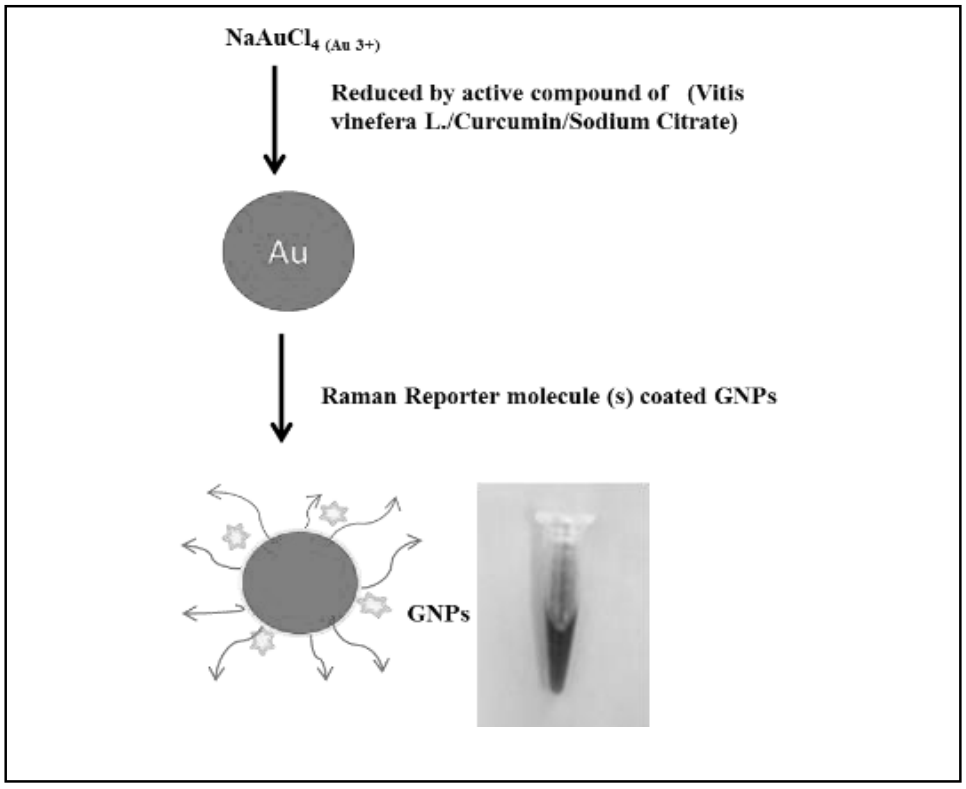

Figure 3.5 Systemic representation of GNPs synthesis

3.1.2 $NaAuCl_4$ reduced by *Curcuma L.*

Preparation of *Curcuma L.* (Curcumin (Diferuloylmethane) solution

The 0.1M curcumin ([HOC6H3 (OCH3) CH=CHCO] 2CH2) (Figure 3.3) solution was prepared by dissolving 18.415 mg curcumin powder (C7727 SIGMA, M.W. 368.38) in 0.5ml of boiling Milli-Q water. Since, curcumin was hydrophobic their dissolution in water was favored by boiling them at high temperatures (90-100°C).

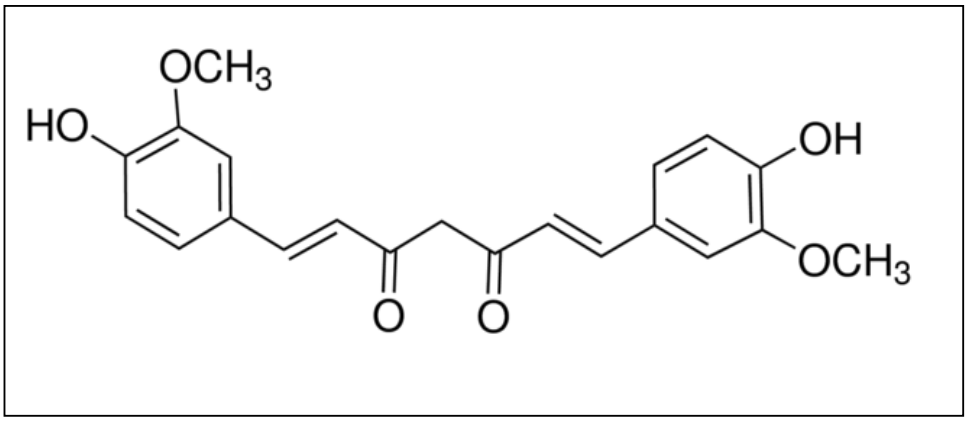

Figure 3.2Chemical structure of curcumin [234]

Procedure of synthesis

100mL of Milli-Q water was taken in boiling flask and was heated to 100°C. At this temperature 33.3mg, gum Arabic was added, followed by the addition of 0.5ml (0.1M) curcumin solution. After 5 Min, 400µL of 0.1M NaAuCl4was added drop-wise under constant stirring. The mixture was continuously stirred for 5-10 min for completion of the reaction and then stop the reaction by cooling in the ice bath. The change in color indicates the reduction of NaAuCl4. The synthesized particles are concentrated by centrifugation at 10,000 rpm for 30min at 25ºC to remove the unreacted reducing agents (Curcumin). The concentrated GNPs were purified and used for characterization and cytotoxic studies.

3.2 Chemical method; $NaAuCl_4$ reduced by Sodium citrate

3.2.1

Preparation of Sodium citrate solution

Sodium citrate solution (Na3C6H5O7) (Figure 3.4),1% (w/v) (3.4mM) was prepared by dissolving 0.99mg Sodium citrate powder (SIGMA,6132-04-3 M.W.294.1) in 1 ml of Milli Q water.

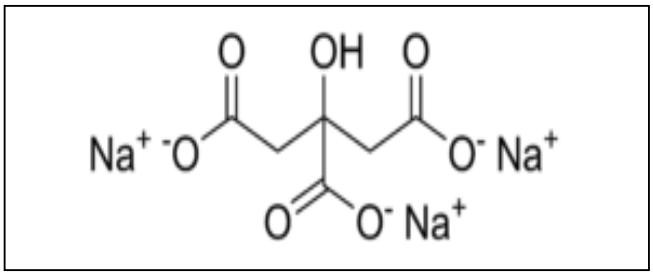

Figure 3.3 Chemical structure of tri-sodium citrate [235]

Procedure of Synthesis

300 ml of Milli-Q water in round-bottom flask was heated up to 100 ºC and 1ml of 0.1M NaAuCl4 was added dropwise with vigorous stirring for 15 minutes followed by addition of 1ml of 1% (w/v) sodium citrate solution. The pale yellow color of the mixture changed into a dark wine red resulted in the completion of the reaction and indication of Au^0 state which interns from the GNPs.

3.3 Physico-chemical characterization of GNPs

3.3.1 UV-vis absorption spectroscopy

The light energy passes through the sample, and its small fraction of energy gets absorbed by the sample molecules which results in a unique pattern of the spectrum, which can be monitored to study their spectrum. Absorbance (A) of light energy at a particular wavelength (λmax) is the spectra of the GNPs. The as-prepared GNPs were characterized

by the UV-Visible spectrophotometer to observe the surface plasmon resonance band (SPR) and blank solvent used was Milli-Q water. The spectra were taken in the scanning range of the 400-800nm using DU 800 Spectrophotometer, Beckman Coulter Inc, CA, USA.

3.3.2 Size and surface potential characterization by Dynamic Light Scattering

In the colloidal state, particles are suspended in a liquid which is due to Brownian motion. The motion of the particles is inversely proportion to the size of the particles. The Dynamic Light Scattering (DLS) measures the intensity fluctuation in the scattered light. Whereas the zeta potential is the measurement of the potential of the samples with the surrounding medium through the electrophoretic mobility of the particles. The zeta potential of the samples determines the stability of the particles in the particular solvent. The zeta potential greater than 30 mV is considered to be highly stable in its solvent [236]. The average hydrodynamic size, size distribution and zeta potential of synthesized GNPs were measured using DLSaaa [237]. The parameters used in the measurements include the viscosity of 0.34 poise, a reflective index of 1.054 and an ambient temperature of 25^0C. A total of three readings was collected, and its average was calculated for each experimental results.

3.3.3 Transmission electron microscopy (TEM) and particle size distribution

A high-resolution electrons (up to 300 kV accelerating voltage) which accelerate at the speed of light passes through the sample are used for the structural analysis of the sample. The electron beam passed through the material results in scattering of electrons, which are captured by electromagnetic lenses into an image. For the TEM study, GNPs were coated on the copper grids (300 mess size) followed by overnight drying.

Subsequently, a voltage of 200 kV was used for the size and shape analysis of GNPs. The size distribution and frequency measured was plotted using origin software (Origin 8).

3.3.4 X-Ray Diffraction

XRD, was performed to identify the crystalline nature and different phases present in the GNPs. The XRD machine (Phillips PW, 1830) was used with 2θ varying from 20° - 60° and the scanning rate of 1 °/min. The XRD was performed at 40 MV current 40 KV voltage and using Cu-Kα radiation (λ =1.5405 Å, 0.15056 nm scan rate 1^0 /min). The acquired data and obtained diffraction patterns were matched to the International Center for Diffraction Data (ICDD).

3.3.5 Fourier Transform Infrared Spectrum (FTIR)

The characteristic functional groups present in the as-prepared GNPs and GNPs - peptide conjugate was studied by FTIR analysis of the samples (Vortex 70, BRUKER). The FTIR analysis not only provide information about the functional moieties of the molecules, but also about its vibrational resonance its chemical interaction with other molecules can be analyzed through peak shift [238]. The FTIR was performed in the range of 500-4000 cm-1. The FTIR in transmittance mode using potassium bromide (Kbr) pellet method.

3.3.6 Matrix Assisted Laser Desorption/Ionization (MALDI)

The mass spectrometry was studied using MALDI (Bruker Daltonics flex Analysis, FLEX-PC autoflexTOF/TOF, MA, USA) in reflector mode (Symprex Technology, Chennai, India) Cyano-4-hydroxycinnamic acid (CHCA) matrix was used for the analysis of GNPs cluster and peptides were coated on the surface of GNP [239, 240]. The solvent was 50% MeCN containing 0.1%TFA in water at 1:1 ratio. The concentration of the sample

was 10-100 pmol/µl, equal volumes (1µl) of HCCA matrix and sample was mixed and 2µl of the mixture was spotted on the MALDI target plate and sample allowed to dry before analysis.

3.3.7 Raman Spectroscopy

Raman spectroscopy utilizes inelastic light scattering associated with the creation and annihilation of a quasi-particle. The Raman Spectra was recorded with the argon ion laser, wave number region of 3000–500 cm-1 at a laser power of 8 mW using an incident light with a wavelength of 512 nm(CRM 200, WITec, Germany with λ = 543 nm).GNPs were drop coated on the glass slide/silicon wafer and scanned for the Raman shift measurement.

3.3.8 Surface Enhanced Raman scattering (SERs)

The SERs effect of the dye-doped GNPs was measured by Raman dyes Rhodamine 6G (R6G). 1 g of GNPs (*Vitis vinifera L.*) was dissolved in 500 µL of Rhodamine 6G (R6G; 20 µm) solution and incubated overnight. The doped GNPs were centrifuged and washed twice with MQ and they were collected in 50 µL MQ water. Aliquots (10 µL) was used for the SERS measurements [241]. The R6G solution was used as a control. The Raman enhancement (RE) was calculated for R6G-doped GNPs with respect to R6G dye only.

3.3.9 *In vitro* stability of GNPs in various biological solutions

The *in vitro* stability of the GNPs in different buffers was studied for ionic strength in different solvent based on their colloidal stability. 1 ml of GNPs was added to 0.5 ml of 0.5% (w/v) cysteine, 0.25% (w/v) histidine, HSA, RPMI+ab, RPMI+FBS+ab, 1X PBS, 1% (w/v) NaCl, respectively followed by incubation for 30 Min at room temperature. The stability and identity were confirmed by UV-Visible spectrophotometer for the stability

analysis. After 15 days of synthesis GNPs were again tested for the mono disparity as well as long term stability. The Plasmon resonance band was measured to confirm the stability of GNPs in all the solutions *in vitro*.

3.4 *In vitro* cell culture

3.4.1 Human Retinoblastoma (RB); Y79 and WERI cells line

Y79 is a RB cell line obtained from Cell Bank, RIKEN Bio Resource Centre (Ibaraki, Japan). RPMI 1640 cell culture media supplemented with 2 "mM L-glutamine, 10 mM HEPES, 1 mM sodium pyruvate, 4.5 g/L glucose, 1.5 g/L bicarbonate" with 10 % (v/v) FBS and 1% antibiotic cocktail (v/v). Cell morphology was in the form of clusters growing as suspension culture.

3.4.2 Human breast cancer; MCF-7 and MDA-MB-453 cells lines

These cells were obtained from National Centre for Cell Science (NCCS), Pune, India. The cells are maintained in DMEM supplemented with 750 µl/dl calf insulin (40 IU/ml) and 10% (v/v) fetal bovine serum. All the cell lines were cultured with the appropriate culture media along with antibiotic-antimycotic solution (Hi Media, Mumbai, India). All the cell lines were maintained at 37°C in a standard cell culture condition in a CO2 incubator.

3.4.3 Human Muller glial; MIO-M1 cell lines

The MIO-M1 cell line was a gift from Dr. G. A. Limb, Institute of Ophthalmology, University of London UK. The cell grows as an adherent cell culture with epithelioid morphology. It is grown in Dulbecco's minimum essential media (DMEM) with 10% FBS (v/v) and 1% (v/v) antibiotic cocktail.

3.4.4 Trypsinization of adherent (MCF-7, MDA-MD 473 and MIO-M1) cells line

A confluent monolayer (~ 90%) of cells were trypsinized with a sterile trypsin solution (0.02% trypsin, 0.5% dextrose and 0.03% EDTA in PBS). The flasks were incubated for 5 min at 37°C with 90% humidity and 10% CO2. After trypsin treatment, the cells get detached from the cell culture flask, which were then removed with culture medium. The cells were then maintained for further passages and were used in experiments.

3.5 *In vitro* quantification of metabolically active cells (MTT assay)

The cytotoxicity of the nanoparticles were assessed using a tetrazolium salt, 3-(4,5-dimethylthiazol-2-yl) -2,5-diphenyltetrazolium bromide (MTT). The cytotoxicity study with MTT was reported for the first time by Mosmann in 1983 [242]. The primary enzyme is succinate dehydrogenase from the mitochondria that, react with the tetrazolium ring of MTT*[243]*. The reaction product after breaking the MTT tetrazolium ring form the dark blue formazan crystals. The crystal was solubilized with an organic solvent DMSO, and the optical density was measured by spectrophotometer. This is a colorimetric assay that measures the mitochondrial enzyme activity. Since, MTT reduced by the metabolically active cells, therefore, the activity is the proposal with the viability of the cells.

3.5.1 Cytotoxicity evaluation of GNPs by MTT assay

Breast cancer (MDA-MB 453, MCF) and Retinoblastoma (RB; Y79, WERI) non-cancer (MIO-M1) cells were used for the cell cytotoxicity study of the GNPs synthesized by Vitis vinifera, Curcumin and Tri Trisodium Citrate. Approximately, 5x103 cells/well Y79 and WERI were seeded in 96-well polystyrene plate coated with poly-L-lysine whereas, MDA-MB-453, MCF, and MIO-M1 seeded without coated plate. The cells were treated with 10, 25, 50 and 100µM of GNPs for 6, 12 and 24 hours. After the treatment,

the cells were removed and washed with 1% PBS, following to this 10 µl MTT solution /100 µl media were added to each well and incubated till purple formazan crystal formed. The MTT solution was removed followed by the addition of 100 µl DMSO to each well to dissolve the crystals. The optical density (OD) was measured at 570 nm (BioTek, ELISA, USA). The percentage cell viability was calculated with respect to control, according to formula:

Cell Viability = (Sample OD/Control OD) x 100

3.6 Functionalization of GNPs with peptide

The antioxidant peptides Pep-A: Pro-His-Cys-Lys-Arg-Met (PHCKRM) and Pep-B: Thr-Arg-Asn-Tyr-Tyr-Val-Arg-Ala-Val-Leu (TRNYYVRAVL) were procured from AnaSpec, Bi Biotech India Pvt Ltd, New Delhi. The thiotic acid modified Pep-A were custom synthesized by Custom Peptide Synthesis, USV Limited India (CPS 1514-1) with >95% HPLC purified form.

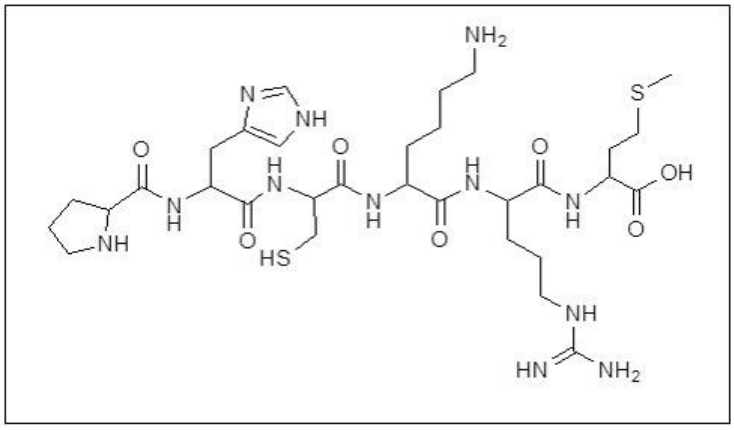

Figure 3.4Chemical structure of Peptide -A

3.6.1 Cellular toxicity of Peptide-A and Peptide-B

The cellular toxicity of the peptide-A and peptide-B was analyzed by MTT assay (Section 3.5). The exponentially growing Y79 retinoblastoma and MIOM1 cells were used

for the toxicity measurements. The Trypan blue exclusion test was used for cell viability, and Haemocytometer was used to count the cells. 5x103 cells/well was seeded in a Poly-L-lysine coated 96 well polystyrene plate and incubated at 37^0C overnight. The cells were treated with varying concentration 10, 30, 60 and 100 μM of peptide-A (Pep-A) and peptide-B (Pep-B), in a fresh medium and was incubated for specific time periods (6, 24 & 48h). After, incubation time intervals the MTT protocol follows as mentioned in section 3.5.

3.6.2 Preparation of GNPs-Pep-A conjugate

The filtered GNPs (synthesized from *Vitis vinifera L.*) were used to prepare the conjugate (GNPs-Pep-A), and the conjugation method was adopted from previously published protocol [244]. The thiotic acid (TA) modified peptide conjugate with GNPs in different ratios of peptide for example GNPs-Pep-A1 (18 ml GNPs 1.7 mg) and GNPs-Pep-A2 (18 ml GNPs:4.3 mg). The conjugates were prepared using 18 ml of GNPs ((OD520 nm = 1.00), (2.32 x 10-9, Molar particles/L, (242 x 10-6, Moles of gold /L) mixed with 4.3 mg of Pep-A dissolved in 1 ml of water and stirred overnight. A similar protocol was followed for the other conjugate preparation, and the synthesized conjugate was subjected to purification. GNPs-Pep-A was centrifuged at 15,000 rpm for 30 minutes. The unbound peptide was removed by washing with MQ followed by centrifugation. The thiotic acid (TA) is a sulfur-containing antioxidant linker molecule that binds with GNPs to form Au-S bond between peptide and GNPs [245]. The GNPs-Pep-A was pelleted, and the supernatant was measured for the presence of the peptide by reading the absorption at 280 nm. The final concentration of GNPs-Pep-A was 50μM, which was used for the in vitro studies. The conjugate (GNPs-Pep-A) concentration was measured using the GNPs

concentration. The GNPs-Pep-A was then characterized using UV-Visible, DLS, MALDI and FTIR spectroscopy as described in section 3.3 to confirm the functionalization of GNPs with peptide.

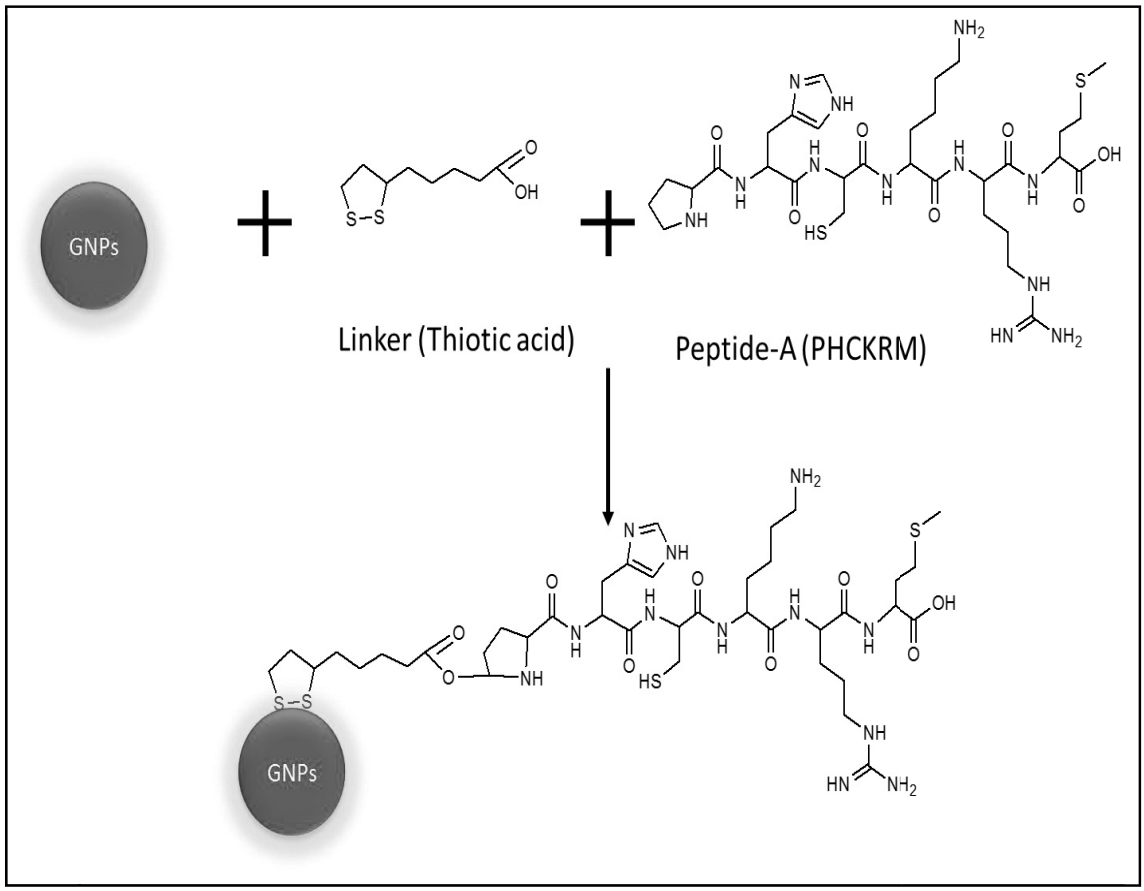

Figure 3.5 Schematic presentation of chemical reaction for functionalization of GNPs with thiotic acid modified Peptide-A

3.6.3 Uptake and internalization by Fluorescent Activated Cell Sorter (FACS) and fluorescence microscopic analysis (Peptide-A, GNPs and GNPs-Pep-A)

For studying the localization and internalization of the peptide by fluorescence microscopy, Y79 cells were seeded on the lysine (0.01mg/ml) coated glass slide. The cells were cultured overnight and treated with 50 and 100μM concentration of FITC tagged Pep-A. The microscopy internalization of GNPs and GNPs-Pep-A were carried by doped GNPs with the R6G dye as describe in section 3.3.8. The doping was carried out as per the protocol published previously [246]. The internalization of the peptide, R6G doped GNPs and GNPs-Pep-A after 4h was qualitatively detected by Zeiss LSM, 710 Laser Microscope by Axio Vision (Germany). The flow cytometric analysis (FACS) was performed using Y79 cells. Cells were seeded at 2 x 105 cells/well in six-well plates and treated with different concentrations (50 and 100μM) of Pep-A for 4h. The cells were then spun at 1,500 rpm for 5 min and then resuspended in FACS buffer (PBS with 10% v/v FBS and 1% sodium azide). The cells were then analyzed for uptake of the peptide on a FACS Calibur (BD Biosciences, CA, USA) using the CELL QUEST PRO software. The fluorescence of FITC positive cells was recorded at excitation/emission at 488/530 nm. The FITC positive cells were a measure for the peptide uptake by the cells and fluorescence intensity was measured as a function of concentration dependent uptake of the peptide.

3.6.4 *In-vitro* stability study of GNPs-Pep-A

The stability of GNPs-Pep-A conjugates were tested in a variety of different ionic strength solvents and buffers using previously reported method [244]. 1 ml of GNPs-PepA1 and GNPs (as a reference material) was mixed with 0.5 ml (10mM) each of Dithiothreitol (DTT), cysteine, histidine, and NaCl. The solution was incubated for 2h at RT and the

stability of the conjugate was determined using UV-Vis spectrophotometer (DU 800 Spectrophotometer, Beckman Coulter Inc, CA, USA).

3.6.5 Measurement of intracellular Reactive Oxygen Species (ROS) levels in peptide-A&B, GNPs and GNPs-Pep-A treated cells by Dichlorodihydrofluorescein (DCF) assay

The ROS species activity measured within a cell by a fluorogenic probe 2', 7'-Dichlorodihydrofluorescin diacetate (DCFH-DA) which is permeable to the cells. Cellular esterases deacetylated the DCFH-DA to nonfluorescent 2', 7'-Dichlorodihydrofluorescin (DCFH), which is quickly oxidized to fluorescent 2', 7'-Dichlorodihydrofluorescein (DCF) by cellular ROS. The fluorescence intensity of DCF is proportional to measure of the ROS level within the cell cytosol. The ROS level in unknown samples was determined by DCF standard calibration curve. DCF stock (1 mM) was diluted with culture media and concentration range is 0, 0.01, 0.1, 1, 10, 100,1000, 10,000 nM was prepared. 100 µl of the diluted standards were used, and fluorescence was measured at 480/530 nm, excitation/transmittance.

The intracellular ROS levels were measured using an OxiSelect ROS Assay Kit (Cell Biolabs, Inc, CA, USA) and the protocol follows according to the procedure provided in the kit. Y79, a RB cells were seeded at 7 x 103 cells/well in 96-well plates and culture overnight. The cells were washed thrice with sterile 1X PBS and treated with 100 µl of 1X DCFH-DA (2', 7'-Dichlorodihydrofluorescin diacetate) for 1hat 37°C. The solution was removed, and 1XPBS was used to wash the cells. The cells were treated with 10, 50 and 100µM of Pep-A and Pep-B for 24h. The reaction was terminated by adding 100µl of cell lysis buffer and mixed thoroughly for proper cell lysis and incubated for 5min. For the measurement of ROS inhibition with GNPs and GNPs-Pep-A1 and GNPs-Pep-A2, 50µm

of each treatment was added and incubations for 24h and similar procedure were repeated for the ROS analysis as described for the Pep-A& Pep-B. The fluorescence was read with a Spectra Max, M4 multi-detection microplate reader (Molecular Devices, CA, USA) at 480nm excitation/530nm emission. The ROS levels in cell lysates were then calculated using the DCF standard curve.

3.6.6 SOD activity measurement of peptide A & B, GNPs and GNPs-Pep-A

Superoxide dismutase (SOD), is an anti-oxidative enzyme that catalyzes the superoxide anion into H2O2 and O2. SOD enzymes are categorized based on its activity in the cell. The three main SOD is Cytosolic Cu/Zn-SOD, mitochondrial Mn-SOD, and extracellular Ec-SOD of™ Superoxide Dismutase kit that uses a xanthine/xanthine oxidase (XOD) to generate superoxide anions and produce the chromagen, a water-soluble formazan dye by the reduction with superoxide anions. The SOD activity was determined as the inhibition of chromagen reduction.[247, 248].

Y79 cells were seeded at $2X10^5$ cells/well in a 12 well cell culture plates with 1000 µl of cell culture media and was incubated at 37°C overnight. The cells were treated with Pep-A Pep-B (10, 50 and 100 µM) GNPs and GNPs-Pep-A (50 µM) in a fresh cell culture medium and incubated for 6h followed by washing using ice cold PBS followed by cell lysis using buffer containing, 0.1M Tris/HCl, pH 7.4 containing 0.5 % Triton X-100, 5mM β-Mercaptoethanol, 0.1mg/ml PMSF. The cell lysates were subjected to centrifugation at 14000 x g for 5 minutes at 4°C. The SOD activity from the cytosol and mitochondria was measured in the supernatant using the superoxide dismutase (SOD) activity assay kit, (BioVision, CA, USA, Sigma-Aldrich, MO, USA) according to the protocol described in the kit. Briefly, the cell lysate, buffer, enzyme and the WST reagent were diluted and was

added as per the protocol and incubated at 37ºC for 20min and read at 450nm in a microplate reader (Biotek, VT, USA). SOD activity was then calculated as a percentage of inhibition activity of xanthine oxidase using the formula;

"SOD Activity of sample (inhibition %) = (OD control-OD sample) / (OD Control) x 100"

3.6.7 Quantitative gene expression (qRT-PCR) study of GNPs and GNPs-Pep-A

Quantitative Reverse Transcription Polymerase Chain Reaction (QRT-PCR) is a used to generate many copies of a DNA sequence in real exponential phase of amplification. The working principal of qRT-PCR is to convert RNA into complementary DNA (cDNA) with the enzyme reverse transcriptase, and the resulting cDNA is amplified using gene specific primer in real-time quantitative PCR. It is recorded the fluorescence of reporter molecule, i.e. SYBRR Green. The gene of interest (GOI) to amplify by qRT PCR involved RNA isolation, cDNA synthesis form mRNA and real-time gene amplification using a set of specific primer for the GOI.

3.6.7.1 RNA extraction by Trizol method

Cells were collected after the completion of treatment of reaction time and cells were centrifuged at 10,000 rpm for 5-10 minutes. The cell pellet was mixed with the TRI reagent (Sigma, T9424) with slight vortex and was incubated at RT for 5 min. Subsequently, cells were incubated for 15 minutes with 500 µl of chloroform ($CHCl_3$) and subjected for centrifuge at 12,000 rpm for 15 min. The aqueous layer that has RNA was collected and transferred to a new vial and mixed with 500 µl isopropanol. The cells were centrifuged at 12,000 rpm for 10 min, and the supernatant was discarded and the pellet was air dried with 75% alcohol at room temperature for 2 min and was re-suspended in 20 µl diethyl pyrocarbonate (DEPC) treated water. 5 µl of the total RNA extracted was then run

on a 2% agarose gel for the qualitative analysis, and nanodrop was used for the quantification of total RNA.

3.6.7.2 cDNA conversion from total RNA

cDNA synthesis was prepared by the total RNA. The high capacity cDNA (AB-4368814) reverse transcription kit was used for the conversion of mRNA to cDNA. The master mix was prepared according to the kit protocol.

Table 3.1 cDNA conversion from total RNA master mix

Master mix 2X RT (20 µl)	
Reaction component	Volume (µl)
10X buffer	2.0
10X dNTP (Mix) 100mM	0.8
10X Reverse Transcriptase Random Primer	2.0
MultiScribe™ Reverse Transcriptase	1.0
RNase Inhibitor	1.0
Nucleae –free H20	3.2
Total RNA	10.0
Total Reaction volume	**20.0**

Table 3.2 Thermal cycling for semi-quantitative PCR

(cDNA conversion)	
Temperature	**Time (Minute)**
25°C	10 .00
37°C	120 .00
85°C	5 .0
4°C	∞

3.6.7.3 Real-time quantification of CAT, SOD, GPX gene

The effect of GNPs and GNPs-Pep-A on mRNA expression were studied using antioxidant genes [superoxide dismutase (SOD), glutathione peroxidase (GPX) and catalase (CAT)] in retinoblastoma cells (Y79) were seeded ~ 1x106 cells/well on a 6 well plate and treated with GNPs and GNPs-Pep-A for 24h. After incubation of cells, the total RNA was isolated using Trizol method (section 3.6.6.1), and concentration of RNA was quantified using a Nanodrop (Biospec-Nano, Shimadzu, Japan). The total RNA was converted into cDNA using an Applied Biosystem kit (High-Capacity cDNA Transcription Kit, USA). Quantification of GOI expression was performed in a triplicate in a 20µl reaction mixture containing 0.1 µg of cDNA, specific primers (CAT, SOD, GPX) and SYBR green reagent in 96-well plates on a real-time PCR system (7500, Applied Biosystems,). GAPDH and β actin were used as internal controls, and the fluorescence of SYBR Green was measured. The relative quantitation of GOI was calculated using the ΔCT method. The relative amount of gene-specific cDNA to housekeeping gene was calculated using $2^{-\Delta\Delta Ct}$. Ct denotes the cycle's threshold, infer that at this stage of cycle GOI reached a threshold that determined by SDS software version 1.3. Protocol.

Table 3.3 qRT-PCR, reaction component for quantitative gene expression study

Master Mix	
Component	**Volume (µl)**
2X buffer	5.0
Forward primer	0.5
Reverse primer	0.5
DEPC	3.0
cDNA (100ng)	1.0
Total Reaction volume	**10.0**

Table 3.4 Thermal cycling for qRT-PCR

Real-time gene expression	
Temperature (°C)	**Time (Minute)**
95	5.00
95	30.00
63	1.00(45 cycles)
72	1.00

Table 3.5 Primer sequence for functional study of GNPs-Pep-A by qRT-PCR

Primer sequence		
Gene name	**Forward primer(F) 5'-3'**	**Reverse primer (R) 5'-3'**
Catalase (CAT)	TCTGGAGAAGTGCGGAGATT	AGTCAGGGTGGACCTCAGTG
Superoxide dismutase (SOD1)	GATGAAGAGAGGCATGTTGGAGAC	GTCTTTGTACTTTCTTCATTTCCACC
Glutathione peroxidase (GPX)	GCACCCTCTCTTCGCCTTC	TCAGGCTCGATGTCAATGGTC
Glyceraldehyde-3-phosphate dehydrogenase (GAPDH)	GCCAAGGTCATCCATGACAAC	GTCCACCACCCTGTTGCTGTA

3.8 HDM2 expression study in human Retinoblastoma tumor samples

The proposed study was reviewed and was approved by the ethics committee of Sankara Nethralaya - Chennai, India. The study approval no. is 383-2013-P. The general principal of research which follows the good laboratory practice (GLP) was used to conduct the study. The RB samples were collected from the SN hospital. During the treatment the

affected eye was enucleated and the consent was obtained from the patient attendant to use the sample for the research purpose.

3.8.1 Collection of RB tumor samples

RB tumors were freshly collected by the Ocular Pathologist from the enucleated eyeballs. The samples were snap frozen in at -80°C and stored until use. The samples were thawed on ice and subjected to RNA and protein extraction. For the immunohistochemical studies, the tumor tissue sections were sourced between the years 2009 to 2013. Fresh RB tumor tissues were collected, fixed in formalin before analyzing for immune histochemistry (IHC) and gene expression studies. Donor retina tissue was obtained from the CU Shah eye bank, Sankara Nethralaya India.

3.8.2 HDM2 expression study in RB tumor sample

Approximately 100 mg of RB tumor tissue was homogenized with 1 ml of Trizol in diethyl pyrocarbonate (DEPC) treated glass tissue homogenizer. The cells were then processed further as per the RNA extraction protocol, describe earlier (section 3.6.6.1). For protein extraction the RB tumour tissues were homogenised using RIPA buffer and the homogenate was then processed in the lysate preparation and proteins were estimated using BSA standard.

3.8.2.1 mRNA and protein extraction from Retinoblastoma (RB) samples

Approximately 250 mg of RB fresh tumor tissues were homogenized in a homogenizer and RNA was isolated by TRizole reagent. The cDNA conversion and the qRT-PCR performed for the HDM2 as described in the section.

Table 3.6 Real time gene expression, primer sequence for HDM2 expression in tumor sample

Gene name	Forward primer(F) 5'-3'	Reverse primer (R) 5'-3'
HDM2	CGGAAAGATGGAGCAAGAA	GGGAGGTGGTTACAGCAAC
P53	GTCCCAAGACAATGGATGATTTG	CTGGGAAGGGACAGAAGATGAC
GAPDH	AACAGCGACACCCATCCTC	CATACCAGGAAATGAGCTTGACAA

3.8.2.2 Western blot study for HDM2 protein expression analysis

Electrophoresis is a technique to study the protein expression in the tissue sample using approximately 250 mg of tissue (retinoblastoma fresh tumor) which was homogenized, the homogenate tissue sample was then sonicated at 10 cycles for 10 sec each a with lysis buffer on an ice cold conditions. Protein was estimated using the Bradford's method. The assay was run along with a set of standards using bovine serum albumin (BSA), ranging from 50 to 200 µg. The absorbance was recorded at 570 nm using spectrophotometer.

Acrylamide (10-12 %) separating gel was prepared and allowed to solidify. Following to this 4% stacking gel was poured over the separating gel by removing the butanol layer and the wells were introduced by comb. 50 µg of tumor lysate containing proteins were mixed with 3X sample loading buffer and was boiled at 100^0C for 3-5 min. Then the sample was loaded on the gel and was run till the dye reaches the bottom of the gel at 120 V. The gel was then removed carefully from the glass-assembled plates.

3.8.2.4 Electro-blotting

The electrophoresed gel was wet transferred onto the nitrocellulose membrane for 1 h under 100 V using transfer apparatus (Bio-Rad). The blot was stained with 0.5%

Ponceau stain to ensure the transfer is completed and visualizes protein bands and then washed with distilled water. The transferred membrane was blocked with 5% skimmed milk for 1h. Primary antibodiesHDM2 (1:2000) and anti-β actin monoclonal antibody (Sigma A 1978) in 1: 2000 at 4°C for overnight. The blots were washed three times with TBST buffer 30 min each using a rocker. The secondary antibody, HRP-conjugated secondary antibody (sc-2005) at 1:10,000 dilution and blot incubate for 1-2h at RT and followed by washing thrice with TBST buffer for 10 min each time and was finally washed with 1XPBS buffer. The presence of HDM2 and βactin proteins were detected by Pierce western blot detection reagents by chemiluminescence (Thermo Fisher Scientific Inc., IL, USA).

3.8.3 Immunohistochemistry detection of HDM2 in xenograft RB tumor sample

The paraffin wax embedded tumor sections (7-10μM) was taken with a microtome. The anti- MDM2 (Cat no. Santacruz sc-965 and antibody (1:100 dilution) was used to HDM2 protein detection. The secondary, anti-mouse/rabbit IgG-Poly-HRP was (NovoLink Max Polymer detection) used as per the protocol mentioned in the kit. The slide was analyzed by Ocular Pathologist and based on staining intensity was intense (+), dull (±) and negative (-). The number of positive cells was classified on the basis presence of HDM2 positive cells -33 %, negative, 34-67 % dull and 68-100% positive.

3.9 Functionalization of GNPs with HDM2 peptide and *In vitro* functional study in RB cell line

HDM2 peptide (QETFSDLWKLLP) a 12–amino acid peptide derived from the p53 sequence that mediates binding to HDM2 were selected and evaluated for targeting HDM2 oncoprotein [249]. The peptide was customized from Sigma-Aldrich Japan (OE-14045-

001) with >95% HPLC purged, 50% hydrophobicity. The N-terminal of the peptide was modified with 3-mercaptopropionic acid [250].

3.9.1 Functionalization of GNPs with HDM2 peptide (V-GNPs-HDM2 and C-GNPs-HDM2)

The GNPs-peptide conjugates were prepared by mixing varying concentration of 3-mpa (mercaptopropionic acid) modified anti-HDM2 peptide with purified GNPs. Initially, three different ratios of GNPs with peptide were prepared by mixing 50 μM of GNPs with different concentration of the peptide with 50, 100 and 150 μM of the peptide. V-GNPs (Vitis vinifera reduced GNPs) and C-GNPs (tri-sodium citrate reduced GNPs) were used for the synthesis of the GNPs-HDM2 conjugate. The conjugate was prepared by mixing18 ml of GNPs (242 x 10-6, moles of a gold / liter, O.D, 1.0) with 4.2mg of peptide (dissolve in 0.01 cell culture grade DMSO) on continuous stirring for 24h. After 24h of continuous stirring, the conjugate was purified by ultra-centrifugation at 15,000 -30,000 rpm till a clear supernatant was obtained, and the pellet was washed with DI water twice. The unbound peptide was removed by washing through centrifugation, and the pellet was collected after re-suspending the water/cell culture medium. The mPEG-thiol stabilized GNPs were prepared by mixing18 ml of GNPs with 1 mg of MPEG-SH-1000. The solution was stirred for 12h followed by removal of unreacted PEG by washing through centrifugation. The PEG stabilized GNPs were mixed with 4.2 mg of HDM2 peptide followed mixing for 24h. The final conjugates were subjected for washing and re-suspended in a distilled water. The optical density (OD) was measured at 520nm and the final concentration of GNPs was calculated in GNPs-HDM2.The conjugates were characterized by the UV-Visible, FTIR, DLS and TEM.

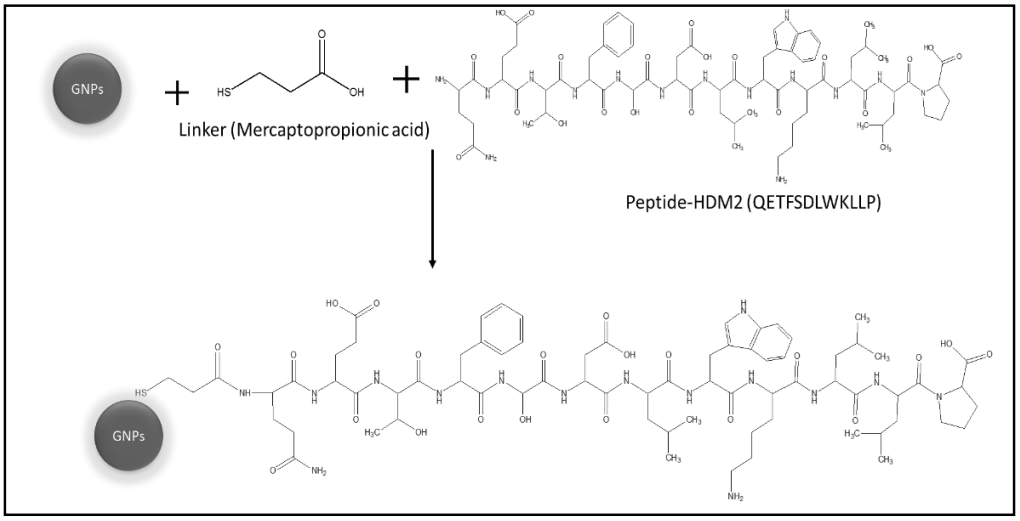

Figure 3.6 Schematic presentation of HDM2 peptide functionalized GNPs

3.9.2 Internalization of GNPs and GNPs-HDM2

3.9.2.1 Transmission Electron Microscopy (TEM)

The internalization study was performed using Y79 cells in vitro. The exponentially grown Y79 cells (Section 3.4.1), of density 1x106, were cultured in 6 well plate and after 12 h of culture, cells were treated and incubated with 50µm/well with the GNPs and GNPs-HDM2 for 24h. After incubation, the cells were washed thrice with PBS and the resultant cell pellets were then washed and fixed in a primary fixative, which is 2.5% glutaraldehyde prepared using 0.1M sodium cacodylate buffer at pH 7.2-7.4.

3.9.2.2 Processing of sample for TEM analysis

The cells fixed in a primary fixative were washed with 0.1M sodium cacodylate buffer thrice for every 10 mins followed, by which the cells were fixed in a secondary fixative for 2h at 8 0C using 0.1% Osmium tetroxide (OsO4) prepared in 0.1M sodium cacodylate buffer. The excess fixative was removed by washing the cells thrice for every 10 mins and was dehydrated with a series of acetone from 30%, 50%, 70%, 80%, 90%

(v/v) for10 minutes in each concentration and with 100% acetone it was washed twice for 10 minutes followed by propylene oxide treatment twice for every ten minutes. The cells were then infiltrated with the resin mixture and acetone, where the resin mixture consisted of Epon 812 resin, DDSA (Dodecenyl Succinic Anhydride) and NMA (Nadic® Methyl anhydride) starting with 25%, 50% and 75% for 2 hours in each concentration and then finally with 100% resin twice for overnight and finally in the resin mixture with added catalyst (DMP 30) in "easy molds" at 60°C for 48 hours.

3.9.2.3 Sectioning and Imaging

The resin blocks were removed from the mold, trimmed and sectioned using Leica Ultra cut R ultramicrotome with diamond or glass knives. The semi-thin sections were cut and stained with toluidine blue and screened using the light microscope to check for area of interest followed by ultrathin sections, collected on a copper grid with 300 mess size and stained with saturated solutions of uranyl acetate followed by lead citrate. The samples were air dried and was screened in JEOL JEM 1400. TEM was operated at an accelerating voltage of 80 kV. The micrographs were taken with the Olympus Keep view CCD Camera attached to the microscope. The TEM performed at the Cancer Institute, India.

3.9.3 HDM2 knockdown study in Y79 cells treated with GNPs and GNPs-HDM2

HDM2 knockdown in Y79 cells treated with GNPs and GNPs-HDM2. The cells were used for the treatment of different time 12, 24 and 36 h with C-GNPs and C-GNPs-HDM2, V-GNPs, V-GNPs-HDM2 form RNA and protein expression study. The exponentially growing cells were seeded at 10□ 105 cells/well in a 6 well plate and treated with final concentration of 50μM of each sample after the 24h of treatment completion cells were processed for total RNA (TRizol method) and protein isolated. After

optimization of the time point with gene expression (functional study), all experiments were performed with 24h of treatment time point. The protocol follows as mentioned in the section 3.7.2.

3.9.4 Apoptosis study in GNPs and GNPs-HDM2 treated cells by Annexin V-Propidium Iodide (PI) staning

Apoptosis is a cell death process, which can be identified by the change that occurs at the cell membrane. One of the change occur in plasma membrane phosphatidylserine (PS) which expressed on the outer surface of apoptotic cell from the inner part of the plasma membrane to the outer layer, by which PS becomes exposed at the external surface of the cell [251, 252]. The analysis of Phosphatidylserine on the outer side of the apoptotic cell membrane was performed using Annexin V- and PI for the differentiation of necrosis of apoptotic cells. Whereas, PI dye binds to the nucleic acid of dead cells and is excluded from the living or apoptotic cells. Thus, the combination of annexin V and PI enables to distinguish apoptotic and dead cells.

A cell apoptosis dye, Annexin V-FITC (Apoptosis Detection Kit I, Brand, BD Pharmingen™, Cat. No. 556547) was used for the apoptosis, cell labeling and identification using flow cytometry (FACSCanto II flow cytometer, BD Biosciences, USA). ~10 × 105, Y79 cells were seeded in a 6 well plate after overnight incubation the culture, cells were treated with a 50µM concentration of C-GNPs and C-GNPs-HDM2, V-GNPs, V-GNPs-HDM2 for24h. After the treatment period, cells were collected followed by washing and centrifugation in a cold 1xPBS. The cells were diluted in the 1×annexin-binding buffer to make the cell density equal to ~10 × 105cells/mL. 5 µL of Alexa Fluor 488 annexin-V in 100 µL of cell suspension was incubated for 15 minutes. Subsequently, 1 µL of PI

(propidium iodide) were added and incubated for 5 minutes. After incubation, the cell suspension was mixed with 300 µL 1×annexin-binding buffer and was kept on ice. This was followed by the analysis of the stained cells by the flow cytometer, involving the measurement of fluorescence emission at 530 nm and 617 nm using a 488 nm excitation laser. For this, flow cytometry tubes (Cat. No. 352054, BD Falcon, USA) was prepared with each containing 300 ml of stained cell suspension in 1×annexin-binding buffer at a final cell concentration of ~ 1 × 106 cells/ml and 10,000 events were recorded for each sample. The experiment was performed in triplicate.

3.9.5 Cell cycle analysis in GNPs and GNPs-HDM2 treated cells

A mammalian cell has four different stages, G1, S, G2 and M, known as the cell cycle. Four distinct phases could be recognized in various phases of the cell cycle: the G1-, S- (DNA synthesis phase), G2- and M-phase (division). However, G2- and M-phase, which both have identical DNA content could not be discriminated based on their differences in DNA content. FACS study of cell cycle based on the singlet was used for calculating the percentages of cells occupying the different phases of the cell cycle. A cell cycle analysis was performed using Propidium Iodide (PI) staining to study the effect of the material in a different stage of the cell. PI is the fluorescent nucleic acid dye, which can identify the cells, which are at different stages of cell cycle [253, 254].

Y79 cells of density ~10 x 105 were seeded in a 6 well plate after overnight incubated culture cells was treated with a 50µM concentration of C-GNPs and C-GNPs-HDM2, V-GNPs, V-GNPs-HDM2 for 24h. Following to this cell were harvested and washed in cold 1xPBS. After the washing, cells were fixed in 1ml cold 70% (v/v) ethanol to ensure fixation of all cells and minimizes the clumping of the cell pellet with slow vortex.

Cells were fixed on ice for 30 minutes, and the cells were washed twice with ice cold1XPBS. Subsequently, cells were incubated with PI (556463, BD Biosciences), and Ribonuclease-A (Sigma, R6513). The cell pellet was treated with Ribonuclease-A to remove the RNA. Followed by 10µl of Ribonuclease-A (10µg/µl) was added to the cell pellet and 50µl of PI (50µg/µl) was added into 300µl of cell suspension. Before FACS analysis, cells were incubated for 3h at 370C and analyzes the samples in PI/RNase-A solution.

3.10 *In vivo* therapeutic efficacy study of GNPs-HDM2 treated RB xenograft mice model

The *in vivo* study was performed as per the regulations of the Committee for the Purpose of Control and Supervision of Experiments on Animals (CPCSEA) facility under the Government of India and followed the Association for Assessment and Accreditation of Laboratory Animal Care (AAALAC) guideline. The experimental protocol was reviewed for carrying out animal experimentation and was approved by Institutional Animal Ethics Committee (IAEC Protocol Approval No: SYNGENE/IAEC/430/10-2013).The experiment was performed with the second safety level under in a laminar flow hood following sterile condition.

Table 3.7 Animal detail and experimental condition to induce Retinoblastoma xenograft in nude mice model

Animal details	
Source	Harlan, Netherlands
Strain	Hsd: Athymic Nude-Foxn1^{nu}
Sex	Female
Age at the start of experiment	5-6 weeks
Body Weight of animals	18-22g
No. of animals/group	n= 7
Cancer cell line	Y79 (Retinoblastoma)
Cell concentration	1 x 10^7 cells/animal
Xenograft induction	Subcutaneous cell injection

3.10.1 Animal maintenance

Animals were maintained in standard condition with 50 (20 % humidity, 22 (3°C temperature, with light/dark cycle of 12 hours each with certified irradiated laboratory rodent diet. The drinking water was RO purified and autoclave provided *ad libitum* via bottle fitted with nozzle during the study period.

3.10.2 Animal selection

The animals were selected for the study was acclimatized for a period of 5 days, and a thorough physical examination was performed before study initiated. The health, animal was selected and labeled individually with details like date of tumor implantation and, randomization, tumor type, mouse strain, gender. After randomization, the animal was grouped in 3 different treatment categories, which include vehicle control, GNPs-1-HDM2 and GNPs-2-HDM2 group.

3.10.3 RB tumor induction

Human RB cells (Y79) with a viability of >90 % were chosen for the study. Ideally 10 X 10^6 Y79 cells were re-suspended in 200 µl of serum free media containing 50% of matrigel kept in ice. Nude mice (Hsd: Athymic Nude-Foxn1^{nu}) housed in Individually Ventilated Cages (IVCs) was injected with Y79 retinoblastoma cell subcutaneously in the flanks or back of theanimalsand implanted area was monitored for tumor growth [255]. Once the tumor attained palpable size, the animals were randomized based on tumor volume (TV≈80mm^3) and the treatment was started.

3.10.4 Tumor growth inhibition study in GNPs-HDM2 treated RB xenograft mice

24 mice were divided into 3 groups with 10 in vehicle control and 7-7 in each treatment group. The first group was used as a vehicle control and the other two groups, was used for treatment with C-GNPs-HDM2 and V-GNPs-HDM2. The group one was treated with 100µl of sterile water, whereas the second and third group were treated with 5µg/100µl/animal of V-GNPs-HDM2 and C-GNPs-HDM2 till 24 days. The treatment was injected in two-cycle, the first cycle was from 0 till 16 days with a daily dose of 5µg/100µl/animal and the second cycle was started after 17th till 24th day and the treatment dosage was repeated twice a day.

3.10.5 Apoptosis array study for analysis of apoptotic protein involve in RB tumor growth reduction

Apoptosis-related proteins profiling was performed to understand the effect of the therapeutic molecules on the apoptotic and signaling pathways. The “Human Apoptosis Array”(Cat.No.ARY009,R&D) is a fast, sensitive and economical method to detect the relative levels of expression of 35 apoptotic pathways related protein.

The RB xenograft tumor from treated (V-GNPs-HDM2 and C-GNPs-HDM2) and an untreated group was used for the apoptosis array analysis. 400 µg tumor lysates was used for the analysis of apoptosis. The protocol was followed according to kit instruction. 2.0 mL of array buffer was added into each well to block the membrane followed by 1h incubation on a rocking platform shaker. 250 µl/array (400µg) tumor lysate from each sample were added, and the array was incubated at 2-8 °C overnight in bark on a rocking shaker. After incubation, the array was washed thrice with 20 mL of1X wash buffer for every 10 minutes on a rocking shaker and 15 µL of reconstituted antibody cocktail to 1.5 mL with 1X array buffer 2/3 were added. The excess wash buffer was allowed to drain from the array. The array was placed in 4 well plate and incubated for 1h with an antibody cocktail using rocking shaker followed by washing. The Streptavidin-HRP was prepared by diluting in 1X using, array buffer 2/3, and pipette 2.0 mL on each array followed for 30 minutes incubation and washing. The array was placed on the plastic and pipette 1 mL of "Chemi Reagent" and evenly spread on each membrane and incubate for 1 minute and was detected by Chemi Doc. The analysis was confirmed using Image J software.

3.10.6 Cytokines array study for analysis role of cytokines in tumor growth reduction in RB xenograft model

Cytokines and chemokines are extracellular signaling molecules and can change their expression in a disease condition. It can be released out from the cells and have an important role in cellular growth, differentiation, gene expression, migration, immunity and inflammation. Most of the immunological responses were regulated by the network of cytokine. The "Mouse Cytokine Array (Cat.No.ARY006, R&D) was used for the expression profiling of cytokines in the RB nude mice xenograft model serum sample.

The RB (xenograft animal) serum treated (V-GNPs-HDM2 and C-GNPs-HDM2) and untreated (control) group was used and the protocol was followed according to kit instruction. Briefly, 2.0 mL of array buffer-6 was added into each array and then blocking buffer was incubated for 1h on a rocking platform shaker. 1 ml (300µg) of serum sample mixed with 0.5 mL of array buffer 4 was adjusted to a final volume of 1.5 mL with array buffer 6. Following to this 15 µL of reconstituted "mouse cytokine array panel A detection antibody cocktail" was added to the array and incubated for 1h. After 1h blocking the sample/antibody mixtures was added to each array and was incubated overnight at 2-8 °C on a rocking shaker. After incubation, each array was washed with 20 mL of 1X wash buffer for 10 minutes on a rocking platform shaker and was repeated 6 times. Streptavidin-HRP conjugated antibody was diluted in array buffer 6 and 2.0 mL of diluted streptavidin-HRP was added into each array and incubated for 30 minutes at RT on a rocking shaker followed by washing using wash buffer. The 1 ml of Chemi Reagent was added on each array and spread evenly with 1 minute incubation at RT.

3.10.7 Xenograft RB tumor tissue preparation for FTIR analysis

Tumor specimens were obtained from 3 mice, including one without any treatment which was used as a control, and the other two mice having their tumor treated with GNPs-1 and GNPs-2 as a test, respectively. Fresh tumor samples were snap frozen in a liquid nitrogen immediately after tumor excision without fixatives and anti-freeze media. For each type of RB tumor sample, two 7 m-thick tissue sections were obtained from a cryostat and transferred onto a glass slide for histopathological assessment after hematoxylin and eosin staining, and onto an IR-transparent calcium fluoride (CaF_2) circular window (0.5 mm thickness by 13 mm diameter, Crystan Ltd, Dorset, UK) for FTIR imaging

measurement, respectively. All tissue sections were dried in a dry cabinet before FTIR spectral data collection.

3.10.8 Focal Plane Array (FPA) FTIR microspectroscopic imaging

The FTIR study of the ex-vivo RB xenograft tumor samples was performed to identify the difference between the samples. FPA-FTIR microspectroscopic images were recorded using a Cary 620 FTIR microscope using cooled liquid-N2 environment with 128 ×128 element FPA detector objective lens, 15× (0.62 NA) attached with FTIR spectrometer (Cary 670 FTIR spectrometer, Agilent Technologies at School of Chemistry, Centre for bio-spectroscopy, Monash University, VIC, Australia). The FTIR Spectra were collected in a transmission mode in the spectral range between 3800-900 cm-1. A single FTIR image was acquired in an area of 700 × 700 cm^2. A single FTIR spectral image contain the array of 64 × 64 spectra obtained from binning of the signal captured on detectors from each square of 4 on FPA array consist of 128 × 128 element. A resultant a single spectrum of sample collected in FTIR image acquired on ca. 10.9 × 10.9 m^2 revealed the molecular information about the sample functional group. From each tumor sample 5 FTIR spectral images were obtained with a resolution of 4-cm^{-1} with 128 co-added scans, Blackman-Harris 3-Term apodization, Power-Spectrum phase correction and a zero-filling factor of 2 using Resolutions Pro software package (Agilent Technologies)". Before each sample measurement, background measurements were performed using a clean surface of the substrate with the same acquisition parameters [256].

CHAPTER 4

4 Synthesis, characterization and biocompatibility evaluation of self-therapeutic Surface-Enhanced Raman-scattered (SERs) active gold nanoparticles (GNPs)

This chapter discusses the first specific objective of the dissertation on the synthesis of GNPs using biological and chemical methods. The in vitro cellular compatibility of GNPs/has been studied using human breast cancer, retinoblastoma and non-cancer in order to study the application as synthesized GNPs for cancer therapy. The SERs dye doping has been used to show the potential application of the as-synthesize GNPs as a Surface Enhanced Raman (SERs) substrate.

4.1 Background

The use of naturally occurring biomolecules for reduction of Au salt agent is the growing field of research which can bridge the gap between green chemistry and nanotechnology. The green chemistry based method of GNPs synthesis has an advantage over the chemical method of synthesis of nanoparticles to decrease or remove the use of substances toxic to the human health as well as environment [130, 257]. The appropriate choice of the reducing agent, capping agent and solvent used in the GNPs synthesis process can reduce the toxic effect of metallic nanoparticles [258]. The use of natural occurring plant extracts and its derivatives could be an attractive ecofriendly alternative method for the synthesis of nanoparticles. The GNPs have been synthesized using phytochemicals from *Terminalia chebula, Breynia rhamnoides*, *Memecylon edule* leaf extract, *Cinnamomum zeylanicum*, *Macrotyloma uniflorum*. These reports indicate that phytochemicals could be an active compound for the reduction of the Au salts [259, 260]. The sub cellular organelle, chloroplasts also used for the GNPs [241]. These biologically

derived GNPs have high impact in the field of biomedical especially cancer theranostic. Antioxidant and anticancer molecules are present in the seeds, fruit, rhizomes and stem of the various part of the plant have been existed in use for instance curcumin, an active component of the turmeric and *Vitis viniferea*. Among nanomaterial, metal nanoparticles have an added advantage due to their Surface Plasmon Resonance (SPR) and the SERs properties [261, 262]. The application of GNPs in cancer theranostic is more promising when compared to other metal nanoparticles because of such as biocompatibility and controllable size, shape, surface charge.

GNPs are good substrate for the Raman enhancement and GNPs with SERs signatures are used extensively for imaging and diagnosis due to high sensitivity and stability compared to fluorescent based imaging [263]. The introduction of noble metal substrates leads to enhanced Raman intensities by as much as 10^{14}-10^{15} times compared to the weak Raman signal exhibited inherently by the molecules [264]. Several advantages of SERs include high spectral specificity, improved contrast, long term stability and availability of large pallets of reporter molecules for multiplexing capabilities [265-267]. The SERs active GNPS are useful for bio labeling, bioassay, clinical diagnosis and therapy. The promising properties of GNPs and emerging nanotechnology enabled the target specific efficient use of GNPs as a nanocarrier in biomedical applications [268].

However, synthesis of green method based SERs active GNPs is a need of an hour for biocompatible material synthesis. The most common method to obtain the SERs encoded nanoparticles involves conjugation of the Raman active dye on the surface of nanoparticles and further encoded with the polymers molecules or biomolecules to retain the functionality of the dye molecules [269, 270]. Since, the synthesis process reported

earlier involved has complicated processes involving multiple steps, there is a need for rapid synthesis of gold nanoparticles with SERs signature instead of using synthetic chemicals for stabilization of metallic nanoparticles as reported earlier, here we used phytochemicals from fruits of *Vitis vinifera L*. and Curcuma L. (Curcumin) to reduce $NaAucl_4$ for the synthesis of SERs active GNPs. GNPs synthesized with different reducing agent of anticancer and antioxidant property as a new ecofriendly platform to synthesize the novel self-therapeutics GNPs to obtain multi-functionality such as biocompatibility, and SERs substrate, etc.

4.2 Materials and Methods

The methodology used for the experiment performed in this chapter has been explained and discussed in detail in Chapter 3. A brief outline of the experiments performed has been mentioned in the Figure.4.2.

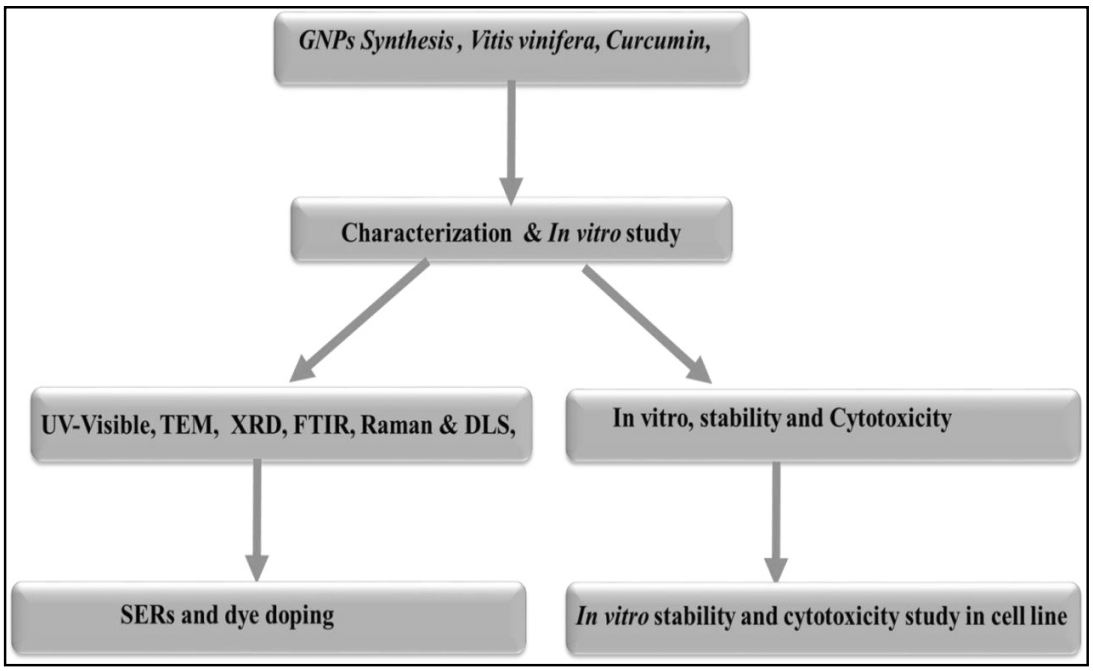

Figure 4.1 The schematic representation of the experimental plan for the synthesis and characterization of GNPs

4. 3 Results

4.3.1 Synthesis of GNPs using *Vitis Vinifera* L. and *Curcuma* L.

The GNPs synthesis reaction is presented in equation 1&2. In brief, the synthesis involved the heating of the $NaAuCl_4$, reducing agent and stabilizing at boiling temperature. The aqueous solution of $NaAuCl_4$ upon heating dissociate into ionic from $Au\ (III)Cl^{-}3$. The following reaction represents a typical reaction for GNPs synthesis.

$$NaAuCl4 \xrightarrow{\triangle\ (80\text{-}100°C)} Au\ (III)\ Cl_3^{-} + Nacl \quad \text{----------(1)}$$

The $Au\ (III)Cl_3^{-}$ react with the reducing agent to form GNPs presented by the following reaction.

$$Au\ (III)Cl_3^{-} \xrightarrow[\text{Reducing agent}]{} Au^0 \quad \text{----------(2)}$$

The synthesis involved the addition of the preheated gum arabic and *Vitis vinefera* L.and curcumin 80°C to $NaAuCl_4$, followed by rapid cooling on ice to stop the reaction (Figure 4.2). In case of curcumin GNPs, curcumin was used for the reduction of $NaAuCl_4$. The long term stabilization of the GNPs was attained by the addition of the gumarabic, therefore, gum arabic was used as a stabilizer to avoid aggregation of GNPs. It is a highly branched polysaccharide structure containing arabinogalactan and glycoproteins. The glycoprotein coating is known to reduce the toxicity of the metal nanoparticles [271]. The glycoprotein is a plant derived green component, provides an additional advantage as a stabilizing agent. The glycoproteins can function as a biochemical active multifunctional GNPs with controllable uniform size and shape [272].

Metallic nanoparticles, particularly GNPs coated stabilized with natural polysaccharides are covalently linked to the gold cluster and have found important applications in MRI. Moreover, in biological system, carbohydrate protein interactions, which are ubiquitous therefore presence natural polysaccharides on GNPs as a coating inhibit the aggregation of the GNPs but it also help in the interaction/binding of the peptide or other molecules with GNPs. Multiple interactions between carbohydrates and protein systems have a unique application in ligand-receptor-mediated delivery of the specific molecules [273]. The *Vitis vinifera* L. The extract could reduce $NaAuCl_4$ salt and produce GNPs, but the long term stability required the stabilization the GNPs.

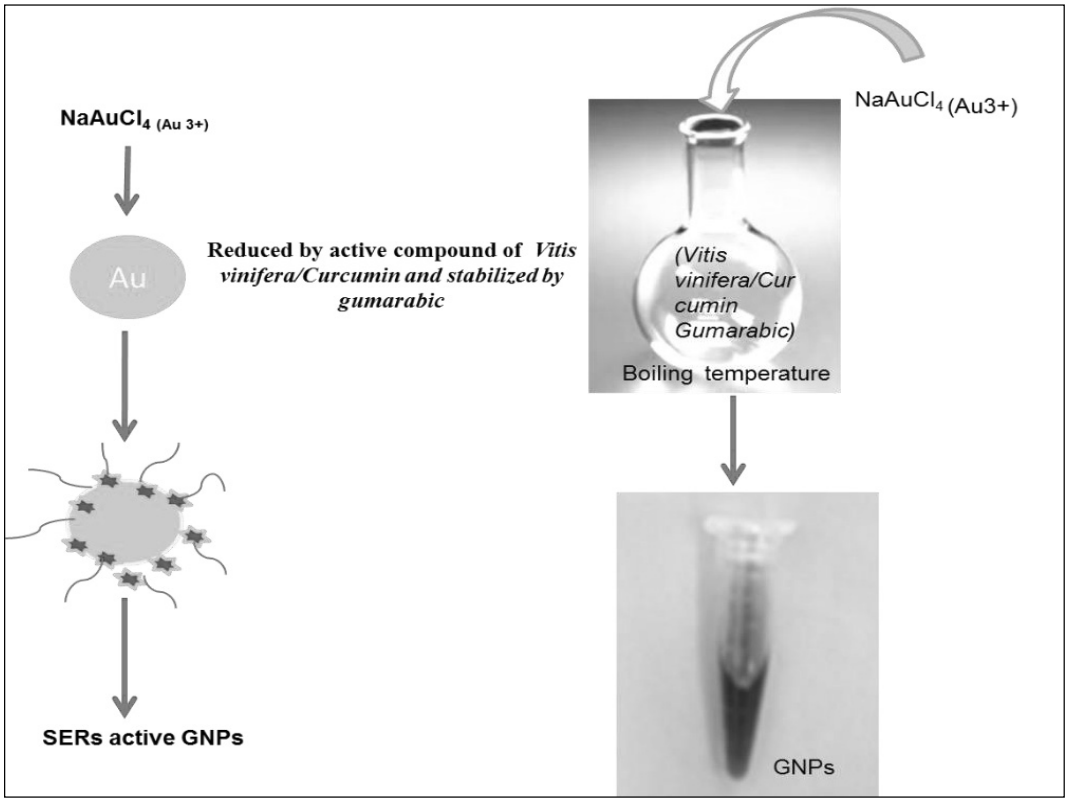

Figure 4 2 A schematic process for GNPs synthesis using *Vitis vinifera L.*and *curcumin L.* , reducing agent

Table 4.1 Important aparameters which have a critical role in the GNPs synthesis

Size of GNPs (Mean ± SD)	**NaAucl4 (0.1mM)**	**PDI**	**Zeta Potential (mV)**	**Temperature (°C)**	**Time (minutes)**	***Vitis Vinifera* Extract (µl)**	**Gum arabic (mg)**	**Reaction Volume (ml)**
14±1	100µl	0.422	-32	80	1-2	600	72	36
28±2	600 µl	0.625	-24	80	2-3	600	72	36
61±2	600 µl	0.411	-22	45	2-5	600	72	36

4.4.1 Characterization of GNPs synthesized by *Vitis vinifera L.*

4.4.1.1 Uv-Visible spectroscopy and DLS

GNPs were characterized using UV-visible spectroscopy (Figure 4.4). GNPs with a diameter of 14±1 nm shows the maximum absorption at 528 nm. This absorption indicates the size of the GNPs as homogeneous isotropic spheres [274]. Furthermore, the λ maximum of the SPR band can also predict the size of the GNPs [275]. The absorption of the maxima (SPR band) of the GNPs depends on the size of the gold nanoparticles. Whereas, the absorption intensity depends on the concentration of the GNPs of the same size. The λ max at wavelength 520-540 attributed the spherical size of GNPs. According to Mie theory, the red shifts in SPR is because of dielectric properties of the medium of the GNP or due to the specific adsorption of materials on the surface of the GNPs. The SPR band at 528nm, (Figure 4.4a) is indicative of spherical particles less than 20 nm diameter. The λ maximum (SPR band) of 28±2 nm and 61±2 nm showed a red shift at 530 nm and 541 nm respectively, (Figure 4.4c and e) with respect to 14±1nm (Figure 4.4a). A similar red shift of the bigger nanoparticles was observed with different sizes of GNPs [276]. Consistent with the prediction of particle size of SPR analysis, the average size measured by the Dynamic Light Scattering (DLS) number distribution is 14±1nm (Mean±SD)

(Figure 4.4b). The size analysis of DLS technique measures is based on random motion (Brownian motion) of particles in suspending fluid. DLS the size measurement is calculated by "Stokes-Einstein (Furth 1956) theory of Brownian motion" in a coherent light source [277]. The Stokes–Einstein relation is described in Equation 3.

$$D0 = kBT / 3\pi\eta d \text{----------(3)}$$

kB------- Boltzmann constant, T --------Temperature in Kelvin, η --------solvent viscosity at T, D0----- "Particle's translational diffusion coefficient at zero solution concentration".

Whereas, the monodispersity of GNPs is express by autocorrelation function g1 (τ) is express as per the following equation (4) (Figure 4.3).

$$g1(\tau) = \int dt\, F(\Gamma) \exp(-\Gamma\tau \text{ ----------(4)}$$

"where Γ is the particle relaxation rate (s−1) and is equal to q^2D, q being the scattering wave vector ($q = 4\pi n \sin(\theta/2)/\lambda$,n is the refractive index of the solvent, θ is the scattering angle and λ is the wavelength of the incident laser beam) and D is the particles' collective translational diffusion co-efficient, τ is the delay time. F (Γ) gives the distribution function of Γ,i.e. D, which in turn gives the particle size distribution". The previous studies found GNPs size <20 nm to be more suitable for biological application compared to the particles of bigger sizes as their cellular uptake is higher and they can cross the blood brain barrier in the animal models, therefore, for the present study, we selected GNPs sized 14±1nm (DLS size) for characterizations [278].

In accordance with the predicted shape of the particles from absorption measurements, TEM micrographs (Figure 4.5 a) also showed spherical GNPs <20 nm. The GNP size calculated from the TEM analysis is 16±2 nm (Figure 4.5 b). This value is closer to the size measured by DLS (14±1nm). The GNPs were characterized by X-Ray diffraction to understand its composition. The autocorrelation function indicates the monodispersity of the spherical shape of GNPs (Figure 4.3).

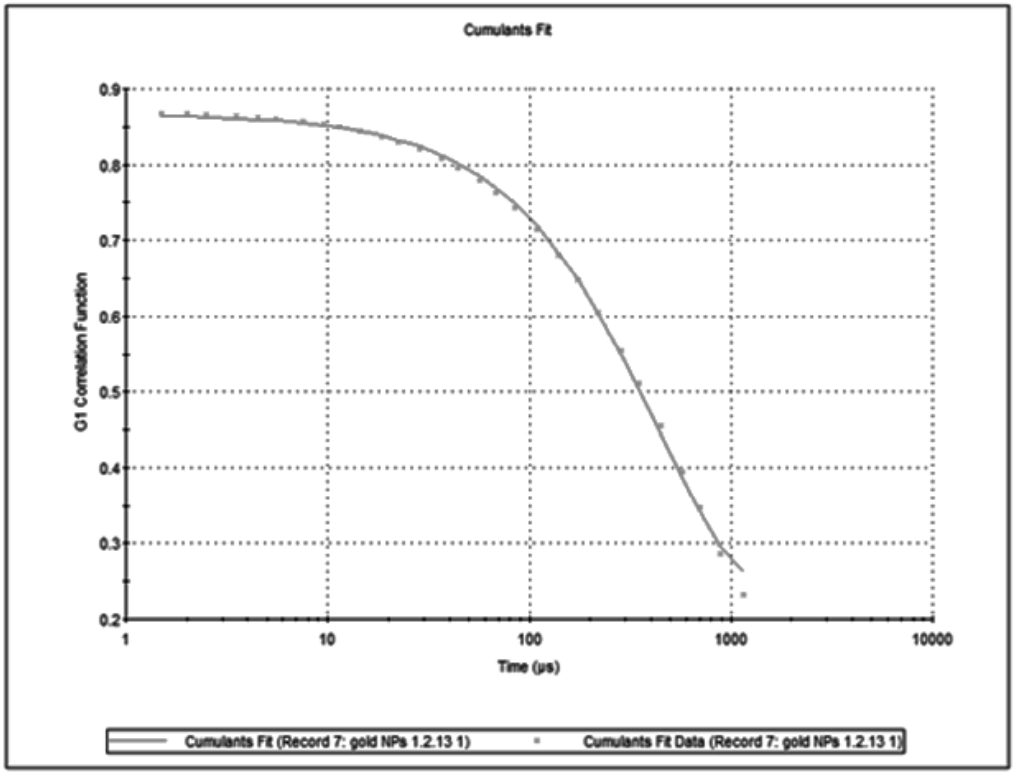

Figure 4.3A autocorrelation graph is an indication of mono-dispersion of GNPs. The mono-modal (only one peak) fitting and also indicates the spherical or nearly spherical shape of the particles.

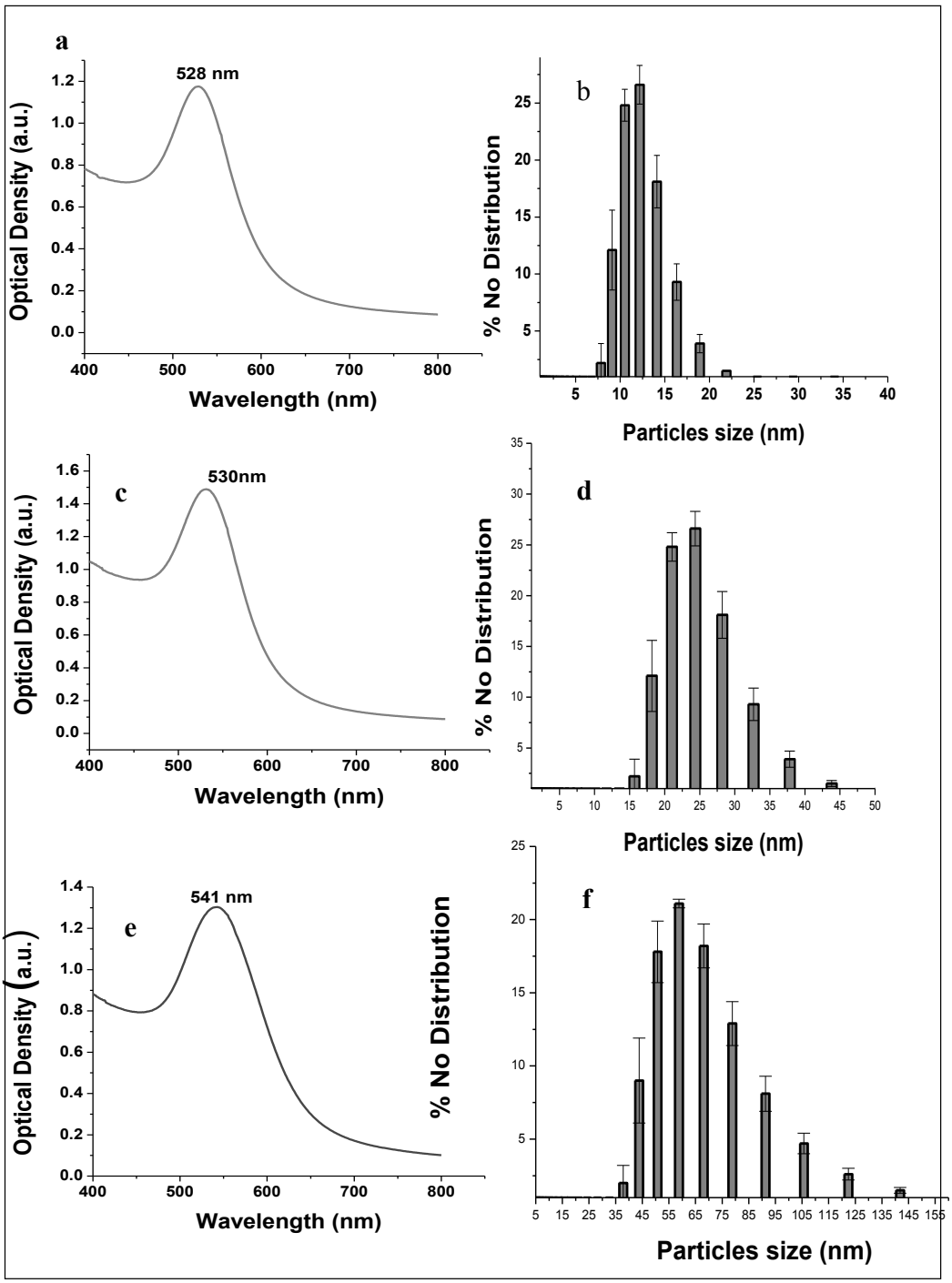

Figure 4.4 UV-Vis spectra of the different sizes of GNPs. a) 20 nm c) 60 nm and e) 93 nm. DLS histograms of the gold nanoparticles showing the distribution of GNPs b) 20 nm d) 60 nm f) 93 nm.

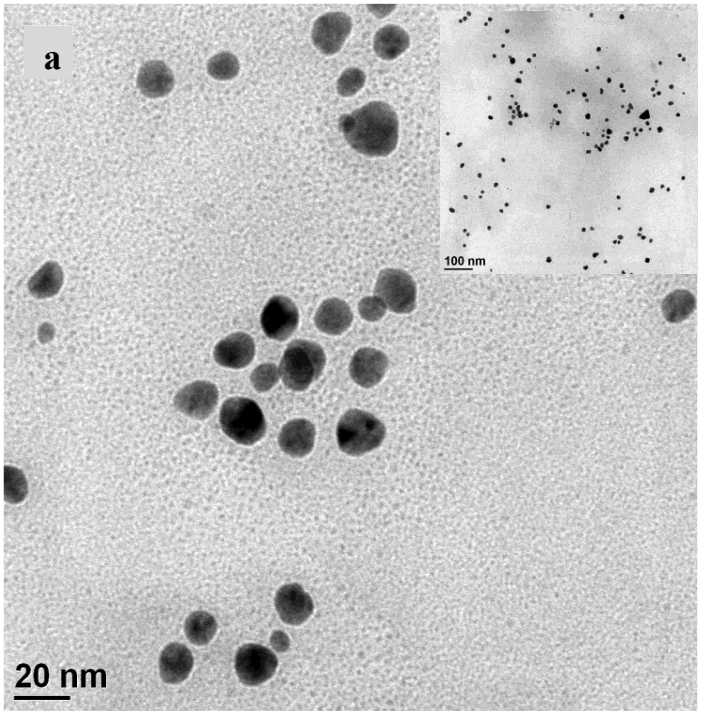

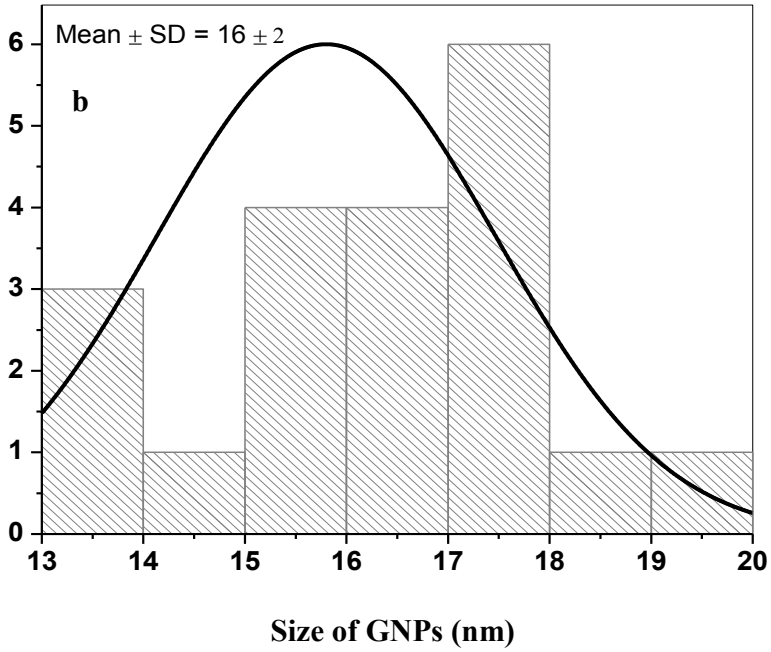

Figure 4.5 TEM micrograph shows particle morphology, size and shape (a). The mean particle size is analyzed by the image J software (b).

4.4.1.2 XRD analysis

The XRD spectrum exhibited peaks at 38°and 44° which is indicative of planes of the face-center-cubic (fcc) of gold respectively, indicates the crystalline nature of the GNPs (Figure 4.6). The indexing of the peaks using ICDDC (International Committee for Diffraction Data) files reveals that the characteristic X-ray peaks could be attributed to face-centered cubic Au structure. Earlier, reports of synthesis of GNPs exhibited additional diffraction peaks at additional diffraction peaks at 64.8° and 78.8° were ascribed to (214) and (311) planes, respectively [241]. The diffraction intensity of the (111) plane is much higher compared to that of the indicating that planes are predominant in our fabricated GNPs. An overwhelmingly strong diffraction peak at (111) plane compared to other facets were observed in earlier reports on GNPs synthesis.

The literature reports that the plane has lower surface energy which results in weak bonding ability and chemical reactivity as compared to other planes [279]. The weak bonding ability and chemical reactivity of might be attributed to the adsorption/coating of the biomolecules from *Vitis vinifera* L. fruit extract on the Au crystal facets. The adsorption of the bio molecules from the *Vitis vinifera* L. influences the surface property of GNPs and make biocompatible as well as SERs active. The *Vitis vinifera* L. mainly contains the sugar; glucose and fructose, organic acid; tartaric, malic, citric, phenolic compound anthocyanins, tannins, nitrogenous compound amino acid, peptides and proteins [280].

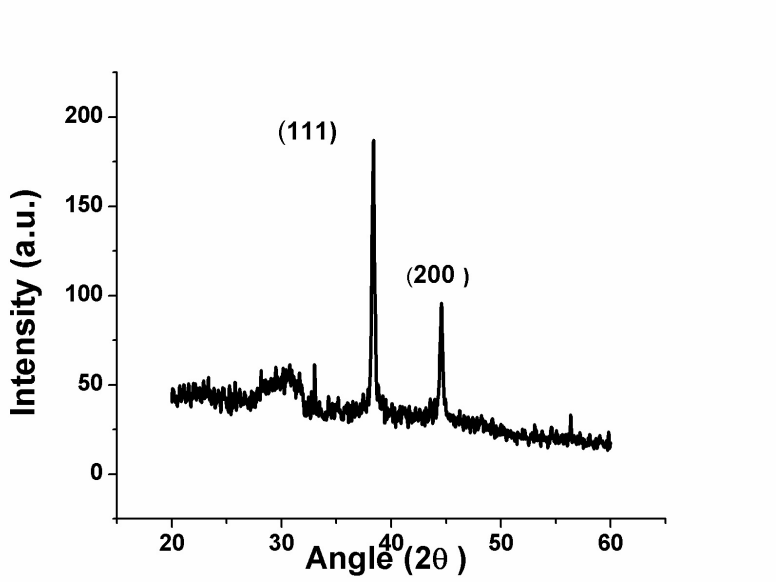

Figure 4.6 XRD spectra from the particles. The particles were recorded at 40 KV voltage and 40 MV current using Cu-Ka radiation (l =1. 5405 Å, scan rate 10 /min)

4.4.1.3 FTIR analysis

The FTIR analysis was performed to detect the vibration mode of the chemical compound and comprehend the biochemical composition of the *Vitis vinifera* L. and GNPs **(**Figure 4.7). The sharp peak of GNPs at 3785 cm^{-1} is due to O-H stretch indicating the presence of the phenols from the *Vitis vinifera* L. fruit extract. The fruit extract consists of a variety of polyphenols, aldehydes, peptides and proteins [281, 282]. The peak of 2934 cm^{-1} and 2071 cm^{-1} indicates the C-H and C≡H of alkenes and alkynes respectively (Figure 4.7 A) Whereas, peaks at 2917 cm^{-1} and 2836 cm^{-1} are indicative of C-H and H-C=O bonds of aldehydes from *Vitis vinifera* L. Fruit extract. The peaks at 1641 cm^{-1} (Figure 4.7 a) and 1659 cm^{-1} (Figure 4.7 b) represents N-H bond vibrations from amide groups of the proteins present in *Vitis vinifera* L. fruit extract as well as in the GNPs [283, 284]. The peak at 1420 cm^{-1} is suggested to be the C-C stretch from the polyphenols of the *Vitis vinifera* L. present on the surface of GNPs. On the other hand peak at 1247 cm^{-1}, 1061 cm^{-1} might

be aliphatic amines with C-N stretch and 630 cm^{-1} from alkanes **present** in the *Vitis vinifera* L. (Figure 4.7 A). The similar peak at 1042 cm^{-1} and 711 cm^{-1} in the spectrum could be from the aliphatic amines C-N stretch and C- H rocks bond of the alkanes respectively present on the GNPs. (Figure 4.7 B). Earlier reports, have attributed this peak to the presence of alkanes [285, 286]. The overlapping peak of the functional group of *Vitis vinifera* L. present on the GNPs also corroborates our results biomolecules from the *Vitis vinifera* L. are coated on the surface of GNPs and might form a covalent bond with GNPs.

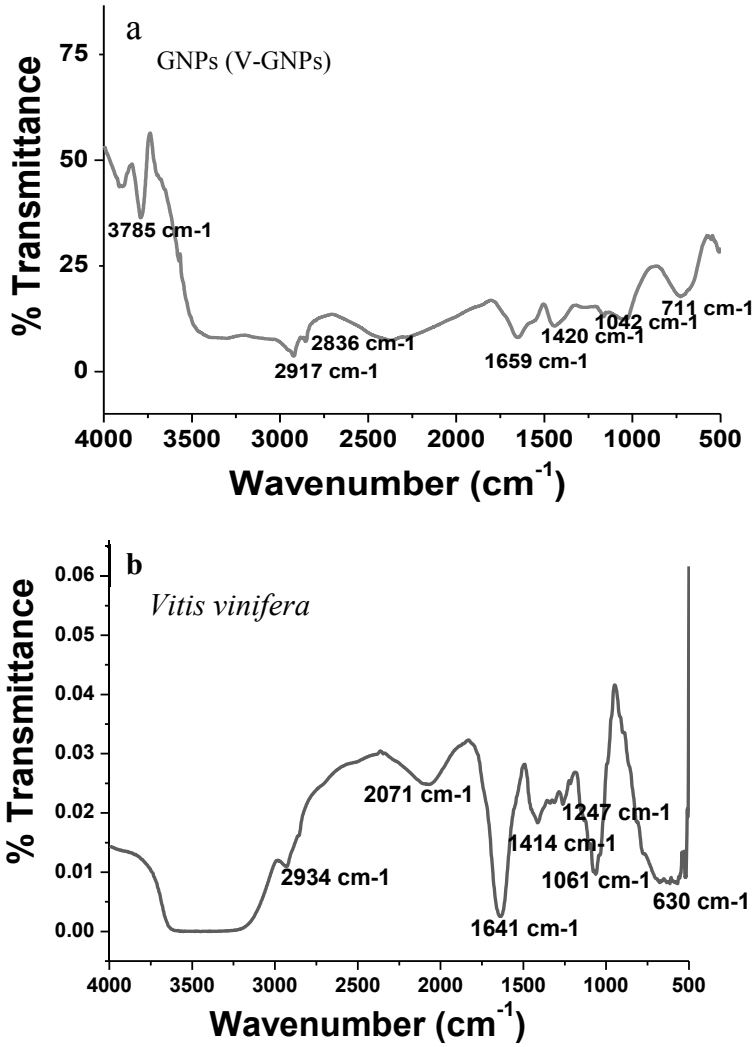

Figure 4.7 FTIR spectra of as-prepared GNPs. The spectrum was recorded from 450-4000 cm-1 in the transmittance mode (a) GNPs and b) Vitis vinifera, a reducing agent for GNPs synthesis.

4.4.1.4 Stability of GNPs

The stability of nanoparticles is an indispensable parameter for biomedical applications. In *in vitro* studies, stability of the GNPs (Figure 4.8 a and b) was evaluated by monitoring the plasmon wavelength (λ max) and in borate buffer, RPMI, NaCl, RPMI+FBS, cysteine and histidine, NaCl (1 and 15 days) after the synthesis of GNPs. The plasmon wavelength in the above buffers did not show a shift in SPR band for 1 day, whereas after 15 days SPR band exhibited a small shift of less than ~ 5nm. The constant

SPR band indicated that GNPs are stable in all buffers and cell culture medium. The 24 h data indicates that there is no difference in the SPR band in all the buffers with respect to GNPs alone (control). Our results are consistency with other studies on the stability of GNPs synthesized from plant compound [155].

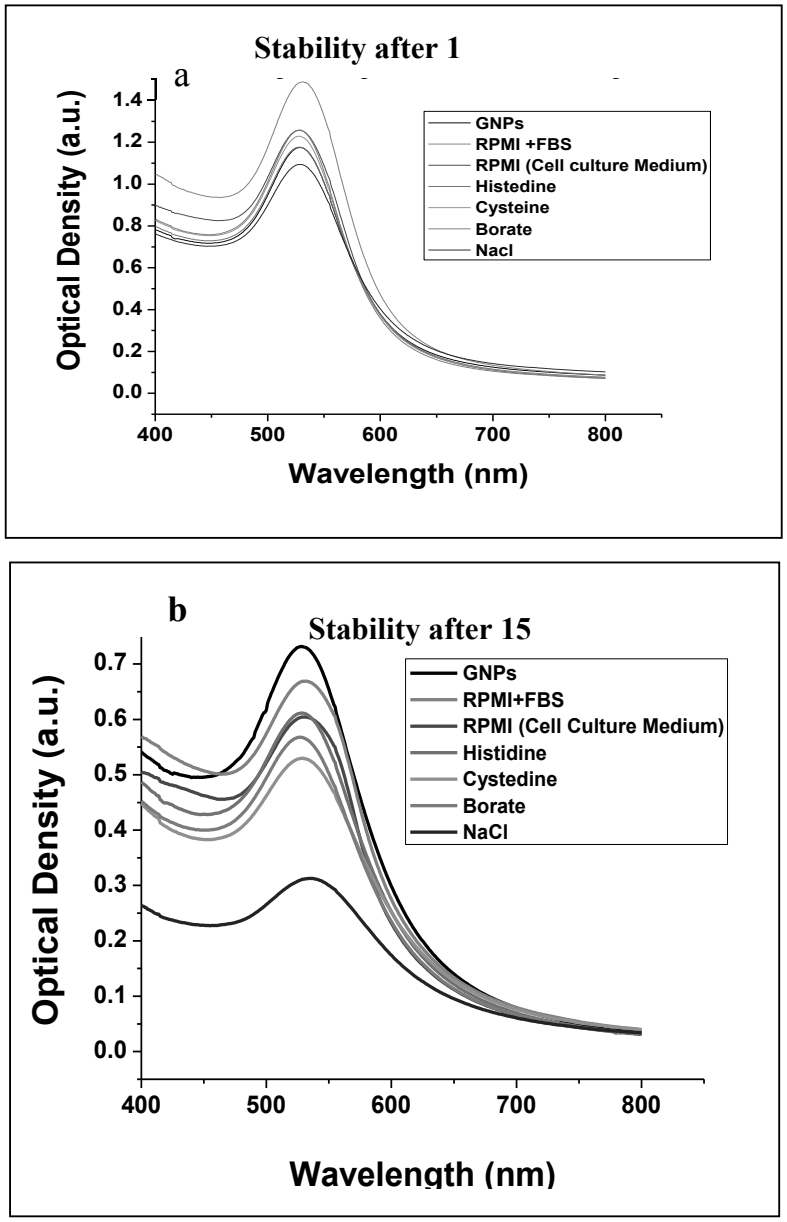

Figure 4.8 Stability of GNPs measured by Uv-Vis spectra of the GNPs in various buffers

SPRs is a function of the time and stability in the different biologically relevant solvents. a) After1day b) After 15 days

4.4.1.4 SERs activity of GNPs

SERs is a unique property of metal nanoparticles that can be used for the imaging applications. Therefore, in the current work the GNPs of various sizes (14±1nm and 61±2nm) were tested for the SERs signature. In our study, the Raman intensity was measured from 500 to 2000 cm^{-1} (Figure 4.9 a). The Raman spectral peak intensity is observed at 570,788 and 1102 cm^{-1}. The peak intensity of the different sizes revealed that Raman intensity is the proposal directly to the GNPs sizes. In agreement with the present work, earlier reported indicates that the increased SERs intensity with the increase in the particle sizes [287]. The Raman spectral peak intensities from the *Vitis vinifera* L. fruit extract is also observed at 570, 788 and 1102 cm^{-1} signifying that the Raman reporter molecule (s) from the extract are retained on the GNPs during the synthesis process [288]. Interestingly, the Raman signal intensity is higher in GNPs compared to the *Vitis vinifera* L. extract alone indicating SERs effect (Figure 4.9 a). The SERS activity of biological molecules such as histidine, cysteine and lysine using gold substrate is reported previously. The RE calculated as described by Chia-Wei –Chang et al., [289].

EF for R6G doped GNPs= $[(I_{R6gGNP}/N_{R6gGNP})] /[(I_{R6g}N/_{R6g})]$…… (5)

I_{R6gGNP} and N_{R6gGNP} is Raman intensities of R6G dye doped GNPs dye at Raman peak 1360cm-1 and the number of R6G molecules on GNPs, respectively. $I_{R6g}N/_{R6g}$ is the Raman intensities of R6G and number of dye molecules. The number of molecules is calculated using the Avogadro number for dye doped GNPs and R6G with the known concentration of R6G. The number of molecules is 120.4 $x10^{14}$and $6.23x10^{20}$, for dye-doped GNPs and R6G, respectively. The EF for dye-doped GNPs are R6G $3.4X10^{7.}$ The EF of 10^{8} has been

reported for R6G doped GNPs previously. The number of the Raman reporter molecules present on the GNPs is unknown therefore we consider peak high for the calculation of RE of without dye-doped GNPs and EF of R6G dye doped GNPs has been extrapolated for without dye-doped GNPs. The RE for GNPs (61 nm) Raman Peak at 1102cm-1 is $4x10^{3.}$

SERs activity is known to be dependent on two key factors: (1) resonant surface plasmon excitation of a metal substrate and (2) proximity of analytic molecules to the metal substrate surface. The surface chemistry of metal substrate was considered as one critical factor for SERs activity because the analysts must be located within 0–4 nm of the substrate surface or the electromagnetic field. Therefore, we proposed that the GNPs had Raman reporter molecule (s) in the close proximity of the Au metal surfaces resulting in SERs enhancements [290]. We hypothesized that the aromatic compounds from the *Vitis vinifera* L. extract acted as SERs nano tags. The Raman peaks at 570 cm^{-1} could be due to in plane bending from carbon and oxygen from the phenolic compound aromatic acids such as p-coumaric acid this phenol is presented in *Vitis vinifera* L. fruit extract and resins [291, 292]. The vibrational peak at 1102 cm^{-1} could be from the trehalos sugar molecules present in *Vitis vinifera* L extract [280]. The vibrational peak at 788 cm^{-1} could be from the amino acid as the Raman reporter molecules. The RE for the R6G reporter molecule is higher than the trehalose Raman reporter indicating the closer proximity of the R6G with Au metal surface associated with the sugar molecules on the GNPs.

The long term stability of the GNPs is assessed for their potential application after storage of the particles. The lack of shift in Raman peaks after one month compared to the freshly synthesized particles indicating the stability of the Raman reporter molecules on GNPs **(**Figure 4.9 b). On the other hand, stored *Vitis vinefera* L. extract cannot reduced

the Au salt to form GNPs with SERs signature. The newly synthesized and stored GNPs can be used for biomedical applications. Earlier studies used SERs active gold nanoparticles for *in vivo* tumor cell targeting and sensitive cancer detection. However, these studies employed GNPs synthesis using $NaBH_4$ as reducing agent and synthetic dyes as SERs reporter molecules. Our method of synthesis of SERs substrate is faster and safe than recent synthesis using $NaBH_4$ and ascorbic acid.

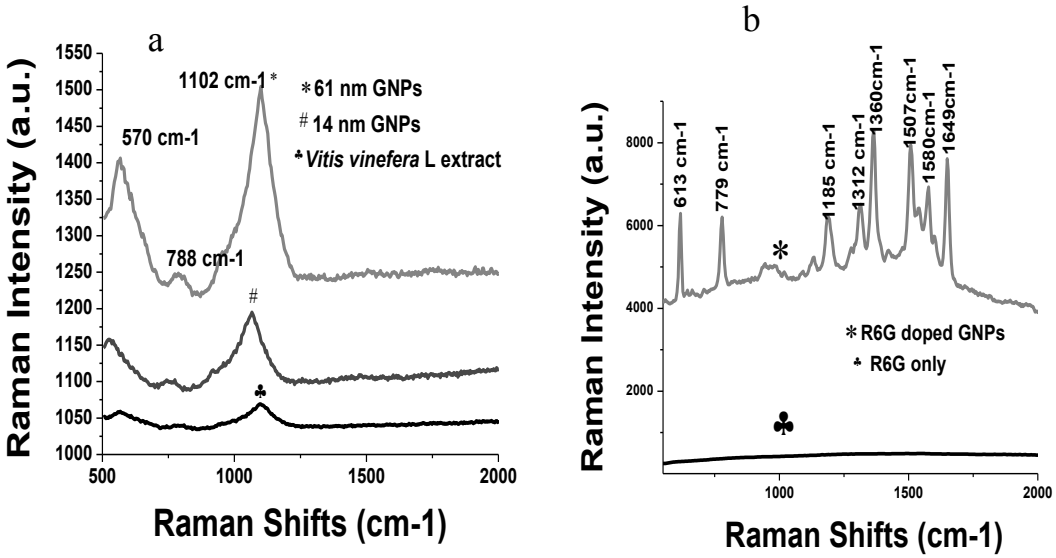

Figure 4.9 Synthesized GNPs function as SERs substrate (a) Raman Spectra from GNPs of different sizes. Black color, *Vitis vinefera L*., black color - spectrum from 14±1nm GNPs and pink color - spectrum from 61±2 nm GNPs (b) Raman spectrum of R6G doped GNPs. Red color

4.5 Biocompatibility evaluation (cell viability evaluation)

Biocompatibility is essential to evaluate before a nanomaterial, can use for the biological application. The *in vitro* cytotoxicity effect of nanomaterials is most often assessed by mitochondrial enzyme activity using tetrazolium salt (MTT assay), with respect to the untreated cell as a control [293, 294]. We have studied the cytotoxicity of the GNPs using MTT assay in non-cancerous Muller glial (MIO-M1) and breast cancer cells

(MDA-MB 453) and Y79, a RB cell line (Figure 4.10 a and c). The GNPs are non-toxic to the cells up to 100 μM concentration. The cell viability does not decrease after 6h and 12h of treatment with increasing concentrations of GNP from 10 to 100 μM ($P<0.05$) in both normal and breast cancer cell lines, when compared to the control untreated cells. Cytotoxicity of the GNPs was previously reported to be dependent on the GNPs concentration, time of treatment and cell types. GNPs synthesized using synthetic and toxic chemicals such as Lithium borohydride ($LiBH_4$) penetrate the membranes at high concentration and decrease cell proliferation via generating ROS, in turn decreasing the mitochondrial enzyme activity ATP content of the cell causing cell damage [295].

In contrast, GNPs synthesized using green nanotechnology were nontoxic even at higher concentrations. The cell viability is more than 85% till 12h of treatment in the MIO-M1 and MDA MB-453 ($P<0.05$). However, 100 μM of GNPs treatment at 24h showed 70.28 % cell viability in MDA MB-453 cells (Figure 4.10 b). Whereas MIO-M1 showed no significant decrease ($P<0.05$) in the cell viability after 24h of GNP treatment (Figure 4.10 c). According to the ISO-10993-5 guideline [296] a material can be used for biomedical application if the material shows more than 70% cell viability. The GNPs from the 10-100 μM concentration are safe to use for *in vitro* biological studies. Whereas in the case of Y79, a RB cell GNPs decreases the cell viability. The cytotoxic effects of GNPs from the 10-100 μM concentration up to 24h of treatment in RB cell line were studied (Figure 4.10c). The percentage of cell viability indicates that 100 μM of GNPs shows anti-proliferative effect on Y79 RB cells at 24h of treatment, which could be due to the presence

of reducing agents (*Vitis vinifera* polyphenols) on the GNPs. The cancer cell death from the treatment of 10-100 µM GNPs concentration was studied (Figure 4.10 c).

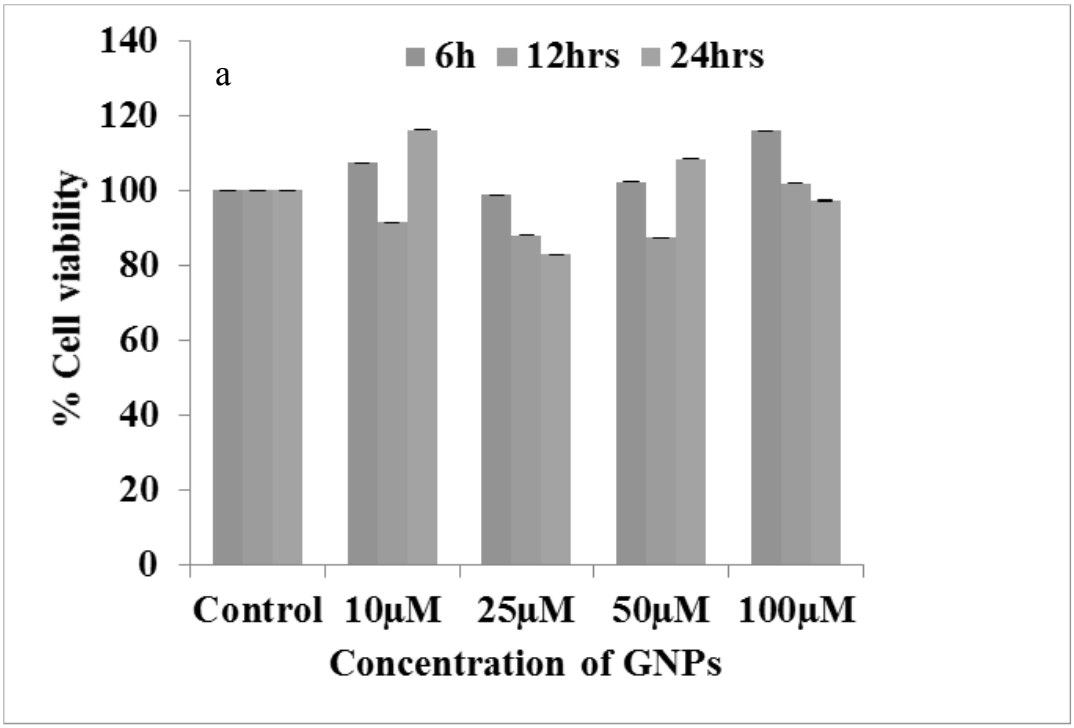

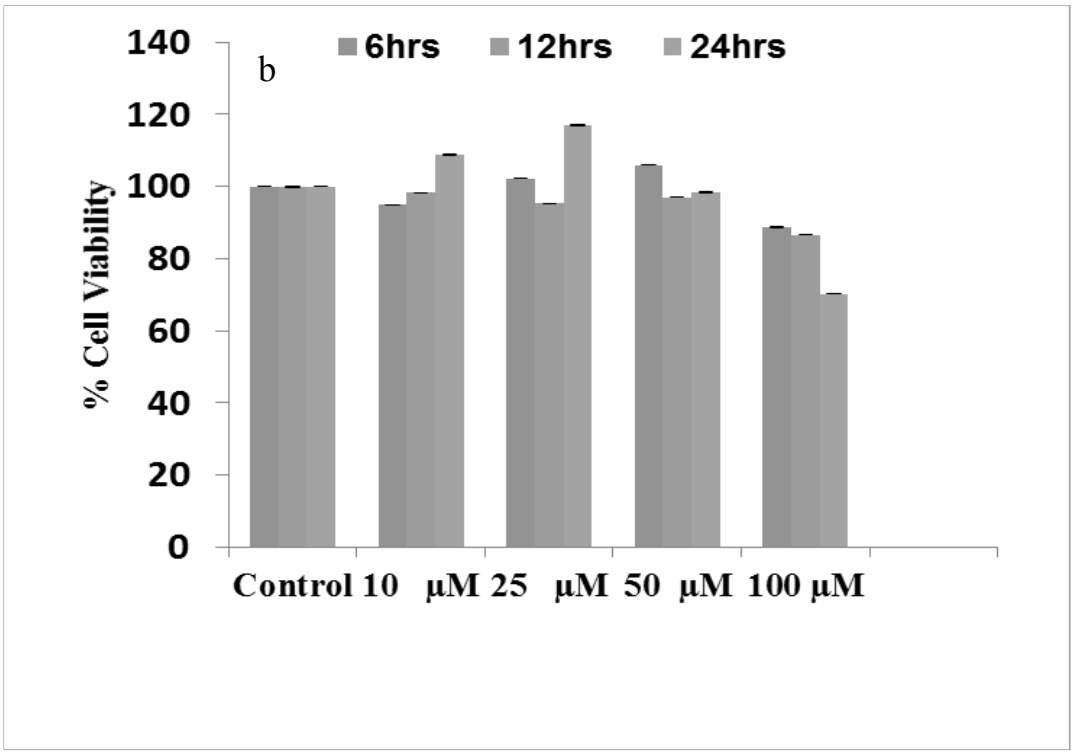

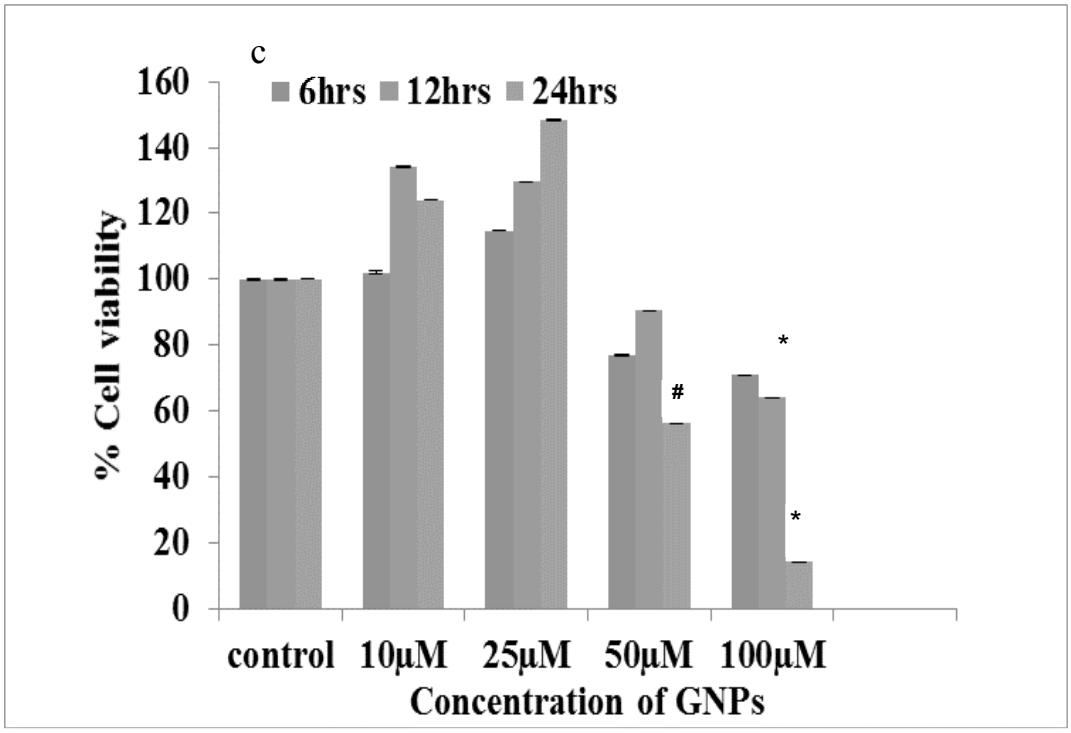

Figure 4.10 Cell viability measurements of GNPs in different cell lines at various concentrations (a) MIO-M1 (Muller Glial, non-cancerous) (b) MDA-MB 453 (Breast Cancer) and (c) Y79 (RB). The cell viability percentage was calculated with respect to untreated cells.

The cell viability percentage was calculated with respect to untreated cells. * Represent the significant difference at $p<0.05$. GNPs treated on Y79 RB cells at varying dosages for 6h, 12h, and 24h showed the decrease in cell viability, which depends on concentration and time of treatment. # indicates the statistical significant difference with respect to the controls at 50µM at 24h. Barr indicates the mean of 3 values and error bars represent the ± standard error of the mean of 1-3 independent experiments.

4.5.1 Characterization of *Curcuma* L. reduced GNPs

The optimized parameters for GNPs synthesis by *Vitis viniferea* the similar synthesis condition was used for the synthesis of curcumin GNPs. The boiling (100 °C) temperature is essential for complete dissolution of curcumin and it has been reported that curcumin can be dissolved at high temperature in the water solvent and can function as reducing and capping agent. The predominant tautomeric forms of curcumin, is phenolic and enolic-OH which donate hydrogen and reduces the Au^{3+} ions [297]. Unlike, *Vitis*

vinifera, curcumin is not soluble at lower temperature and reduction of Au salt required higher temperature for Au salt reduction. As discussed in the preceding section the optimum size of GNPs for targeted therapy and as a self-therapeutics should be in the range of 15-20 nm therefore, the representative GNPs (Cur-GNPs) size range is further characterized.

4.5.1.1 Uv-Visible spectroscopy, DLS, TEM, and XRD

The Cur-GNPs characterized by Uv-Visible, DLS, TEM and XRD (Figure 4.11 A &D). The SPR band at ~530nm is observed predominantly indicates the spherical shape of the particles [266]. The number distribution shows that the sizes of GNP's are in the range of 15 to 30 nm in diameter, however majority of particles are of a size 21nm (Figure 4.11 a &b). The zeta potential of GNP was -40.5 mV, which indicates that GNPs are stable in the aqueous solution. TEM micrographs (Figure 4.11 c) also showed GNPs ~20 nm. The predominant shape of particles as indicates spherical shape, another shape of particles also noticed, this indicates that the synthesis is less controllable in case of Cur-GNPs, which gives different morphology.

X-ray powder diffraction studies of Cur-GNPs confirm the plane at 38.2°C in of Cur-GNPs are shown in Figure 4.11 d. In XRD spectra of Cur-GNPs complex, the characteristic X-ray diffraction of the Au shown at 111 (38.2°C) which reveal the presence Au in the Cur-GNPs. A similar plane has been observed for the *Vitis vinifera* reduced particles also. The diffraction spectra of Cur-GNPs demonstrated an amorphous behavior nature of the GNPs which could be due to capping of the curcumin on the GNPs. The plane confirmed that particles nucleate and grow, and most of them are face- centered cubic (fcc).

The plane surfaces in the nano scale range is lowest-energy facets which also confirmed the crystalline nature of particle [298, 299].

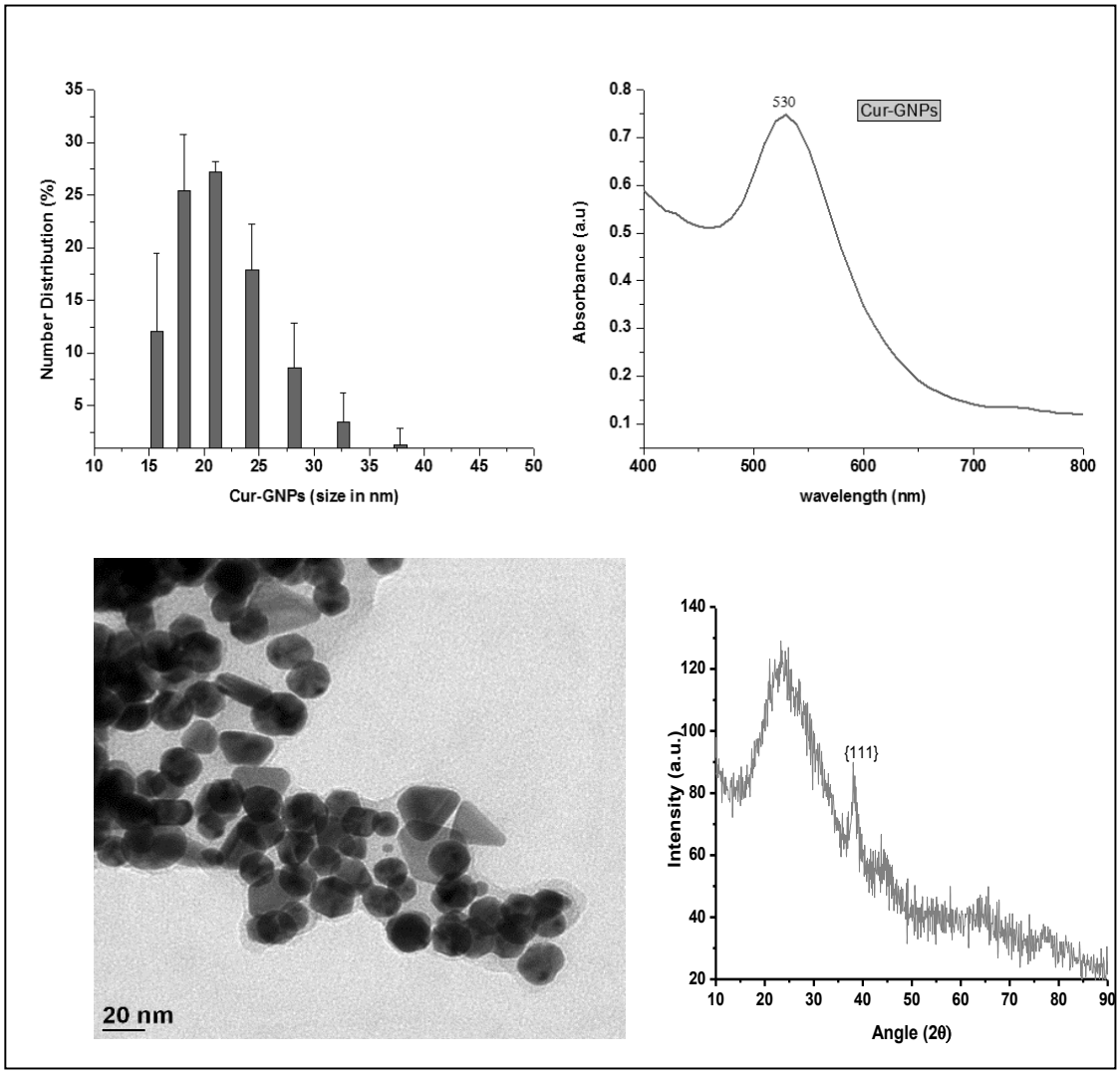

Figure 4.11 Characterization of Cur- GNPs Representative images and graph for Cur- GNPs (a) DLS represents the no distribution (b) UV, visible graph indicate the characteristics SPR band (c) TEM micrograph of the GNPs shows the shape of the particles. (d) XRD spectra which shows a predominant peak at 38.5° [300]

4.5.1.2 Fourier Transform Infrared spectroscopy (FTIR)

The FTIR spectra of curcumin, Cur-GNP, are shown in Figure 4.12. Characteristic peaks of curcumin and change in the spectral pattern in Cur-GNP also proves the coating/capping of curcumin on GNP. From the visible differences in FTIR spectra, it was concluded that the reduction of Au, capping and stabilization GNPs and conjugation of curcumin on GNPs occur successfully.

The broad peak at ~3456 and ~ 3427 cm^{-1} has been shown in the Cur-GNP-and curcumin respectively, corresponded to H-bonded alcohols/phenols present in the curcumin. The narrow band 2923 and 2933 cm^{-1} is assigned to the signal (C-H stretch of alkanes) in the Cur-GNPs and curcumin, respectively (Figure 4.12). The narrowly spaced peak at 1645 and 1635cm^{-1} can be assigned for the symmetric and an unsymmetrical stretch of the strong diketones group present in the curcumin and also assigned the Enol form of the curcumin [301]. The stabilized cur-GNPs shows the 10 cm^{-1} (1645cm^{-1}) shift in the C=O peak of a cur in (1635 cm^{-1}) could be an SPR effect of GNPs. It is predicted that C=O of an enolic group of curcumin help in capping and reduction of Au salt. Cur-GNPs formation is supported by the density function theory . The other important peak at 1509 cm^{-1} C=C aromatic ring of the Curcumin after the stabilization with the GNPs the shift in the peak which appears at 1441 cm^{-1} in the case Cur-GNPs [302].

4.5.1.3 Stability analysis in different biological relevant solvents

The *in vitro* stability is an important parameter, which has been studied using various biological relevant solvents of different pH. The curcumin GNP which shows stability in a range of solvent namely NaCl, Cysteine, Histidine, borate, DTT, RPMI, and DMEM. It has been noticed from the stability graph that of Cur-GNPs (Figure 4.12 b) SPR

bands are unaltered and characteristic peak of GNP remains unaltered in aqueous solution after 24h of incubation at room temperature except culture medium. The cell culture medium which contains the 10% serum protein from a red shift was observed ~530 to ~555 nm (Figure 4.13) (indicates by the arrow). The serum protein binding with GNPs, which could increase the absorbance and also shows the Red shift in SPR band.

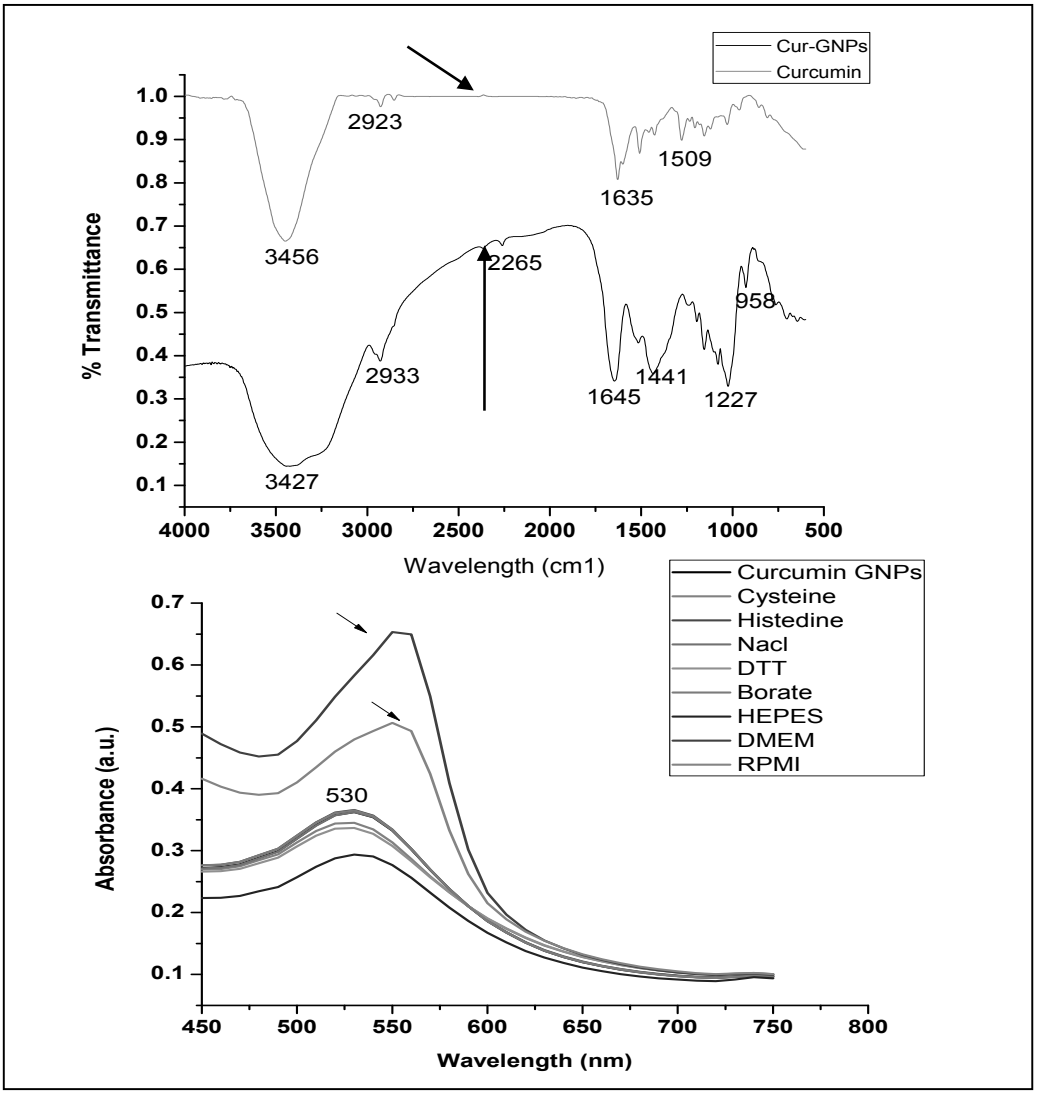

Figure 4.12 a) FTIR spectra of as-prepared GNPs and curcumin stabilized nanoparticles. The spectrum was recorded from 450-4000 cm-1 from the GNPs in the transmittance. (b) Stability of curcumin GNPs in various solvent and culture medium. The arrow indicates the SPR shift.

4.5.1.4 Raman Spectroscopy of Cur-GNPs

The Raman shift has been observed at 1417, 1570, 1381, 1321, 1172 and 1464 cm^{-1}, which are notated to the vibration band of the curcumin coated on the surface of GNPs (Figure 4.13) [303, 304]. The major advantage of Raman over the FTIR includes, fewer water molecules interfere and large Raman scattering cross section [305]. 1570 cm^{-1} could be assigned to the benzene ring, and 1172 cm^{-1} were signified to C–O–C and C–O–H vibrations of the curcumin. The most intense bands appearing at 1417 cm^{-1} could assign for the $_{v}$ (C=C) of an aromatic moiety. Whereas, 1381 and 1321cm^{-1} represents the bending of the phenolic group presents in the curcumin. The decrease intensity of Raman shift except 1417 cm^{-1} indicates that the C=O carbonyl band and C-OH hydroxyl group participates in the binding with the metal in the Cur-GNPs complex [306].

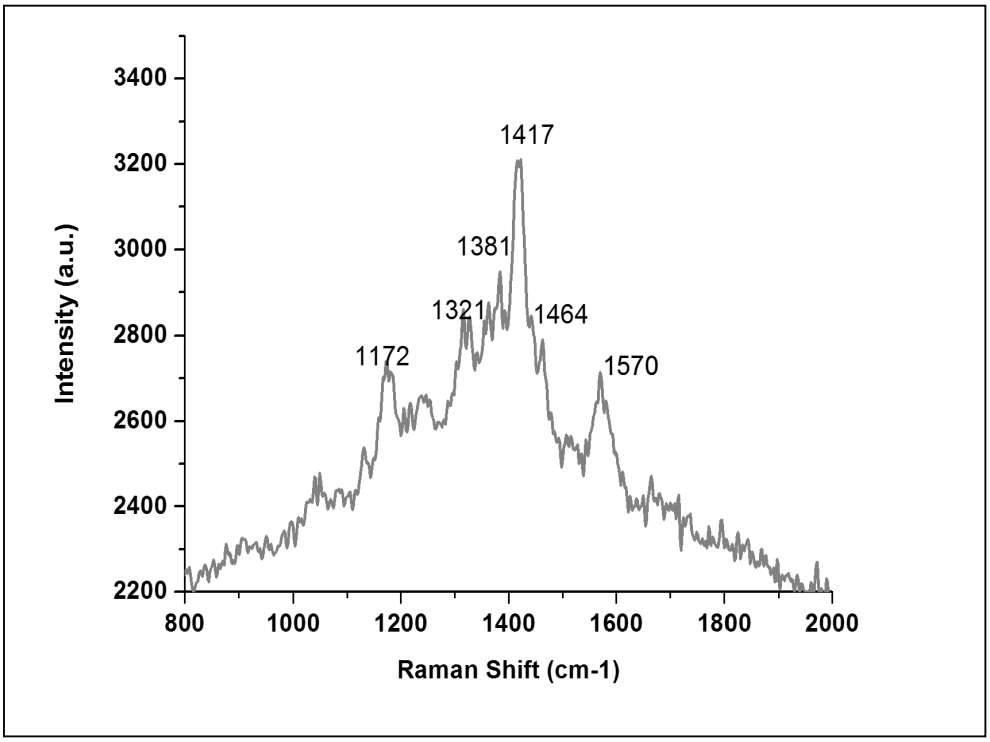

Figure 4.13Represent the Raman spectra of Cur- GNPs. The spectra indicate the SERs effect.

4.5.1.5 Cell viability (MTT Assay)

The cell viability of cell treated with curcumin GNPs was calculated with respect to control (Figure 4.14). The cell viability in Y79 and WERI, RB after 6 h of treatment was 73% and 48% respectively, at 150 μm of GNPs. Whereas, at the same concentration (150 μm) after 24 of treatment cell viability was decreased significantly ($P<0.05\%$) with maximum cell viability was 16% and 17% in Y79 and WERI, respectively. The maximum cell viability noticed at 50 μm was 21% ($P<0.05$) proves that Cur-GNPs has an anti-proliferative effect on RB cells. MCF-7 and MIOM-M1, the adherent cell lines show the difference in the cell viability compared to the RB, the suspension cell line. In both cases, there is no significant ($P<0.05$) cytotoxicity observed for 6hr treatment. The cell viability was observed more than 90% with 150 μm of GNPs concentration. Whereas, the cell viability was 33% and 60% ($P<0.05$) in MIO-M1 and MCF-7 respectively, after 24h of treatment. The result infers that cell viability reduced significantly with respect to control at a 24h treatment time for all the cells treated with Cur-GNP. This data clearly indicates the Cur-GNPs shows anti-proliferative effect, which is desirable for cancer cells. However, it could also be noted that there was significant reduction in viability of MIO-M1 cells, especially for 24 hour treatment that is a non-cancerous human neuronal cell. The cell viability data confirm that Cur-GNPs are anti-proliferative in nature and more effective as an anticancer self-therapeutic particles compared to MCF breast cancer cell line with same concentration.

4.6.1 Sodium citrate reduced GNPs

Citrate reduced particles were synthesized by Turevich's method using sodium citrate as a reducing the NaAuCl4 [307]. The citrate reduces GNPs were used as a control

material for the comparison of the biological synthesized GNPs for the *in vivo* experiment. The sodium citrate reduced particles are comparable in size and shape with the sodium citrate reduced GNPs procured from the British Biocell International (BBI).

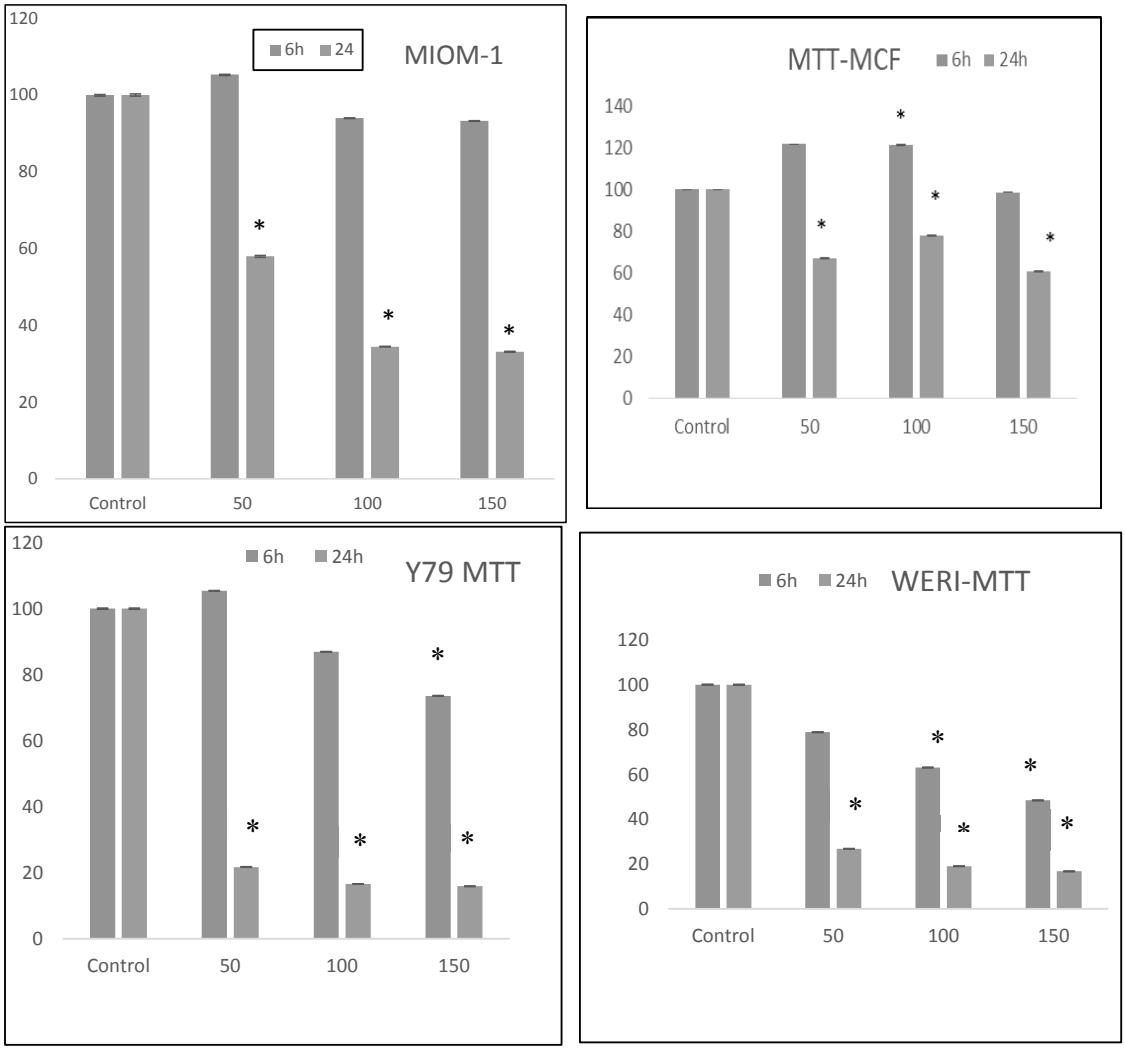

Figure 4.14 Cell viability using MTT assay after treatment with of GNPs in different cell lines at various concentrations (a) MIO-M1, (b) MCF, (c) & (d) WERI and Y79

The cell viability (% of treated cells with respect to untreated cells) of different cell lines treated at various time periods. Muller Glial, non-cancerous, Breast Cancer (adherent cell lines). RB, (suspension cell line). * Represent the statistical significant at $p<0.05$.

4.4 Discussion

The data obtained in the current experimental condition are discussed further with an emphasis on the synthesis procedure, parameters which affect the size of particles and the cytotoxicity effect of GNPs using different cancer and non-cancer cell line. The different sizes of GNPs were synthesized by changing the temperature, concentration of NaAucl4 and reducing agent (Table 4.1). GNPs with a diameter of ~20nm (Figure 4.2 D) size were synthesized at 80°C. Increasing the time of reduction resulted in particles of bigger size (~60nm). The ~93nm GNPs were synthesized at 45^{o}C with higher Au salt concentration. The different sizes of GNPs are dependent on two independent processes of growth and nucleation of the Au atoms during particles synthesis [308, 309].

The bigger size of nanoparticles can form due to increase in time of growth and nucleation processes during synthesis. At higher temperatures and less Au salt, the atoms vibrate strongly at their lattice positions and exchange energy with neighboring atoms [310]. The lower temperatures resulted in the reduction in the diffusion and the higher strain energy that lead to the formation of bigger sized particles The GNPs of different sizes were reported previously with varying the annealing temperatures on the seeded ZnO sacrificial template and polymethyl silsesquioxanes [311]. The zeta potential of the particles is -32mV and the bigger GNPs had reduced zeta potential of -22mV, indicating a lower stability of the particles compared to ~20 nm (TEM size) GNPs. Similarly, the result observed in current data the zeta potential of the 14±1 nm (DLS size) particles is -32mV. The bigger GNPs had reduced zeta potential of -22 mV, indicating a lower stability of the bigger particles compared to the 14±2 nm GNPs (Table 4.1). However, the negative zeta potential for all the GNPs indicates the relative stability in biological relevant solvents.

Apart from the temperature, pH is a vital parameter which controls the growth and nucleation at the time of the reduction of Au salt and synthesis of nanoparticles. It has reported that low pH facilitates the reaction kinetics of gold ions which increases the size of the GNPs and this effect is responsible for the ellipticity and different size of GNPs form during the growth and nucleation process .

The metal intrinsic toxicity is the major concern in the field of nanomaterial for biomedical applications. The potential adverse effects of nanomaterial in biological application could reduce to a greater extent with the use of the GNPs synthesized from the natural plant compounds such as polyphenolics and phytochemicals that are known to have abundant antioxidant and anticancer properties [312, 313]. Curcumin as a reducing agent helps in the delivery of Curcumin through GNPs as a capping agent and increases its bioavailability. Hence, it can act as the most effective drug for cancer therapy with sustained-release on the tumor site. In addition to this, coating of Curcumin on GNPs solve the problem of solubility during the synthesis of GNPs at 100˚C at this temperature the Curcumin is completely dissolved [314]. The anti -carcinogenic, anti-oxidant properties of Curcumin and *Vitis Vinifera* have been demonstrated in different types of cancer for therapy [315].

A single step economic and eco-friendly method of bio-synthesizing SERs substrate is successfully established using *Vitis vinifera* L. extract and same procedure used to synthesize the GNPs with the *curcuma L*. The synthesis of Cur-GNPs indicates that the method of the SERs active GNPs synthesis is reproducible with different reducing agent. The synthesized GNPs were spherical in shape, coated with aromatic compounds (proteins/peptides) from the *Vitis vinifera* L. and the phytochemicals from the *Vitis vinifera*

L. extracts a reducing agent for synthesis and a Raman reporter molecule. The multivalent glyconanoparticles have been employed in many areas including the identification of biomarkers by glycan coated on GNPs which can bind with proteins present on the cell surface [316, 317].

In this consideration, multifunctional gold nanoparticles (GNPs) synthesis and functionalization is the quest for targeted cancer therapy. Over the decades therapeutics for the cancer has been changed significantly towards nanotechnology to deliver biomolecules, in particular carbohydrate and protein coated multifunctional metal nanoparticles is a new venture for biomedical application. The toxicity of the metal nanoparticles is reduced by surface coatings [318]. This coating might be responsible for the observed low toxicity in the normal and breast cancer cell lines as it inhibits the direct interaction of the metal nanoparticles to the cells and makes these particles more biocompatible than the uncoated particles. The gum arabic coated GNPs were previously tested in animal models and found to be non-toxic [319]. The method is rapid, simple and highly reproducible, studies demonstrate a promising potential of a new class of GNPs as a self-therapeutics which can be a candidate material for cancer theranostic. In the current method, phenolic compounds and polysaccharides might have reduced the aurochloric acid into GNPs. The *Vitis vinifera* reduced GNPs is more promising due to stability, uniformity shape, and monodispersity index and reproducibility compared to the Curcumin GNPs therefore, the further work has been carried out with the *Vitis viniferea* GNPs. Apart from this the role of *Vitis vinifera* as a major component is studied in RB cancer for the anti-proliferative activity.

4.5 Chapter Summary

- The *Vitis vinifera L*. and *Curcuma L.* (curcumin) shows the kinetic potential to reduce the Au salt.
- The GNPs are SERs activity, and the reducing agent can act as a Raman reporter molecule
- The method of GNPs synthesis can be used for synthesis of GNPs using different reducing agents
- GNPs act as a self-therapeutic as it shows the anti-proliferative activity in the cancer cell
- The bioavailability and aqueous solubility of the anticancer molecules can overcomes with the current method of GNPs synthesis.
- *Vitis vinifera L. (V-GNPs*) is crystalline in nature with better therapeutic potential compared to *Curcuma L.*

CHAPTER 5

5 Evaluation of radical scavenging property of antioxidant peptide functionalized GNPs in Retinoblastoma *in vitro*

This chapter addresses a specific aim of the project to target the reactive oxygen species in a cancer cell. The antioxidant property of the novel tri-conjugate (GNPs-Pep-A) prepared by conjugation of thioctic acid, modified peptide-A with GNPs (*Vitis vinifera*) discussed in Chapter 4. The delivery of thiotic acid modified antioxidant peptide using GNPs as a carrier molecule to study the radical scavenging property of peptide in the RB cancer cell.

5.1 Background

Cancer cell reported to show higher ROS compared to the normal cell due to the stressed condition. Chemotherapy is the most common method in use for cancer treatment and during the treatment many anti-neoplastic agents (anticancer agent) produce oxidative stress, reactive oxygen species (ROS) in the cancer cell. ROS negatively interfered with the cellular component such as DNA/RNA, proteins and lipids, which impaired the cellular functionalities [320]. Some of the chemotherapy drugs such as doxorubicin, carboplatin, "anthracyclines, most alkylating agents, platinum coordination complexes, epipodophyllotoxins, camptothecins and etoposide" are known to generate ROS above threshold and thereby leading to apoptosis [321, 322]. However, this method has many disadvantages such as the evolution of more aggressive drug resistance, invasion and metastasis of tumor cells. In addition to this, ROS generated during cancer therapy may interfere with the anti-neoplastic activity and hence reduce the efficacy of the treatment [323, 324]. Redox-active agents such as antioxidants can enhance the benefits of

conventional anti-cancer therapy, without affecting the normal cells and would be an effective strategy in the clinical management of RB and other cancers [325, 326].

5.1.1 Reactive oxygen species (ROS) and oxidative stress

The redox imbalance in a cell due to ROS can be correlated with the oncogenic stimulation of the cancer cell **(**Figure 5.1). The ROS is oxygen-free radicals, which generated during the natural metabolism are an important signaling molecules [327, 328]. ROS can induce DNA damages, which increase the genetic instability and this is the ultimate cause of mutations and tumor genesis [329]. The DNA damage and ROS also increase nitrous oxide N_2O exposure. RB tumor aggressiveness can be correlated with the presence of iNOS (inducible nitric oxide synthase) and (NT) nitrotyrosine in the RB [330, 331]. The most common form of the radical species is oxygen ($O^{\cdot 2}$), superoxide ($O^{\cdot 2-}$), hydroxyl ($OH^{\cdot}$) and peroxyl ($ROO^{\cdot}$) radicals Apart from the ROS, the reactive nitrogen, sulphur, iron, copper and chlorine species are collectively called as 'reactive species'. Hypochlorous acid (HOCl), hydrogen peroxide (H_2O_2), ozone (O_3) and aldehyde (HCOR) are non-radicals. Transition metals such as Fe^{2+}, Cu^{2+} ions act on hydrogen peroxide to release the reactive hydroxyl radical.

This reaction is called the Fenton reaction, as described in equation (1)

$$Fe^{+2} + H_2O_2 \longrightarrow Fe^{+3} + OH^{\cdot} + OH \qquad (1)$$

5.1.2 Biomolecules, targets of reactive oxygen species

An increase in ROS generation causes oxidative injury to cell's biomolecules mainly DNA, proteins, and lipids, which increases more chances to enhance the disease. Protein oxidation usually forms aldehydes, keto compounds, and carbonyls. 3-nitrotyrosine serves as a marker for oxidative damage of protein. The hydrogen peroxide and superoxide

radicals, mainly target the proteins and peptides predominately which contain the SH such as cysteine and methionine amino acid. This interaction leads to the change in the confirmation of the proteins and peptides which causes the structure changes or degradation of the peptide/protein molecules. The most common lesion observed in the DNA is the C-8 position to yield 8-hydroxydeoxyguanosine (8-OHdG) which causes mutations in the genetic material, and it is the extensively studied DNA lesion [332]. Cancer cell showed more ROS compared to normal cell due to oxidative stress and it can be targeted for the cancer therapy [333, 334].

Figure 5.1 Multiple roles of ROS in cancer. It can inhibit or stimulate the cancer cell different

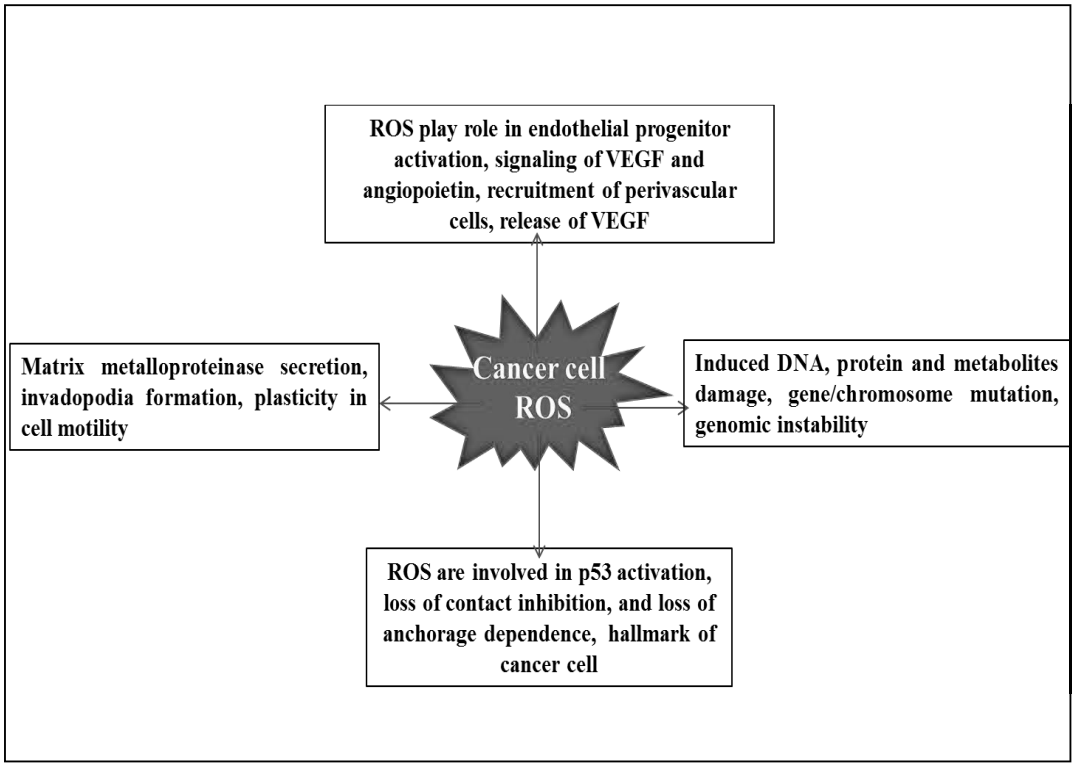

cellular process such as “survival, proliferation, invasion, angiogenesis, and metastasis”.

5.1.3 Antioxidant and targeted therapy

An antioxidant is a molecule that protects a cell against the electrophilic stress, and oxidative damage by reducing the ROS increased scavenging of radicals, bind metal ions and enhanced the antioxidant effect. Antioxidant molecules are widely studied for targeting reactive oxygen species [335, 336] and their use may lead to suppression of tumor growth [337]. Antioxidants have the property to counterbalance free radicals by electron exchange. The physiological conditions of the oxidation state decide cellular redox reactions in which an antioxidant can play dual roles as antioxidants, it donates the electron and a pro-oxidants it accepts an electron both these forms favored and reduced the ROS burden in the cell [338]. It has been reported that neuronal damage due to with L-Glutamate (Glu) -induced cytotoxicity can be protected by active antioxidant therapy [339]. Phenolic antioxidants (PA) play an important role in the reduction of inflammatory cytokines by inflammatory stimuli [340]. PA of *Vitis vinifera* acts as a chemopreventive agent by preventing DNA damage induced by mitomycin C. When an antioxidant neutralizes free radicals, it becomes inactive, thereby protects the cells from ROS, which cause excessive oxidative damage to the membrane lipids, protein and DNA [341]. Every cell develops either antioxidant enzymes or non-enzymatic antioxidants based protective mechanism against the ROS generated in the cell. The first line of defensive enzymes are “superoxide dismutase (SOD), glutathione peroxidase (GPx), and catalase (CAT)” and other low-molecular weight antioxidants are ascorbic acid (Vitamin C), α-tocopherol (Vitamin E), glutathione (GSH), carotenoids and flavonoids are shown effective in antioxidant function. Paradoxically, superoxide active sites of dismutase (SOD) and catalase contain metal ions to combat ROS generated by metal ions. Cancer cells, in general, have 10-100 times less catalase than normal cells, requiring them to use externally administered antioxidants such

as vitamin C for repair [337, 342]. Antioxidant treatment can increase hydrogen peroxide levels, and induce cancer cells to undergo apoptosis [343, 344].

In contrast, cancer cells can adapt to increased ROS levels, which promotes cell survival and drug resistance [343, 345, 346]. ROS can alter the genes, which has an important role in proliferation and signal transduction pathways [347-350]. Antioxidant molecules have been extensively studied as biomarkers, targeting agents, and as diagnostic tools in diseases like atherosclerosis, diabetes, and cancer [351-354]. The biological significance of antioxidant peptide is understood by ROS scavenging activity. Peptides are emerging as versatile materials that can be modified to perform specific tasks by functionalization on nanomaterial [355, 356]. Peptides have therapeutic potential due to their small size, biocompatibility and a stability in a wide range of pH in the different solvent *in vitro* and *in vivo* .The therapeutic application of peptide/protein molecules in its native form is difficult limited due to the instability of these molecules in the *in vivo* system. Therefore, the functionalized nanomaterials are attracting more attention, as it can provide stability to the biomolecules. The metal nanomaterials are a choice for the delivery of such molecules, but the toxicity is a major concern. Hence, nanomaterial synthesized based on natural materials such as those obtained from plants, and its derivatives can be explored for biomedical applications as an alternative.

Understanding and controlling bio-Physio-chemical properties of nanoparticles are biological system is a big task. Therefore, it is imperative to develop a suitable biocompatible material for specificity [357] using natural plant products like polysaccharides, phenolics and phytochemicals for the synthesis of nanoparticle [358]. GNPs synthesized using natural polyphenols could reduce the effect of toxic chemicals and

increase the potency of functionalization biomolecules [359-361]. Recently, we have reported the synthesis of GNPs from *Vitis vinifera* L. extract, and showed the dose and time dependent biocompatibility of GNPs with non-cancerous Müller glial (MIO-M1) and breast cancer (MDA-MB-453) cell lines [94]. The inhibitory effect of Resveratrol, a major component of *Vitis vinifera* L. on Y79 (RB) cell proliferation was observed by Sareen D et al. [362]. In this study, an effort has made to synthesize a novel nano-bio conjugate using short peptide (PHCKRM) and GNPs to develop a nanocarrier mediated delivery of peptide. The i*n vitro* functional study was performed using Y79 (RB cancer) cells as a tumor model.

5.2 Materials and Methods

The methodology used for the experiment performed in this chapter has been explained and discussed in detail in Chapter 3. A brief outline of the experiment performed is mentioned in the Figure.5.2

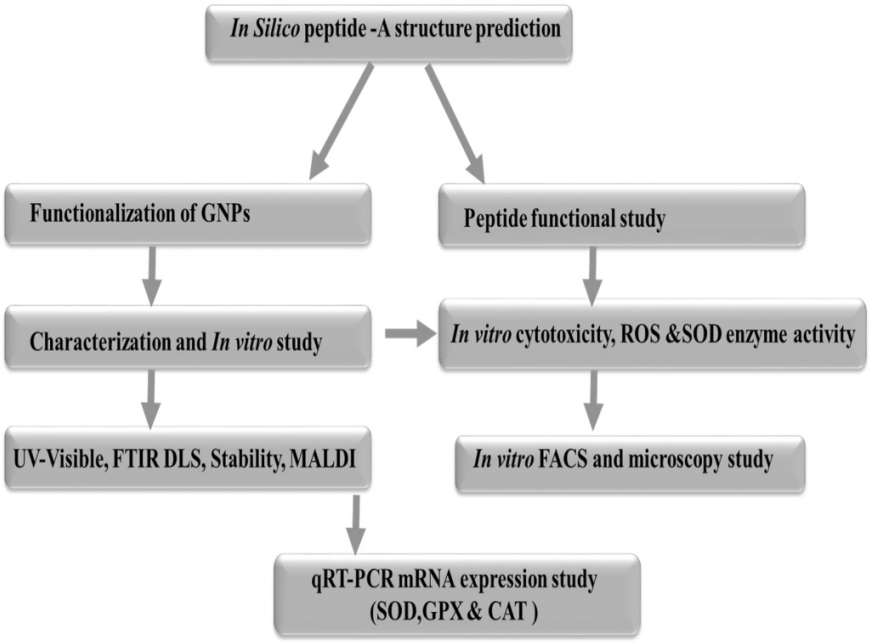

Figure 5.2 Schematic presentation of experiment performed in the chapter

5.3 Results

5.3.1 Structure prediction of the (PHCKRM- Peptide) Modelling and Dynamics

Fasta sequence of the peptide sequence was taken as an input, and a sequence based search against PDB database was carried out using protein BLAST (BLAST-P) search. BLAST-P search was performed using a very low e-value threshold=0. 001 and a threshold of expect (e) -value = 0.001, in order to extract only homologous sequences. From the BLAST-P results, it was observed that the given peptide showed very high sequence identity (83%), and 100% query coverage to the C - terminal Domain of transcription factor IIB from *Trpayanosoma Bruce* (PDB ID: 3H4C).Three-dimensional structure of given peptide was modeled using Modeller 9.12 taking 3H4C as template.

DOPE (Discrete optimal potential energy) score was used to select the best model from the generated 1000 structures. Further, the stability of the peptide structure was assessed by performing molecular dynamics (MD) simulations. Conventional molecular dynamics simulations were carried out using GROMACS-4.5 suit package [363] using the AMBER force field. The system was prepared by solvating the homology modeled structure of peptide in a cubic box of SPCE water molecules. The additional charge on the system was neutralized by adding counter ions (2 Cl^- ions). The neutralized system was then energy minimized using steepest descent and conjugate gradient methods. The stability of the predicted structure was assessed by calculating c-alpha backbone RMSD (Root mean square deviation), grms programme in gromacs was used to plot c-alpha RMSD. Moreover, the potential energy of the structure at all frames were plotted using g_energy programme of gromacs. The conformations with lowest potential energy were averaged to obtain the final optimal conformation. C-alpha backbone RMSD trajectory

analysis of the peptide in simulated conditions suggest the stability of the predicted structure, as it showed least deviation (>1 Angstrom) throughout the simulation (Figure 5.3 a & b). These results confirm the stability of Pep-A through *in silico* approach. Further studies were carried out *in vitro* to demonstrate its chemical and biological properties.

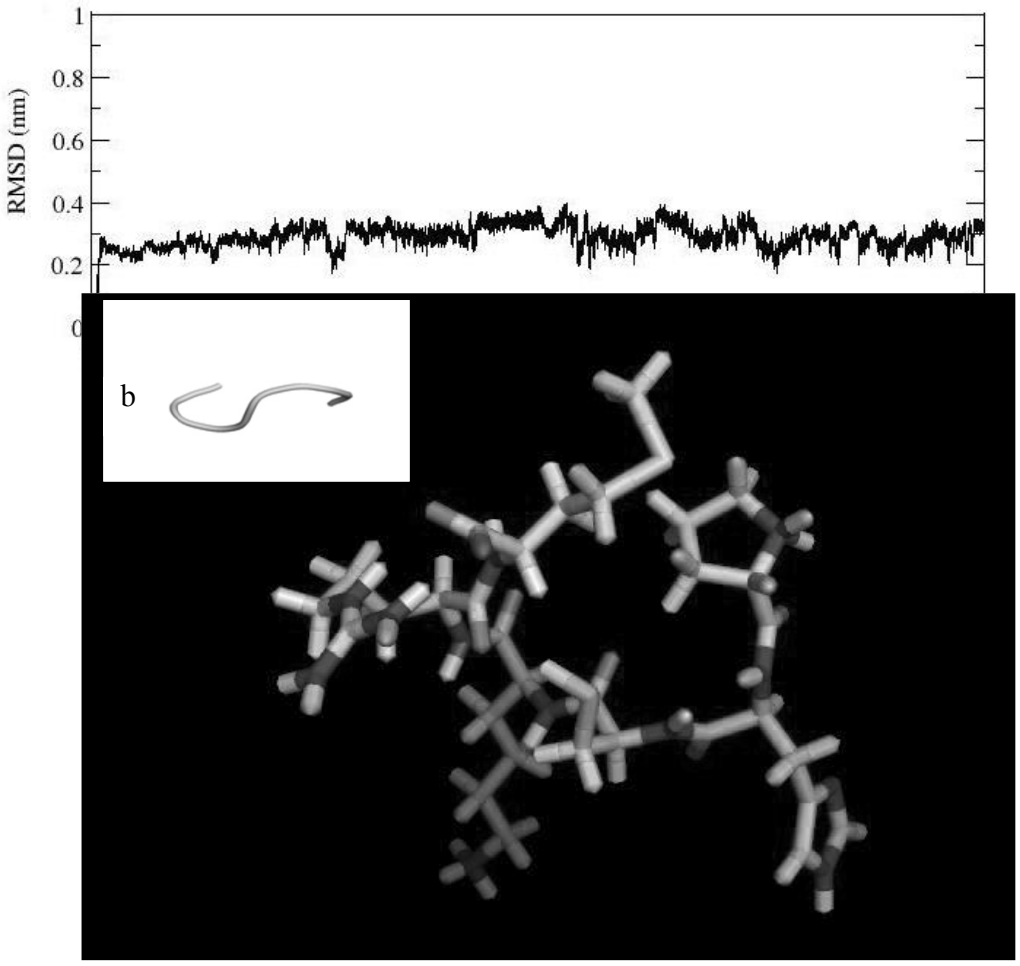

Figure 5.3 a) Showing c-alpha RMSD of peptide structure formed during the course of 50ns simulation, which suggests the stability of the predicted structure to be least deviation (>1 Angstrom) throughout the simulation. (b) Optimal confirmation as averaged from low po potential energy structures from Molecular Dynamics Simulation.

5.3.2 Cytotoxicity (MTT) Assay with Pep-A and Pep-B

Cell viability analysis results showed that the peptide was non-toxic to non-neoplastic (MIO-M1) and cancer (Y79) cells up to 48h of treatment (Figure 5.4 a & c). The Y79 RB cell viability ranged between 115-157% and 111-126% after 24 and 48h of exposure with Pep-A, respectively, with respect to control (untreated cells) (Figure 5.4 a) Whereas, Pep-B showed 89-107% and 93-114% of viability after 24h and 48h (Figure 5.4 b), respectively in Y79 cell line. These peptides were also tested on non-neoplastic MIOM1 cells, which showed an average of 105% of viable cells (Figure 5.4 c). This further confirms that this peptide is not toxic to non-neoplastic MIOM1 cells as well as to the cancer cells. The increased in the cell viability is due to the enhanced mitochondrial enzyme activity, which is more than the control cell and this could be the reason of showing the cell viability more than 100% in peptide treated condition.

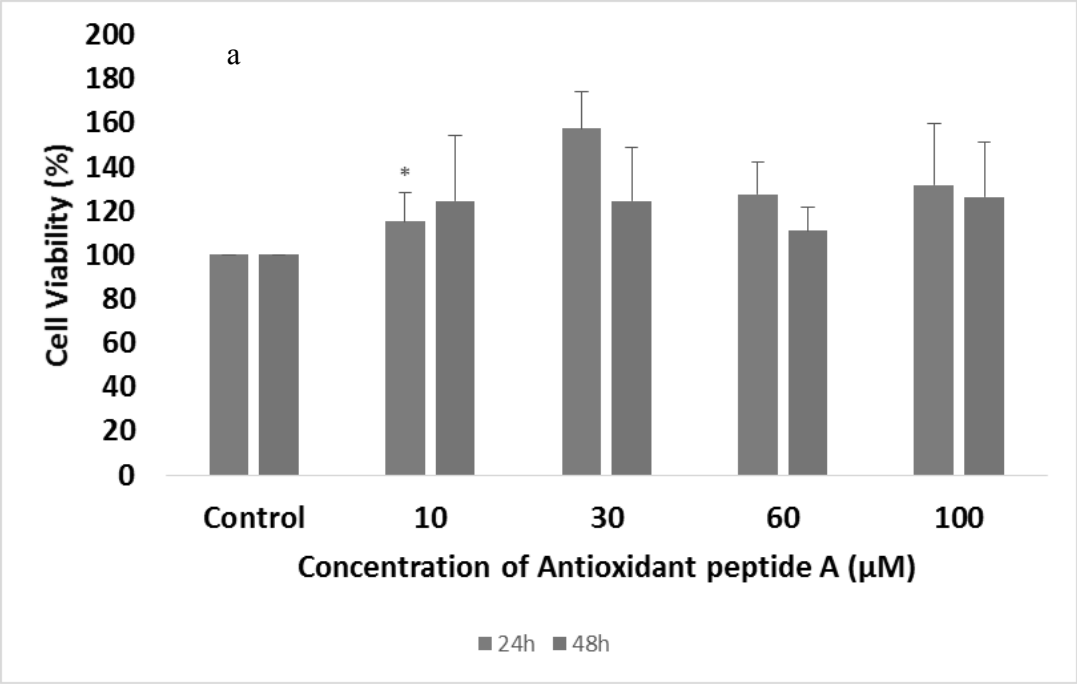

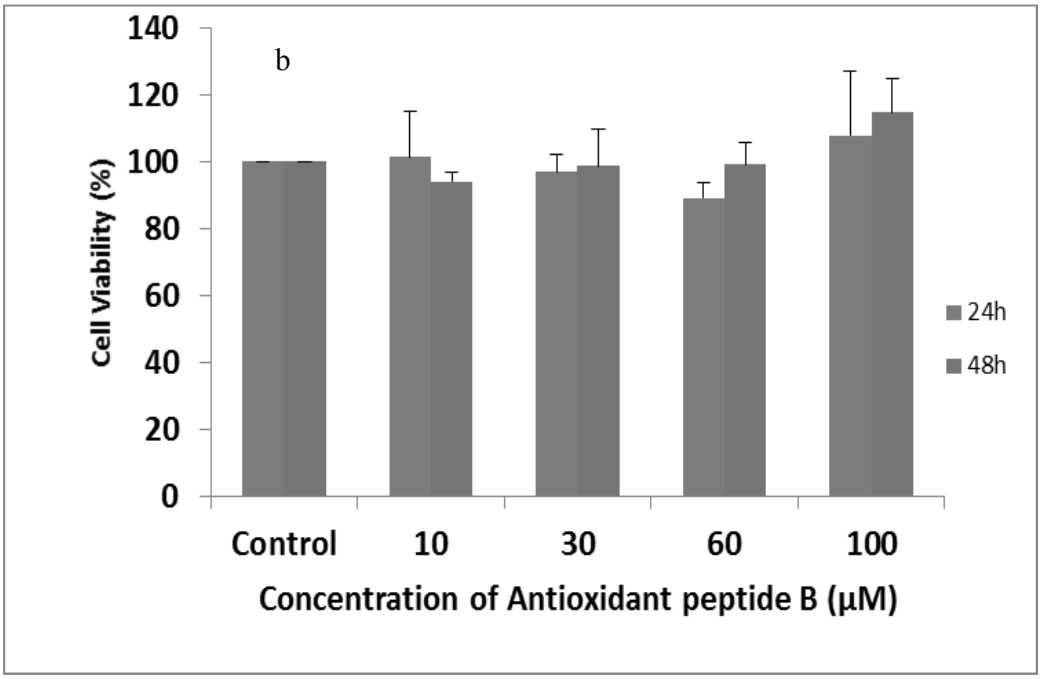

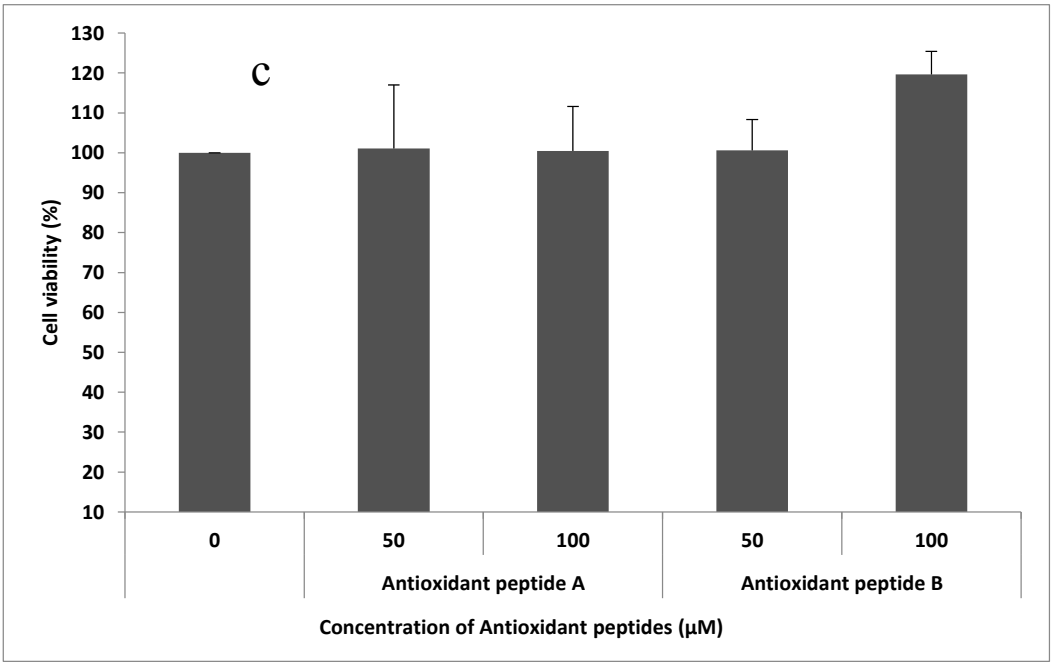

Figure 5.4 Cell viability assay. Effects of Peptide A and B were analyzed at 24 and 48h in Y79 RB cells (a) & (b), and MIO-M1 non-neoplastic cells (c), which were found to show no cytotoxicity in vitro.

* indicates the statistical significant at $P<0.05$ relative to control (without peptide only cells).

5.3.3 Evaluation of intracellular ROS reduction levels upon Pep-A and Pep-B treatment

Proteins and peptides with sulphur containing amino acids and aromatic side chains can protect lipids from oxidative damage [364, 365]. The antioxidant property of the peptides (Pep-A and Pep-B) was determined by inhibition of intracellular ROS with and without peptide treatment. Pep-A showed a dose-dependent inhibition of ROS levels from 4-40% relative to untreated control. In contrast, Pep-B showed inhibition in the range of 32-38%, and the inhibition level was inconsistent (Figure 5.5). Nutritionally, peptides are normally more bioavailable than proteins and free amino acids, and this property enhances their functional specificity [366-368]. Higher inhibition of ROS levels with Pep-A treatment could signify the occurrence of sulfur containing amino acids (Met & Cys) that are involved in the radical scavenging activity compared to Pep-B. Furthermore, a cysteine-containing tri-peptide has been reported to exert peroxynitrite activity [369]. Thiol based antioxidant systems are present in mammals to provide antioxidant functionality that is necessary for disease prevention [345, 359]. Amino acids with aromatic or sulfur-containing side chains are involved in ROS scavenging. For example, “His (imidazole group), Trp (indolic group) and Tyr (phenolic group)” act as a hydrogen donator while methionine and cysteine are hydrogen acceptors [368]. Change in the catalytic activity of cancer cells using antioxidants is a potential approach to cancer therapeutics [245, 370].

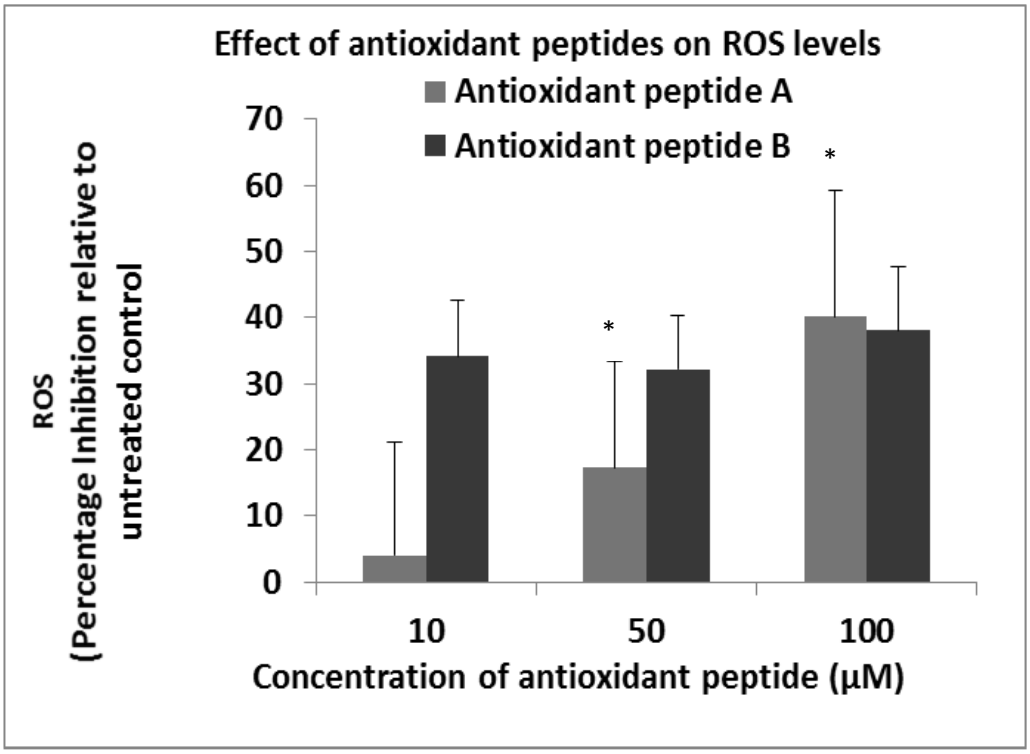

Figure 5.5 Evaluation of Antioxidant activity of Pep-A and Pep-B, Inhibition of ROS and levels by antioxidant peptide. The antioxidant activity of Pep-A and Pep-B was evident from the decrease in ROS levels in Y79 RB cells in peptide treatment. The figure shows the percentage decrease in ROS levels relative to untreated control. Data point indicates ± SEM and * indicates statistical significance at $P<0.05$ relative to 10µM of peptide A

5.3.4 Evaluation of SOD enzyme activity on Pep-A and Pep-B treatment

Superoxide dismutase (SOD) enzyme activity levels decrease with increasing concentrations of an antioxidant peptide from 10-50 µM. At 100µM peptide concentration, SOD activity increased by 1.79 folds for Pep-A, indicating that this is an optimum dose required to exert the antioxidant function (Figure 5.6). Whereas, Pep-B showed concentrations independent SOD enzyme activity in Y79 RB cells. Earlier reports showed on free radical scavenging peptides derived from gelatin hydrolyzate, increased the first line defense antioxidant enzymes suggesting that the peptides it is involved in the maintenance of redox balance [371, 372]. Based on the above results Pep-A was selected for conjugation with GNPs as Pep-A showed effective antioxidant properties compared to Pep-B.

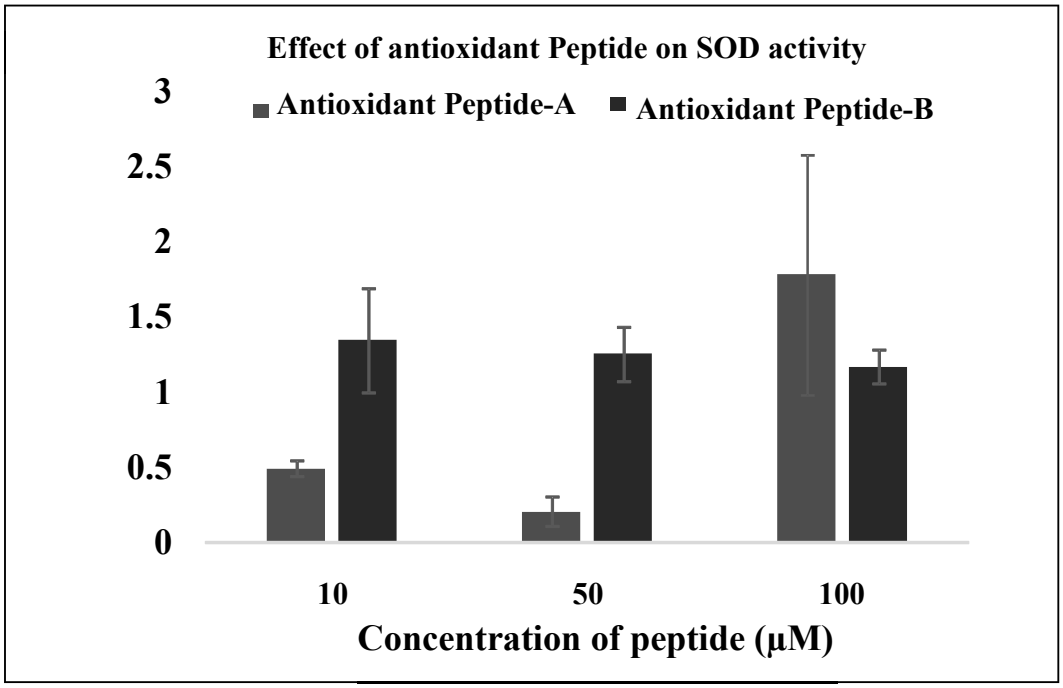

Figure 5.6Antioxidant Pep-A and Pep-B treated Y79 RB cells.

The initial decrease in SOD activity, when treated at 10-50µM and as 100 µM the enzyme activity increased. SOD activity was calculated as an inhibitory activity of xanthine oxidase and depicted as increase /decrease relative to untreated control. The data indicates a mean of two or more independent experiment Error bar is ± SEM of duplicate values.

5.3.5 Uptake of Pep-A, GNPs-Pep-A, and GNPs

The Peptide-A (Pep-A) uptake was measured by the FACS (fluorescence activated cell sorter) in Y79, a RB cell line. The FACS analysis results for Pep-A showed a concentration dependent uptake into the Y79 cells. The histogram statistic indicates that there is a significant shift in the FITC positive population (Figure 5.7 a, X-axis) from M1 to M2. In the control samples (cells without Pep-A) shows M1 population 99.99 whereas the M2 population is 0.01 whereas in the case of 50μM of Pep-A, M1 population 99.97 whereas the M2 population is 0.03. Similarly, 50μM of Pep-A shows M1 population 99.95 and the M2 population is 0.05. The shift of the population from M1 to M2 in the peptide is an indication of the peptide internalization. In addition to the histogram statistic, overlay graph (Figure 5.7 b) further confirms the concentration-dependent internalization of the peptide into the Y79 RB (Figure 5.7 b). The increase in the number of counts (Y axis, Figure 5.7 b), as well as the FITC positivity M2 population, compared to the control, indicates that peptide is internalized by the Y79 cells[373]. It has been reported that the uptake of the peptide is mainly by CPP (cell penetrating peptide) that follows the endocytotic pathways, endocytosis, macropinocytosis and clathrin-mediated endocytosis. The proteoglycan contributes mostly for internalization of the peptide by increasing the concentration of the peptide at the membrane surface by enhancing recruitment of peptide via electrostatic interactions and helps in the reorganization of the F-actin to facilitate the internalization of the peptide [374, 375]. The amino acid composition also significantly alters the internalization of the peptide [376]. Arginine is an important amino acid, which enhances the internalization of the peptide, this could be due to the cationic nature of arginine, which disrupts the membranes of macropinosomes and this may lead the peptides into the cytosol. Alternatively, hydrophobic counter-anion molecules may help the

translocation of arginine peptides into the cytosol. In the case of Pep-A (PHCKRM) the P (Proline) and M (Methionine) amino acid are hydrophobic in nature which could help in internalization of peptide in addition to the arginine (R) [377].

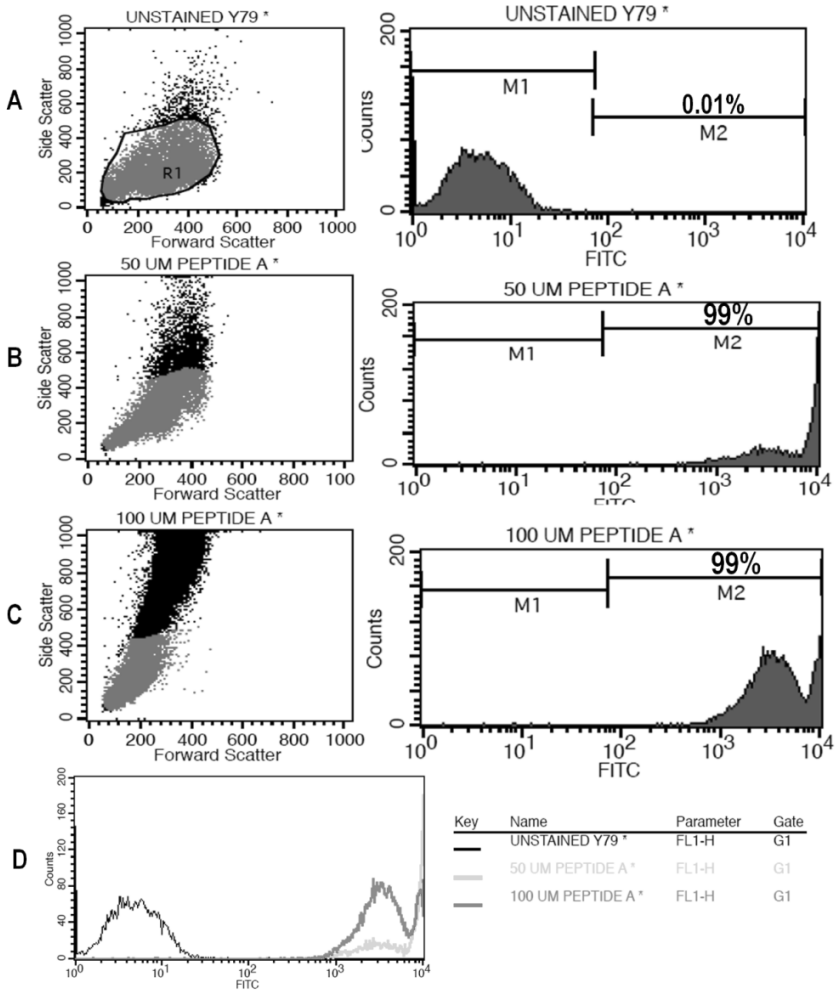

Figure 5.7 FACS, the histogram showed the FITC positive population in untreated (a) and treated (Peptide-A) Y79 RB cells. Cells treated with 50 and 100 µM of Pep-A showing maximum 99% of the FITC positive population in M2. d: Overlay picture shows concentration dependent peptide uptake of the peptide**.**

5.3.5 GNPs-Pep-A (conjugate) characterization

5.3.5.1 UV-Visible Spectroscopy and DLS

UV-Visible was performed confirming the presence of the peptide on the GNPs (Figure 5.8 a & b). The surface plasmon resonance (SPR) absorbance band peak of GNPs shows a Red shift at 540nm after the addition of Pep-A (Figure 5.8 a). The arrow indicates the SPR band of the GNPs. The similar red shift was observed in surface plasmon absorbance peak observed after the binding of cysteine molecules to the GNPs. The red shift in plasmon absorbance is attributed to the presence of peptides on GNPs [378, 379] .

The hydrodynamic size of the conjugate has changed since 49.6±0.4 to 91.7±1.17, which is likely to because of the peptide on GNPs rather than from the aggregation of GNPs (Table.5.1). The zeta potential of the GNPs-Pep-A (-26.5±0.2) is larger than that of GNPs alone (-22.5±0.2) indicating a greater stability of these nanoparticles than the GNPs *in vitro.* The absorbance, hydrodynamic size, its distribution and increase in zeta potential indicate that the conjugate is very stable. The size of GNPs (%, number distribution) of GNPs-Pep-A in the range of 25-60 nm whereas V-GNPs in the range 15-35 (Figure 5.9b inset). The increase in hydrodynamic size (GNPs are 49.6 ± 0.4 and the size increased to, 91.7 ± 1.7 in GNPs-Pep-A) and % number distribution is due to the presence of peptide molecules capped on the surface of the GNPs (Table.5.1). The DLS measurements (Figure.5.8b) indicate a mono-dispersion of GNPs-Pep-A in the solvent water [380]. A similar study using bombesin peptide conjugated with GNPs is reported earlier. The concentration of bombesin peptide increased the hydrodynamic size of the nanoparticles

(Au–BBN-1 115, Au–BBN-2 137, Au–BBN-3 155, whereas the core size of particles was ported as 16 ±7 nm [381].

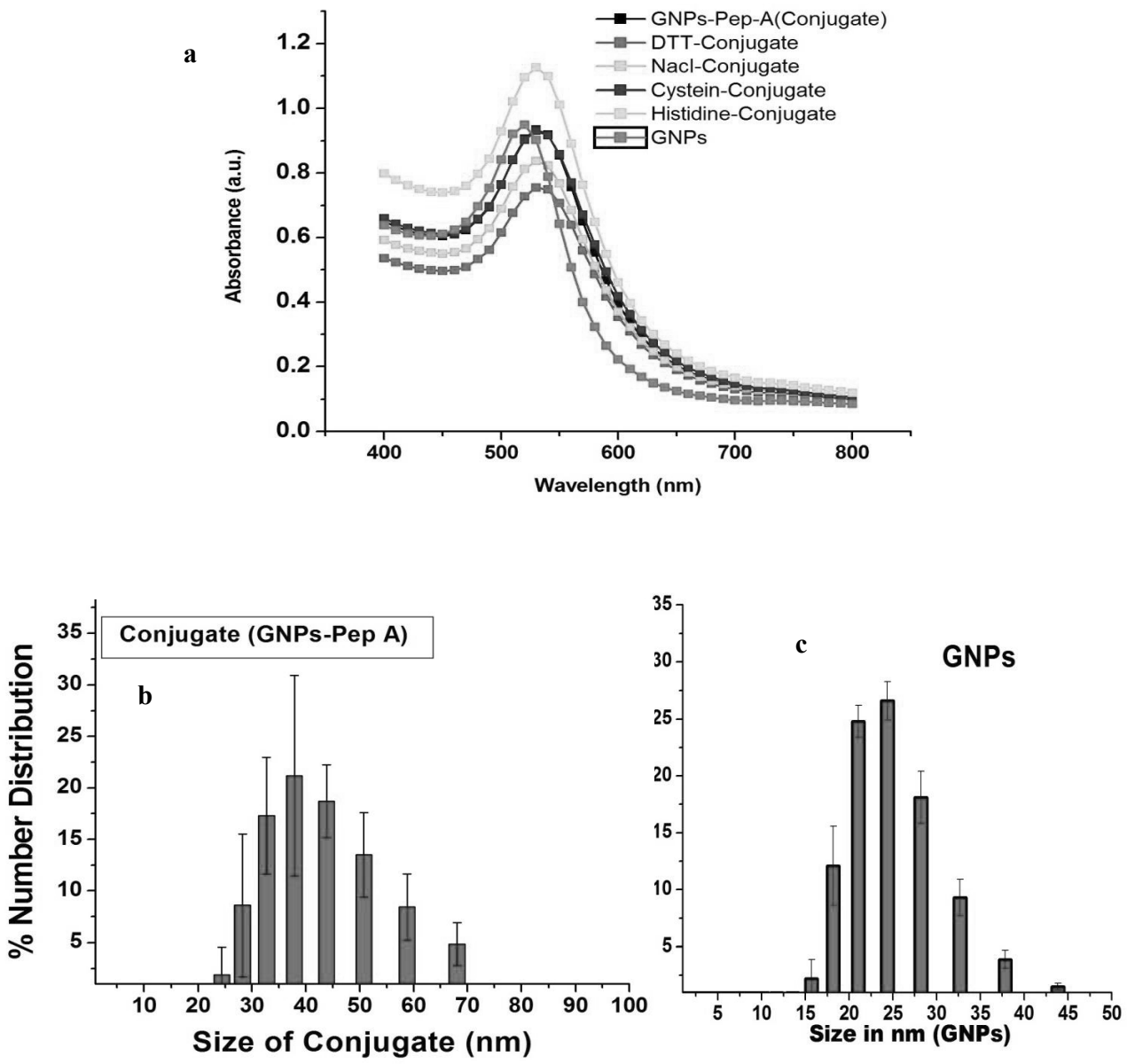

Figure 5.8 The graph shows a shift in SPR for GNPs-Pep-A.

(a) GNPs-Pep-A stability of conjugate in different solvents. Black which is actually not visible, but is merged with blue line and for GNPs-Pep-A in the different buffers did not alter the shift which confirms the stability of the conjugate in vitro, (b) Size distribution of GNPs-Pep-A. (c) Size of GNPs.

5.3.5.2 Stability analysis of the GNPs-Pep-A in various biological solvent

The stability of the GNPs-Pep-A was tested in different solvents using UV-Visible spectroscopy and DLS measurements (Table 5.1). The absorption peak of GNPs-Pep-A at 540 nm remained unaltered in various solvents except histidine (Figure 5.9a) and zeta potential has been altered all the solvent except NaCl. The Zeta potential of the GNPs and GNP-Pep-A increased from -22.5±1.77-26.5±2.02, respectively (Table.5.1). The increased zeta potential of the conjugates indicates that there is no aggregation occurring. However, the sulfur containing amino acid cysteine and DTT also increased the zeta potential to -36.96±1.17 and -35.4±3.95, respectively. This increase in absorbance with histidine indicates its binding with GNPs-Pep-A hybrid could be due a positive charge on a histidine imidazole functional group which changes its binding affinity with the metal nanoparticles [382]. The zeta potential of GNPs-Pep-A-His is also higher (-32.0±0.25) than GNP-Pep-A indicating a greater stability in this solvent (Table 5.1). Even the ionic strength salt such as NaCl does not alter the zeta potential due to an electric double layer of the GNPs and decreases the probability of the salt Na^+ ions to cause any aggregation to the hybrid [383, 384]. Thus, the GNPs-Pep-A is stable in various biologically relevant solutions, making these agreeable for their potential applications.

Table 5.1 Effect of different solvents on stability of GNPs-Pep-A

Sample	**Zeta Potential (mV)**	**DLS Size (HD- Hydrodynamic)**
Conjugate (GNPs-Peptide A)	-26.5± 2.02	91.17± 1.17
DTT + Conjugate	-35.4± 3.95	92.36 ± 0.30
NaCl + Conjugate	-22.6± 1.98	89.48± 0.31
Cysteine + Conjugate	-36.96± 1.17	91.05± 0.99
Histidine + Conjugate	-32.0± 0.25	95.96± 0.88
GNPs	-22.5± 1.77	49.6± 0.4

5.3.5.3 FTIR and MALDI characterization

The Pep-A attachment to GNPs is either by covalent or electrostatic attraction. This is evaluated by using FTIR vibrational spectroscopy as this method gives specific vibrational patterns for the ligand bound to GNPs [385]. Spectroscopic analysis of GNPs-Pep-A by FTIR (Figure 5.9) showed specific vibrational bands at 3446-2365 cm^{-1}, 2620 cm^{-1} and 1641-663 cm^{-1}. The presence of 1641 and 1669 cm^{-1} bands of Pep-A and GNPs-Pep-A confirms the presence of the amide bonds. The peptide coating on the GNPs exhibited a characteristic IR band at 3448 cm^{-1}, indicating the presence of O-H and COOH functional group, whereas, 2920 and 2854 cm^{-1} can be assigned to the symmetric and anti-symmetric vibration bands for CH_2 and CH_3 group and C=O stretch of an amide I. In a study, COO^- band assigned in 1600 and 1390 $cm^{-1}$are asymmetric and symmetric whereas a band at a broad range 3000–3500 cm^{-1} range was assigned for $NH_3^+$of amino acids.

The FTIR spectral differences between Pep-A and GNPs-Pep-A (conjugate) corroborate with the DLS and UV-visible data. Specifically, FTIR data show a shift in wave number from 1641 for Pep-A to 1669 for the GNPs-Pep-A conjugate, this shift in amide bond could be due to the SPR effect of GNPs on the amide bond for the conjugate. The peak at 2129 cm^{-1} in the spectra of the conjugate indicates Au-S bond formation after Pep-A conjugation. The spectrum of Pep-A conjugated with GNPs is quite different from that of GNPs alone (Discussed in Chapter 4) and Pep-A alone (Figure 5.9). The GNPs-Pep-A nanoparticles showed a significant peak shift from 1641 to 1669 cm^{-1} when compared to Pep-A alone indicating an effect of metal surface on selective surface–induced functional group shift. A similar changes in vibrational modes in the presence of metallic nanoparticles are observed before [386]. The shift in the vibration peak intensities may indicate covalent binding of Pep-A to the GNPs to form GNPs-Pep-A nanoparticles [380].

The peak at 2129 and 2365 cm^{-1} in the spectra of the Pep-A indicates a S-H bond in the peptide molecule whereas the disappearance of these peaks in GNPs-Pep-A may suggest the absence of S-H bonds and the presence of the Au-S bond.

The GNPs-Pep-A was characterized by the mass spectroscopy to detect the additional mass of the peptide from GNPs-Pep-A nanoparticles compared to GNPs alone (Figure 5. 10 a & b). The Au metal is confirmed by the presence of spectral peak masses in 1379.74, 1576.77 and 1772.98 which indicate Au_7, Au_8 and Au_9 gold clusters, respectively [239, 240]. The presence of peptide mass (959.47) apart from the gold clusters indicates the presence of the Pep-A in GNPs-Pep-A nanoparticles.

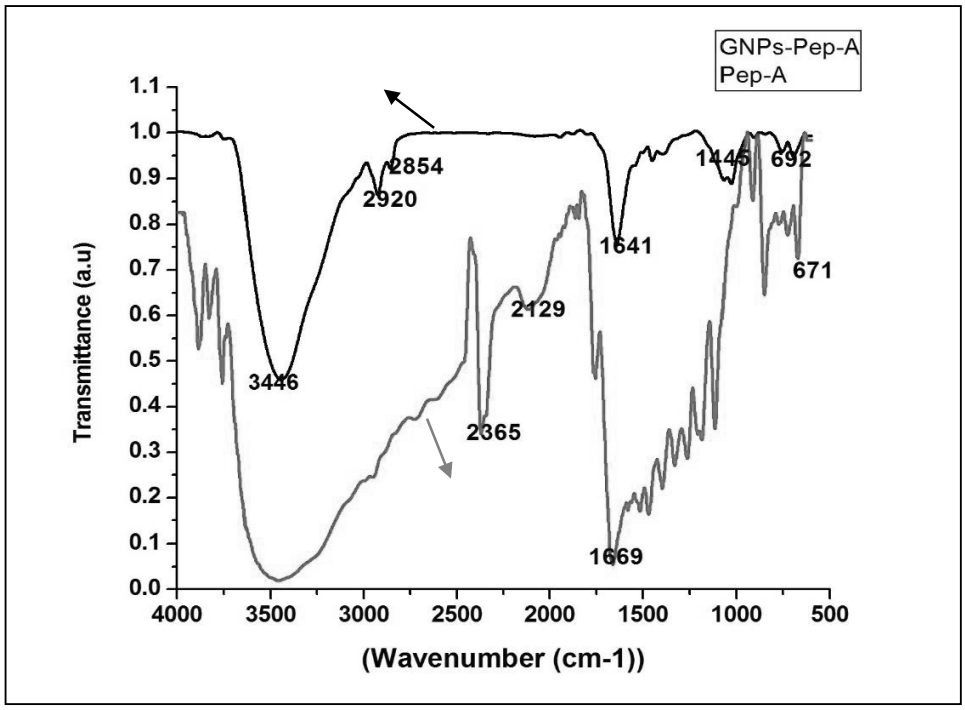

Figure 5.9 The FTIR spectral of the VGNPs-Pep-A and Pep-A conjugate formation. Disappearance of 2365 cm-1 and SPR shift of 1669 cm-1 to 1641 cm-1 along with the spectral difference indicates the formation of the bond between GNPs-Pep-A.

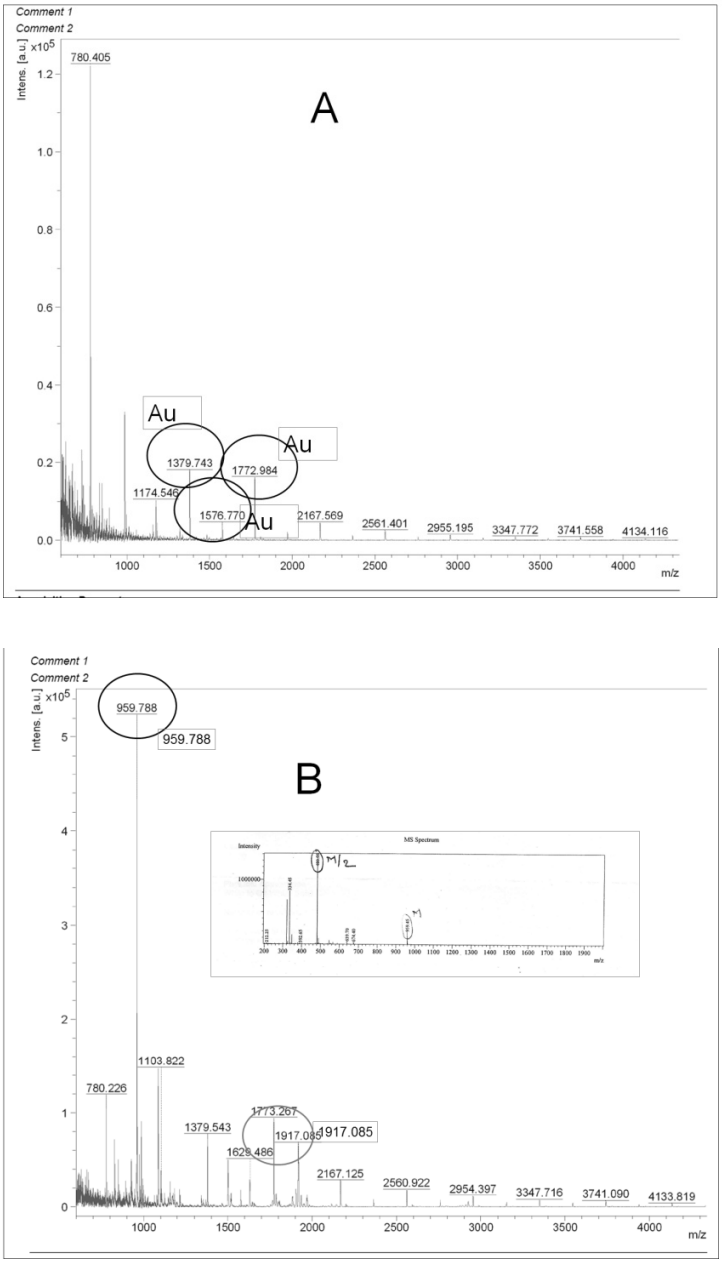

Figure 5.10 MALDI spectra of the GNPs (A) GNPs-Pep-A (Inset-Pep-A). The Au7-9 cluster confirmed the presence of gold atoms and highlighted peak confirms the presence of the peptide on GNPs (B). The molecular weight of Pep-A is 959.80 (Inset).

5.3.6 Internalization and morphological study

The internalization of the nanoparticles is further visualized by the presence of red fluorescent signal from the cells treated with the R6G dye doped GNPs and GNP-Pep-A1 nanoparticles (Figure 5.11). The R6G doped GNPs had been successfully used as a fluorescence sensor to detect heavy metals [387]. In our current results, the GNPs (Figure.5.11c & d) and GNPs-Pep-A1 (Figure 5.11) shows the red fluorescence of the R6G dye on V-GNPs. However, when FITC conjugated peptide was attached to the GNPs, green fluorescence of the dye was not observed (Figure 5.11). The fluorescence quenching could be the reason of disappearance of FITC signal, which is due to the proximity of the metal atoms in GNPs. [388]. The optical microscopic images of Y79 (RB) cells treated with the peptide, GNPs and GNPs-Pep-A1 (Figure 5.11) show the morphological changes compared to the untreated cells. The cells treated with the peptide alone (Figure 5.11) have a similar cell surface morphology as the control untreated cells (Figure 5.11) whereas the cell morphology treated with GNPs and GNPs-Pep-A1 showed significant differences. The cell fragments were observed, indicating apoptotic bodies formed during the process of membrane blebbing (Figure 5.11c & f). The cell membrane blebbing, clustering of cells, shrinkage, change in size and condensation of the cytoplasm is in accordance with apoptotic or necrotic cell death, are most commonly observed microscopic features. [7, 389, 390]. The better performance of the GNPs and GNP-Pep-A compared to the peptide alone in cell death the cells indicate the potential application of the nanoparticles for cancer.

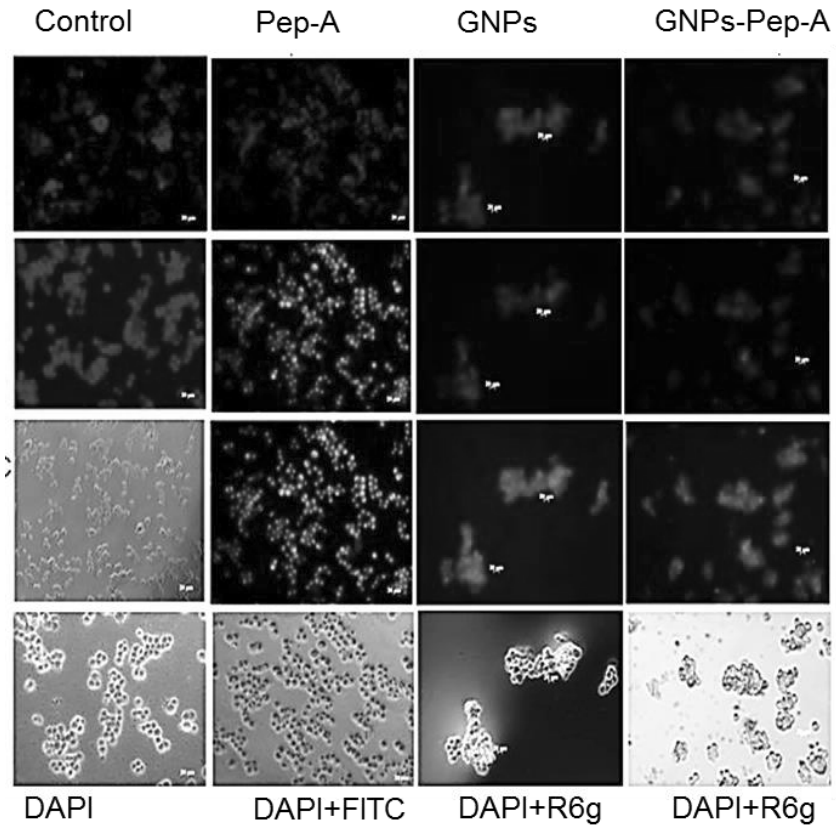

Figure 5.11 Micrographs showing internalization of FITC labeled peptide Pep-A after 3h of treatment in Y79 RB cells. First panel: Control, second panel: Pep-A, third panel: GNPs, fourth panel: GNPs-Pep-A. Magnification 10 x Magnification: 10X (Scale bar: 10μm)

5.3.7 ROS scavenging and SOD enzyme activity of GNPs and GNPs-Pep-A

GNPs-Pep-A1 (100μM of Pep-A) and GNPs-Pep-A2 (250μM of Pep-A), have used for ROS measured in Y79 a RB cell. In the case of GNPs-Pep-A1 ROS levels decreased significantly (75% at $P<0.05$) compared to GNPs alone (9%) (Figure 5.12a). The peptide concentration on the GNPs was increased to 250 μM (GNPs-Pep-A2) to study the concentration-dependent effect on ROS inhibition. There was a 66% decrease in ROS production at this concentration. Very high dosages of antioxidant Pep-A may prevent them from exerting their antioxidant action, and it may also alter the biological redox state. Combination therapy with multi-scavengers and sustained release formulations are

suggested for antioxidant therapy [336]. Therefore, 100 μM of Pep-A could be the optimum dosage, which showed (Figure 5.5) about 30-40% decrease in the ROS production. The GNPs-Pep-A1 nanoparticles were more efficient at scavenging ROS than their individual component GNPs and Pep-A (Figure.5.12a) indicating a synergistic antioxidant effect due to the combination of the two metals and organic phases in the conjugate. After confirming the effectiveness of ROS inhibition with the GNPs-Pep-A1 and GNPs-Pep-A2 for the SOD enzyme activity for GNPs-Pep-A1 was selected which shows 81% SOD enzyme is reduced compared to 61% for the untreated control, implying that the innate antioxidant defense function of the SOD enzyme is reduced by GNPs-Pep-A1. The 20% reduction in the SOD activity in GNPs-Pep-A1 could be the synergistic effect since GNPs alone showed 70% reduction in SOD activity compared to the control (Figure 5.12b). The SOD enzyme activity inhibition in both; GNPs and GNPs-Pep-A1 could be attributed to the presence of polyphenols on the GNPs and Pep-A in conjugate (GNPs-Pep-A) [391].

The presence of alternating aromatic and cationic amino acids also provides effective antioxidant properties and efficient membrane penetration .The supramolecule system utilizes monolayer protected gold nanoparticles (GNPs) and the antioxidants improves its functionality, which is consistent with the assertion that the organic molecules in organized assemblies have a reactivity enhanced than the monolayer as an individual layer. Thus, the constituent amino acids in a peptide determine its effectiveness [369, 393]. Au@Trolox, an organic drug, organic, inorganic nano composite is 8 fold more reactive than the with the Trolox monomer, indicating that the cooperative effect of supra-molecular assemblies to increase the free radical scavenging. Trolox is water-soluble analog of

vitamin E and functions as an antioxidant, supporting the current findings that not only the peptides but other antioxidant molecules perform better in organic-inorganic hybrid form. Reactive oxygen species (ROS) are formed as a by-product of normal cellular metabolism as well as physical stress to the cell. ROS damage DNA, oxidizes amino acids and lipids, and inactivate essential enzymes. Cells scavenge these species with the help of first line defense enzymes: GPX, CAT, and SOD. Resveratrol is known for its antioxidant function and the peptide under the current study (PHCYAM) is an antioxidant peptide [394]. The antioxidant effect of total polyphenolic content (TPC) of *Vitis vinifera*, shows antioxidant effect in (HepG2) and cervical (HeLa) cancer cell against oxidative DNA damage caused by the ROS. It has been shown that polyphenolic also inhibited OH- and ROO-induced DNA damage in the cancer cell [395].

Cancer cell shows intrinsic oxidative stress, which hindered the action of the anti-neoplastic, hemotherapeuticals agent and inactivate caspases . Similarly, polyunsaturated fatty acids, which are in use along with chemotherapy can cause oxidative stress [396, 397]. Antioxidant can help in reduction of oxidative stress by enhancing the apoptosis in the cancer cell and oxidative stress, which may further help in enhancement of cancer therapy [398, 399]. Similarly, polyunsaturated fatty acids which are in use along with chemotherapy can cause oxidative stress which can reduce by antioxidants to prevent polyunsaturated fatty acid-induced oxidative stress may further enhance the impact of cancer therapy [401, 402].This finding confirmed that antioxidant therapy might be advantageous. Trolox, with arsenic trioxide has shown to induce the ROS mediated cell death of some types of cancer, such as leukemia, myeloma, and breast carcinoma, etc. In addition to this, vitamins are known for its antioxidant activity, one such

example is vitamin C enter via glucose pumps which highly expressed in cancer cells and enhanced the cancer cell apoptosis [272]. Similarly, Menadione and Thioredoxin,, a synthetic derivative of vitamin K which induces cytotoxicity in cancer cell induced by the ROS [400]. The action of thioredoxin can enhance the cytotoxicity effect of daunomycin in human breast carcinoma MCF-7 cells. The current findings indicate that antioxidant molecules can be used to target cancer cell. Apart from targeting ROS, an antioxidant enzyme up regulation also used for antioxidant molecules based cancer therapy [401-404].. The SOD enzyme which is known for the oxidative stress modulator which target the superoxide [401]. The up regulation of the SOD in GNPs-Pep-A condition confirms that the antioxidant function of the peptide which is due to enhancing the antioxidant function of peptide tagged GNPs. On the other hand, the down regulation of SOD in case of GNPs treated cells confirmed that nanoparticles can induce the oxidative stress, which has confirmed *in vitro* using different types of inorganic nanoparticles [402-404].

5.3.8 Quantitative mRNA expression study

Quantitative real-time PCR analysis of GPX, CAT and SOD in the Y79 cells treated with GNP and GNPs-Pep-A1, showed 2 fold down-regulation of SOD and GPX and 2.7 fold down-regulation of CAT enzymes (Fig.5.12c) GNPs-Pep-A1 showed 2.1 fold up regulation of CAT and SOD and 2.5 fold up regulation of GPX enzyme gene expression. The current results indicate that polyphenols from grapes are synergistically acting with Pep-A. It has been reported that Resveratrol, a key component of *Vitis vinifera* controls apoptosis and regulate antioxidant enzymes in cancer cells, and this could increase apoptosis in Y79 cells [372]. Cells scavenge ROS species with the help of first line defense

enzymes. The results indicate that polyphenols from *Vitis vinifera* are synergistically acting with Pep-A to decrease the oxidative stress in the Y79, RB cells *in vitro*.

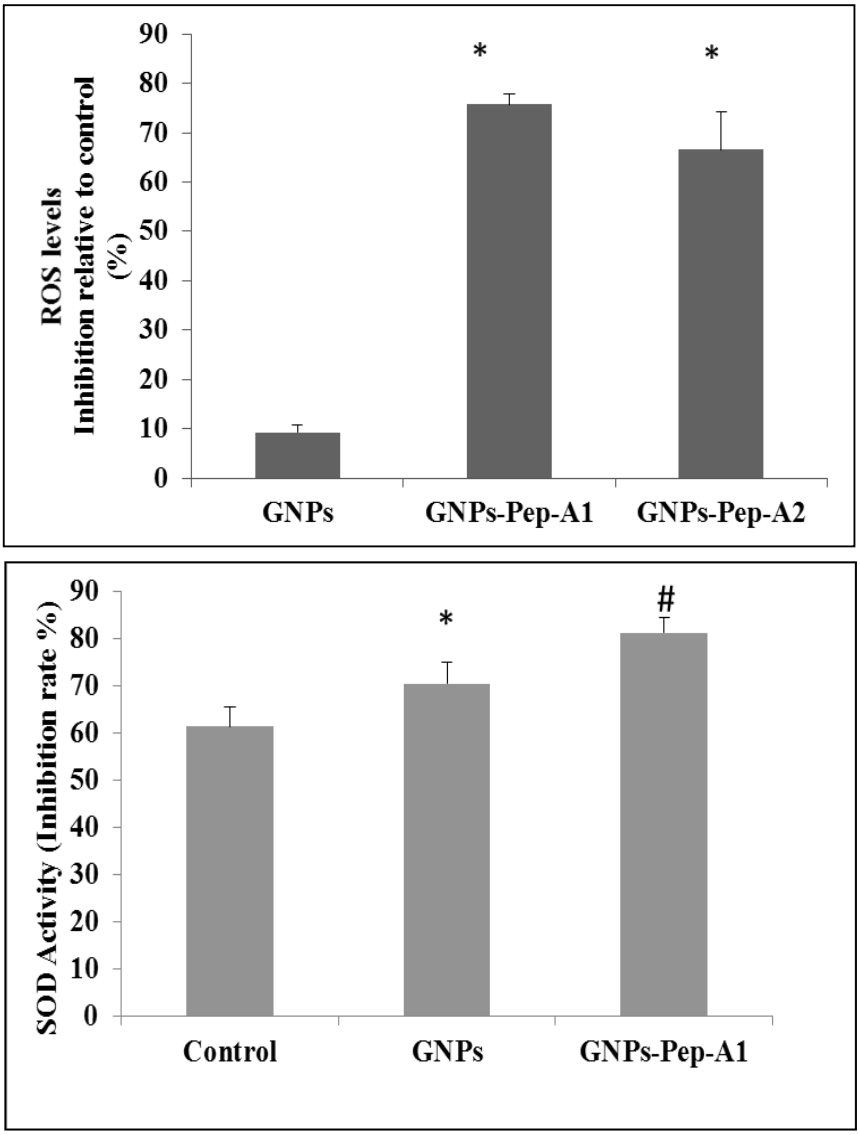

Figure 5.12 GNPs-Pep-A1 ROS, and SOD effect.

ROS decreased the ROS levels in Y79 RB cells adequately compared to GNPs alone and peptide alone (Figure 2a). The final concentration 50 µM of GNPs (Moles of gold) was used for functional study. GNPs-PepA_1 and GNPs-PepA_2 contain the final concentration of Pep-A is 100 and 250 µM, respectively. Each column indicates mean percentage inhibition of ROS levels from triplicate values relative to untreated cells. Error bars: SEM of triplicate values. (b) GNPs-Pep-A1 increased the SOD enzyme activity by 1.3 fold compared to 1.1 fold increase by GNPs alone. Each column indicates SOD activity (inhibition rate %) from triplicate values. Error bars indicate SEM from triplicate values. * Represent the statistical significant compared to control at $P<0.05$; # represent the significant difference relative to GNPs at $P<0.05$.

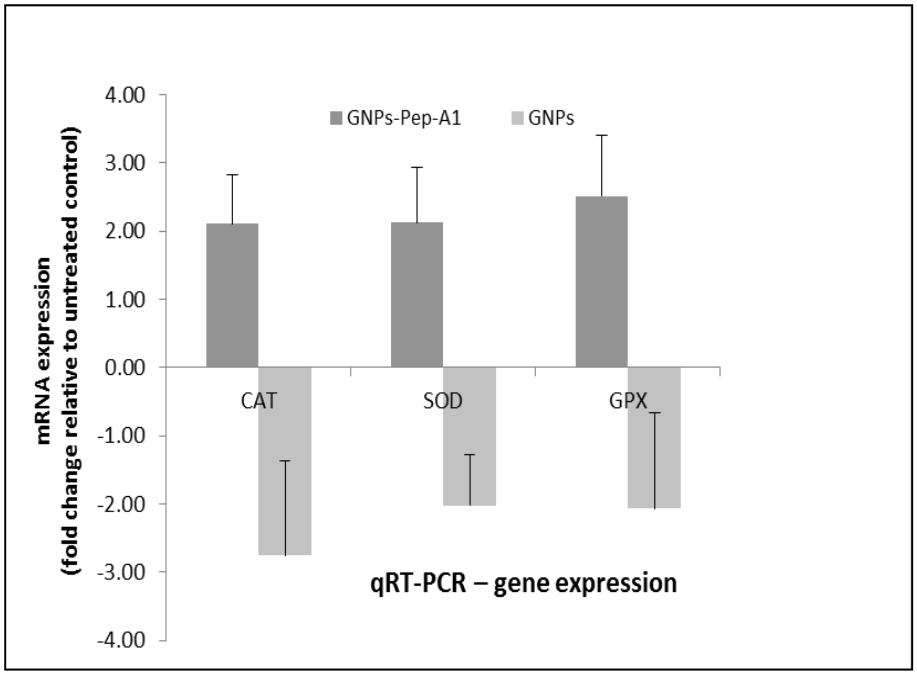

Figure 5.13 C) Y79 RB cells treated with GNPs and GNPs-Pep-A were analyzed for mRNA expression of first line defense antioxidant enzymes.

GNPs and GNPs-Pep-A down-regulated and up-regulated the SOD, GPX and CAT enzyme gene expression levels respectively. Each column indicates mean ±SEM of duplicate values.

5.4 Discussion

The results obtained in the current study is discussed to understand the organic-inorganic bio conjugates functional properties, with a particular focus on ROS scavenging property of Pep-A and GNPs-Pep-A. Nanomaterials are in use for a wide range of application, which includes biosensor, drug delivery, imaging and therapy [405, 406]. The bio-functionalization of nanoparticles requires particular modification which confers them with specific functionality. The proteins or peptides are of specific interest as because it helps in internalization of the gold nanoparticles. The multi-functional nanoparticles have an added advantage due to its unique coating and reduction of the metal ion exposure to cells directly.

It has been reported that the organic-inorganic hybrid material retains its original property along with the improved properties such as stability, thermal behavior, aqueous solubility and additional novel properties are introduced in conjugated material which shows the synergistic effect of the hybrid materials [407]. The assembly and degree of organization between targeted moiety and nanomaterial not form hybrid material and improve the functional property of material in terms of structure, function, dimension and availability of the materials at the interface. Therefore, it is imperative to develop suitable biocompatible nano-materials for specific applications [357, 408, 409]. The gold nanoparticle has many therapeutic applications due to its unique biocompatibility property, which increases its application as a delivery and next generation imaging agent. Nanotechnology can open novel avenues by target specific delivery of these antioxidants to the cancer cell through nano carrier to target ROS in a cancer cell. Small antioxidant peptide (Peptide-A) which contain alternative aromatic or sulfur-containing amino acid side chains are hypothesized to enhance the radical scavenging property of Pep-A and can regulate oxidative stress (Figure 5.5) [185]. However, the stability of peptides in the body fluids is of great concern, therefore, nanoparticles for delivery of peptide improve the delivery and target therapy. The conjugation of biomolecule on the inorganic nano materials generates hybrid material with very specific interaction with the targeted group by ligand exchange, electrostatic adsorption and non-covalent interactions [40]. Here we have used a tri conjugate approach to increasing the stability and therapeutic efficacy to target ROS in the cancer cell. Tri-conjugate prepared by conjugation of GNPs with thioctic (TA) acid, modified Pep-A and GNPs used in the conjugation was synthesized by *Vitis vinifera,* known for antioxidant and anticancer property [410]. The bio-inspired GNPs

synthesized using natural polyphenols could reduce the effect of toxic chemicals, inherent metal toxicity and increase the potency of functionalized molecules through change in the reactivity due to co-existence of different phases in a conjugate [361, 411, 412].

The improved functional activity of the novel hybrid nanomaterial is assessed by studying cancer cell death by controlling the oxidative stress in RB cancer cells *in vitro*. Thiol based antioxidant systems are present in mammals to provide antioxidant functionality that is necessary for disease prevention [359]. The change in the catalytic activity of cancer cells using antioxidant peptide is an efficient approach for cancer therapeutics [370]. The GNPs synthesized from polyphenols are self-therapeutics as it would function as an antioxidant and anticancer agent due to coating of these compounds on the GNPs [413, 414]. The organic-inorganic combination in hybrid not only provides the stability to the conjugated peptides but can introduce the new functionalities and stability to the biomolecule [131, 415].The final material could gain the large synergistic effect due to their coexistence of the two phases and their interaction though the size and chemical reactivity of individual can be altered [416]. Moreover, resveratrol an essential compound in *Vitis vinifera* L. present on the GNPs as a coating, has been reported as an anticancer molecules that lead to the apoptotic cell death of retinoblastoma cells [362].

Earlier the functionalized GNPs have been reported as anti-cancer and antioxidant bio-functionalized nanomaterial [417, 418]. Modification of the GNPs with smaller molecules such as peptides and proteins determines its interaction and stability in biological system. The current findings give an insight that V*itis vinifera* coated and reduced GNPs can be a candidate material for the antioxidant peptide delivery. Our findings confirm the stability of Pep-A by *in silico* studies, and its antioxidant activity in

the biological system. The dose-dependent increase in ROS inhibition and modulation of SOD enzyme activity was observed after treatment with GNPs-Pep-A treatment, which greatly enhanced the Pep-A antioxidant efficiency. Thus, antioxidant peptides conjugated with GNPs may be a candidate biocompatible hybrid nanocomposite for therapeutic application. With research evidence of oxidative stress and its contribution to RB pathogenesis, we evaluated the effectiveness of this novel GNPs-Pep-A using retinoblastoma as a tumor model. There is promising scope for further research on evaluating antioxidants in cancer therapy in combination with self-therapeutics or GNPs and chemotherapeutic agents.

5.5 Chapter Summary

- Antioxidant peptide (A & B) up to 100μM found nontoxic to the RB (Y79) and non-cancer cell (MIO-M1) cells.
- The inhibition of ROS is more effective in GNPs-Pep A conjugate compared to GNPs and peptide-A, alone. The gene expression results confirm that the first line defense genes are altered in the GNPs-Pep A treated condition.
- SOD activity and ROS levels were altered after treatment with the GNP-Pep. The GNPs-Pep A, regulate the expression of antioxidant gene SOD, CAT, GPX. The increase the antioxidant activity of GNPs-Pep-A leads to Y79 RB, cancer cell death by ROS scavenging activity

CHAPTER 6

6 *In vitro* and *in vivo* preclinical study for tumor growth inhibition by anti-HDM2 peptide functionalized GNPs

This chapter discusses the therapeutic application of GNPs-HDM2 conjugate using the RB model system. The study carried out to understand the therapeutic efficacy of the newly synthesized GNPs-HDM2 conjugate using *in vitro* and *in vivo* system using Retinoblastoma cell line and xenograft study in nude mice model.

6.1 Background

Nanocarriers based approach to targeted therapy has emerged as an attractive strategy for the cancer therapy [419, 420]. Nanomaterial functionalized with target specific biomolecules like peptide, proteins help in the delivering and homing of molecules at tumor sites can serve [169]. Gold nanoparticles (GNPs) are the most suitable therapeutic molecule nano carrier due biocompatibility and colloidal stability, physical and chemical properties that could utilize to carry the biomolecules [44, 421]. Functionalized GNPs has many applications in therapy. Henceforth, a novel GNPs-HDM2 conjugate is synthesized to target the HDM2 (Human Double Minute 2) oncogene, a potential therapeutic inhibitor of the HDM2. It is a proto-oncoprotein which is over-expressed in many cancers, including Retinoblastoma (RB) and are used as a clinical target. HDM2 bind with tumor suppressor protein p53, which has a vital function to prevent the proliferation of damaged/abnormal cells to induce malignancy in normal cells. The feedback inhibition of HDM2 and p53 maintain the cellular homeostasis of p53 and HDM2 in the normal cell. E3 ubiquitin ligase activity of HDM2 degrade the p53, whereas HDM2 is transcriptionally activated by p53. Hence, in normal cell HDM2 and p53 form a feedback loop, which control expression of

HDM2 of p53 in a healthy cell. HDM2 is amplified in certain tumors and results in inactivation of p53, which contribute to the malignant growth of the cell [422, 423]. Because of the crucial role of the HDM2 and its interaction with p53 in human cancer, it is imperative to identify the target molecules which inhibit the HDM2 expression and activates the apoptosis in the cancer cell. Therefore, identification of anti-HDM2 peptide against the HDM2 onco- protein up-regulate in cancer is an approach for targeted cancer therapy. Here, we developed a GNPs-HDM2 nanocarrier conjugate, which inhibits the interaction between the HDM2-p53 through blocking the HDM2 loop that has p53 binding site **(**Figure 6.1). This conjugate destabilizes the interaction and subsequently attenuates HDM2-mediated the p53 polyubiquitination and degradation, which could enhance the p53 activity. The p53 leads to apoptosis and cell death by slowing down the cell cycle progression [424]. When DNA is damaged, HDM2-p53 interaction decreases and p53 is activated to arrest the abnormal proliferation of the cells. The p53 is not required for the noncancerous cell and maintains its low level through HDM2 pathways. HDM2 protein breakdown the p53 in the cytoplasm through ubiquitin-mediated or suppression of p53 in the nucleus [425]. In a cancer cell, which shows HDM2 and p53 interactions only un-phosphorylated HDM2 can reside in the cytoplasm. The apoptosis is induced by releasing the endogenous, wild-type p53 from its negative inhibitor, HDM2. HDM2's over amplified in many cancers and is selective targeted through small molecular inhibitor, which bind with HDM2 protein that can inhibit the binding between HDM2 and p53. Several, studies have shown that the distribution of p53 and HDM2 interaction shows the promising therapeutic application in cancer [426-429].

HDM2, the peptide is explicitly derived from the p53 domain and deliver through the GNPs explored for the first time in RB [249]. Apart, from the delivery of HDM2 peptide for targeted therapy of RB, the significance of the type of reducing agent used in the GNPs synthesis was explored as a complementary approach along with HDM2 for antitumor effects. In addition to this, the lack of understanding of GNPs used for the targeted therapy, interested us to explore the effect of the V-GNPs and C-GNPs in combination with anti-HDM2 peptide for efficient tumor targeting. The RB xenograft mice *in vivo* model were used to study the *in vivo* response of GNPs-HDM2.

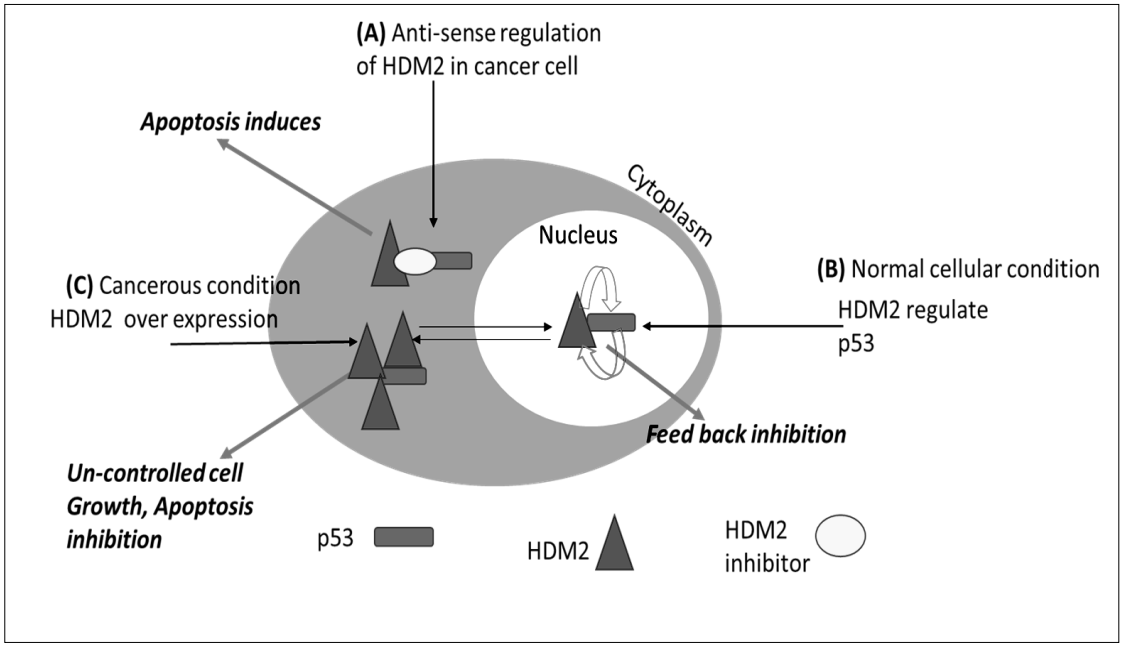

Figure 6.1 Schematic presentation of the regulation of HDM2 by anti-HDM2, a potential therapeutic strategies to target HDM2 oncogene.

(A). In normal cells, the tumor suppressor gene, P53 is regulated by an auto regulatory feedback mechanism between HDM2 and p53. The wild-type p53 gene unregulated the expression of HDM2 protein, which bind to the p53 and control the transcription activity p53 (B). In a cancer cell HDM2 over express and inactivation of p53, which contribute to malignant growth (C). The nucleocytoplasmic transport of HDM2 and P53 is an important mechanism of the regulation of HDM2 [430].

6.2 Materials and Methods

The detailed experiment and protocol for each method has been explained in Chapter 2. An outline of the experiment performed in the current chapter is described in Figure. 6.2

Figure 6.2 Schematic representation of the experiment performed in the current study

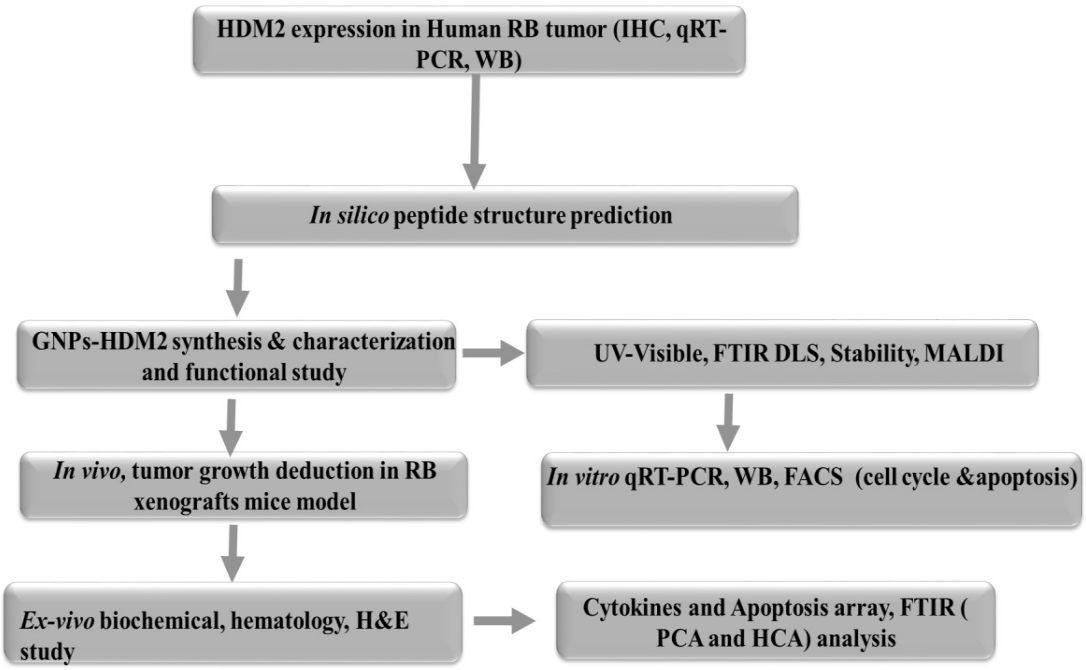

6.3 Results

6.3.1 HDM2 expression in RB tumor sample with clinical, pathological feature RB

6.3.1.1 HDM2 mRNA expression in RB tissue by qRT-PCR

RB tumor tissues and normal retinal tissues were analyzed for HDM2 expression at mRNA level, which were studied by qRT-PCR and normalized by using GAPDH a housekeeping gene. The clinico-pathological information on RB tumor tissue has been shown in Table 6.1.a. The figure 6.3a shows the mRNA overexpression of maximum ~6 fold compared to control sample. All samples showed statistically significant ($p<0.01$) up regulation of HDM2 and two RB samples did not show the significant change in expression compared to control sample. The significant difference in the tumor sample correlated with the tumor differentiation stage. The clinicopathological feature of these two samples shows that RB is poorly differentiated with no invasion found in the choroid and optic nerve in both the samples. Whereas, the other sample, which shows the significance with normal retina is well and moderately differentiated and are invasive tumors.

Table 6.1 Represent the clinicpathological detail of RB sample included for the HDM2, mRNA expression study

Sample	Sex/Age Y&m	OS/OD	Clinicopatholoigcal information
1	F/90	OS/ OD	NR
2	M/2Y	OS	RB ,Ex, WD, NI
3	F/3Y	OD	RB, PD, Inv; FC (<3mm), ON , LC
4	M/3Y	OS	RB, MD, NI;
5	F/5Y	OD	RB, PD Inv;Ch (<3mm), Pre.L,Post.L and ON
6	M/3Y	OD	RB, MD, Inv; RPE, Pre.L,Post.L
7	F/3Y	OS	RB; PD, NI
8	M/3 m	OS	RB,PD NI
9	F/11Y	OS	RB, MD , Inv; FC (<3mm) and Post L.
10 (@)	F/3Y, 4m	OS	RB, PD , Inv; RPE

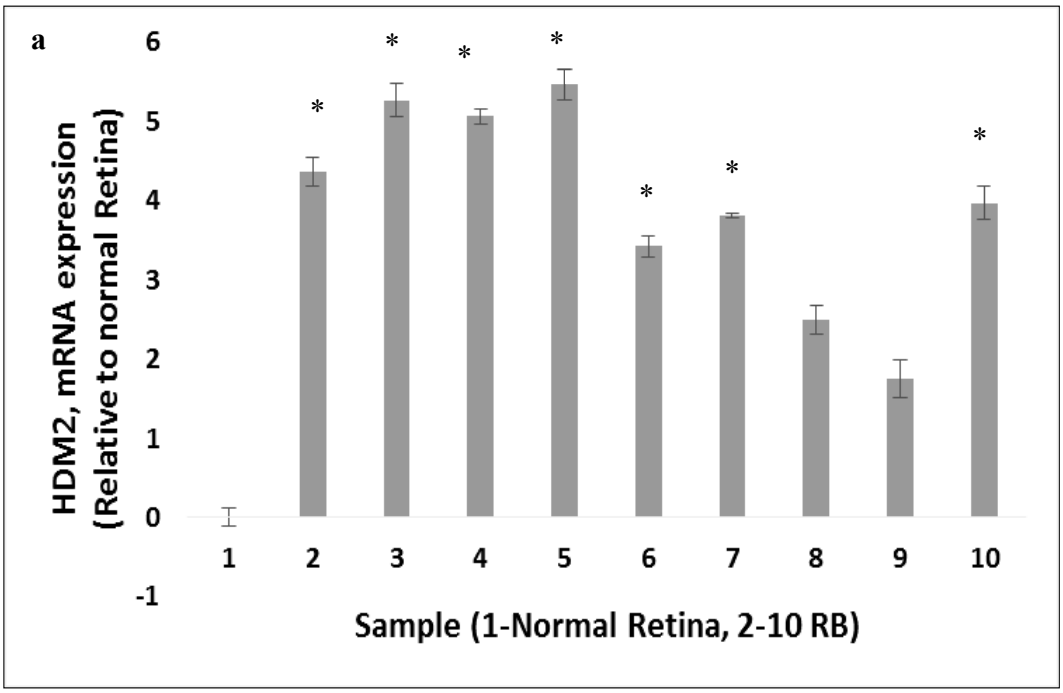

Figure 6.3 (a) Representative q-RT-PCR data on the HDM2 expression. Transcriptional (mRNA) level expression of HDM2 in RB cancer tissue sample normalized with corresponding (β actin). RB samples, clinical details are tabulated (Table 4.5). The HDM2 mRNA expression in 9 tumor tissue is expressed as fold change with respect to normal retina. The * represent the significant difference with respect to the normal (Sample 1) at $p<0.01$. The HDM2 mRNA expression in 9 tumor samples relative to the normal retina.

Abbreviation: NR- Normal Retina, RB- Retinoblastoma, M- Male, F- Female, y- years, Mon- Months, OD- right eye (unilateral), OS- left eye (unilateral), Ex- Exophytic. WD- well differentiated, PD- poorly differentiated, MD- moderately differentiated, NI-No Invasion, Inv- Invasion, ON- optic nerve, Post L- post laminar, PreL- pre laminar, RPE- retinal pigment epithelium, LC- Lamina cribrosa, Ch- Choroid. (@) Indicate that the sample used for protein expression study also

6.3.1.2 HDM2 protein expression in RB tumor tissue

HDM2 protein expression was measured in RB tumor tissues and compared with normal retina tissue by immunoblotting using human HDM2 antibody. The WB specific band of HDM2 indicated at 55 kDa in all tumor samples with difference in the protein expression (Figure 6.3b) The clinicopathologic features of RB tissue used in the protein

expression study are tabulated in Table 6.2. The protein band intensity was measured and normalized with respect to β- actin protein band intensity (Figure 6.4). It is observed that HDM2 is over-expressed in all the samples while there is no invasion of the optic nerve, choroid, and RB tissue is also poorly differentiated. All samples are coming under to D and E category of ICRB classification of RB. Group A- RB up to 3 mm in size; Group B - RB > 3 mm in size, macular location, or minor sub-retinal fluid; Group C - RB with localized seeds; Group D-RB with diffuse seeds; and Group E-massive RB necessitating enucleation [431]. The different size HDM2 protein have been reported, and it could be due to proteolytic cleavage, alternative splicing or post-translational modification [432]. The immunohistochemical analysis of tumor samples was performed to exemplify the protein in RB samples.

Table 6.2 Represent the clinic-pathological detail of RB sample included for the HDM2 protein expression by WB

Sample	**OS/OD**	**Sex/Age Y&m**	**Clinicopatholoigical feature**
1 (D)	OS	M /3 Y	RB, PD, NI
2 (E)	OS	M /2 Y	RB, PD, Inv; Pre.L, Post.L and ON
3(D)	OD	2y/m	RB, PD, NI
4 (E)	OS	3 m/m	RB, PD, NI
5 ((E)@)	OS	3/ 4F	RB, PD, Inv; RPE

Abbreviation: - RB- Retinoblastoma, M-Male, F-Female, y-Years, Mon- Months, OD- right eye (unilateral), OS-left eye (unilateral), PD-poorly differentiated, MD-moderately differentiated, WD-well differentiated, MnD-Minimal differentiated, ON-optic nerve, Inv-Invasion, NI- No Invasion, PostL- post laminar, PreL- pre laminar, LC- Lamina cribrosa, Ch-Choroid, RPE-retinal pigment epithelium.(@)Indicate that sample used for protein expression study as well. D and E classification as per the norms of ICRB (International Classification of Retinoblastoma) [17].

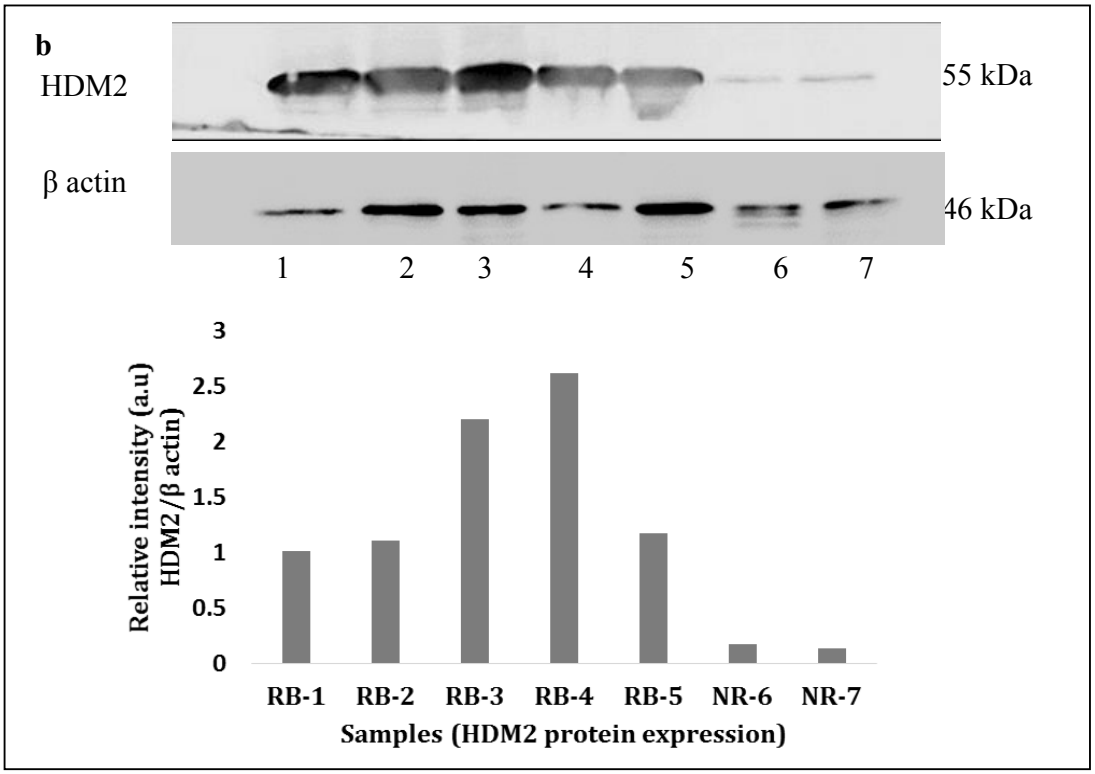

Figure 6.4 (b & c) HDM2 protein expression data, studied by western blot. 2-3 fold more expression in RB compared to NR confirmed the up-regulation of HDM2 in RB

6.3.1.3 Immunohistochemical analysis in RB

RB tissue sections were used for the HDM2 protein expression using immunohistochemical analysis. The clinicopathological information of the sample was described in Table 6.3. The sample shows HDM2 expression based on their differentiation, the nature of the invasion of optic nerve and choroid. The cytoplasmic immunoreactivity observed in RB samples is variable due to the invasiveness of tumor in different part of the eye (Figures 6.5). All the 7 tumor tissue stained positive for HDM2 protein and heterogeneous of the protein was observed between 20-100% positivity. The moderately differentiated RBs exhibited 60-90% positivity for HDM2 protein. The HDM2 expression have been previously reported in the cytoplasm and nucleus in RB [68].

Table 6.3 Represent the clinicopathological detail of RB sample included for the HDM2 expression by IHC analysis

S. N.	Age/Sex	Age/Sex	(%) Positive Cells & Staining	Clinicopatholoigcal Results
1	3Y/F	OD	(-)	RB, PD, Inv; FC, LC, ON and Post L
2	4Y,3m/F	OS	(±) 90-80	RB, PD , Inv; RPE
3	2/M	OS	(±) 70	RB, WB, Ex
4	2/M	OS	(-)	RB, WB Inv; Fc, RPE, ON and Post L
5	4/F	OD	(±) 40	RB, MD , Inv; RPE
6	2/F	OD	(+) 60	RB, MD, Inv; FC
7	5/F	OD	(+) 90	RB, PD, Inv; Ch (<3mm) , Pre L. Post L and ON

Abbreviations RB- Retinoblastoma, , M- Male, F- Female, y- years, mon- Months, OD- right eye (unilateral), OS- left eye (unilateral), Ex- Exophytic. WD- well differentiated, PD- poorly differentiated, MD- moderately differentiated, MnD- Minimal differentiated, ON- optic nerve, PreL- pre laminar, PostL- post laminar, Inv- Invasion, NI- No Invasion, RPE- retinal pigment epithelium, LC- Lamina cribrosa, , Ch- Choroid. Positive (+), Dull (±) and Negative (-)

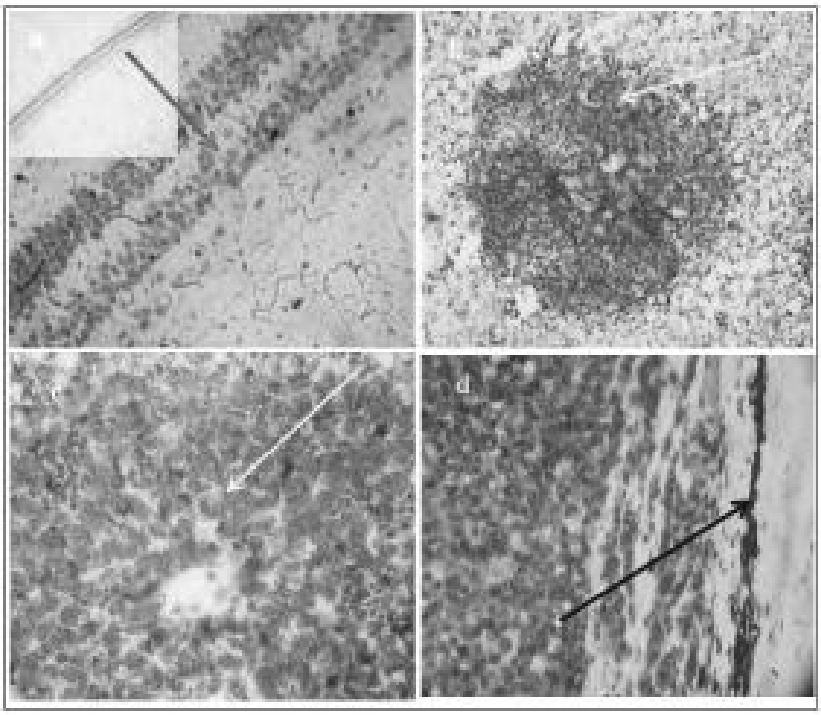

Figure 6.5 Photomicrograph shows HDM2 immunoreactivity in RB tissue sections. (a) Retina shows negative staining for HDM2 40X, (Inset 10X). (b&c) immunoreactivity (DAB staining with hematoxylin counter stain and rosette formation indicated by Yellow Arrow 10X & 40. (d) Choroid invasion and HDM2 positivity.

6.3.2 Structure prediction of anti-HDM2 peptide (QETFSDLWKLLP)

Molecular dynamics were performed to predict the structure of peptides by simulation. All the simulations were performed using GROMACS 4.5 suite [363, 433]. The AMBER force field was employed to calculate the interactions of simulation. The peptide was solvated in a cubic box of TIP3P H_2O, and the charge of the system was neutralized by adding either chloride or sodium ions. The neutralized system was minimized and then equilibrated with NPT-NVT ensembles. The production run was initially carried out for 10ns and extended up to 50 ns depending on the convergence of the system. The structure for the peptide sequence was modeled by performing homology modelling with PDB (PDB_ID: 1YCR) structure as a template. Further, the model was

refined using molecular dynamics simulations. RMSD plot was used to assess the stability of the model. The *in silico* data confirm that the peptide is linear in structure (Figure 6.6). The peptide shows 50% hydrophobicity, which anchor peptide into the cell membrane. The HDM2 peptide QETFSDLWKLLP, with aromatic ring Phe (F) and Trp (W) amino acid shows more fluctuation which could increase the fluctuation of peptides on the GNP surface. In a study using the di/tripeptide and mono, amino acid confirm that tri-peptides are more flexible after adsorbed on GNPs and fall farthest from the GNPs other. In addition to this, the aromatic ring amino has an important role in the fluctuation of the peptide on the GNPs [434].

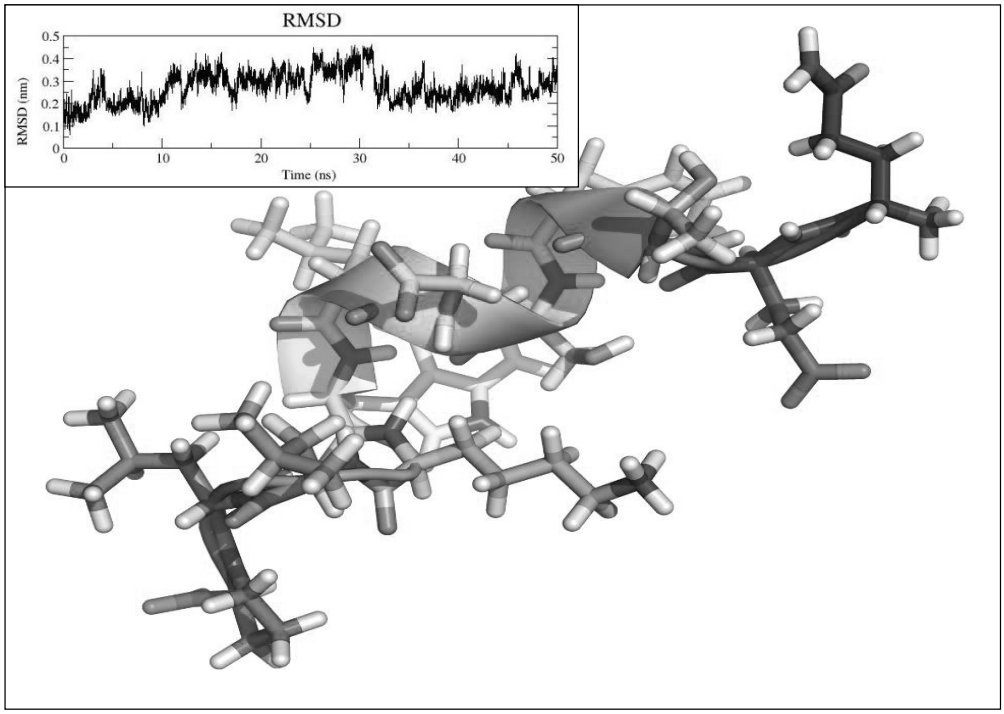

Figure 6.6 Lowest energy confirmation attained at 380 72th time frame and RMSD plot of Anti-HDM2 peptide where the structure, after initial fluctuation, converges (after 30ns) into stable conformation with RMSD between 1 and 2 Å (Inset).

6.3.4 *In vitro* characterization and functional study of GNPs-HDM2

6.3.4.1 UV- Visible and DLS

Prefix V- indicates the *Vitis vinifera* reduced GNPs and C-indicates sodium citrate reduced GNPs. The suffix HDM2 indicates that the peptide conjugated with GNPs

The GNPs-HDM2 peptide synthesis was characterized by UV-Visible and FTIR (Figure 6.6). The optimization of the saturation of the GNPs was performed by using a different ratio of the peptides (Figure.6.6a) which confirms that 1: 3 GNPs: peptide was the optimum ratio which saturates the GNPs. The increased absorbance (Figure 6.6a) with respect to GNPs in the GNPs-HDM2 conjugate confirms that peptide absorbed on the GNPs. The SPR absorbance peak of GNPs-HDM2 conjugate in both types of GNPs indicates the shift of SPR band ~ 5nm in comparison with GNPs used for the formation of GNPs-HDM2. A red shift from 532 nm indicates that peptide molecules are coated on the surface of the GNPs, which could be due to aggregation of GNPs in the presence of peptide on the surface of GNPs as indicated in the Figure.6.6.a. As discussed previously (Chapter-5) the similar red-shift was observed in the conjugation of GNPs-Pep-A. As, already observed by the Red shift in plasmon absorbance is attributed to the presence of peptides on GNPs [378, 379].

The “hydrodynamic diameters (HD)” and “polydispersity index (PDI)” of the V-HDM2-GNPs and C-HDM2-GNPs were measured by the DLS showed the increased HD compared to the respective GNPs used for the formation of GNPs-HDM2 conjugate. The observed HD of V-GNPs-HDM2 were 267±13.47 with PDI of 0.42 compared to the V-GNPs which was reported 14±1 with PDI of the 0.422 (Chapter-4). Whereas, the C-GNPs -HDM2 showed the HD 84.76±0.45 with PDI of 0.03 compared to the C-GNPs which

showed HD 38.71±.243nm. The change in the HD was increased, according to the surface modification with an amount of the agglomerate, however the DLS quality report was good and autocorrelation function shows the mono-modal fitting dispersion of the solid line [380]. A similar increase in size was reported using bombesin peptide conjugated with GNPs is reported earlier. Similarly, increases in size were observed in a study with gold nanoparticles, which was reported size and surface charge dependent bio-distribution of different sizes of GNPs injected into the rats as *in vivo* model [435].

6.3.4.2 FTIR characterization

The V-GNPs-HDM2 and C-GNPs-HDM2 conjugation further confirmed by the FTIR (Figure 6.7d). The broad IR band centered at 3482 cm^{-1} can be specified to phenolic O-H stretch H-bonded. The bands at 2914 and 2904 cm^{-1} can be assigned to the asymmetric stretching of methyl functional groups. The strong asymmetric band at 1645 cm^{-1}signifies the carbonyl stretching characteristic to both GNPs-HDM2 and HDM2 peptide present in the conjugate. This band at C=C 1645 cm^{-1} is typically a weak absorbance. The series of bands between 1500 and 1200 cm^{-1} can be accounted for the asymmetric and symmetric stretching and bending modes of aliphatic and aromatic amino acids presented in the HDM2 peptide sequence (QETFSDLWKLLP), respectively. Additionally, the weaker bands between 850 and 450 cm^{-1} can be associated with the phenyl ring stretching and out of plane vibrational modes of CH moieties presented in the HDM2 peptide or the molecules coated on the GNPs surfaces. The presence of peaks at 2914, 2904 in V-GNPs-HDM2 and C-GNPs-HDM2 respectively, and 2855 cm^{-1} in HDM2 (peptide alone) are attributed C-H stretch of the methylene groups of 3 mercaptopropionic acid attached to the HDM2 peptide (MPA) [436]. Reduced transmittance of MPA peak in the case of V-GNPs and C-GNPs

indicates MPA is contributing to the formation of the bond between the HDM2 peptide and GNPs. The presence of a strong peak at 1625 cm^{-1} is ascribed to the amide between the MPA and the HDM2 peptide (Peptide alone) (Figure 6.7 d). The shift of 1625 cm^{-1} peak of the HDM2 peptide alone in case of V-GNPs-HDM2 and C-GNPs-HDM2 1655 and 1645 cm^{-1} respectively, compared to the HDM2 peptide alone (1625 cm-1) provide a confirmation for the formation of the amide bond. Remarkably, the broad O-H band in HDM2 peptide spectra has missed while a distinct alkyl stretching vibration have observed in GNPs-HDM2 spectra. The FTIR data give good evidence that HDM2 peptide is conjugated with the GNPs though the difference are observed in the spectral peak intensity. Since, the spectral peak is similar in both the conjugate is documented that the MPA-functionalized HDM2 peptide is covalently bound with GNPs.

Interestingly, the majority of the peaks obtained in (Figure 6.7 d) HDM2 peptide alone disappears, leaving sharp, intense bands at around 1600 and 1450 cm^{-1}, which can be attributed to C=C vibrations in aliphatic aromatic compounds presented in the amino acid. An additional peak at around 1025 cm^{-1} observed in the V-GNPs-HDM2 and C-GNPs-HDM2 ascribed to alkene C-H bend. The rest of the bands can be accounted for considering various vibrational modes of aliphatic and aromatic CH moieties present in the peptide.

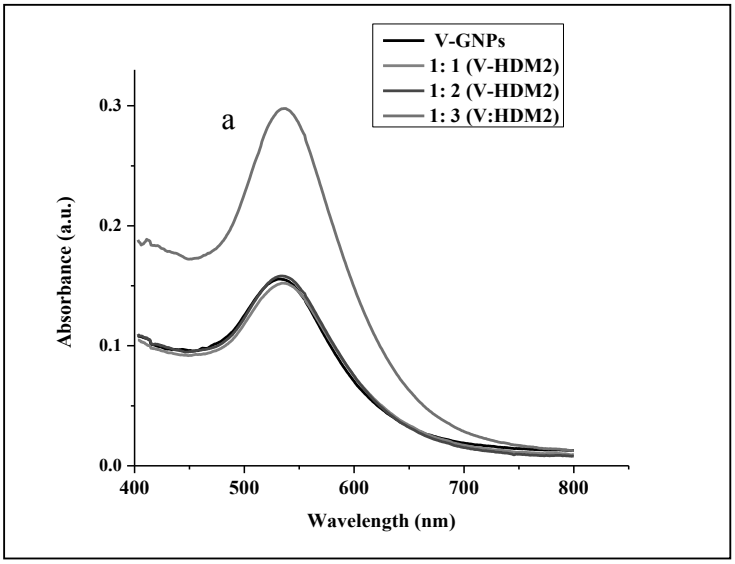
V-GNPs
1: 1 (V-HDM2)
1: 2 (V-HDM2)
1: 3 (V:HDM2)
a
Absorbance (a.u.)
Wavelength (nm)

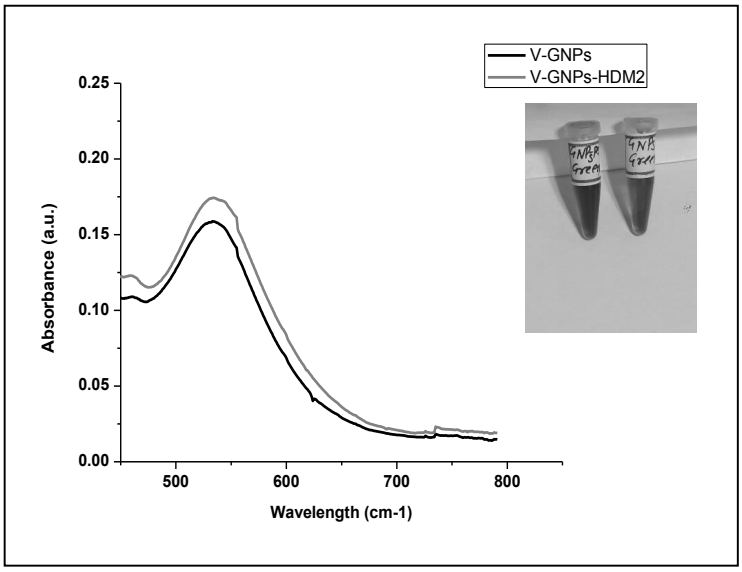
V-GNPs
V-GNPs-HDM2
Absorbance (a.u.)
Wavelength (cm-1)

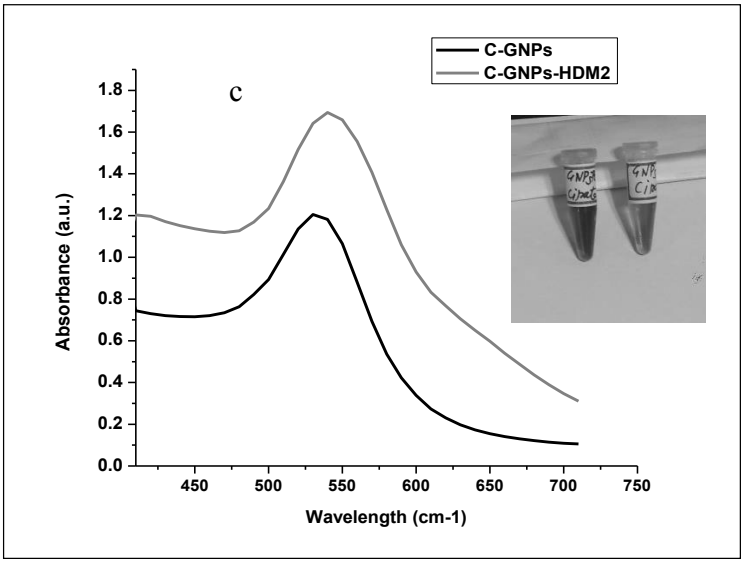
C-GNPs
C-GNPs-HDM2
c
Absorbance (a.u.)
Wavelength (cm-1)

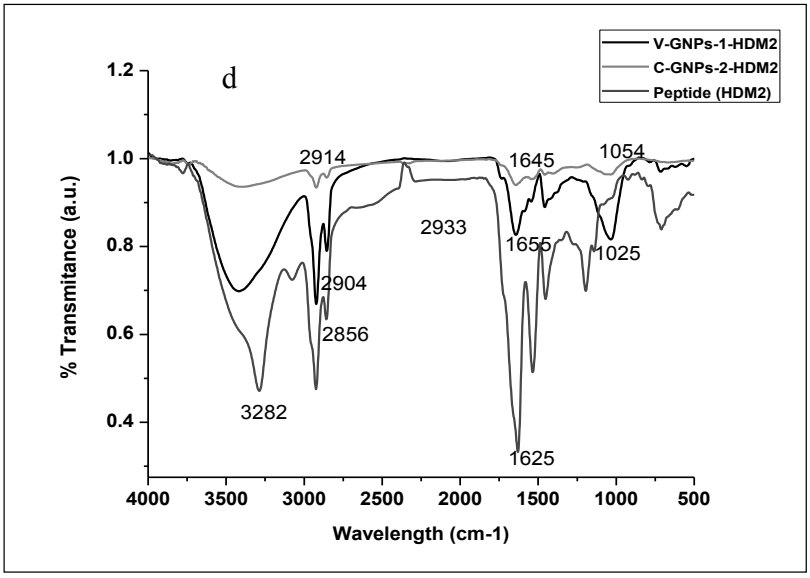

Figure 6.7 The figure shows the character of the GNPs- HDM2. The peptide coated on the GNPs confirmed by the shift in SPR band with respect to the GNPs (without peptide) (Indicated by the arrow).

The inset picture indicates the GNPs and GNPs coated with the peptide (Change in color of conjugate due to an aggregation of the peptide on the surface of GNPs). The Red shift indicates the binding of the GNPs with peptide (a, b & c). FTIR spectra show the changes in spectral peak and FTIR band assigned to the functional group (d). V-GNPs-1 (GNPs synthesized by *Visit vinifera*), C-GNPs-2 (GNPs synthesized by sodium citrate). HDM2-Peptide sequence (QETFSDLWKLLP), V-GNPs-1-HDM2 (HDM2 conjugated with V-GNPs) and C-GNPs-2-HDM2 (HDM2 conjugated with C-GNPs).

6.3.4.3 Internalization of the particles (TEM)

The GNPs and GNPs-HDM2 internalization was visualized by the TEM after 24h of culture in the Y79 a RB cells to confirm the uptake of the particles as well as to confirm the stability and the morphology of particles inside the cells in culture medium to confirm the stability of the nanoparticles. The TEM results indicate that GNPs are stable *in vitro* in a high ionic salt concentration of the biological medium until 24h of treatment. It has been observed that in the case of C-GNPs (Figure 6.8c), particles tends to aggregate whereas, in cases V-GNPs, V-GNPs-HDM2 and C-GNPs-HDM2 which is coated with the polyphenols

and proteins respectively prevent the aggregation (Figure 6.8a,b &c). This protein coating changes the basic physiochemical interaction of GNPs by the dynamic interfaces between the nanoparticles and the biomolecules inside the cell. This interaction could affect the internalization of nanoparticles and consequently change the cellular responses, therefore, it is imperative to consider the stability of the GNPs inside the cellular environment [437].

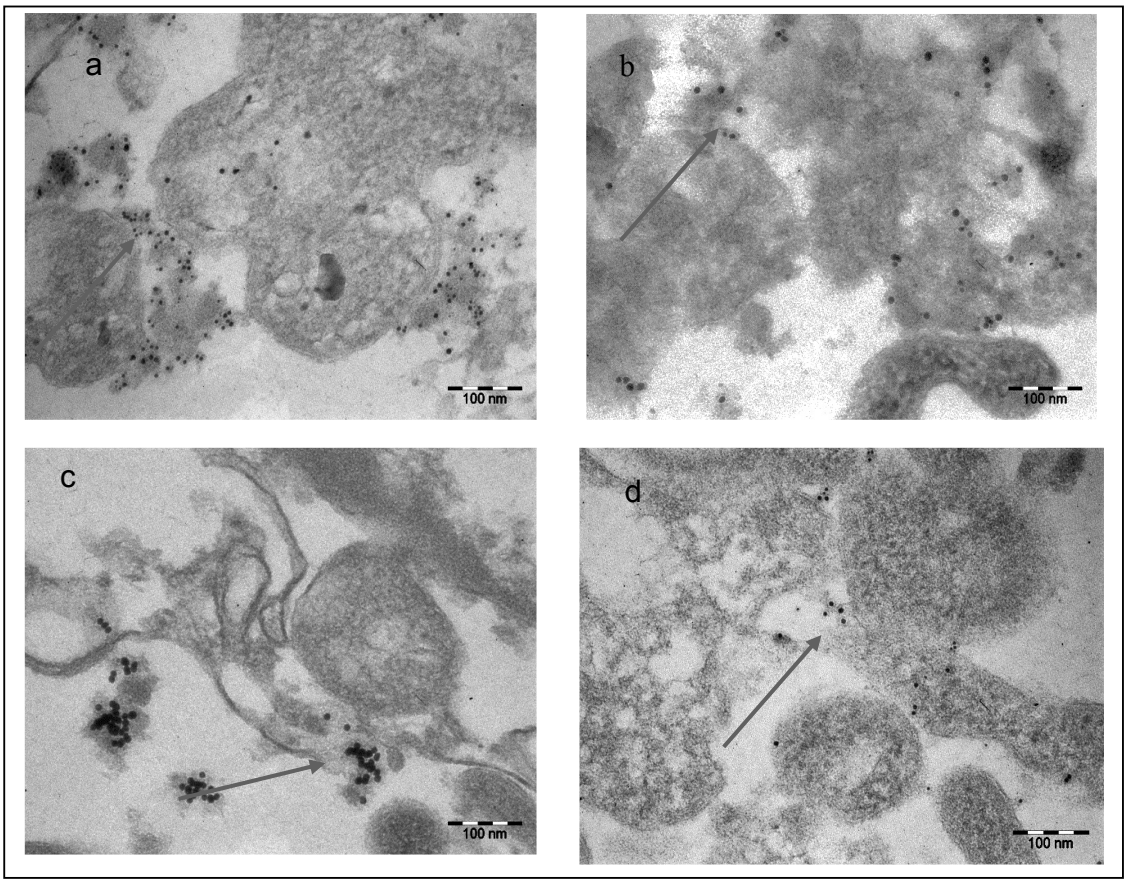

Figure 6.8 The TEM micrograph represent the internalization of the GNPs in Y79 cells.

A) V-GNPs (GNPs-1), B) V-GNPs-HDM2, C) C-GNPs (GNPs-2) and D) C-GNPs-HDM2. The arrow indicates the particles inside the cells. The size and shape of particles, and scale bar represent 100 nm.

6.3.4.4 *In vitro* HDM2 knockdown in Y79 cells

The HDM2 at a concentration of 50μM of V-GNPs-HDM2 and C-GNPs-efficiently knockdown HDM2 at 24h of treatment compared to the V-GNPs & C-GNPs. An optimized concentration and time related (12, 24 and 48 h) knockdown study determines the optimal time and concentration required for the HDM2 gene knockdown. The down regulation of

HDM2 at transcription level significantly ($P<0.05$) was observed compared to control sample (untreated Y79 cell) (Figure 6.9). HDM2 down regulation of 5.8 and 4 fold was observed in V-GNPs-HDM2 and C-GNPs-HDM2, respectively. The down regulation of HDM2 was also observed in the protein level by the western blot. As noticed, the significant down regulation of the HDM2 in C-GNPs-HDM2 and V-GNPs-HDM2 ($P<0.05$) (Figure 6.9a) whereas the C-GNPs and V-GNPs is not effective in HDM2 down regulation compared to untreated (control sample). Interestingly, V-GNPs-HDM2 and V-GNPs showed the up-regulation p53 significantly ($P<0.05$). However, C-GNPs-HDM2 and C-GNPs does not up regulate the expression of p53 after the treatment. The difference in the knockdown of the HDM2 and p53 with respect to C-GNPs and V-GNPs conjugated anti-HDM2 peptide indicates that apart from the anti-HDM2 peptide, type of GNPs used for the conjugation affect the knock down of HDM2 and p53 in treating Y79. Interestingly, it is noticed that V-GNPs-HDM2 is more promising with respect to the knockdown of the HDM2 compared to the C-GNPs-HDM2 at both mRNA and protein level.

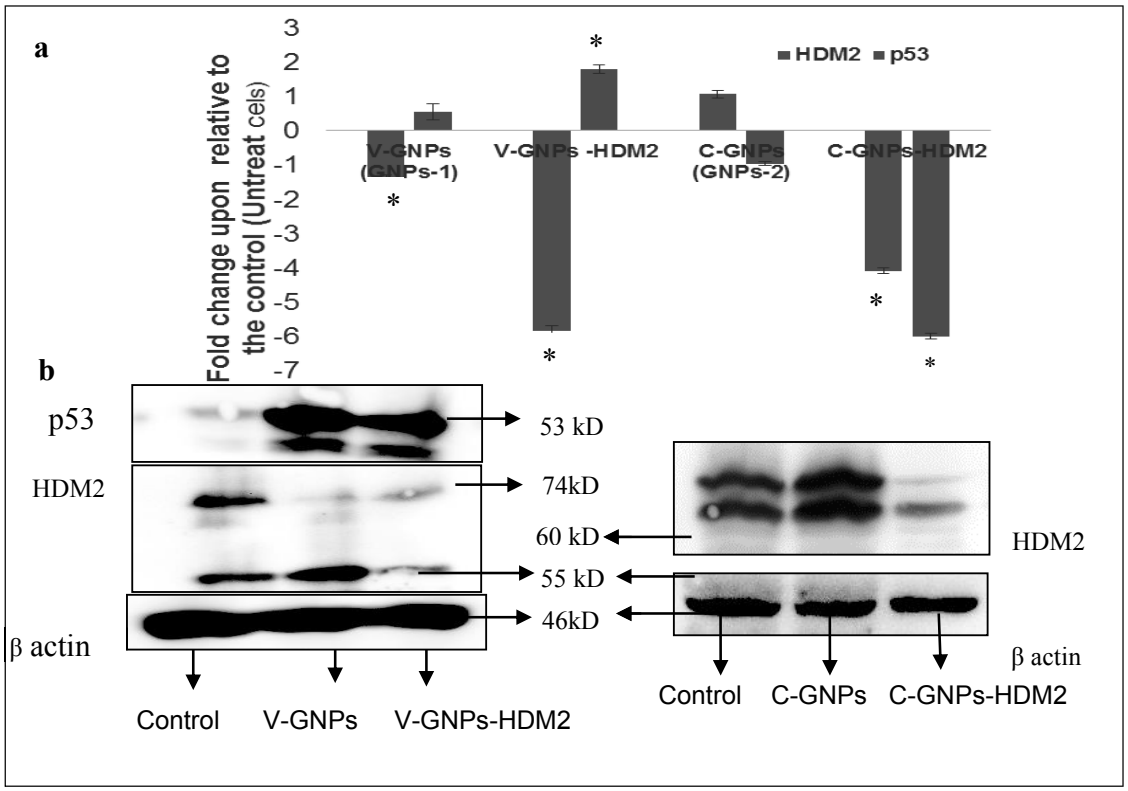

Figure 6.9 (a) qRT-PCR study for the functional analysis of mRNA reveals that the HDM2 peptide is functional

* (b) Represent the significant difference in fold change with respect to the control sample at $p<0.05$. The Western blot results indicate the knock down regulation of the HDM2 in the case V-GNPs-HDM2 and C-GNPs-HDM2, whereas, p53 up-regulated in V-GNPs-HDM2.

6.3.4.5) Knockdown of HDM2 by GNPs and GNPs-HDM2 lead to apoptosis

The *in vitro* apoptosis study was performed to understand the effect GNPs-HDM2 and GNPs in the Y79 cells. The knock down effect of HDM2 in treated Y79, a RB cell after 24h of treatment, was analyzed by the annexin-V/PI staining. The proportion of cell viability significantly decreased after treatment compared to control (Figure 6.11a & b). A significant difference was observed in the V-GNPs, V-GNPs-HDM2, and C-GNPs-, C-GNPs--HDM2 compared to control. Interestingly, it has observed that V-GNPs-HDM2 inducing the cell death by apoptosis, whereas the C-GNPs-1-HDM2 shows more of

necrosis population. The necrosis population is not statistically significant compared to control. However, a statistical significant difference ($P<0.05$) was noticed in C-GNPs-HDM2 compared to C-GNPs (Figure 6.10b).

This finding indicates that the cell death exclusively induced due to the effect of HDM2 although it is not an apoptosis. Whereas, in case of V-GNPs-HDM2 a statistical significant difference ($P<0.01$) was noticed in the apoptotic population compared to untreated cells. Moreover, the V-GNPs-HDM2 showed statistical significant necrosis compared to the V-GNPs. The current result confirmed that apoptosis is due to knockdown of HDM2. Interestingly, V-GNPs-HDM2 confirm that there is a significant effect of the reducing agent on the cell death and a statistical significant ($P<0.01$) apoptosis population noticed. C-GNPs-HDM2 instead showed the necrotic population with respect to control cells.

Figure 6.10.a

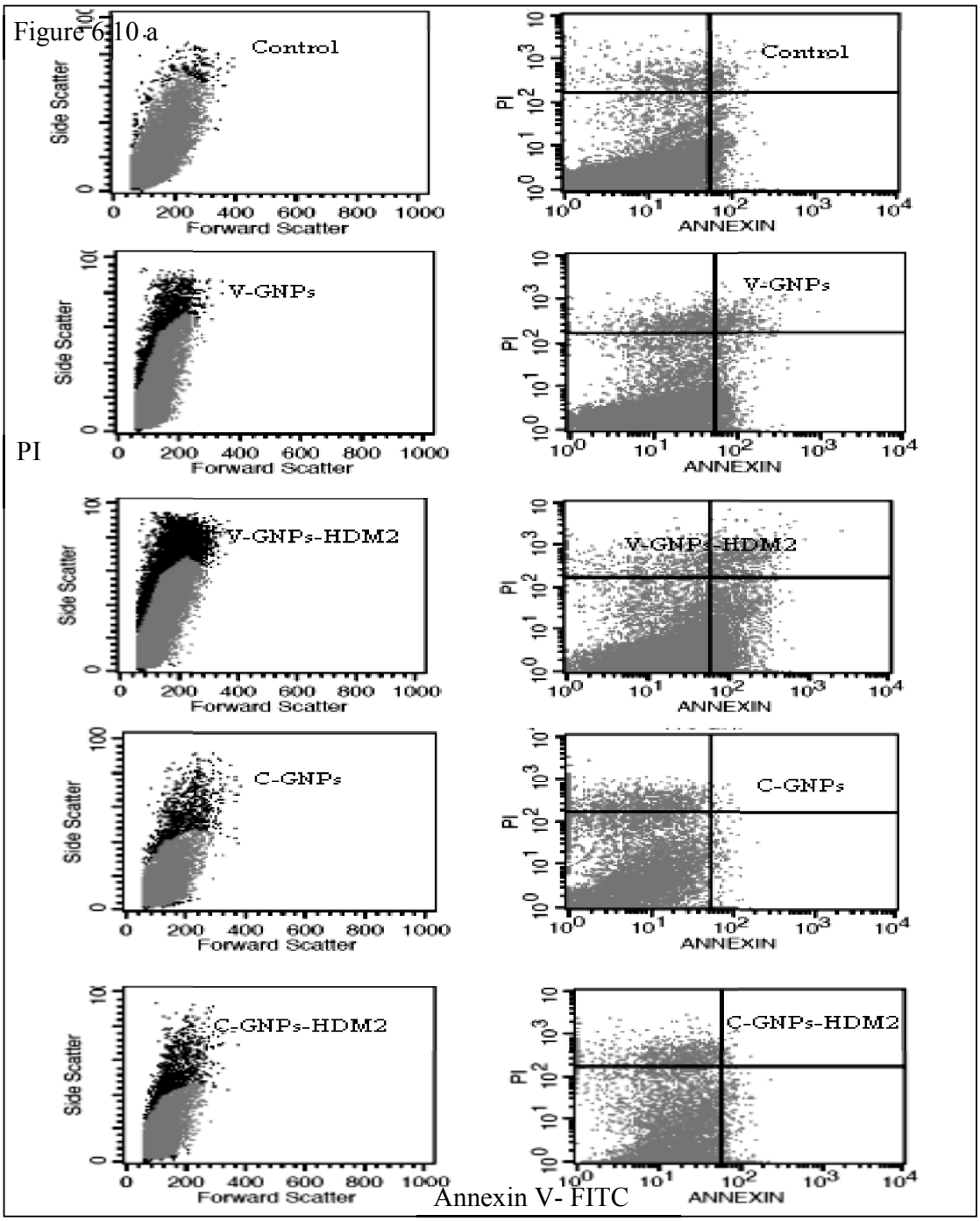
Control
Side Scatter
Forward Scatter
PI
ANNEXIN
V-GNPs
V-GNPs-HDM2
C-GNPs
C-GNPs-HDM2
Annexin V- FITC

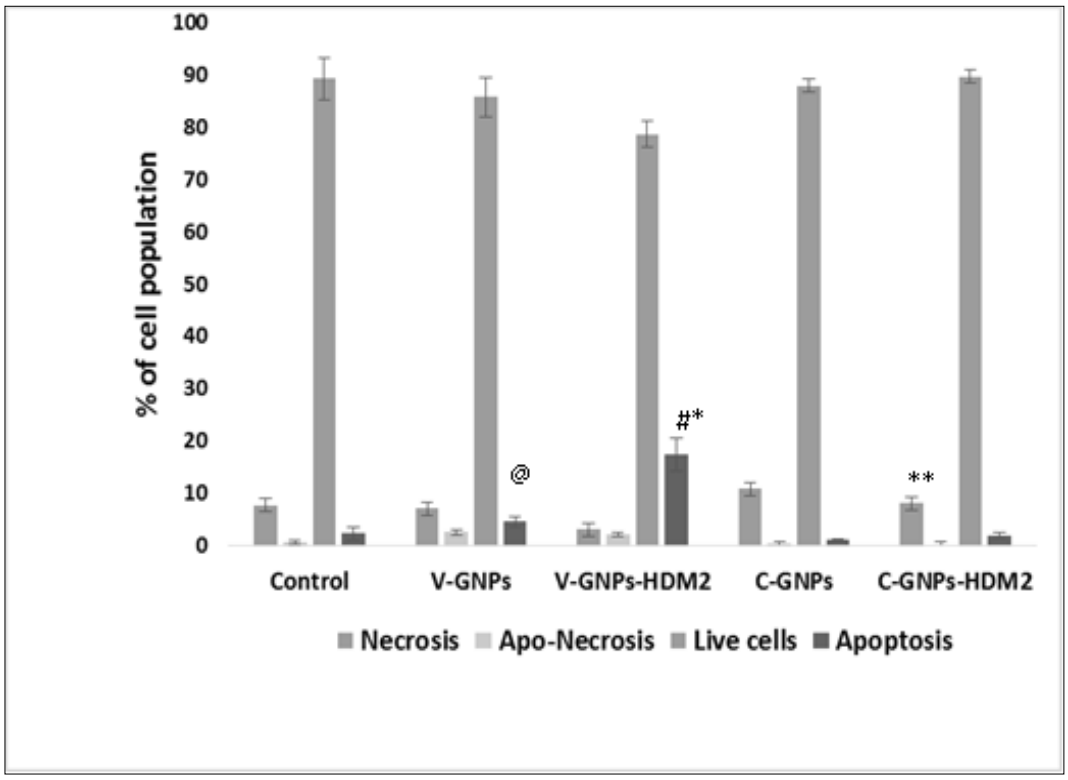

Figure 6.10 (a) Represent the apoptosis data by. The Y79 RB cells treated with V-GNPs, C-GNPs, V-GNPs-HDM2, and C-GNPs-HDM2.

The Y79, RB cells were evaluated for the concentration 50μM (Concentration of GNPs atom of gold) at treatment for 24 h. Quadrants portions indicates: lower left: Live cells (Annexin and PI –ve), lower right: early apoptotic (Annexin+ve and PI–ve), upper right: Apo-Necrosis (late apoptotic) (Annexin +ve and PI +ve), upper right: necrotic cells (Annexin –ve and PI +ve). (b) Apoptosis population was observed in treating Y79 cells. Error bar represents the mean ± SD of triplicate samples. The '@' represent significant difference with respect to V-GNPs to V-GNPs-HDM2, # and * represent with respect to control and V-GNPs to V-GNPs-HDM2 at $p<0.05$ and 0.01. Whereas ** shows significant GNPs-2 to GNPs-2-HDM2 at $p<0.05$.

6.3.4.6 Cell cycle analysis in treated Y79, RB cell

Cell cycle regulation is one of the important cell fate process and deregulation of cell cycle associated with cancer progression. A strategic response of cancer cell can modulate cell cycle associated proteins and switch the cell cycle from apoptosis to cell cycle arrest which leads to tumor inhibition. The anti-proliferative effects of C-GNPs-HDM2 and V-GNPs-HDM2 are due to cell-cycle and altered phosphorylation of pRb.

Analysis of a cell population in a different stage of the cell cycle can be studied by fluorescence labeling of nucleic acid of cells. Since the amount of DNA is different in the different stage of the cell cycle, the amount of fluorescent observed is also varied. This can be established by quantifying the fraction of cell populations in G1, S, and G2 phases. As the histogram clearly indicates that, after the treatment with the GNPs and GNPs-HDM2 the increasing population in the S phase and G0/G2 phase compared to the control. The significantly increased population in G0/G1 stage in the case of V-GNP from 19.26 ± 0.322986 compared to the control, 13.77 ± 3.5 ($P<0.01$) indicates that V-GNPs has effects on cell cycle whereas, C-GNPs does not show significant difference with respect to control. Whereas, in the case of V-GNP shows the statistical significant change in the S phase, which shows 17.49 ± 0.6 compared to control, 14.23 ± 1.5 ($P<0.05$). This data clearly indicates that V-GNPs arrest the cell in S phase, which is synthesis also when V-GNPs conjugated with the HDM2 peptides it affected the G2/M, which is a transition between DNA synthesis and division. Both are significantly increasing compared to the control indicates that the cells are not in the dividing stage (Figure 6.11 a). On the other side, C-GNPs-HDM2 and C-GNPs also show the increased population in the S-phase of the cell cycle. The significantly increased population of the V-GNPs in G2/M and S phase of cell cycle indicates that the cell cycle arrested in the V-GNPs treated sample whereas, in case of V-GNPs-HDM2 the effect is not statistically significant. Similarly, C-GNPs-HDM2 also statistically non-significant. V-GNPs which has polyphenols shows a significant S phase arrest ($P<0.01$) and G2/M phase arrest ($P<0.05$). It has been reported that Resveratrol, a major component of *Vitis vinifera* polyphenols control apoptosis and different stage of the cell cycle in Y79 cell line [438]. The growth and apoptosis arrest by Resveratrol have been

reported in many types of cancer such as colorectal, epidermoid carcinoma cancer cell [439]. Therefore, resveratrol has been identified as a as novel promising agent for cancer therapy which would be a altered the in signal transduction pathways which intern induced apoptotic cell death [440]. The cell cycle results confirmed GNPs has the significant effect on the cell cycle.

Figure 6.11 a

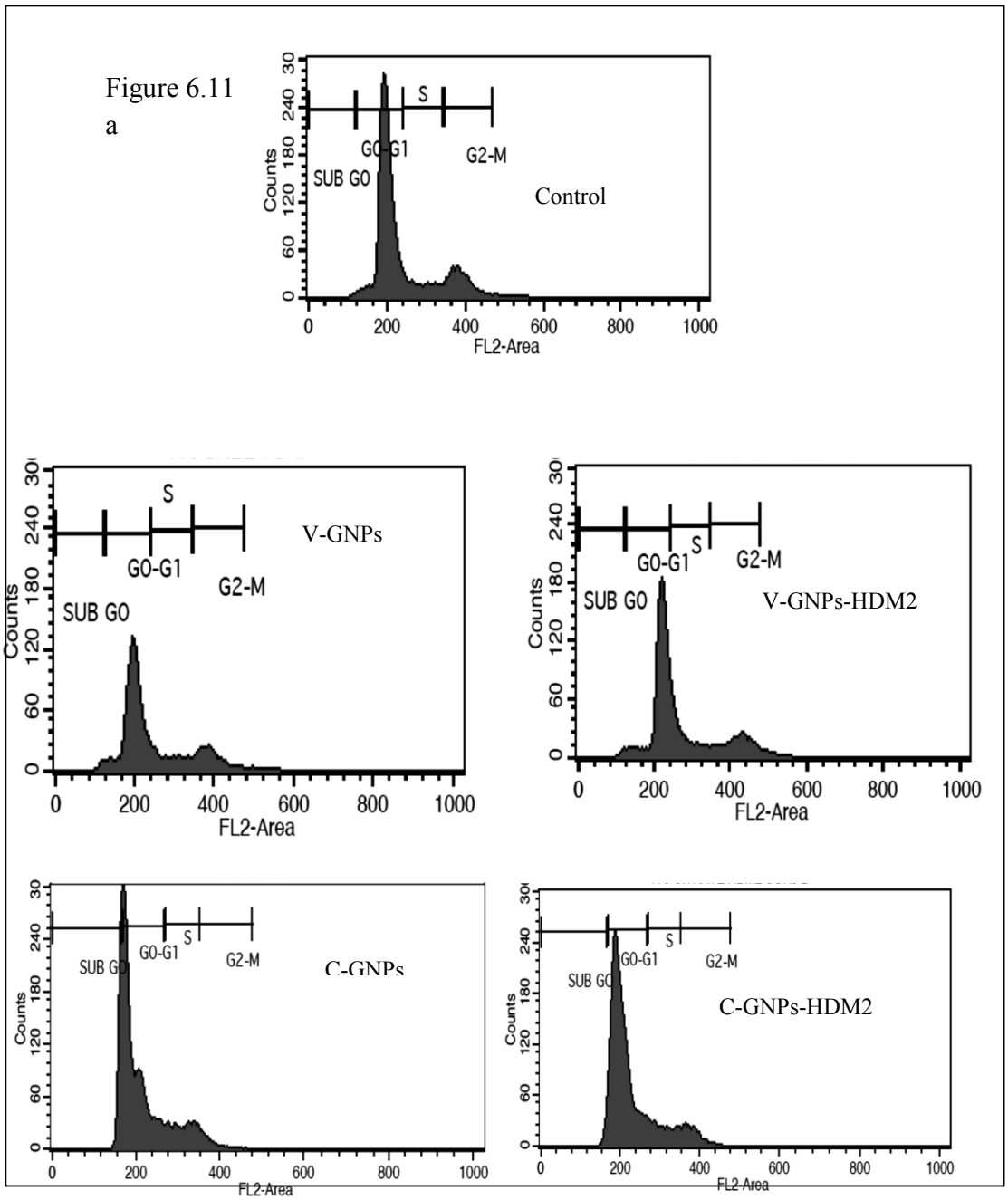

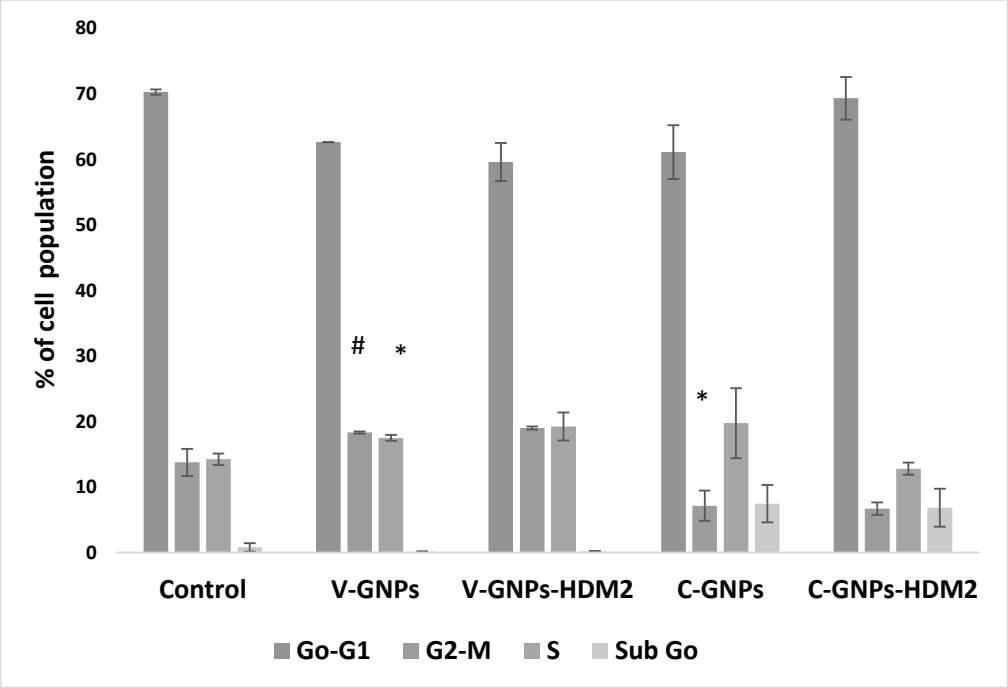

Figure 6.11 (a) Y79 cell cycle analysis in treating the sample with V-GNPs, C-GNPs, V-GNPs-HDM2 and C-GNPs-HDM2 treated.

The Y79, RB cells were treated with 50µM concentration (Concentration of GNPs) for 24 h of treatment. The treated cells were washed, fixed and stained with PI and subjected for FACS analysis. Cells in sub-G1 phase represent the hypodiploid DNA content an indication of apoptotic cell death by DNA fragmentation. Due to treatment S phase cell population increased. (b) Cells in G0/G1, S, and the G2-M phase of the cell cycle are plotted and present as a histogram. (A, B) Mean ± SD of triplicate sample. * and # represents as compared to untreated control sample at $p<0.05$ and $p<0.01$, respectively.

6.3.4.1 *In vivo* preclinical evaluation of antitumor effect of GNPs-HDM2 using RB xenograft model

After successfully showing functionalization of GNPs with HDM2 and functional study showing the knockdown of HDM2 *in vitro* in RB model, the novel conjugate were tested for the targeting therapy for tumor growth reduction, in Y79 induced xenograft nude mouse model. The pharmacokinetics of GNPs-HDM2 increased in the animal model by coating of this particle with the PEG. The PEGylation help in the reduction of the nonspecific adsorption of proteins and limit the non-specific interactions of the GNPs in RB xenograft animal model *in vivo* in the current study. The PEGylation and the chain length of the PEG (PEG-1000 kD) does not affect the biocompatibility of the GNPs-HDM2, and the current formulation and dose of administration confirms that GNPs-HDM2 is non - toxic to the cells. The targeted therapy using nano-carrier works in the solid tumor through homing of the target molecule at the tumor site, which is attributed to the EPR effect of cancer cells. The passive accumulation of the GNPs can be attained due to the unique property of the tumor, which shows characteristics feature such as leaks and immature blood vessels [441].

6.3.4.2 In-life study (body weight measurement)

Body weights were measured once every three days during the study period. Animals were observed for visible clinical signs once every three days during the study period, mortality and body weight changes. The results of the percentage change in body weight following the treatment with V-GNPS-HDM2 and C-GNPs-HDM2 represented in Figure 6.12 a. The change in body weight by the treatment with the V-GNP-HDM2 and C-GNP-HDM2 confirmed that the given dose of the treatment was relatively well tolerated with no mortality. During the experimental period (until 24 days) there was no significant

body weight loss in control, V-GNP-HDM2, and C-GNP-HDM2. There was a transient body weight loss (-0.5%, Day 6-9) in C-GNP-HDM2. However, in subsequent treatments the body weight was regained, and there was no visible sign of abnormal behavior or clinical symptoms in any of the treatment groups.

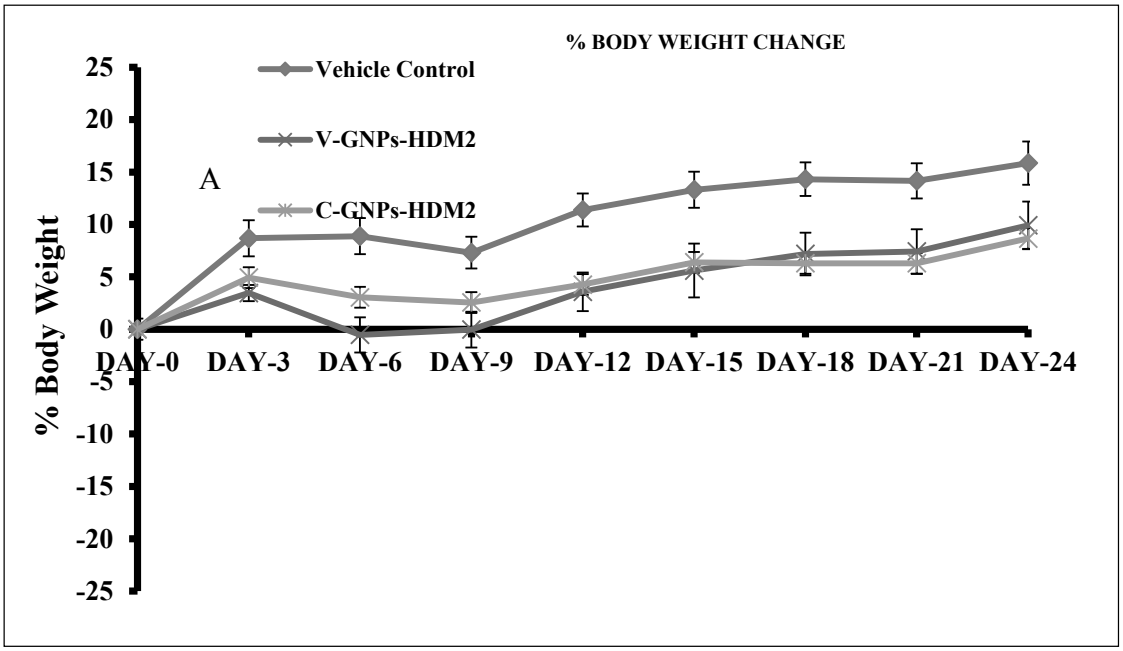

Figure 6.12 Mean body weight of T 79 tumor xenografts in nude mice. C-GNPs-HDM2 shows mean body loss between days 6-9.

6.3.4.3 In-life tumor growth kinetics and antitumor activity measurement

The tumor volume was measured by caliper on the day of randomization (Day 0) and then once every three days (i.e. On the same days when body weight was taken). Using a vernier caliper the length (L) and width (W) of the tumor was measured.

Tumor volume (TV) was calculated using the following formula:

$$\text{Tumor Volume } (mm^3) = L \times W^2 / 2, \quad \text{----------(1)}$$

Where, L = Length (mm); W = Width (mm).

Standard Deviation (SD) and Standard Error of Mean (SEM) were calculated for individual groups.

6.3.4.4 Antitumor activity measurement using the following criteria

Antitumor activity was evaluated as maximum tumor volume inhibition versus the vehicle control group.

I) Test/Control Value in % (% T/C)

Tumor inhibition on a particular day (T/C in %) was calculated by using the below formula:

$$T/C\ (Day\ X) = \frac{(\text{Mean TV of the test group on Day } X - \text{Mean TV of the test group on Day } 0)}{(\text{Mean TV of the control group on Day } X - \text{Mean TV of the control group on Day } 0)} - \text{x } 100\%$$

The minimum (or optimum) % T/C value recorded for a particular test group during an experiment represents the maximum antitumor activity for the respective treatment.

TV= Tumor volume (mm^3)

II) Tumor growth inhibition (TGI)

TGI was calculated using the following formula:

$TGI = (1 - T/C) \times 100$

Where, T = (Mean TV of the test group on Day X - Mean TV of the test group on Day 0)
C = (Mean TV of the control group on Day X - Mean TV of the control group on Day 0)

The GNP peptide conjugate shows tumor growth reduction in Y79 xenograft tumor model. The mean tumor volumes on Day 24, for control group (Injected with sterile water), V-GNP –HDM2 and C-GNP –HDM2 groups were 1755 ± 116 mm^3, 1463 ± 109 mm^3 and 1288 ± 210 mm^3, respectively (Figure 6.13 b). The tumor growth reduction during this

period is shown in Figure 6.12 C & D. An optimal T/C value of 83% and 72% with shows % tumor growth inhibition (TGI) was found to be 17% and 28% respectively on Day 24.

The current data indicate that there GNPs-HDM2 conjugate is homed at the tumor site [281] without toxicity and mortality of the animal during the study period. Also the retention of the GNPs-HDM2 at the tumor site. A similar kind of findings was observed in a study using glucose and polyethylene glycol (PEG) coated GNPs confirmed that ½ life of GNP improved the *in vivo* coating of the particles. This finding also emphasized that the selective system due to the homing of GNPs at the tumor site helps in effective radiotherapy through the interaction of X-rays with GNPs [279].

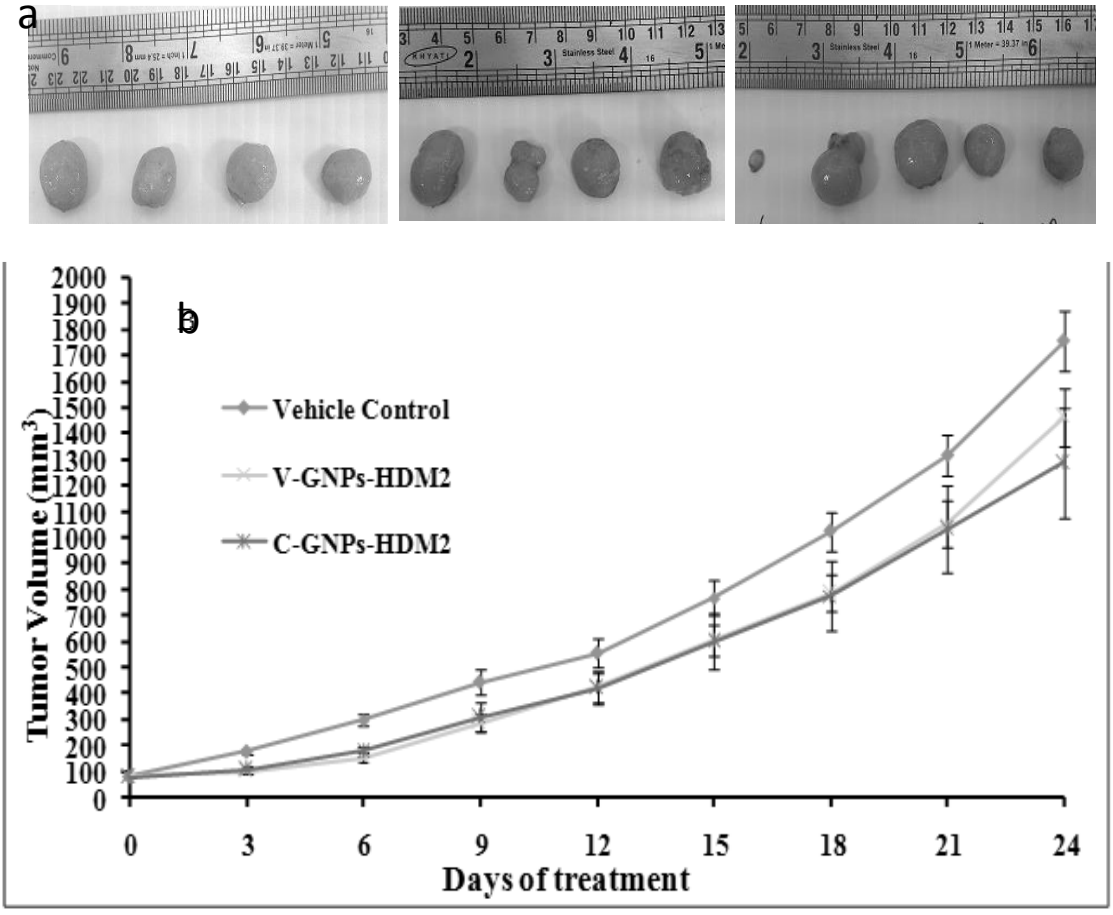

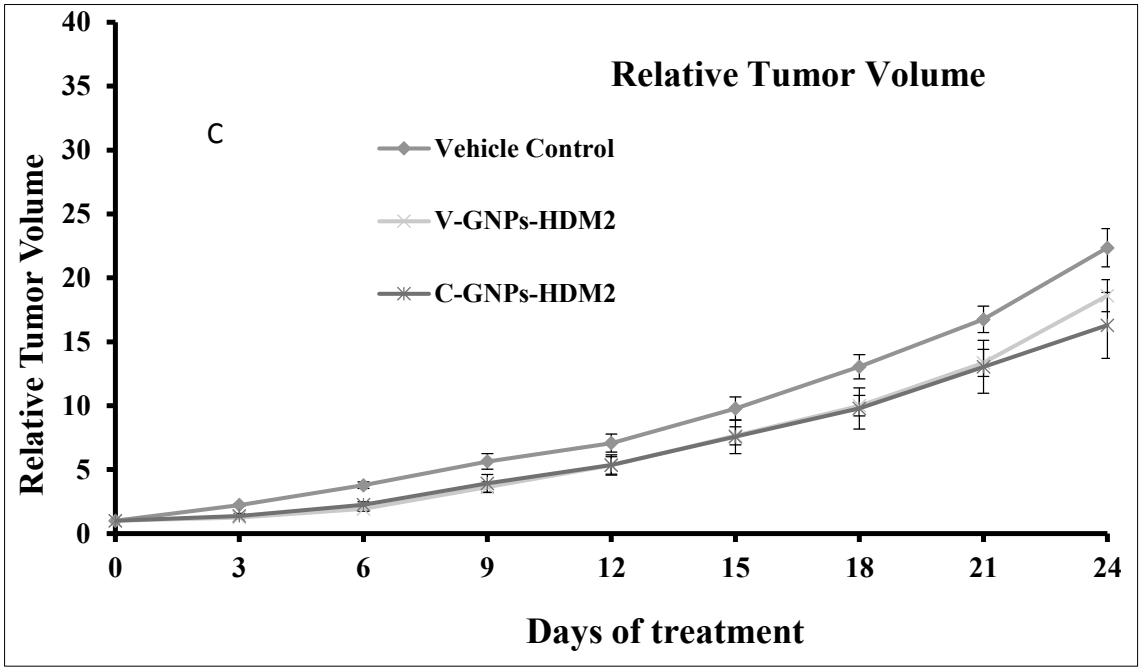

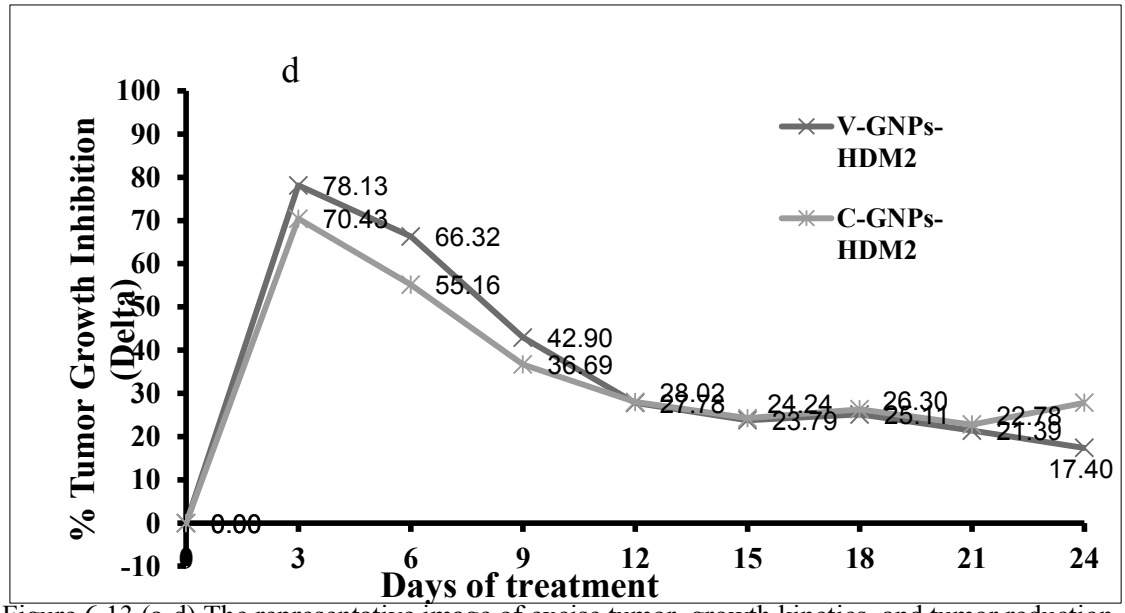

Figure 6.13 (a-d) The representative image of excise tumor, growth kinetics, and tumor reduction.

(a) The representative image of the tumor. (b & c) tumor growth kinetics and tumor volume (d). In life tumor growth reduction. C-GNPs-HDM2 shows the statistical significant difference in comparison with a control sample $P<0.001$ using two ways ANOVA followed by Bonferroni post-hoc test was performed using the Graph Pad Prism v5.

6.3.4.5 Biochemical and Hematological analysis

The biochemical and hematology analysis was performed at the end of the experiments, on the day of the euthanization. The blood was collected under light isoflurane anesthesia from all the groups for clinical assessment of liver function, Serum glutamic oxaloacetic transaminase/ Serum Aspartate Aminotransferase (SGOT/AST)) and Serum glutamic pyruvic transaminase/ Serum Alanine Aminotransferase (SGPT/ALT) ((Fig.6.14 a) & Kidney function Blood Urea Nitrogen (BUN, Creatinine) (Fig.6.14 b). Additionally peripheral blood smears were prepared and stained with May-Grunwald Giemsa stain and evaluated for the Differential Leukocyte Count (DLC) (Fig.6.14c).

Kidney function (BUN, Creatinine) & Liver function (SGOT, SGPT) parameters between the V-GNPs-HDM2, C-GNPs-HDM2 and vehicle control group (Figure 14.a & b). This indicates that there is no possible evidence of treatment related to specific organ toxicity (Liver/Kidney). Similarly, the results of Differential Leukocyte Count (DLC) revealed no significant changes in the percentage of lymphocytes, neutrophils, monocytes & eosinophils compared to control (Figure 14.a). The current results from DLC indicates that there is no possible evidence of bone marrow suppression (Figure 14c). In the current work, no signs of toxicity were noticed in liver and kidney functions with the dose of 5 µg/100µl/animal of C-GNPs-HDM2 and V-GNPs-HDM2 in terms of such as (Figure 6.14 a, b & c). The liver and spleen, which consist reticuloendothelial system confirms that the treatment given to the animal was not phagocytize; instead the treatment homed at the tumor site [442].

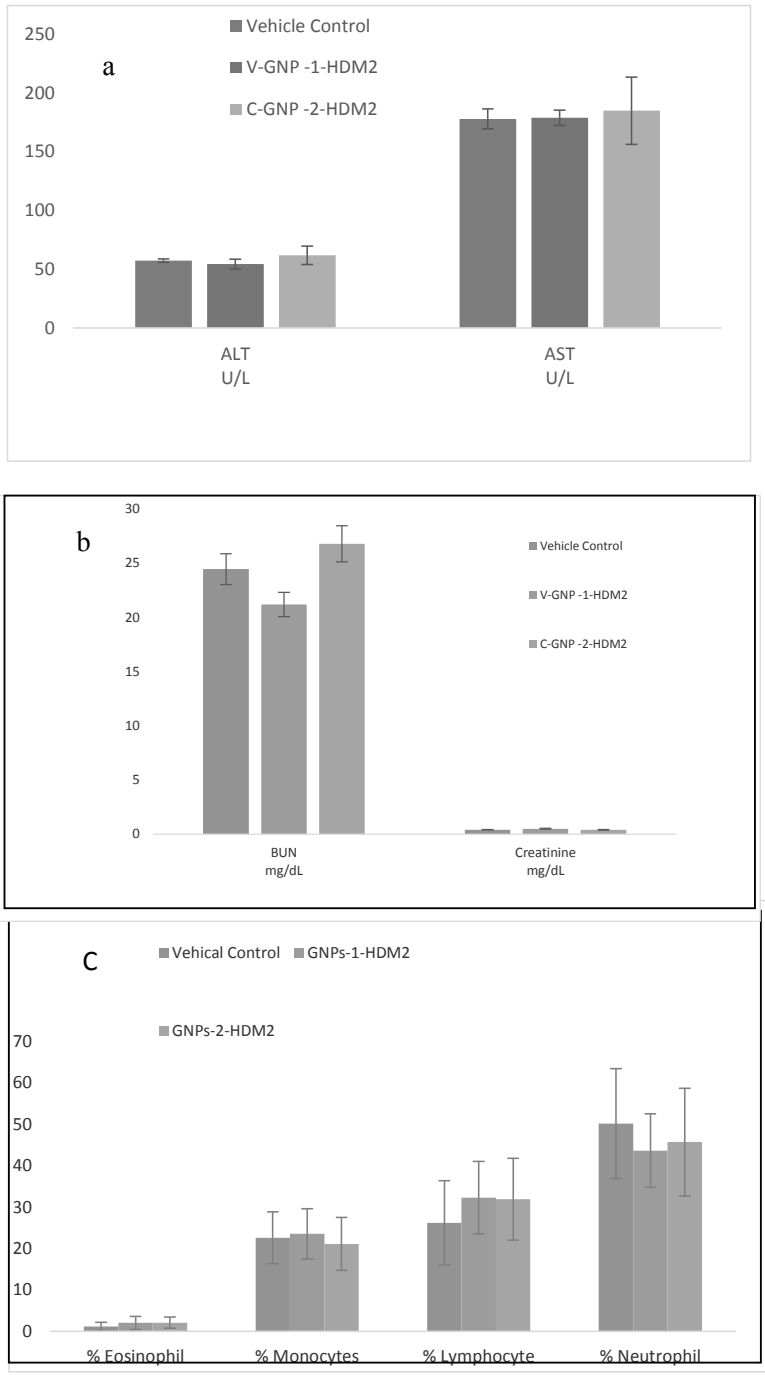

Figure 6.14 (a) Biochemical parameter; ALT (Serum glutamic oxaloacetic transaminase SGOT) AST (Serum glutamic pyruvic transaminase, SGPT), b)BUN and urea. C) %Total cell count Data expressed as the mean of 2-4 animals in each group.

Statistical analysis is carried out by one-way ANOVA. The data are statistically non-significant when V-GNPs-HDM2 and C-GNPs-HDM2 compared to control group.

6.3.4.6 Histology (Hematoxylin-eosin staining)

The histopathological analysis of the preserved tumor tissue and organs, liver, spleen, lung, heart, and kidney, was performed. The tissue was trimmed, processed, embedded in paraffin blocks and sectioned at 4-5 microns thickness. Tissue sections were stained with hematoxylin and eosin stains for microscopic evaluation.

(I) Histological features of tumor xenograft

The tumor tissue was evaluated for the histopathology analysis from C-GNPs-HDM2 and V-GNPs-HDM2 and control groups (Figure 6.15 a). The common feature all the 3 group includes the arrangement of cells & type of stroma. The cells are arranged loosely in sheets with a moderate amount of fibro-vascular stroma confirms the epithelial origin of the cells without any attachments. The cytological features of cells indicate cells are round with medium sized and the minimal amount of eosinophilic cytoplasm and distinct cell borders. The nucleus is large a characteristic feature of the RB cell rounded in shape with centrally located, hyper chromatic with finely stippled chromatin. The nucleus to cytoplasm ratio is altered with the nucleus occupying majority of the cell and each nucleus shows the presence of 1 or 2 nucleoli.

(II) Histological features of liver tissue

The liver tissue was analyzed for control, C-GNPs-HDM2 and V-GNPs-HDM2 appeared normal (Figure 15.b). The hepatic lobule hepatocytes were arranged in cords radiating away from the central vein with sinusoidal spaces in between lined by endothelium. The hepatocytes were normal sized with distinct cell boundaries, large nucleus with 1 or 2 nucleoli and vesicular cytoplasm containing many secretory vacuoles giving it a vacuolated appearance. Portal area at every alternate corner of the hepatic lobule

are present the portal area comprising of a branch each of the hepatic artery, portal vein and bile duct in fibrous connective tissue septa.

(III) Histological features of lung tissue

The lung tissues from different groups appeared normal including the vehicle control group. The common features include- Alveolar spaces - The alveolar sacs lined by flattened epithelial cells in close conjuncture with thin-walled capillaries were observed which was spread evenly over the lobes. There was no evidence of emphysema or atelectasis and the alveolar spaces were free of any exudate. Bronchioles -Terminal and tertiary bronchioles lined by simple ciliated cuboidal epithelium were seen at regular intervals. The lumen was clear of any discharge.

(IV) Histological features of spleen

The spleen from all the groups appeared normal with the following features- white pulp aggregates of mostly lymphocytes and macrophages, which are arranged around the arteries in the form of follicles in the white pulp (Figure 15d). Red pulp- majorly consists of vascular tissue with multiple erythrocytes in the vascular sinuses. These are sinusoids a specialized type of capillary, which is very leaky. The sinuses are interspersed with cords forming the framework.

(V) Histological features of heart

The heart tissue from various groups seemed to have the following normal features, Myocardium- the cardiac muscles appeared striated with intercalated discs and a single nucleus. The individual muscle fibers, were in close association with other fibers and no separation was seen (Figure 15 e).

(VI) Histological features of kidney

Kidney tissue appeared normal across all groups with the following features- Cortex- the cortical tissue showed multiple glomeruli/renal corpuscles associated closely with capillaries as well as tubules (PCT and DCT). No interstitial or tubular exudation or inflammation was noticed. Medulla- the medullary tissue consisted of multiple tubules, mainly collecting ducts with no renal corpuscles. No inflammation was seen in the medulla as well (Figure 15 f).

In summary, the tumor tissues obtained from animals of various treatment groups and the untreated vehicle group showed no significant differences and showed common characters in all the tissues. The other organs collected, namely liver, lung, spleen, heart and kidney appeared normal across all groups with no deviations.

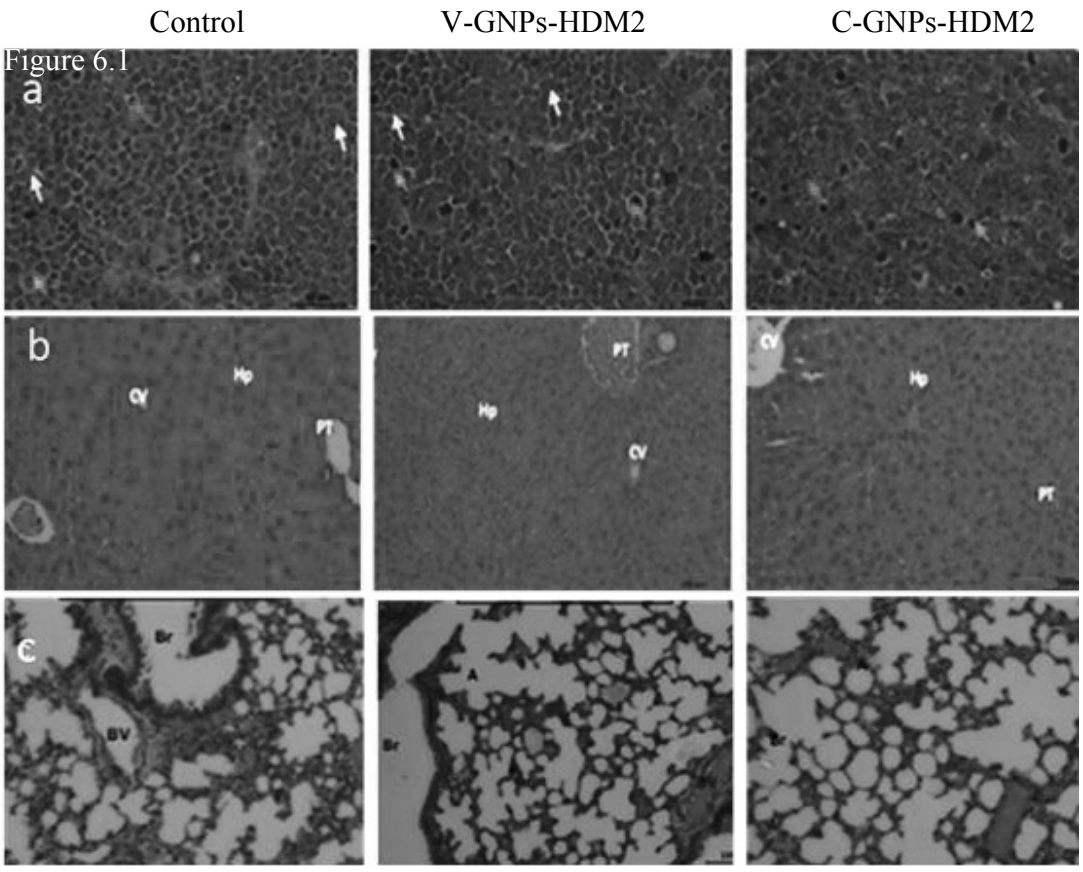

Figure 6.1

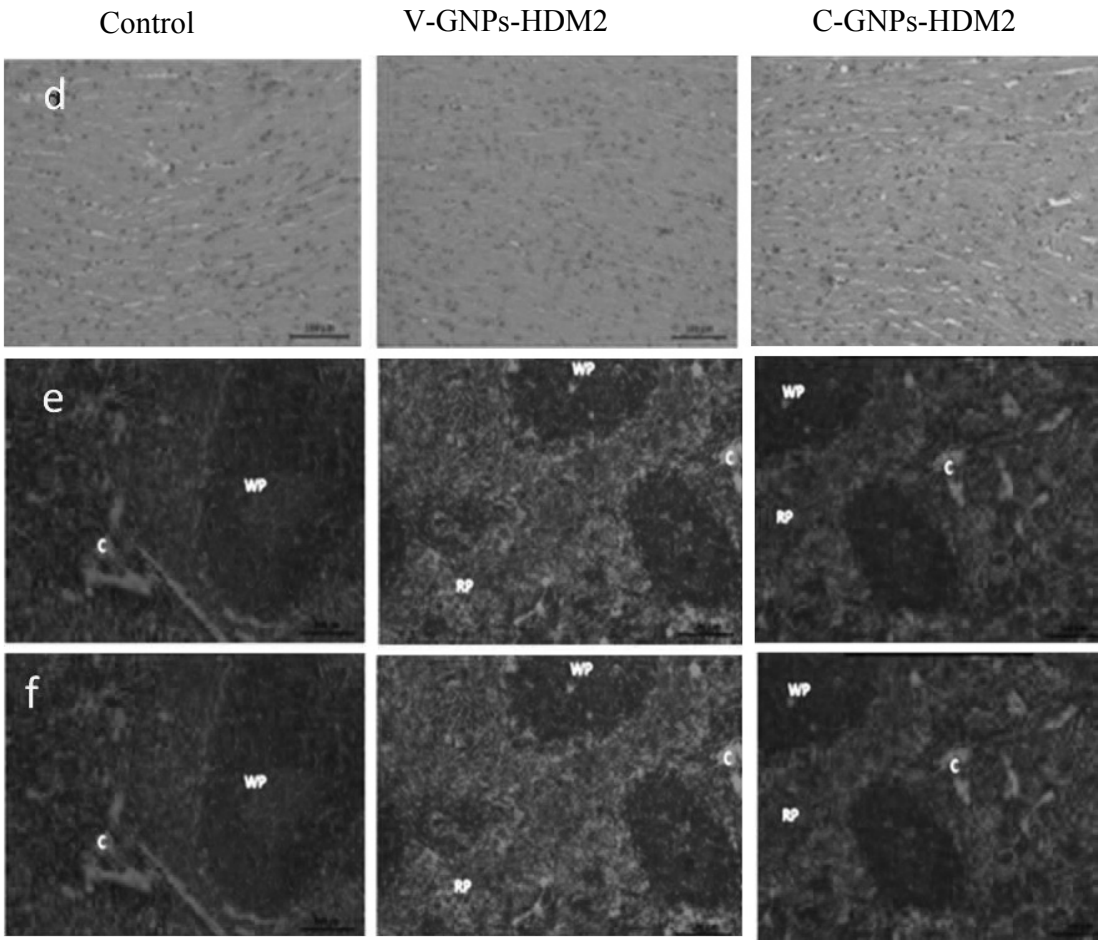

a) Tumor tissue, b) Liver, c) Lung, d) spleen e) Heart and f) Kidney

Figure 6.15 (a-f) Representative histological photographs (40X) of tumors from nude mice bearing Y79 xenograft

(a) Representative histological photographs (40X) of tumors from nude mice bearing Y79 xenograft. Mitotic figure (White arrow); Fibro-vascular stroma (Yellow arrow); Apoptotic figure (Red arrow); Neutrophil (Green arrow). Mitotic features: 1 to 2 multinucleate cells/ mitotic figures seen in a single field. Apoptotic figures: multiple (5-6) cells undergoing apoptosis seen in a single field (40X magnification). The other features a few neutrophils and monocytes have seen. **(b)** Representative photographs (20X) from the liver. PT- portal triad; CV- central vein; Hp- hepatocytes. (**c**). Representative photographs (20X) lungs. A-Alveoli; Br- Bronchiole; BV- Blood vessel. All photographs taken at 20X magnification. (d) Representative photographs (20X) of the spleen. WP- White Pulp; RP-Red pulp; C-cords. All photographs were taken at 20X magnification (e) Representative, photographs (20X) of heart from two animals in each group. All the fields show evenly arranged striated, cardiac muscles with a few RBCs in between the muscle fibers. Representative photographs (20X) of kidney.

6.3.5 RB, xenograft tumor sample apoptotic protein profiling

The apoptosis, is a natural process, which shows distinct biochemical changes and regulated by both apoptotic and anti-apoptotic molecules expressed in the cells. The two important families involved in the apoptosis are inhibition of apoptosis (IAP) and B-cell lymphoma 2 (Bcl 2). It has observed that an apoptotic maker X-linked Apoptotic Protein (XIAP) increased 0.36 fold and survivin 0.19 fold ($p<0.05$) (Figure 6.16 c), can act as an inhibitor of the apoptosis which shows increased expression in the C-GNPs-HDM2 treated animal [443]. SMAC/Diablo, a mitochondrial protein that negatively regulates XIAP expression is increased 0.27 fold ($p<0.05$) in C-GNPs-HDM2. The increase in the expression of the SMAC/Diablo enhanced the apoptosis by inhibiting the action of XIAP through binding of XIAP with Caspases. This interaction leads to the activation of Caspases activity and which induces the apoptosis of the tumor cell. Caspase activity which is a protein involved in cell death induced in the tumor sample could be specifically activated due to the targeting of the HDM2 through GNPs-HDM2.P^{21} (CDKN1a) protein down-regulate by 0.84 and 0.5 fold in C-GNPs-HDM2 and V-GNPs-HDM2 treated condition, respectively (Figure 6.16 c). The regulation of p21 gene is (CDKN1a) is controlled by the p53 dependent cell cycle arrest in G1 phase during the stress condition. The CDKN1a regulate the cell cycle through interaction with the proliferation of cell nuclear antigen (PCNA), which is a DNA polymerase accessory factor which plays an important role in S phase of cell cycle through a DNA replication, damage and repair. This protein was cleaved by CASP3-like caspases though activation of CDK2, and involved in apoptosis by caspase activation.

It is noticed that Pro-Caspase-3 and Cleaved Caspase-3 both are increased in the treated condition infer that the programmed cell death is the case of C-GNPs-HDM2 and

V-GNPs-HDM2 is mediated through the caspase pathways. The activity of the caspase in C-GNPs-HDM2 and V-GNPs-HDM2 is depending of the types of the GNPs used for targeting to HDM2 in RB xenograft tumor model. The current data infer that is target specific inhibition of the function of HDM2 through anti-HDM2 peptide.

Bcl-2 is an important target of the HDM2 which induce the apoptotic cell death through the intrinsic mitochondrial apoptotic pathway is down-regulated 0.2 fold ($P<0.05$) in case of V-GNPs-HDM2 whereas, Bcl-Xl up regulated, 0.67 fold ($P<0.05$). However, Clusterin a negative regulator of the apoptosis 0.4 fold decrease the expression in C-GNPs-HDM2, support to our findings that HDM2 peptide induce the cell death and reduces the tumor growth through targeting the HDM2 protein (Figure 6.16) [444]. In case of V-GNPs-HDM2, the clustering up-regulated compared to control. The significant increase 0.11 fold ($p<0.05$) expression of the Cytochrome-c, protein in C-GNPs-HDM2 and Smac 0.27 ($P<0.05$) in both conditions confirms the anti-proliferative effects in the treatment [445]. Survivin is an apoptotic protein of the IAP family member and shows significant increase by.0.2 fold and 0.19 fold ($p<0.05$) in V-GNPs-HDM2, C-GNPs-HDM2 respectively, indicates that stress induced amplification of Survivin protein. The up regulation of Survivin may correlate with the GNPs induced resistance of malignant with the cell. It has reported that the anticancer compound in combination with metal as a composite drug can induction the alternative cell death pathways [446, 447]. Similarly, here we observe that Survivin amplification, which is an alternative effective approach to combat with the cancer cell in stress condition. It can be an alternative method adopted by the cells to reduce the oxidative stress and enhanced the cell apoptotic cell death.

Figure 6.16 a

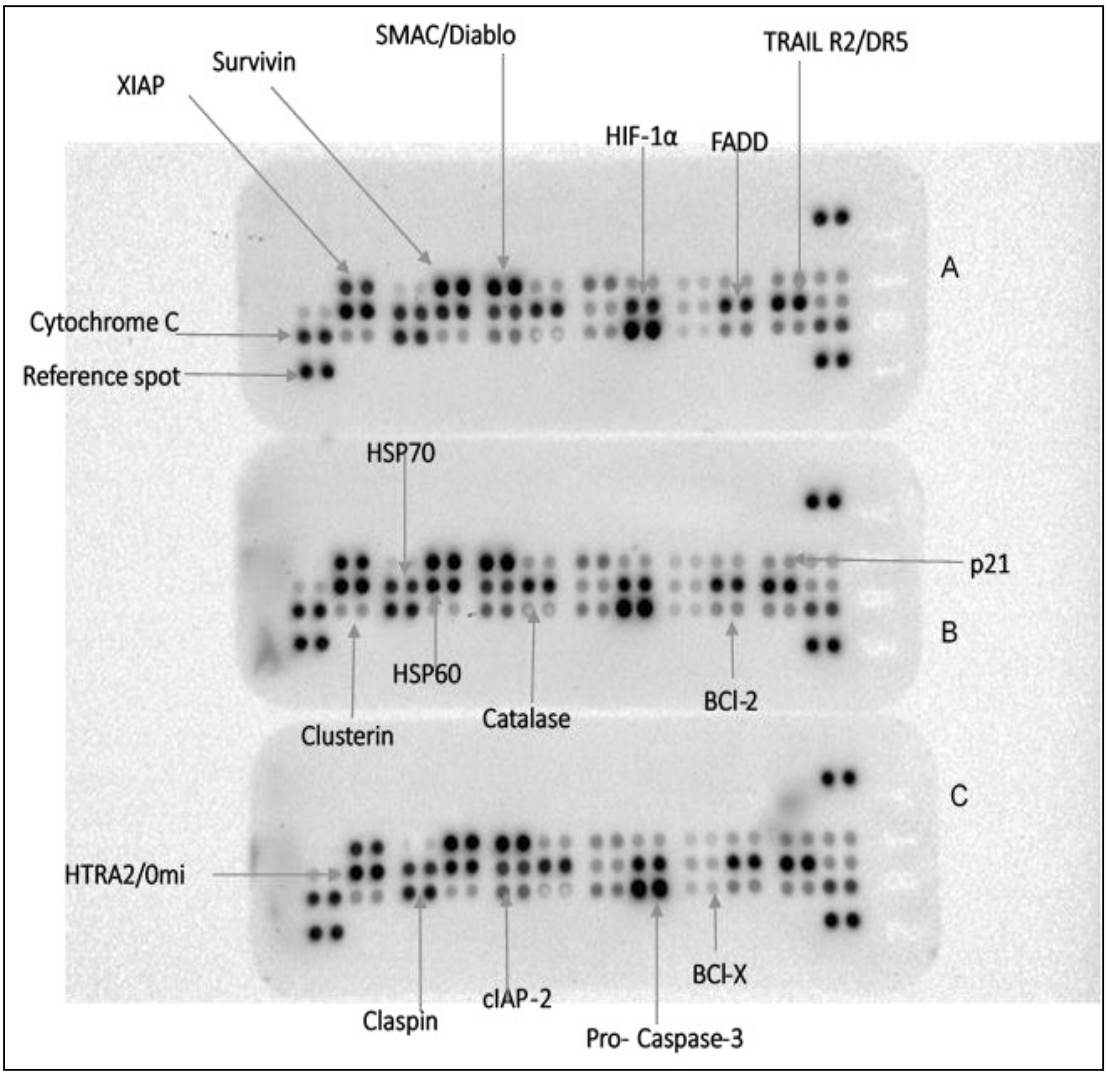
SMAC/Diablo
TRAIL R2/DR5
Survivin
XIAP
HIF-1α
FADD
A
Cytochrome C
Reference spot
HSP70
p21
B
HSP60
Clusterin
Catalase
BCl-2
C
HTRA2/0mi
BCl-X
cIAP-2
Claspin
Pro- Caspase-3

.

Figure 6.16 b

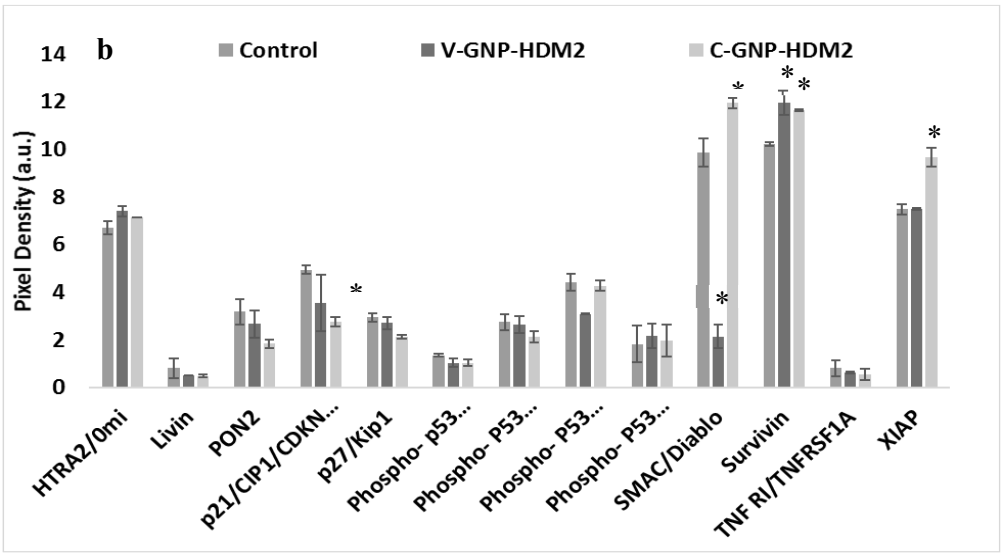
b
Control
V-GNP-HDM2
C-GNP-HDM2
Pixel Density (a.u.)
0
2
4
6
8
10
12
14
HTRA2/0mi
Livin
PON2
p21/CIP1/CDKN...
p27/Kip1
Phospho- p53...
Phospho- P53...
Phospho- P53...
Phospho- P53...
SMAC/Diablo
Survivin
TNF RI/TNFRSF1A
XIAP

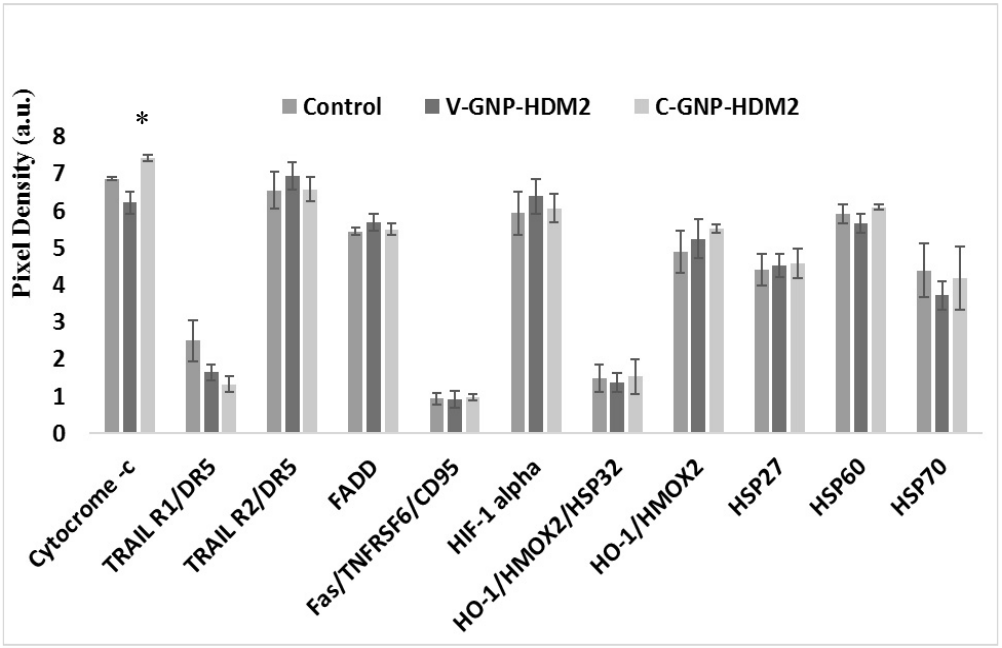
Control
V-GNP-HDM2
C-GNP-HDM2
Pixel Density (a.u.)
0
1
2
3
4
5
6
7
8
Cytocrome -c
TRAIL R1/DR5
TRAIL R2/DR5
FADD
Fas/TNFRSF6/CD95
HIF-1 alpha
HO-1/HMOX2/HSP32
HO-1/HMOX2
HSP27
HSP60
HSP70

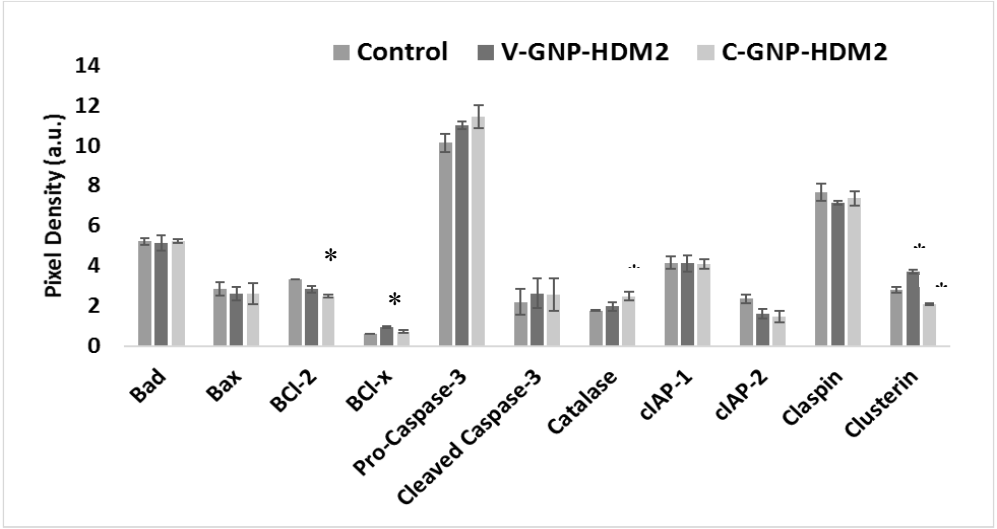
Control
V-GNP-HDM2
C-GNP-HDM2
Pixel Density (a.u.)
0
2
4
6
8
10
12
14
Bad
Bax
BCl-2
BCl-x
Pro-Caspase-3
Cleaved Caspase-3
Catalase
cIAP-1
cIAP-2
Claspin
Clusterin

Figure 6.16 c

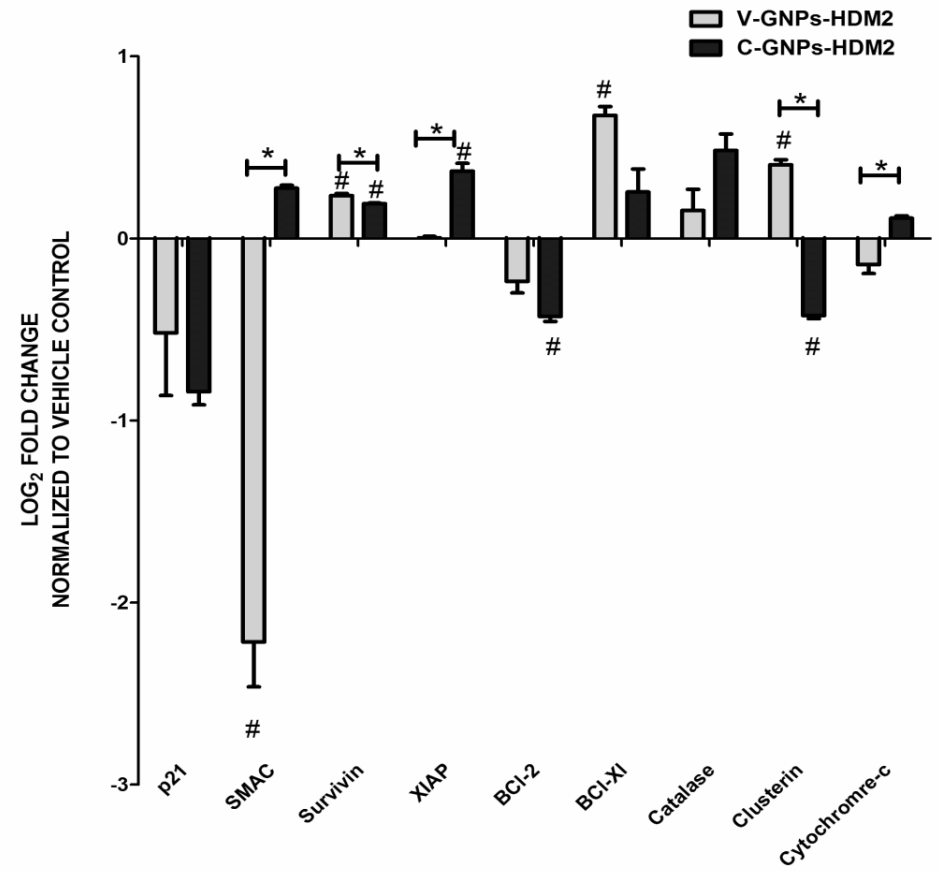

Figure 6.16 (a-c) Represent the expression profiling of important apoptotic protein. Apoptotic array panel indicates 30 proteins and the important which shows significant difference are marked.

(a) Represent the expression profiling of important apoptotic protein .a) Control sample, b) C-GNPs-HDM2 and c) V-GNPs-HDM2. It has Pro-apoptotic intrinsic proteins, extrinsic death receptors, and anti-apoptotic, cell cycle checkpoint, and stress responsive proteins**.**

(b) Apoptotic protein profiling A) V-GNPs- 1-HDM2 B) C-GNPs-2HDM2 2. * represent the statistical significance at $P<0.05$. p21, Bcl-2, XIAP, Catalase, Cytochrome c specifically show the significant difference in C-GNPs-HDM2 treated animals whereas SMAC Bcl-x in V-GNPs-HDM2 treated animals. Clusterin and Survivin, in both the condition.

(c) Apoptotic protein profiling, relative fold change with respect to untreated sample # represent the statistical significance with control and * between the group at $P<0.05$. Statistical analyzed was performed by one-way ANOVA and Turkey's post-hoc was used for multiple comparisons between groups. P^{21} though the significant difference was noticed in the intensity of due to high standard deviation in the mean in a mean density post-hoc test of multiple comparison does not show statistical significance difference.

6.3.6 Serum cytokines profiling in treating mice samples

Cytokines have a role in immunotherapy, which can lead to the destruction of tumors by either direct antitumor effect or an indirect improved of the antitumor responses of an immune system. A direct antitumor cytokines, like necrosis factor (TNF) alpha, interferon (IFN) alpha, TNF-α expression has decreased after the treatment with the V-GNPs-HDM2 and C-GNPs-HDM2 compared to the control sample which indicates that the macrophages mediated inflammation is not induced after the treatment with the GNPs-HDM2 in both the condition. Moreover, in the case of V-GNPs-HDM2 treated animal the expression of the TNF-α is further down-regulated by 0.7 fold (Figure 6.17 c) in comparison with the C-GNPs-HDM2 suggest that is due to *Vitis vinifera* as a reducing agent and the TNF-α is down regulated significantly [448].

This infers that there is no inflammation associated with the TNF-α. In addition to TNF, other cytokines which act directly with tumor cells is interleukin-6 (IL-6) to stop the growth of tumor cell. Although these cytokines are more effective with a combination and have a synergistic effect accruing from different cytokines. TNF-alpha have shown down-regulation compared to the control and in both the samples C-GNPs-HDM2 and V-GNPs-HDM2. Whereas, the IL-6 expression is not altered in treating samples, indicate that there is inflammation occurs after the treatment with the GNPs-HDM2. The cytokines change in TNF-α without alteration the IL-6 in treating samples confirms that there is an antitumor activity, which occurs after treatment with GNPs-HDM2. The GM-CSF, sICAM-1 and BLC/CXCL13, IL-1a is increasing significantly in the case of C-GNPs-HDM2. Whereas, the sICAM-1 and GM-CSF expression is down regulated by 1.9 and 1.2 respectively, compared to control in the case of V-GNPs-HDM2. The expression of Il-1a and BLC/CXCL13 decreased further in case of V-GNPs-HDM2 compared to C-GNPs-HDM2

[448]. GM-CSF (granulocyte–macrophage colony-stimulating factor) can act with indirect pathways for the tumor reduction by intecting without cytokines. It has been reported that GM-CSF can interact with antigen-presenting cells (APCs) and enhanced the synthesis of cytokines which can facilitate the activation of lymphocytes. It is clearly indicated that increasing GM-CSF has antitumor activity through immune response in case of C-GNPs-HDM2 whereas V-GNPs-HDM2 the antitumor activity is not associated with the immune response infer that this sample inhibiting the tumor growth through direct pathways. Whereas, in case of C-GNPs-HDM2 immune responses is dominated, it corroborates because, IL-1a another cytokine act indirectly through immune response and it is also up-regulated in the C-GNPs-HDM2 treated condition. In another study using "iron-saturated bovine lactoferrin (Fe-bLf) nanocarriers/nanocapsules" for the colon cancer cell stem cell targeted therapy, confirm that there is a significant change in IL-1β, which induces the apoptosis and is specifically released during apoptosis [36]. Whereas, IL-6 has dual function both proinflammatory, and an anti-inflammatory cytokine was reported less in concentration in nude mice (absence of T cells) compared to wild-type mice [449].

Similarly, in the case of V-GNPs-HDM2 and C-GNPs-HDM2 the IL-6 unaltered support our finding that there is no inflammation induced by the treatment in RB bearing xenograft nude mouse model. ICAM-1 (Intercellular Adhesion Molecule 1) or CD54 (Cluster of Differentiation 54) is a cell surface glycoprotein, which is expressed on endothelial cells as well as cells which are specific to the immune system. As indicated that the il-1a is up-regulating in the C-GNPs-HDM2, which intern up-regulate the expression of CD54, and indicate that C-GNPs-HDM2 treated animals are showing an

antitumor effect due to the immune system. Whereas, in V-GNPs-HDM2 treated tumor bearing animal ICAM-1 is released less compared to regulating similar to the TNF-α.

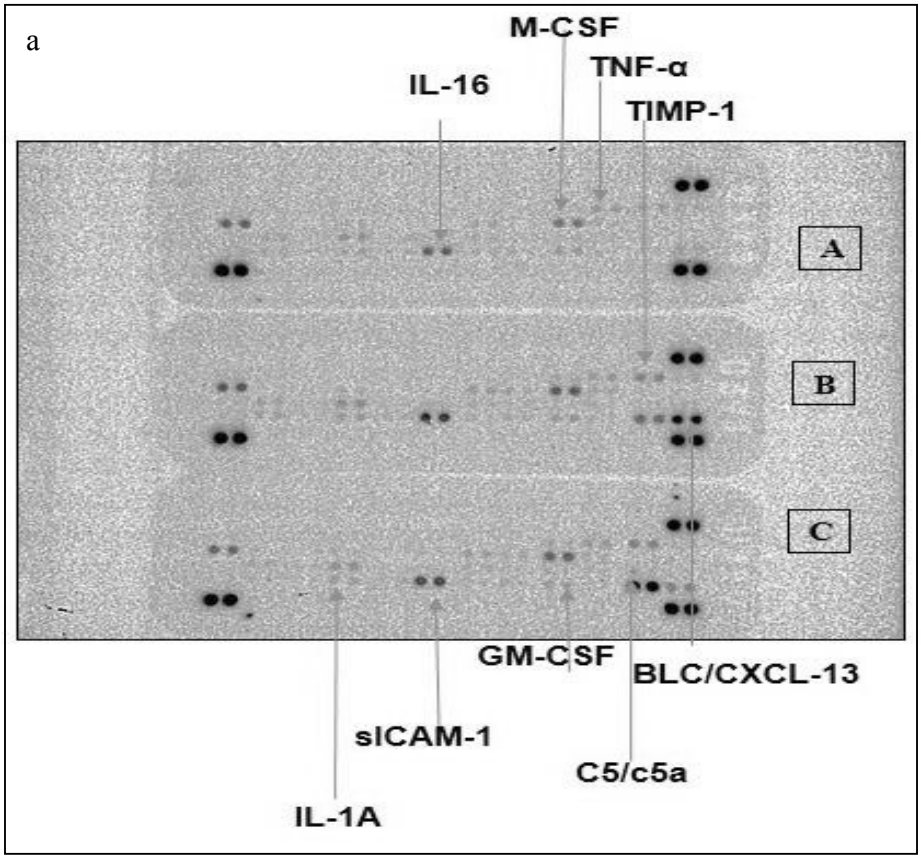

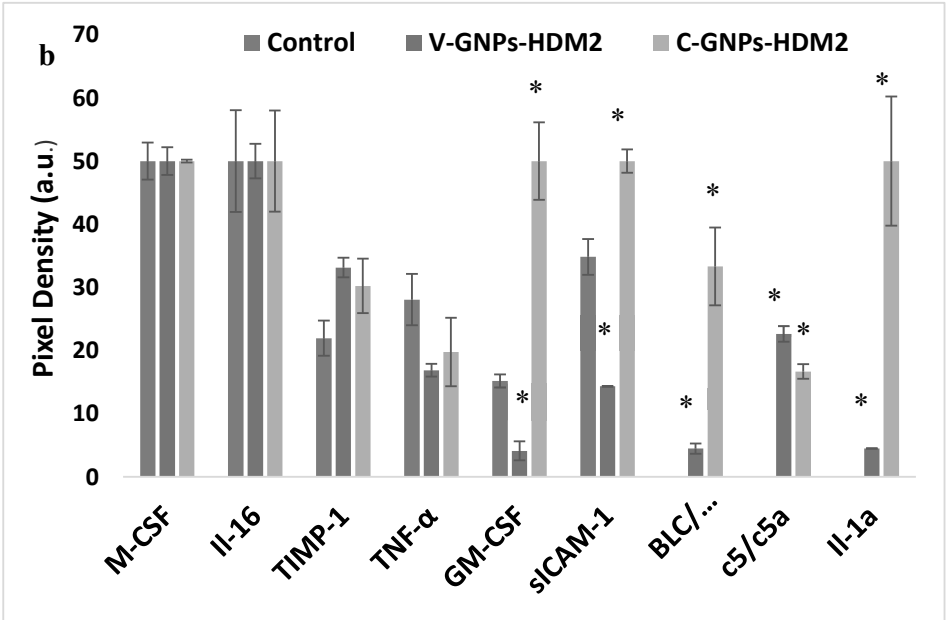

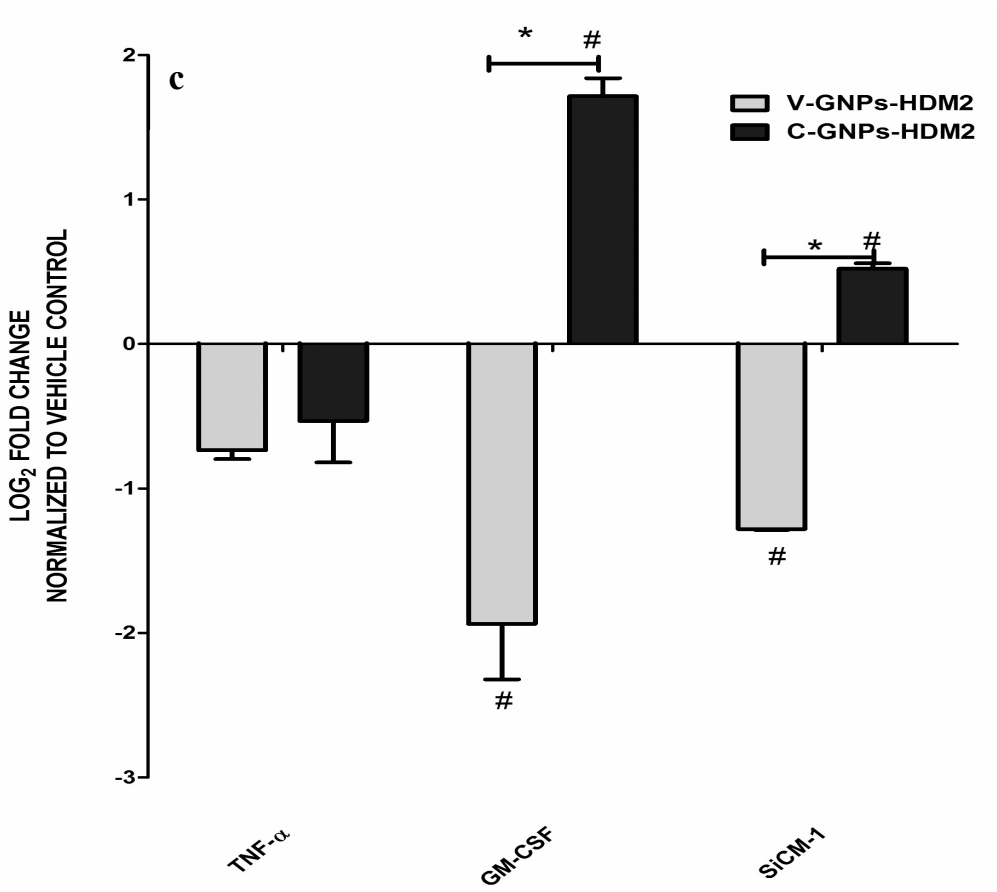

Figure 6.17 (a-c) Represent the expression profiling of important cytokines.

(a) Represent the expression profiling of important cytokines (a) Control sample, b) C-GNPs-HDM2 and c) V-GNPs-HDM2. Cytokines array panel indicates cytokines, chemokines, and acute phase proteins, which involved in signaling, infection/inflammation and regulate the process of an immune system.

(b) The * indicates the significant difference with respect to the control sample at $p<0.05$. The expression of, TNF α was reduced and that of BLC, CXL13, c5/c5a and IL-1a increased in both the groups compared to the controls. Whereas, GM-CSF and sICAM-1 decreased in V-GNP-HDM2 whereas C-GNP-HDM2 shows increase expression.

(c) Cytokines and chemokines profiling, relative fold change with respect to untreated sample # represent the statistical significance of control and * between the group at $P<0.05$. Statistical analyzed was performed by one way ANOVA and Turkey's post-hoc was used for multiple comparisons between groups. TNF-α though significant difference was noticed in the intensity of due to high standard deviation in the mean in a mean density post-hoc test of multiple comparison does not show statistical significance difference.

6.4 Discussion

The experimental results presented in the current study have been discussed with specific emphasis on the antitumor effect of anti-HDM2 peptide GNPs conjugate in RB, *in vitro* and *in vivo* and the significant difference in the responses of the cytokines and apoptosis protein in treating C-GNPs-HDM2 and V-GNPs-HDM2 xenograft tumor samples.

In designing, nanoscale based delivery vehicles for the targeted therapy using peptide it is required to the limit off-target effect without altering the native structure and function of the delivered molecule [450]. Bioconjugation of an anti-HDM2 peptide with PEGylated GNPs could reduce the RES uptake, the common problem encounters in the delivery of therapeutic molecules by the GNPs *in vivo* whereas in *in vitro* condition the RES is not effective. This formulation, GNPs-HDM2 increases the stability of peptide contribution and increased the probability of homing of the peptide at tumor site [451]. By this approach, GNPs-HDM2 do reach to the target site by the existence of favorable pharmacokinetics *in vivo*.

In the line of though, the current work has shown the HDM2 expression in the RB tumor to confirm the expression profile of the HDM2 in the RB tumor (Figure 6.2 and 6.3), which may help in vasculature of tumor. Therefore, the knockdown of the HDM2 could be an attractive approach to target the RB tumor. HDM2 knockdown (Figure.6.9) is more effective after treatment with the V-GNPs-the HDM2 and C-GNPs-HDM2. Whereas, in case of C-GNPs-HDM2 the knockdown of HDM2 is observed at mRNA and protein level shows significant ($p<0.05$). P53 expression doesn't regulate significantly in case of C-GNPs and C-GNPs-HDM2 at both mRNA and protein level. The data indicate that C-GNPs-HDM2 and V-GNPs-HDM2 shows the cell death induced by the knockdown of

HDM2 but the V-GNPs-HDM2 could show the p53 dependent pathways, whereas, C-GNPs-HDM2 could follow p53 independent pathways as because HDM2 knockdown could either regulate by p53 dependent or independent pathways [452, 453]. A similar type of study showed that antisense anti-MDM2 in breast cancer model, confirm that the p53 level elevated by, resulting from specific down regulating MDM2 expression in MCF-7 cell line, which contain the wild type of P53 similarly, RB also has wild type of P53 [44]. Whereas the MDA-MB-468 cell line which containing mutant p53, after specific inhibition of the MDM2 the p53 level hasn't elevated. This finding corroborates our *in vitro* data which shows knockdown in both types of GNPs but the p53 up regulation have observed only in V-GNPs-HDM2 treated Y79, a RB cell could be due to the presence of *Vitis vinifer*a polyphenols in V-GNPs, which help in elevation of p53 [454]. Several studies suggest the anti-proliferative function of *Vitis vinifer*a on different cancer have reported which confirms the anticancer effect of the active component present in *Vitis vinifer*a [455, 456].

To further confirm the effect GNPs-HDM2 for tumor growth reduction in *vivo,* using the subcutaneous xenografts model, induced by the Y79 cells to mimic the *in vitro* studies which can make the link at *in vitro* and *in vivo* results. In a study using anti-HDM2 peptide has shown the effective antitumor function in the RB tumor model, similar results we observed in the current studies *in vivo* level [249]. The nude mice injected with C-GNPs-HDM2 exhibited a significant reduction in Y79 cells tumor growth ($p<0.001$) 28% whereas, the V-GNPs-HDM2, which is more effective *in vitro* shows 17% reduction compared to vehicle control. A, moderate tumor growth reduction was noticed in the V-GNPs-HDM2 until the 9 days of treatment which shows 43% tumor growth reduction. Interestingly, at the same time C-GNPs-HDM2 shows 37% tumor growth reduction

corroborate our finding that V-GNPs-HDM2 is more effective compared to C-GNPs-HDM2 at *in vitro* and *in vivo*. Afterward, both group animals were performing similar tumor growth reduction until 21st days of with a single dose of treatment per days. Ambiguously, one of the mice in the C-GNPs-HDM2 group shows relative tumor volume (RTV) 1.19 compared to other animal which shows RTV in the range of 5-13 %. This could be attributed to better performance C-GNPs-HDM2 over the V-GNPs-HDM2 in a later stage of the experiment, from day 10th till 24th day (Figure 6.13 d). To further understand the difference observed in the *in vivo* response with due consideration of GNPs used for the targeted therapy in RB using anti HDM2 peptide, an apoptotic array was performed.

It has been reported that HDM2 have the multiple mechanism of regulation of cell death either p53 dependent or independent. The apoptotic protein profiling of the C-GNPS-HDM2 and V-GNPs-HDM2 treated xenograft bearing RB, confirms that there is a variation in effect apoptotic protein expressed in treated mice compared to untreated (Control). The apoptotic protein profiling of *ex vivo* tumor sample (Figure 6.13) confirms the cell death mediates through the activation of the apoptotic proteins which shows p53 dependent pathways in V-GNPs-HDM2 treated condition whereas C-GNPs-HDM2 shows p53 independent apoptotic cell death. Inside, a similar kind of study using RNAi -mediated silencing of HDM2 in breast cancer cell confirms that it reduced tumor cell growth and induced apoptosis, cell death by decreased Bcl-2 expression with increased caspase level as well as altered the cell cycle by arresting the cell cycle at G1 phases by suppresses expression of cyclin and Cdk proteins [457]. Similarly, C-GNPs-HDM2 and V-GNPs-HDM2 showed the less the Bcl-2 expression and increased the Bcl-$_{XL}$ confirmed it could follow the p53 dependent, knockdown of HDM2 and induces the antitumor effect [457].

Similarly, findings have been observed using plant flavonoids apigenin (4′,5,7-trihydroxyflavone) in human prostate cancer cell lines and xenografts in a thymic nude mice model [458]. The exposure of apigenin to 22Rv1 cell line led to a decrease expression of Bcl-$_{XL}$ and Bcl-2 and increase the expression of Bax, which interns triggers the caspase activation to lead to apoptosis. These findings reveal that apoptosis mediates through p53-dependent and independent pathways which cumulatively induce the cell death. Apart from that the result also confirms that 22Rv1 cell line apoptosis induced by mitochondrial membrane potential disruption and also by transcription dependent/ independent p53 pathways. The study further confirmed that apigenin-induced p53 stabilization through p14ARF-mediated down-regulation of MDM2 protein.

Apart from the oncogene status of HDM2, the growing evidence confirms that it HDM2 has p53-independent effects and can function as a tumor suppressor gene [459]. Therefore, it can be a remarkable gene and important target in cancer therapy. The p53 independent activity of the HDM2, which leads to apoptosis mediated through the regulation of anti-apoptotic protein XIAP. It has been reported that MDM2 bind to the mRNA that express XIAP and improves it changes, which intern leads to the amplified the expression of XIAP. The MDM2 mediated increased expression of XIAP enhanced the caspase which lead to apoptosis [460]. Similarly, in case of C-GNPs-HDM2, treated the tumor, 20% ($P<0.05$) increased expression of XIAP compared to control could lead to apoptosis in xenograft tumor sample. This finds confirmed that the reducing agent which used in the synthesis of GNPs play an important role, which not only affect the *in vivo* responses, but also change the apoptotic protein profiling through regulating the p53 dependent and p53 independent pathways. A study reports that to cleavage of Mdm2 at

Asp-Val-Pro-Asp (DVPD) via activation of a temperature-sensitive p53 and caspase-3-activity. Moreover, MDM2 can cleave by caspase-3 at a higher level than caspase-2, and it can lead to degradation of Mdm2 through introducing extra cleavage sites [461, 462].

The apoptotic pathways driven by the anti-HDM2 in RB *in vivo*, further studies were carried out and cytokines profiling described the role of immune system in relation to the HDM2 mediated antitumor effect. The current, observation with cytokine profile helps to understand the effect of C-GNPs-HDM2 and V-GNPs-HDM2 mode of action with the change in cytokine profiles. The ICAM-1 and TNF-α are specifically regulated by the V-GNPs-HDM2, which confirms the synergistic effect of *Vitis vinifera* reduced GNPs on the antitumor effect along with the HDM2 peptide [461]. It has been reported that peptide [463] such as cationic cell-penetrating peptide, (cPPs,) Antennapedia homeodomain-derived peptide (Antp), nona-arginine and Tat-derived peptide, inhibit tumor necrosis factor (TNF) induced signal transduction through down regulating the receptor by endocytosis mechanism. The TNF-α has many role in apoptosis and cell survival along with apoptotic pathways as well as inflammation and immunity. The GNPs tagged with TNF- α reached on early-phase of clinical trials in which the 27-nm citrate reduced GNPs used for the tumor targeting. It has shown that GNPs tagged with factor-α (TNF-α) (Aurimmune; CytImmune Sciences, Rockville, MD) has the dual effect of increasing tumor targeting reduce the toxicity of TNF-α and delivery at the target site. TNF-α is known for dual role as a cytotoxic and immunomodulator agent [172].

The recent studies on the regulation of the ICAM-1 of reactive oxygen species (ROS) indicate that ICAM-1 expression up-regulated whereas the antioxidant attenuated the ICAM-1 expression [464]. A similar observation is noticed in V-GNPs-HDM2 and C-

GNPs-HDM2 treated samples. V-GNPs-HDM2, significant down-regulate the ICAM-1expression ($P<0.05$) compared to the control sample (untreated sample). One of the basic functions of the Cell Adhesion Molecules (CAMs) in the multicellular organism is cell-cell interaction. Apart from the cell adhesion it has a various role in the cellular process such as cell migration, cell-cell signaling, and morphogenesis [465]. Endothelial cells expressed ICAMs or CAMs constitutively. ICAMs, helps in the dispersion of T lymphocytes on endothelial cells. Based on the current finding and the fact that resveratrol exhibits antioxidant property corroborate our findings that V-GNPs-1-HDM2 not only better in the tumor growth reduction, but it shows antioxidant potential [466-468]. In a similar kind of study using GNPs conjugated peptide for anti-cancer therapies using murine bone marrow macrophages indicates that the conjugate were recognized by the macrophages indicates that the conjugate was recognized by the macrophages. Consequently, the macrophage proliferation was stopped in GNPs-peptide treated condition which inhibits the pro-inflammatory cytokines TNF-alpha. Similarly, in the C-GNPs-HDM2 and V-GNPs-HDM2 the pro-inflammatory, IL-6 expression does not change, whereas TNF-alpha expression lower in case of V-GNPs-HDM2 significantly ($P<0.05$) which activates the macrophages and suppresses the expression of the TNF-alpha. Furthermore, the study confirms that macrophage activation is independent with the nature of the peptide but dependent on the pattern of peptide coating on GNPs.

The cytokines profiling helps to understand the design of the GNPs-peptide conjugate and its responses with the immune response either activate/deactivate immune responses. The immune responses could base on peptide coating and the sequence of peptide coating [469]. V-GNPs-HDM2, which is coated with the phenolic of the reducing

agent can regulate TNF-alpha expression in macrophages, which is an indicator of the inflammation induced by antioxidants [470]. There is an indeed a need to identify the role of the C-GNPs- and V-GNPs conjugated HDM2 peptide to understand the role of these two type of reducing agent in combination with the peptide for targeted therapy and combination therapy can develop for RB cancer. In general, in order to effectively use this newly developed organic-inorganic hybrid conjugate nano vehicle for targeted therapy. Since, the cytokines profiling of V-GNPs and C-GNPs not only help to understand the role of peptide in tumor growth reduction, but gives an insight to understanding the role of the immune system.

However, further detailed studies with the different mode of injection are strongly recommended to understand the bio-distribution, antitumor effect, molecular pathways and synergistic effect, which complements the HDM2 antitumor effect. There is no statistical significant difference was observed in the accumulation kinetics of GNPs between, V-GNPs-HDM2 and V-GNPs-HDM2 whether it is single or repeated administration. It has been reported in a similar kind of study that the mode of injection, either IV or to intratumoral doses not affect the distribution of GNPs and antitumor property in a laser coupled photoplasmonic treatment the other important parameter to consider is instillation of a single dose or multiple dose and the tumor size. [471, 472].

The use of nanotechnology is continuing to expand within the biomedical application, particularly for targeted cancer therapy, in order to use GNPs (~10 nm and 300 nm) as a nanocarrier, it is necessary to consider the mode of administration, distribution, accumulation, toxicity, apoptosis and cytokine/chemokine, the dose and size of the tumor

during the treatment to consider the nanomaterial as a candidate vehicle for the targeted therapy.

6.5 Chapter Summary

- HDM2 expression studies in RB tumor tissues revealed evidently a high expression of HDM2 protein, significant higher amplification of HDM2 mRNA at different levels, confirmed that HDM2 is a potential molecular target for RB cancer therapy.
- The *in vitro,* mRNA and protein level knockdown and *in vivo* result confirms that HDM2 is functional after conjugation with the GNPs and the tumor growth reduction has observed in both types of V-GNPs and C-GNPs conjugate
- The results suggest that C-GNP-HDM2 conjugate showed 28% ($P<0.001$) in tumor growth reduction, whereas V-GNPs-HDM2 showed 17% compared to control
- The protein profiling and cytokines profiling indicated that the difference in the apoptotic pathways induced by both typed of GNPs which are different at the same time. The cytokine profiling also confirms that the immunogenic responses difference in both samples is due to the presence of the different reducing agent in GNPs.

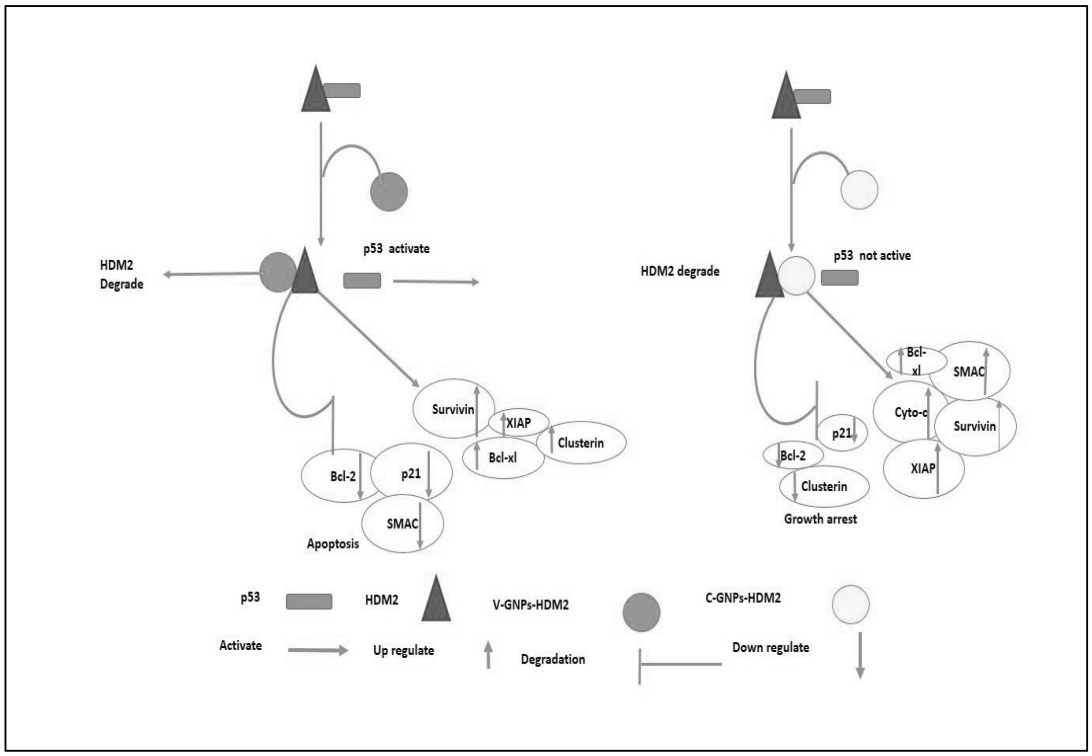

Figure 6.18 Proposed mechanism of apoptotic by V-GNPs-HDM2 and C-GNPs-HDM2 by the dissociation of the active HDM2 after binding with anti- HDM2 peptide.

V-GNPs-HDM2 activate the apoptosis by re p53 targets apoptotic gene such Bcl-2 and SMAC and kept significant protein level low ($P<0.05$). Where as in C-GNPs-HDM2, released HDM2 free to promote the degradation of its other target p21 and thus the level of p21 protein significant low ($P<0.05$) due to HDM2 degradation and insufficient transcription activation of p21 which interns cells undergo to apoptosis**.**

CHAPTER 7

7 FTIR spectroscopic imaging of xenograft RB tumor tissue a tool for molecular diagnosis

This chapter reports the application of vibrational microspectroscopy to understand the differences observed in the tumor growth reduction after treatment with V-GNPs-1-HDM2 and C-GNPs-2-HDM2 in the xenograft RB tumor sample. FTIR, (Fourier Transform Infrared) is a powerful method for imaging macromolecules in biological systems. The non-destructive label free spectroscopic techniques in combination with multivariate data analysis provide the molecular fingerprint to identify the chemical interaction of the HDM2 functionalized GNPs and therapeutic importance of the novel conjugate synthesized for therapeutic application in RB.

7.1 Background

Over the last few decades, FTIR spectroscopy has become a modern photonics technique in the field of cancer diagnosis [284, 285]. It has opened a new path in the field of molecular diagnosis, which can effectively identify the presence or absence of a specific interaction between the biomolecules the cellular component, qualitatively and quantitatively. FTIR microspectroscopy is a potential approach in contrast to the available molecular and histopathological techniques, which rely on the statistical confidence and operator expertise [283]. Whereas, vibrational spectroscopy relies on non-perturbing identification of molecules arising from the inherent chemical composition of the tissue sample [282]. The identification of the differences non-invasively and fast by unique the spectral signature of each endogenous molecular functional group of the biomolecule is the

ultimate aim to achieve with the spectroscopic technique [289, 473]. The microbial cell was used first to identify the biomolecules using FTIR in the mid-infrared frequencies from 4000 to 600 cm^{-1} [301, 474]. The amide I which arises from the coupled C=O stretching and N–H bends of protein is the most common and prominent vibration band observed in biomolecules [297, 302]. The amide I is a very sensitive bond which shows variation according to the protein secondary structure [296, 475].

FTIR technique is to identify the differences in the complex cancer tissue, which involves a wide range of spectral profile contributed by particular vibrational peak shifts, band shapes, intensity [303]. The spectroscopy can be a new diagnostic tool for the analysis of the tumor sample due to the sensitivity and specificity without interference of the chemicals used in the processing of the tissue for the analysis unlike IHC [300]. Early detection of cancer is indeed a primary requisite for the effective treatment of cancer, as it is asymptomatic during the initial stage of disease progression. Similarly, the chemical interaction between the cellular macromolecules and therapeutic molecules can also studied with FTIR, which give an insight for interaction between the target moiety (Therapeutic molecules) and specific macromolecule such as DNA, RNA and protein, lipids, carbohydrates and nucleic acids. This molecule shows a distinct band in FTIR spectra, which is identical with respect to each molecule [290-292].

The detailed study of xenograft RB tumor samples for the identification of interaction with cellular macromolecules such as protein, nucleic acid, and lipids. Our results indicate that the interaction of the novel conjugate (GNPs-HDM2) with tumor cell changes the chemical composition in terms of quantity, which we hypothesize could be due to differences in the specific interaction of the reducing agent used for the synthesis of

GNPs. Similarly, after interaction of GNPs-HDM2 with tumor tissue can change biomolecules quantitatively and qualitatively. This is first attempt to understand the interaction of the GNPs-HDM2 with the cellular component at the molecular level. It can help in understanding of tumor growth reduction attained by V-GNPs-1-HDM2 and C-GNPs-HDM2 treated *in vivo* (Discussed in Chapter-6) [305].

7. 2 Materials and Methods

The methodology used for the experiment performed in this chapter has been explained and discussed in detail in Chapter 3. A brief outline of the experiments performed mentioned below.

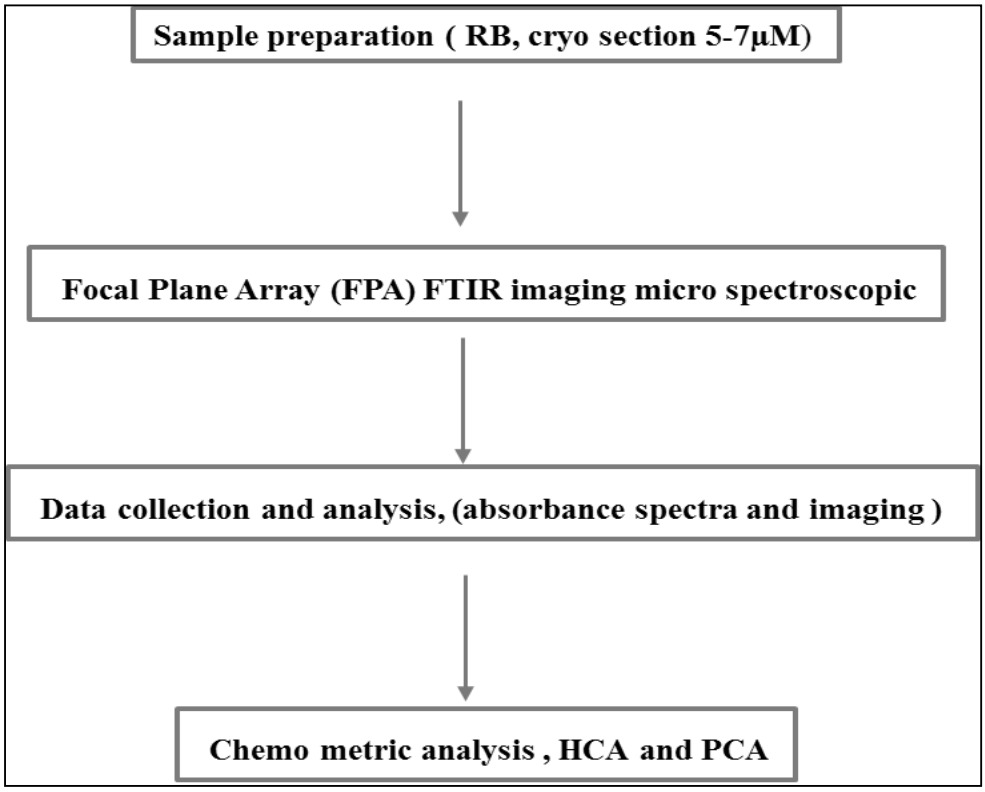

Figure 7.1Flow chart shows the methods used in the FPA-FTIR data analysis

7.3 Results

7.3 .1 Multivariate data analysis, Hierarchical cluster analysis (HCA)

HCA analysis of RB, xenograft tumor sample was performed on, control, (Vehicle control), GNPs-1 (V-GNPs-HDM2) and GNP-2 (C-GNPs-HDM2). The representative tumor from each group has been shown in the Figure7.2. The Multivariate data analysis was performed using HCA CytoSpec v. 1.4.02 (Cytospec Inc., Boston, MA, USA) and PCA uses Unscrambler 10.1 software package (CAMO Sofware AS, Oslo, Norway). The main criteria include the appropriate sample thickness, which includes the absorbance over the 1620-1680 $cm^{-}1$ spectral and the other criteria includes spectral absorbance either less than 0.2 or greater than 0.8.

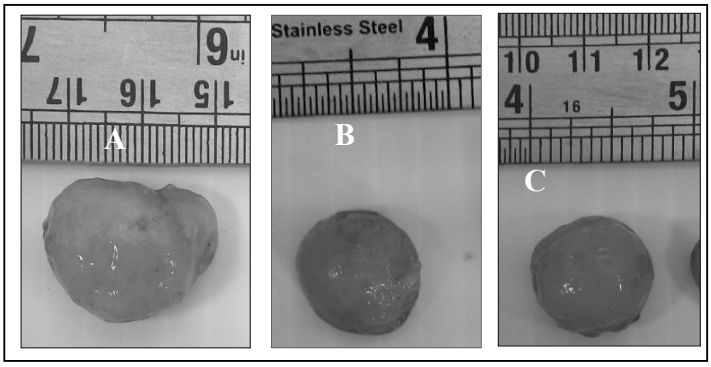

Figure 7.2 The representative image of ex-vivo Retinoblastoma xenograft tumor use for the analysis A) Vehicle control (Control) B) GNPs-1 (V-GNPs-1-HDM2) and(C-GNPs-2-HDM2)

The cluster analysis was performed on pre-processed "2^{nd} derivative" data of the area-normalized spectra in the region 930-3040 $cm^{-1.}$ The spectral range for vector normalized was in between 930-1800 and 2810-3040 cm−1. Figure7.3. Discrimination between the three samples in a hierarchical tree was made with multi-dimensional Hierarchical Cluster Analysis (HCA) using Ward's algorithm, which is the most

appropriate method for quantitative variables and clustering into group [476]. The HCA analysis the similarity between pairs of spectra from all the three samples and groups them into distinct clusters in a dendrogram until the overall analysis is complete.

HCA revealed the intragroup similarity within the control (untreated tumor) and tumor treated with V-GNPs-HDM2 and C-GNPs-HDM2 and generated5 clusters in each group. The average spectra were obtained from the second derivative with a baseline, smooth and vector normalization at 930-1800 and 2810-3040 cm–1. The maximum heterogeneity level was found in the lipids and nucleic acid regions. Lipids were observed in the IR absorption spectrum according to available literature as mentioned earlier in the spectral range 930-1800 and 2810-3040 cm–1. The difference in the spectral range was established by considering the similar areas of biological functional groups in all the sample with the highest possible difference between same tumor samples. The dendrogram clearly showed distinct clusters between control, GNPs-1-HDM2 and GNPs-2-HDM2 treated groups. All samples were clearly discriminated and formed one sub-cluster (Figure 7.4). These results show that the biochemical composition of the RB xenograft tumor sample is influenced by the treatment of the GNPs-HDM2 conjugate differently.

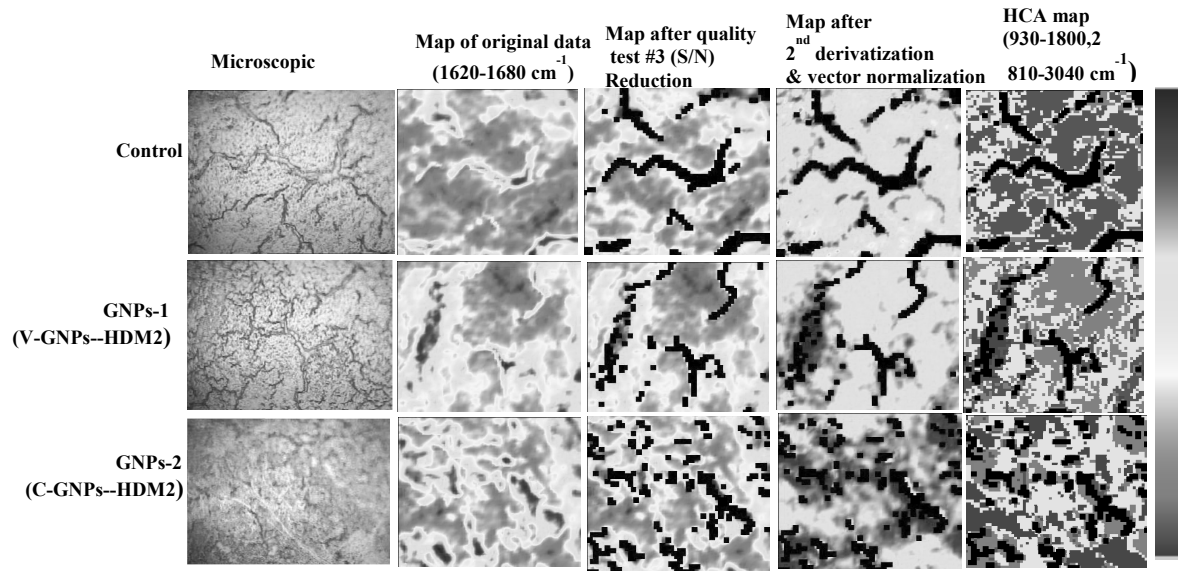

Figure 7.3 Represents the micro-spectroscopic images of Control, V-GNPs-1-HDM2 (GNPs-1) and C-GNPs-2-HDM2 (GNPs-2) tumor from each group were used for the spectral processing for each group after the second derivative analysis.

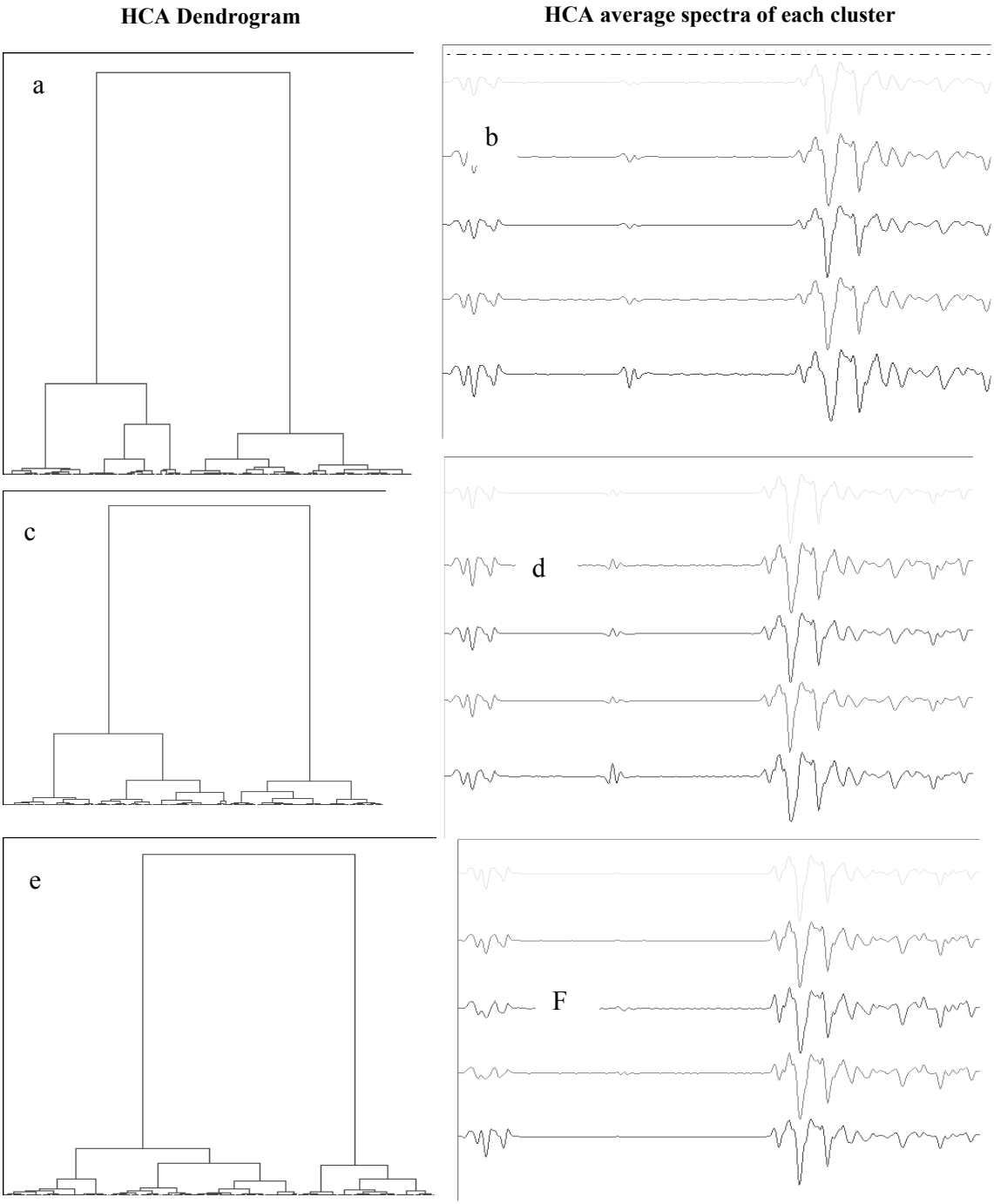

Figure 7.4 HCA on pre-processed 2nd derivative" data (version 3 with quality test and noise Reduction). HCA dendrogram and average spectrum of each cluster. Control (A & B), V-GNPs-HDM2 (C&D) and V-GNPs-HDM2 (E&F). 5 cluster were selected in each sample for the HCA analysis.

7.3.2 Principle Component Analysis (PCA)

PCA was performing on absorbance spectra of the data set of three samples obtained from each group includes control, V-GNPs-HDM2 (GNPs-1) and C-GNPs-HDM2 (GNPs-2). The total raw spectral data are 1493 from all three groups, which include 543 spectra from control, 486 spectra from GNPs-1 and 464 spectra from GNPs-2

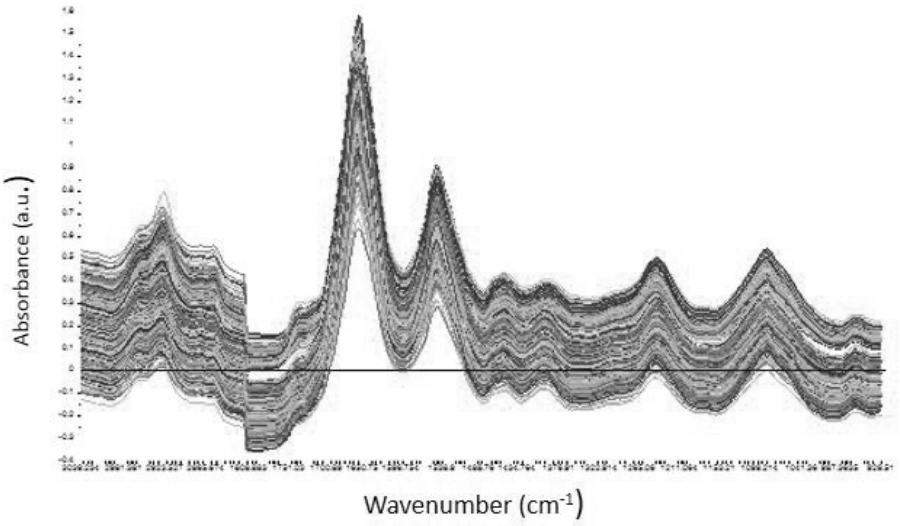

Figure 7.5 Represent the absorbance spectra of the raw data set (Total no. of spectra=1493) with total scattering recorded in the RB sample.

7.3.2.1 Spectral processing in bio bands

The absorbance data were used for the Extended Multiplicative Scatter Correction (EMSC) performance using "biobands". The biobands of the wavenumber between 3040-2810, 1800-930 with interval 1-60,320-548 was selected for analysis. The actual biobands wavenumber is 3039.234-2811.677, 1808.883-929.51. The specific range was selected since, it is useful in identification of the lipids and protein molecules present in the mammalian cells (Figure 7.6). The many spectral bands overlap in the unprocessed

spectrum, therefore it is imperative to process the data and use the second derivative to get the distinct individual bands from the original data set. (Figure.7.6).

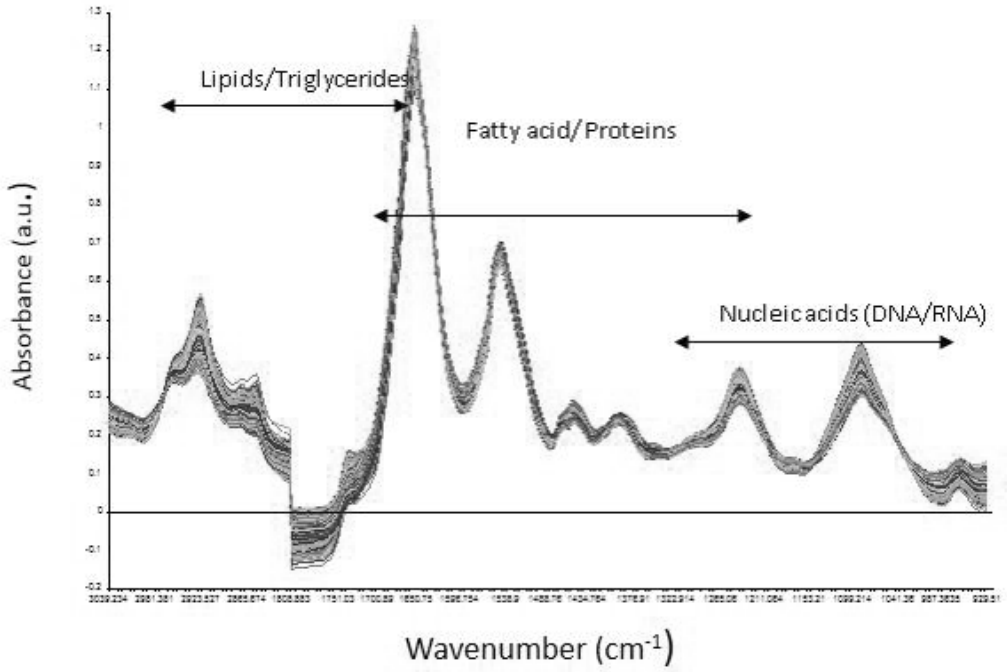

Figure 7. 6 Represent the spectra of bio-band. The marked difference in the spectrum (compared to Figure 7.5) is due to the representation of spectra of interest alone from the bio-band

7.3.2.2 PCA analysis of the raw data set in the bio-band range

PCA performed to extract the most significant difference between the three groups of spectra of the xenograft, RB tumor samples. The score plot visualization of the data in PCA whereas, the loading plot is an indicator of the biochemical functional group obtained in PC level [477]. The total spectral data analysis was carried out using Bioband to extract the most relevant information (Figure 7.7).

PCA was performed on the spectral data of "BioBands" through cross-validation at 7 PCs. The interval = 1-60,320-548 in the range (wavenumber): 3040-2810, 1800-930. The actual biobands wave number was 3039.234-2811.677 and 1808.883-929.51 cm-1. The recommended PC was up to 4 levels, which shows 95.22% of the variance. The clear

discrimination between the three groups is a function of the PC level. It was observed that at PC-1, C-GNPs-HDM2, and V-GNPs-HDM2, PC-3 the clearly showed more loading, respectively. As it has been noticed that in a PC score plot of unpriced original data that all the three groups, (Control, C-GNPs-HDM2, and V-GNPs-HDM2) shows clear scattering at different PC level.

Figure 7.7

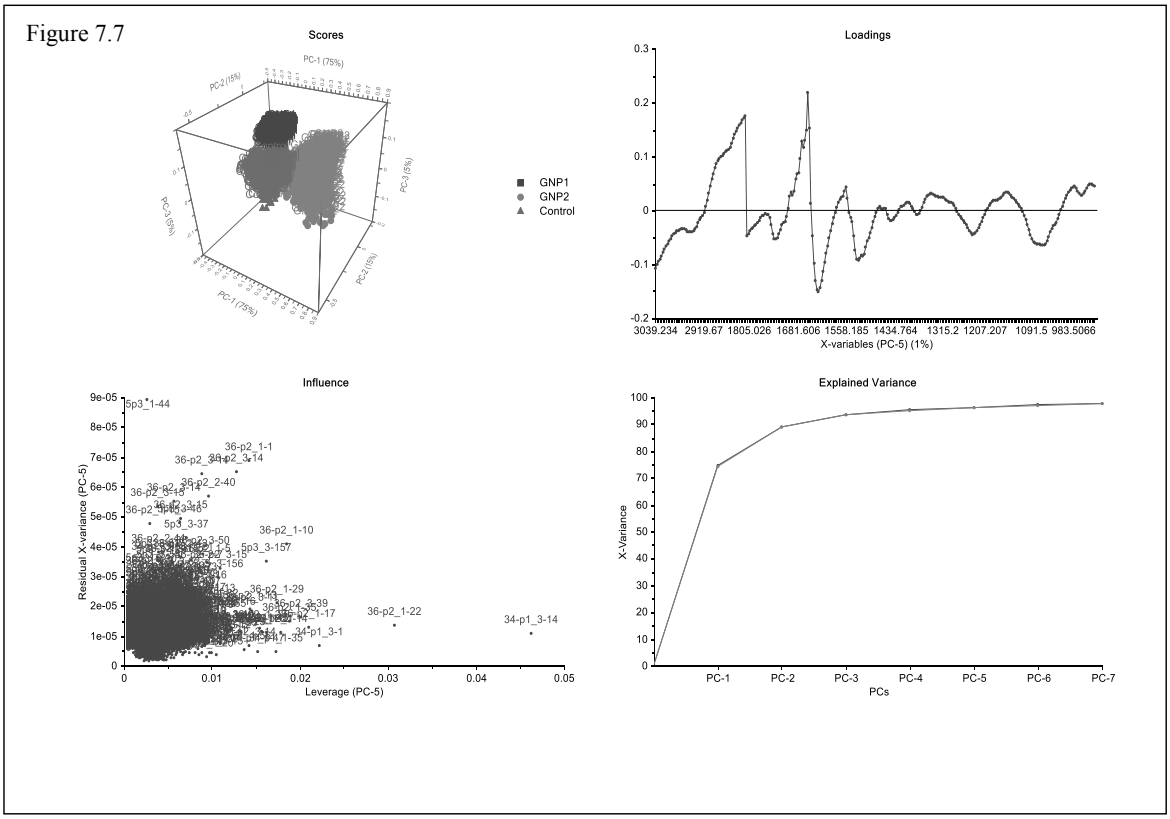
Scores
PC-1 (75%)
PC-2 (15%)
PC-3 (5%)
GNP1
GNP2
Control
Loadings
X-variables (PC-5) (1%)
Influence
Residual X-variance (PC-5)
Leverage (PC-5)
Explained Variance
X-Variance
PCs
PC-1
PC-2
PC-3
PC-4
PC-5
PC-6
PC-7

Figure 7.7 b

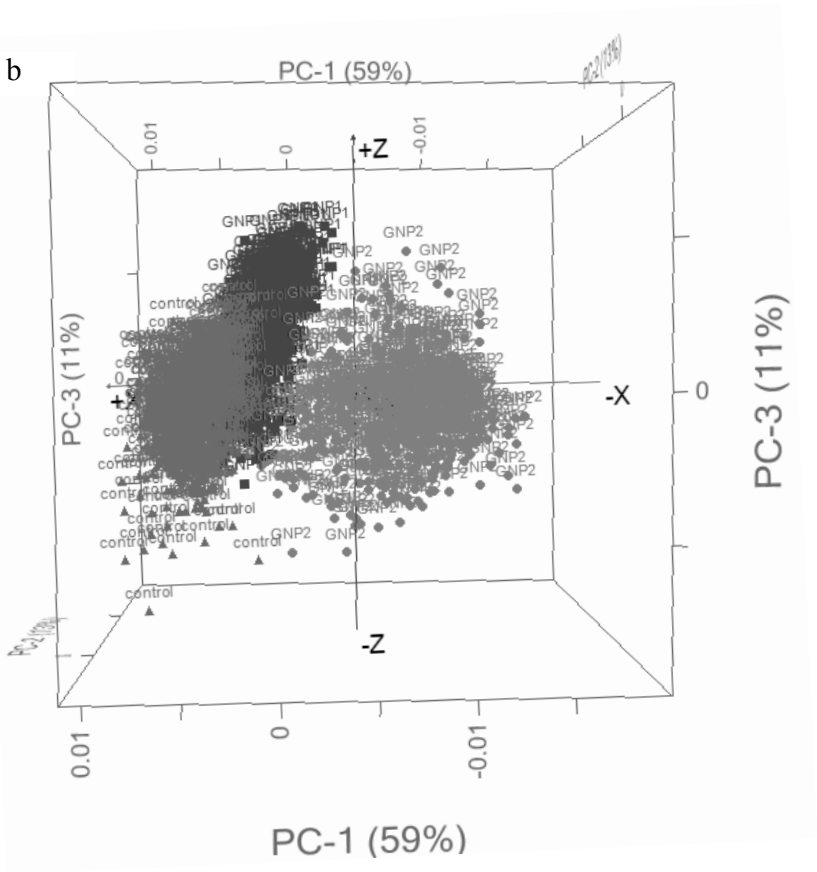

Figure 7.7 PCA score and loading plot shows of un-derivatized dataset (A &D). A -PC-score plot, B) Loading, D) Cumulative variance explained by PC for Control, GNPs-1 (V-GNPs-1-HDM2) and GNPs-2 (C-GNPs-2-HDM2)

7.3.3.1 Spectral processing using 2nd derivative spectra of all the data sets

The second derivative (Figure 7.8) was obtained from the normalized spectra is Figure 7.4 &7.7. 2nd derivate performed with 13-point smoothing and 3 polynomial order. The spectra obtained for second derivative after EMSC was performed using “biobands" in the wave number range 3040-2810, 1800-930 with data interval of 1-60,320-548. The actual wavenumber was 3039.234-2811.677, 1808.883-929.51.

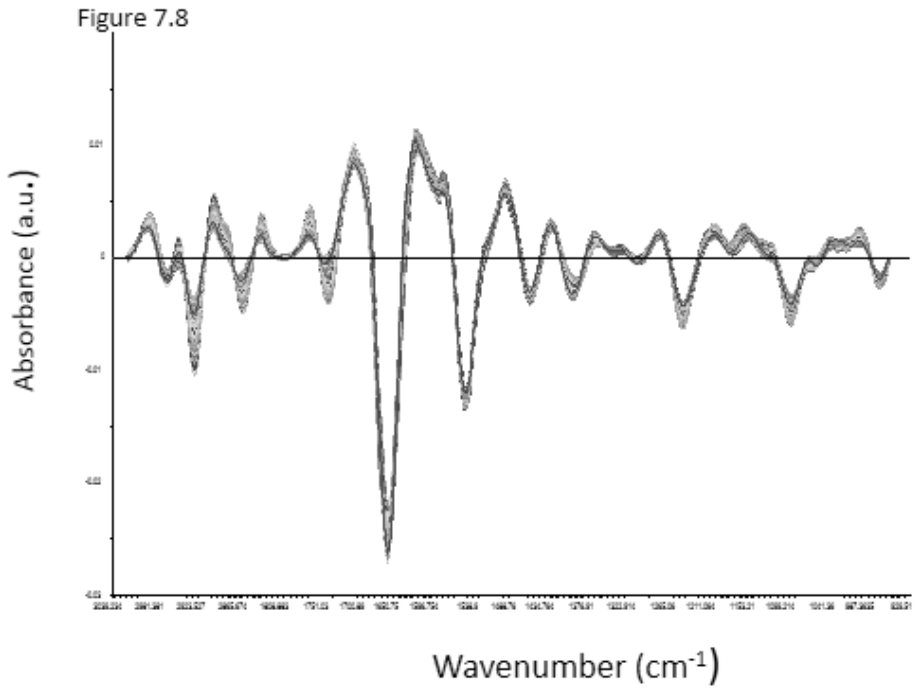

Figure 7.8 The spectra obtained after the EMSC to obtain the maximum difference in the PC to differentiate the Control, V-GNPs-1-HDM2 and C-GNPs-2-HDM2 after EMSC analysis

7.3.3.2 PCA analysis of the 2nd derivative set in the bioband range

The 2nd derivative PCA was performed from spectral sets of "biobands" with cross-validation and 7 PCs with the interval of 1-60,320-548 cm-1.The leverage correction was done in the biobands of wavenumber 3040-2810, 1800-930 cm-1. The actual band wavenumber was 3039.234-2811.677 and 1808.883-929.51 cm-1 the recommended PC-4 which accounts for 89.24% of the variance in the 2nd derivative data set. The scatter plots of PC1 (variability; 51%) and PC2 (variability; 11%) and PC2 and PC3 (variability; 13%) are shown in Figure 7.9, respectively. The scatter plot of PC-1 (Figure 7.9) showed difference between control and C-GNPs-HDM2 whereas, PC3 showed difference against control and V-GNPs-HDM2 clearly confirmed that same type of tissue (RB xenograft) showing the difference due to different treatment condition. The loading difference in all

three samples with the difference at PC-1, PC-2, and PC-3 indicated the difference in the sample. In case of PC-1 (Figure 7.9A) the loading of protein and lipids are in both the direction (negative and positive) while PC-3 shows loading in almost always in the positive direction (Figure 7.9 C). In contrast, PC-2 showed very less loading in both the direction with positive and negative (Figure 7.9 B)

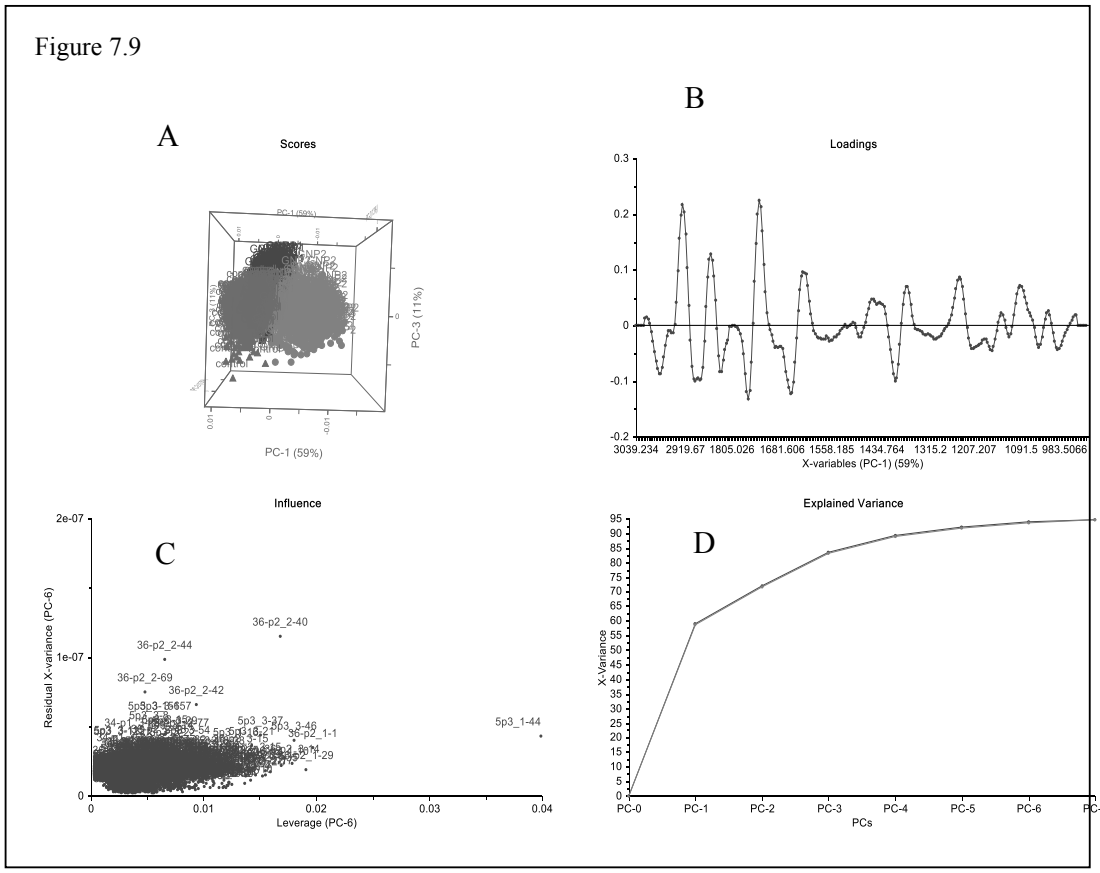

Figure 7.9 Shows the 2nd derivative PCA score indicates the PC-loading and variance. PCA score and loading plot shows of 2nd derivative dataset (A &D).

A -PC-score plot, B) Loading, D) Cumulative variance explained by PC for Control, GNPs-1 (V-GNPs-1-HDM2), and GNPs-2 (C-GNPs-2-HDM2).

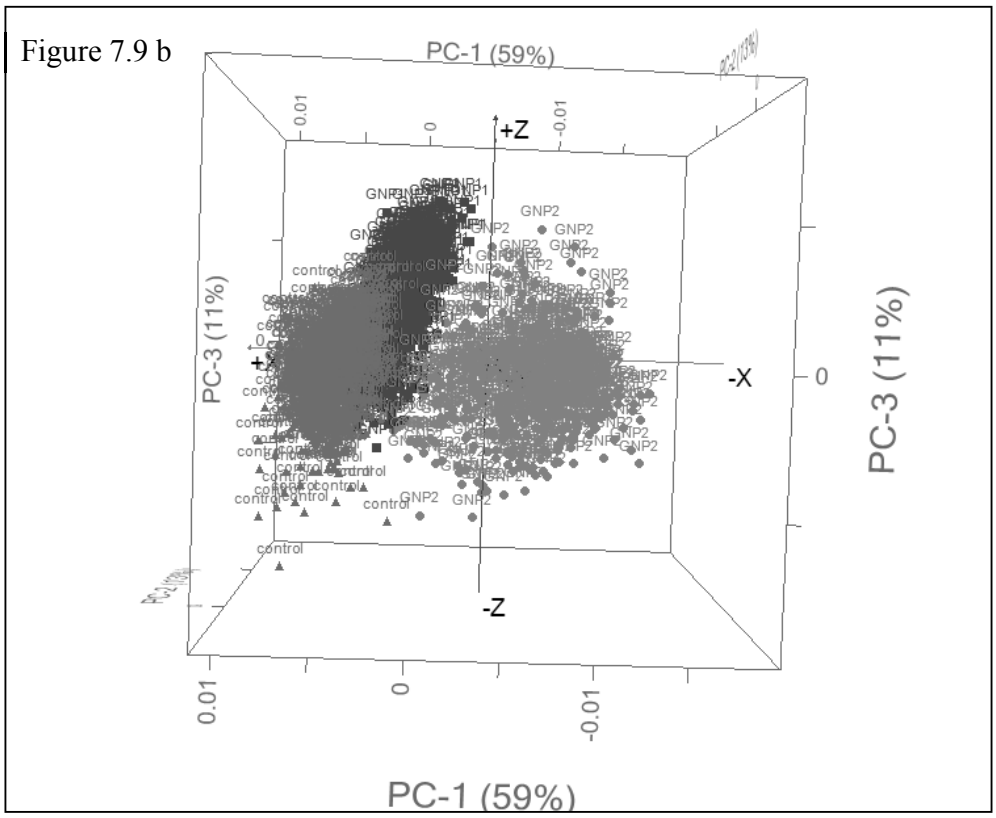

Figure 7.9 (b) PCA score and loading plot shows at PC-1, PC-2 and PC-3 level

7.3.3.2 Interpretation of 2nd PC loadings with Control, V-GNPs-1-HDM2 and C-GNPs-2-HDM2

Classification of xenograft samples shows the difference in PC laden. These differences are expected to be due to the differences in the treatment of V-GNPs-1-HDM2, and C-GNPs-2-HDM2. We attempted to interpret each PC loading in terms of the difference in positivity and negativity loading of the functional group. The PC corresponding to V-GNPs-1-HDM2 (PC3*)* and C-GNPs-2-HDM2 (PC1) has different reducing agent which corresponds to the differences observed in the PC loading. The results of the different bands at different PCs level are compiled in Table 7.1. For the loadings observed in all three samples, there are two common marker stand out are Amide III beta (Amide III: b-sheet) at ~1249 cm-1 in V-GNPs-HDM2 and C-GNPs-HDM2

whereas 2948- $_{v}$as (C–H) from methylene (–CH2) groups of lipids and 2888 $_{v}$s (C–H) from methyl (–CH3) groups of lipids in all three groups suggesting that this marker is informative concerning to the group separation. Based on this result, the loading of PC-1 had a strong positive correlation at 1092 and 2847 corresponding to the phosphodiester backbone of DNA/RNA; and the CH2 group of lipids. In addition, negative loading was detected in 1649- indicating a Amide-1α helix. The loading of PC-3 showed a positive correlation at 982, 1029 and 1675 corresponding to Ribose-2'-OH vibration of RNA, CH_2OH of polysaccharides, and Amide-1β turn respectively. Whereas a negative loading was observed at 955 and 1649 corresponding to Ribose-2'-OH vibration of RNA and the -Amide-1α helix.

The difference in the loading observed between V-GNPs-HDM2 (GNPs-1) and C-GNPs-HDM2 (GNPs-2) could be correlated with the biological response such as difference in tumor growth reduction, variations in gene expression and cytokine profiles as discussed in the chapter-6. The PC-3 corresponding to V-GNP-HDM2 showed the highest number of loading both positive and negative compared to C-GNP-HDM2 and control. (Table-7.1). The GNPs-1 (V-GNPs-HDM2) is reduced with the *Vitis vinifera,* which consists of polyphenols and hence resulted in higher biochemical changes in a wide range of the macromolecules such as lipids, protein and nucleic acid (Table 7.1 Figure 7.10 C). Alternatively, C-GNPs-HDM2 (GNPs-2) synthesized with the sodium citrate showed interaction mostly with the lipid molecules as discussed and could justify the reduction in loading as observed in PC-1.

Figure 7.10

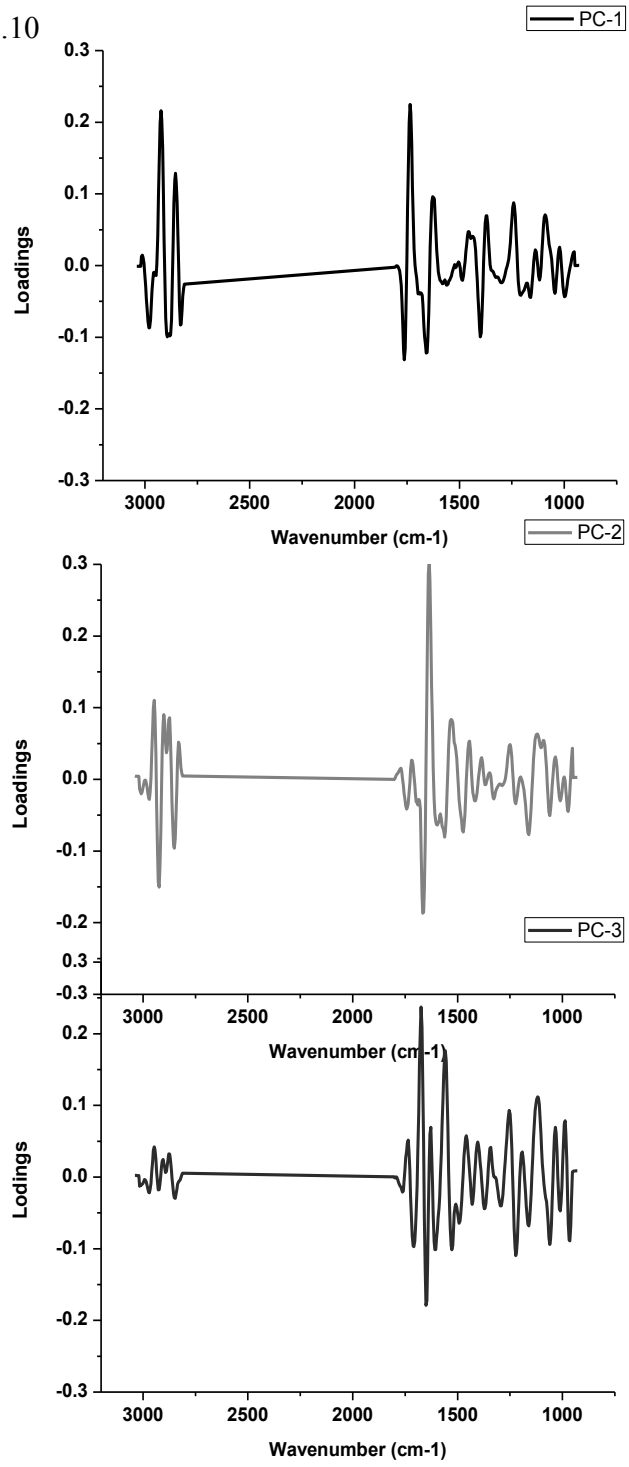

Figure 7.10 PCA score loadings of PC1-PC3. The major band observed, and the positive (+) and negative loading (-) bands are tabulated in the Table-1. PC-1 (C-GNPs-HDM2), PC-2 (Control) and PC-3 (V-GNPs-HDM2)

Table 7.1 The major band assignment for thelevel, which group in each PC level which shows the difference in Control, V-GNPs-HDM2 (GNPs-1) and C-GNPs-HDM2 (GNPs-2) [256, 478, 479]**.**

Level of PC	**Loadings Wavelength (cm^{-1}) ,** ν*-Stretching Vibration,* ν_s *–Symmetric Stretching Vibration* ν_{as}- *Asymmetric Stretching Vibration,* δ- in plane bending vibration
PC-1 (+)	➢ 1092 -PO_2^- group of DNA/RNA and phospholipids backbone ➢ 1242- β-sheet of amide III bond ➢ 1622- Antiparallel β-sheet , ν(C=O) of carboxylate and ν (C=C) of aromatic compounds of amide I bond ➢ 1738- ν(C=O) bond of esters group from fatty acids and lipid triglycerides ➢ 2847- νs(C–H) bond of methylene (–CH2) of lipids ➢ 2929- νas(C–H) bond of methylene (–CH2) of lipids
PC-1 (-)	➢ 1758- ν (C=O) bond of esters group from fatty acids and lipid triglycerides ➢ 1649- ν (C=C) of di substituted cis-olefins and α-helix of amide I ➢ 1388- δs(CH3) and ds(CH2) of lipids and proteins
PC-2 (+)	➢ 1257 ➢ 1377- δs(CH3) from cholesterol and fatty acid radicals ➢ 1441- ν(C–N) of the pyridine ring ➢ 1526- Parallel mode of the α-helix of amide II ➢ 1625- Antiparallel b-sheet of amide I, ν(C=O) of carboxylate and ν (C=C) of aromatic compounds ➢ 2851- νs(C–H) from methylene (–CH2) groups of lipids ➢ 2937- νas(C–H) from methylene (–CH2) groups of lipids
PC-2 (-)	➢ 1675- β-turn of amide I: ➢ 1150- νas(CO–O–C) group of glycogen and nucleic acids (DNA and RNA)

PC-3(+)	➢	982- $_{\gamma}$(=CH) of trans isomers and conjugated trans, vibration involving OH group of ribose rings in RNA
	➢	1029- $_{\nu}$(C–C) coupled with $^{\delta}$(CH2) of $^{\alpha}$CH2 in –CH2OH groups of polysaccharides
	➢	1109- $_{\nu}$s(C–O) at the 2$^{'}$-OH group of ribose rings in RNA
	➢	1249- β-sheet of amide III
	➢	1342- $_{\gamma}$wag(CH2) of $^{\alpha}$CH2 groups in polyethylene chains
	➢	1416-$^{\delta}$rock(CH2) of di-substituted cis-olefins
	➢	1468-$^{\delta}$scissor(CH2) from methylene (–CH2) groups in acyl chains of lipid bilayers in orthorhombic packing
	➢	1555- α-helix and antiparallel β-sheet of amide II
	➢	1675- β –turn of amide I
	➢	2888- $_{\nu}$s (C–H) from methyl (–CH3) groups of lipids
	➢	2948- $_{\nu}$as(C–H) from methylene (–CH2) groups of lipids
PC-3(-)	➢	1649- $_{\nu}$ (C=C) of di-substituted cis-olefins and α-helix of amide I:
	➢	1529- Parallel mode of the α-helix in amide II:
	➢	1056- $_{\nu}$s (R–O–P–O–R) from ring vibrations of carbohydrates
	➢	1229- -(PO_2^-) PO_2^- group of DNA/RNA and phospholipids backbone

7.4 Discussion

The transformation of the tissue states from normal to cancer is attributed to biochemical changes within the tissue. Similarly, after the treatment cancer cell with drug molecules, small molecules can also change the chemical stage of the cell by interacting with the cellular biomolecules. This change can be studied using the FTIR in combination with chemometric analysis at the molecular level, thereby giving a vital information with regard to the interaction of target molecules as the cellular component. The combination of FTIR spectroscopy and multivariate analysis can provide a reproducible and non-invasive method to study the biomolecules changes in treatment condition.

FTIR spectroscopy is currently being employed as a tool to derive biochemical signatures of a wide range of cells and tissues. The FTIR has been used to distinguish the normal and cancer cells due to the presence or absence of macromolecules such as nucleic acids, proteins, lipids and carbohydrates and differences in their configurations [480, 481]. For the first time an attempt was made to identify the difference induced by the treatment of GNPs-HDM2 to RB xenograft tumor samples. The comparison of the FTIR spectra of PC-1- PC-3 clearly reveal the difference induced by C-GNPs-HDM2 and V-GNPs-HDM2. The major difference observed in the amide, nucleic acid, polysaccharides and lipids in the spectral range 3040-2810 and 1800-930. The resultant score plot (Figure 7.10) clearly reveals the separation of 3 ex-vivo xenograft tumor sample. The PC- 1 loading plot shows a strong positive band At 1622 cm-1 of Amide I, antiparallel b-sheet of carboxylate of aromatic compounds which could attribute binding of C-GNPs-HDM2 with the protein molecules and due to the SPR effect of the GNPs it shows the shift of from the 1625 cm-1 observed in PC-2 (Control samples/untreated RB xenograft tumor). In addition to this, a

significant difference was observed in the lipid loading between PC-1 and PC-2. The data indicate that in the case of PC-1 a strong positive peak at 2929 cm-1 is observed, which attributed to methylene (–CH2) groups of lipids. The presence of strong positive loading of these lipids attributes the activation of the fatty acid synthesis, which could be due to the presence of citrate in C-GNPs-HDM2 [482]. It has been reported that citrate has an important role in fatty acid synthesis pathways. Whereas, in the case of V-GNPs-HDM2 treated samples lipids bands completely disappears indicates that there are no lipids loadings. The other important difference, which can consider for the impact on the classification of PC-3 is a strong positive loading at 1555 cm-^{1}Amide II, a-helix and antiparallel b-sheet, 1029 cm-1 for CH2OH groups of polysaccharides and 1109 cm-1 for 2$^{'}$-OH group of Ribose rings in RNA. The PC-3 loading plot reveals that 1343, 1416, 1468 and 1555 cm-1 are accounted for the difference in lipids, proteins and nucleic, acid composition (Figure 7.11) and confirmation in C-GNPs-HDM2 treated tumor samples. The bar graph indicates that the PC-3 (Figure 7.10) shows more positive loading for all the biomolecules compared to control and treated samples a remarkably negative loading of the lipids are observed in the PC-1 (Figure 7.10 &7. 11).

It should be emphasized that the GNPs used in the targeted therapy using peptides, HDM2, complementary affected by the nature of the GNPs used for the delivery of peptide molecules at the target site. In the line of current findings, we can hypothesize that a targeted moiety can interact with the different biomolecules during the treatment. As we have noticed here that although a peptide (HDM2) was used for the targeting the protein molecules due to difference in the carrier molecules (GNPs), the interactions were not limited to the protein and a significant difference was observed in interactions with various

biomolecules as revealed by the PCs loading (Figure 7.10) compared to the control samples. As discussed C-GNPs-HDM2, which shows predominantly lipid loading whereas V-GNPs-HDM2 which shows mostly proteins, lipids and polysaccharides of different composition confirm that both the treatment are showing the difference at the molecular level. The difference in the specific band loading is a mean to identify the difference of the biomolecules. In a similar kind of study using FTIR analysis to differentiate between normal and a mutated genome have been used to screen the mutagenic potential effect of the drug [483]. The application of FTIR in combination with specific biological assays can be utilized for assigning the differential band position and intensity of specific molecular events between samples compared [484].

In addition, most of the research studies widely use molecular biological techniques such as gene expression and protein expression studies to analyze the mechanism of action of drugs, peptides or siRNA. For instance, the validation of peptide or siRNA based experiments is limited to protein expression while the differences in the other biomolecules are ignored. Since, biological systems are complex, modulation of one specific group of biomolecule (eg., Protein) can cause a cascade of changes that does not limit itself to target group for instance, protein, hence a method that would provide a holistic view of interactions between different biomolecules are vital [485]. Application of FTIR, fulfills the above-mentioned criteria. Our results reiterate the need for a method like FTIR for understanding the complete array of biomolecule interactions. Additionally, the combination of FTIR with multivariate analysis could provide a non-invasive and reproducible method of assessing the differences between untreated /treatments, cancerous/non-cancerous stage of the tumor samples. The transformation of the tissue

states from normal to cancer of treated to untreated is attributed to biochemical changes within the tissue. Since the tumor is abnormal stage of the cell associated with the chemical changes at the molecular level, the tumor cells can be monitored in comparison with the normal cells based on their chemical composition, thereby giving a vital information with regard to early diagnosis of the tumor stages, benign or malignant in human tissue.

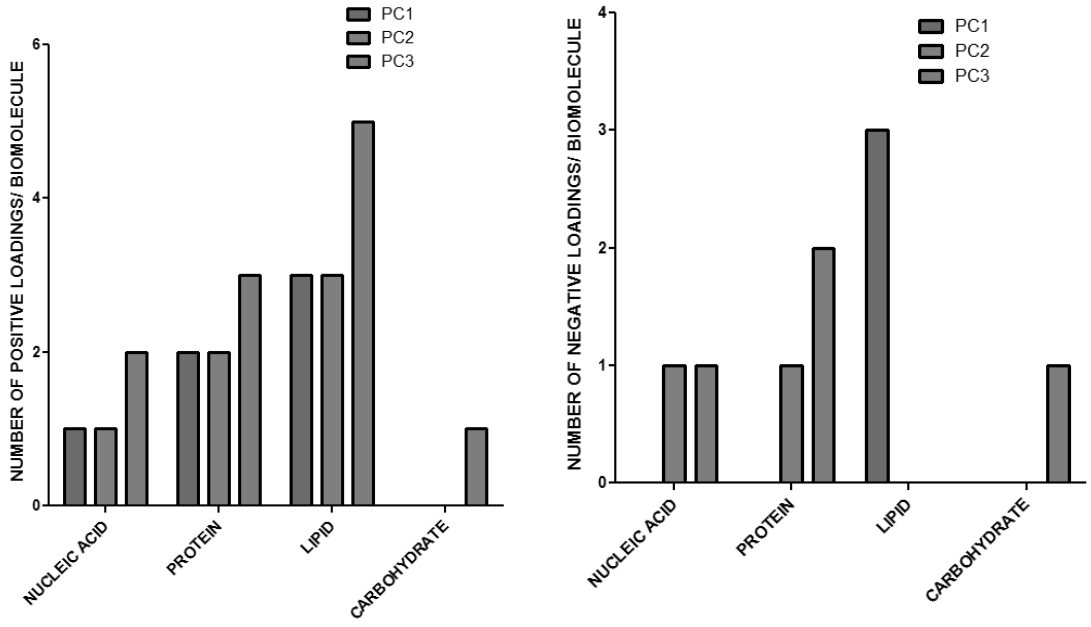

Figure 7.10 Summary of the biomolecules positive and negative loading with respect at PC-1, PC-2, and PC-3 level

The current findings indicate that biological responses observed in the GNPs-HDM2 created RB xenograft cancer model at *in vitro*, *in vivo* (discussed in Chapter 6) and current xenograft RB sample FTIR date corroborate at each level. The molecular fingerprint observed by multivariate analysis (such as PCA) supports our hypothesis that reducing agent used in the synthesis of GNPs is a playing important role apart from the therapeutic response by the HDM2 therapeutic peptide. To understand this effect in depth to get an insight at the molecular level through identify the chemical fingerprint the FTIR

spectroscopic technique has used to divulge the difference at the molecular level. The identification of spectroscopic signature unique for the particular interaction would be highly beneficial for the development of the new chemotherapy drug/therapeutic agent for the targeted therapy [486]. This technique would be a new motivated path in the field of drug-biomolecules interaction for the improvement of chemotherapeutic responses to achieve more target specific treatment modalities [487]. To interaction can be classified by chemometrics analysis. which includes statistical and mathematical methods to analyses and elicit the important information with high sensitivity, selectivity due to FPA technique [488]. Apart from this, the usefulness of the technique lies in the diagnosis, unlike other techniques the spectroscopy like non-invasive, easy sample preparation and unique vibration pattern of each biomolecule. The characteristic band that mainly reveals the information about the interaction and confirmation as a signature.

7.5 Chapter summary

- V-GNPs-HDM2 and C-GNPs-HDM2 interact differently at macromolecule level.
- FTIR molecular fingerprint can aid in understanding the interaction of therapeutic molecules at lipid proteins and nucleic acid level
- These findings would explain better how the chemo-bio interaction affect the biological responses at cellular and genomic levels.

CHAPTER 8

8 Summary and future perspective

This chapter summarizes the major findings obtained in this dissertation. This chapter concludes the results of novel SERs active GNPs and GNPs-peptide (organic-inorganic hybrid nanomaterial) conjugate for cancer theranostic. The conjugate, GNPs-Pep-A, and GNPs-HDM2 showed antioxidant and antitumor effect in RB cancer models, respectively. This chapter also includes the future scope of current work.

8.1 Conclusion

8.1.1 Major findings of the current dissertation;

1) The first report on the GNP synthesis with *Vitis vinifera L*. and *Curcumin L.* successfully stabilized with SERs and self-therapeutic activity in the cancer cell.

2) The *Vitis vinifera L*. GNPs (V-GNPs) is crystalline in nature and showed multifunctional activity and high therapeutic index compared to the *Curcumin L.* in Retinoblastoma (RB) cancer model.

3) The Peptide-A conjugated GNPs (V-GNPs-Pep-A) showed synergistic effect and was more efficient in ROS reduction and SOD enzyme activity compared to V-GNPs and Pep-A alone.

4) HDM2 over-expression was observed in RB tumor samples both at mRNA and protein levels in all the analyzed samples.

5) Knockdown of the HDM2 expression, *in vitro, in* the RB cancer model, confirmed that the anti-HDM2 peptide was functionally active after conjugation with GNPs (V-GNPs-HDM2 and C-GNPs-HDM2).

6) Apoptotic and cytokine profile in xenograft RB tumor and serum sample, respectively, indicates that V-GNPs-HDM2 and C-GNPs-HDM2 induced the cell death through different signaling pathways. In addition to this, the apoptotic gene downstream to HDM2 pathways was different which could be due to the difference in signaling pathways modulated by the metal-peptide complex and the peptide alone.

7) Label free spectroscopy of a xenograft RB tumor sample with FTIR further confirmed that V-GNPs-HDM2 and C-GNPs-HDM2 showed a difference in PC loading at macromolecule level corroborate with our findings that the reducing agent used in the synthesis of GNPs significantly affected the interaction of the conjugate at the molecular level.

More detailed conclusion of each study is summarized below:

I Green technology for GNPs synthesis

The present dissertation resulted in the development of novel SERs active GNPs with polyphenols from the plant molecules. Nontoxic, and eco-friendly plant derivatives known for their anti-cancer and anti-oxidant properties were used for the GNPs synthesis. The gold precursor $NaAuCl_4$ reduced by the *Vitis vinifera* and *Curcumin* to form the gold nanoparticles and gum arabic was used to increase the colloidal stability of GNPs. The GNPs synthesis protocol is quick, easy and highly reproducible to generate the GNPs with different reducing agent. The GNPs of different sizes can be developed in the range from 10-1000 nm by changing the synthesis parameters which includes temperature,

concentration of salt and time of reduction. The therapeutic index of the V-GNPs is more compared to curcumin reduced GNPs and hence V-GNPs are more promising for therapeutic application in the RB cancer model. The *in vitro,* stability studies of GNPs confirmed the stability of GNPs in biologically relevant solvent and culture medium. Furthermore, the GNPs were assessed for their stability and anti-cancer effect on the biological system.

II Novel GNPs- peptide -A (GNPs-Pep-A), an antioxidant for RB therapy

Reactive oxygen species (ROS) generated as an initial signal in the cancer cell during the oxidative stress condition. Antioxidants are the molecules that protect biological molecules such as protein, DNA, lipids, etc., against the oxidative damage caused by ROS generated during anti-cancer therapy. This study for the first time report that an antioxidant peptide (Pep-A) showed an antioxidant effect in RB cancer cell and reduced the ROS level upon treatment with the Pep-A alone. In addition to this, GNPs-Pep-A is more effective due to the synergistic effect of GNPs compared to the Pep-A. The synergistic effect has been observed due to the presence of polyphenols coated on the surface of GNPs (reported in the chapter-4). This enhances the antioxidant effect of the GNPs-Pep-A compared to Pep-A, which corroborate the results reported for the antioxidant effect of *Vitis vinifere*. The expression of antioxidant genes GPX, SOD and CAT at mRNA level were up regulated and SOD enzyme expression after treatment with the GNPs-Pep-A.

III HDM2 knock down for targeted therapy in RB

The HDM2 is an oncogene, which inhibit the expression of a P53 gene. The feedback regulation of HDM2-P53 controlled important cellular function apoptotic cell

death and tumorogenesis. The up-regulation of HDM2 at mRNA and protein level were observed in RB tumor tissues, which confirmed the role of HDM2 in tumor progression. The V-GNPs-HDM2 and C-GNPs-HDM2 conjugate showed significant down-regulation of the HDM2 *in vitro* and up-regulation of p53 in the case of V-GNPs-HDM2. The result (Chapter-6) obtained in the current work is corresponding to the earlier report on p53 expression, enhanced by the *Vitis vinifera*.

The *in vivo* tumor growth reduction data confirmed that C-GNPs-HDM2 and V-GNPs-HDM2 suppress the tumor growth through p53 independent and p53 dependent pathway, respectively. However, knockdown of HDM2 induces the apoptosis irrespective of C-GNPs-HDM2 or V-GNPs-HDM2. The *Vitis vinifera*, a polyphenol, contains the major component resveratrol, which is known for tumor growth inhibition in Y79, RB cells complements the HDM2 peptide and induces the tumor reduction RB *in vitro* and *in vivo*. In conclusion, this study proved that HDM2 could be a good target in RB. The GNPs successfully functionalized with HDM2 peptide and knockdown the HDM2 specifically by anti-HDM2 functionalized GNPs, which lead to apoptosis in RB. The reducing agent used in the synthesis of GNPs plays an important role in biological response, this is evident from observation from the current data which showed clear differences in biological responses such as level of HDM2 knock down, apoptosis protein profiling and cytokine expression.

IV Label-free spectroscopy, a tool for identification of therapeutic responses at molecular level

Spectroscopic imaging in combination with multivariate analysis, principal component (PCA) was performed to study the chemical mapping and detecting the distribution of the cellular macromolecules in C-GNPs-HDM2 and V-GNPs-HDM2

treated xenograft RB tumor samples. The differences observed in the tumor growth reduction during in life study (discussed in chapter-6) in the nude mouse model was studied by the multivariate PCA analysis. The complete disappearance of lipid loading and positive loading for polysaccharides confirm the effect of V-GNPs-HDM2 in xenograft RB samples which are virtue of the appearance of *Vitis vinifera* in addition to an anti-HDM2 peptide, which could affect the tumor growth reduction, apoptosis and cytokine profile observed in V-GNPs-HDM2. This result proved that reducing agent used for the synthesis of GNPs indeed affects the tumor growth reduction as a synergistic effect in the presence of anti-HDM2 peptide, which lead to cell death.

8.2 Future scope of the work

The application of GNPs for cancer theranostic will be more promising by reducing the toxic effect of metal nanoparticles, and hence green nanotechnology holds the promise to reduce the nanoparticles toxicity. The future scope of the current work opens a new path and direction for Nanomedicine research. This requires a determined long-term effort to achieve the real solution in a clinical setup. These include design and development of multifunctional GNPs for integrated cancer therapy and theranostic application. Use of multiplexed nanoparticles for diagnostics to study clinical outcome, treatment response and individualized therapy. The possible new venues are open to continuing the current work as follows;

- Resveratrol, a major component of the *Vitis vinifera*, can be used for the GNPs synthesis, which could be more specific in terms of the self-therapeutics effect of GNPs in RB management.

- Though curcumin act as a reducing agent to form GNPs, it has limitation in terms of the reproducibility and aqueous solubility, in future, it is imperative to optimize the synthesis protocol of GNPs to get the reproducibility and aqueous solubility of curcumin for successful use of Cur-GNPs for biomedical application.
- The identity of the Raman reporter molecule (s) coated on V-GNPs, is presently unknown, therefore in the future work will carry out to study the polyphenols, peptides and protein compounds present in the *Vitis vinifera* L. extract.
- SERs active GNPs will be more specific and multi-functional if functionalized by cancer cell surface-specific biomarkers. This could overcome the non-specific organ uptake and RES uptake of target moiety.
- The V-GNPs will explore further for therapeutic application in another cancer model. Self-assembled GNPs can be synthesized using antioxidant and anticancer biological reducing and capping agent.
- Since, HDMX family member HDM4 over-express in RB, in future it can be studied whether GNPs functionalized with HDM4 along with HDM2 and used for the RB therapy.
- The novel V-GNPs HDM2 showed tumor growth reduction *in vivo* in mice model; the future study needs to explore different modes of administration such as I.V. (Intra venous), I.P. (Intra-peritoneal). In addition to this the dose of V-GNPs-HDM2 can be optimized to enhance the tumor reduction with no toxicity in a vital organ.
- In future, the different gold nano structure can be formed and optimized for the delivery of anti-HDM2 peptide for therapeutic application in RB and other cancer

model. Future studies will focus on photothermal and imaging by SERs active GNRs and GNPs, respectively

- Since, V-GNPs doped successfully with Raman dye (R6G) a multiplexing approach could be used for the targeting multiple biomarkers along with imaging.
- In future, green technology can be explored in detail in terms of the synthesis of GNPs by using the different reducing agent and obtain self-therapeutic GNPs, which could be more useful in terms of cancer cell apoptosis and specific targeting.
- Spectroscopic signature can be identified by vibrational spectroscopic techniques such as Raman and FTIR to generate the molecular spectral signature in RB as a diagnosis tool.
- The orthotropic model of RB would be an appropriate choice better to understand the role of this novel conjugate as an intravitreal delivery vehicle.

References

[1] Sanna V, Pala N, Dessi G, Manconi P, Mariani A, Dedola S, et al. Single-step green synthesis and characterization of gold-conjugated polyphenol nanoparticles with antioxidant and biological activities. International journal of nanomedicine 2014;9:4935-51.

[2] nan'o[middot]tech[middot]nol'o[middot]gy n. Nat Nano 2006;1:8-10.

[3] Wang Y, Herron N. Nanometer-sized semiconductor clusters: materials synthesis, quantum size effects, and photophysical properties. The Journal of Physical Chemistry 1991;95:525-32.

[4] Alivisatos P. The use of nanocrystals in biological detection. Nature biotechnology 2004;22:47-52.

[5] Dykman LA, Khlebtsov NG. Gold Nanoparticles in Biology and Medicine: Recent Advances and Prospects. Acta Naturae 2011;3:34-55.

[6] 'Plenty of room' revisited. Nat Nano 2009;4:781-.

[7] Kumar R, Kalmodia S, Nath S, Singh D, Basu B. Phase assemblage study and cytocompatibility property of heat treated potassium magnesium phosphate-silicate ceramics. Journal of materials science Materials in medicine 2009;20:1689-95.

[8] Porter AL, Youtie J. Where does nanotechnology belong in the map of science? Nat Nano 2009;4:534-6.

[9] Roduner E. Size matters: why nanomaterials are different. Chemical Society reviews 2006;35:583-92.

[10] Chen YS, Hung YC, Liau I, Huang GS. Assessment of the In Vivo Toxicity of Gold Nanoparticles. Nanoscale research letters 2009;4:858-64.

[11] Delong RK, Reynolds CM, Malcolm Y, Schaeffer A, Severs T, Wanekaya A. Functionalized gold nanoparticles for the binding, stabilization, and delivery of therapeutic DNA, RNA, and other biological macromolecules. Nanotechnology, science and applications 2010;3:53-63.

[12] News & Views in ... Nanomedicine. Nanomedicine : nanotechnology, biology, and medicine 2010;5:683-5.

[13] Choi CH, Alabi CA, Webster P, Davis ME. Mechanism of active targeting in solid tumors with transferrin-containing gold nanoparticles. Proceedings of the National Academy of Sciences of the United States of America 2010;107:1235-40.

[14] Liu J, Yu M, Zhou C, Yang S, Ning X, Zheng J. Passive tumor targeting of renal-clearable luminescent gold nanoparticles: long tumor retention and fast normal tissue clearance. Journal of the American Chemical Society 2013;135:4978-81.

[15] weibo cai tg, hao hong, jiangtao sun. applications of gold nanoparticles in cancer nanotechnology. Nanotechnology, Science and Applications 2008;1:17 - 32.

[16] Xu ZaB. Multifunctional Magnetic Nanoparticles as Bionanomaterials. Action Biosciences 2011.

[17] Chen ZF, Liu YC, Peng Y, Hong X, Wang HH, Zhang MM, et al. Synthesis, characterization, and in vitro antitumor properties of gold(III) compounds with the traditional Chinese medicine (TCM) active ingredient liriodenine. Journal of biological inorganic chemistry : JBIC : a publication of the Society of Biological Inorganic Chemistry 2012;17:247-61.

[18] Arvizo RR, Bhattacharyya S, Kudgus RA, Giri K, Bhattacharya R, Mukherjee P. Intrinsic therapeutic applications of noble metal nanoparticles: past, present and future. Chemical Society reviews 2012;41:2943-70.

[19] Knox R, Gell PG, Pollock MR. The selective action of tetrathionate in bacteriological media: A report to the Medical Research Council. The Journal of hygiene 1943;43:147-58 1.

[20] Marton L. The Electron Microscope: A New Tool for Bacteriological Research. Journal of bacteriology 1941;41:397-413.

[21] Richard Klein U-GRHFNR, Department of health and human services, Centers for Disease Control and Prevention. USA. Uni-Gold Recombigen™ HIV: FDA News Release, Department of health and human services, Centers for Disease Control and Prevention. USA. 2003.

[22] K. Jk. "Nanotechnology in clinical laboratory diagnostics". Clinica Chimica Acta 2005;358:37–54, .

[23] Cheng W, Dong S, Wang E. Synthesis and Self-Assembly of Cetyltrimethylammonium Bromide-Capped Gold Nanoparticles. Langmuir 2003;19:9434-9.

[24] Russo M, Spagnuolo C, Tedesco I, Russo GL. Phytochemicals in cancer prevention and therapy: truth or dare? Toxins 2010;2:517-51.

[25] Gao J, Huang X, Liu H, Zan F, Ren J. Colloidal Stability of Gold Nanoparticles Modified with Thiol Compounds: Bioconjugation and Application in Cancer Cell Imaging. Langmuir : the ACS journal of surfaces and colloids 2012;28:4464-71.

[26] Lee KS, El-Sayed MA. Gold and silver nanoparticles in sensing and imaging: sensitivity of plasmon response to size, shape, and metal composition. The journal of physical chemistry B 2006;110:19220-5.

[27] Jain PK, El-Sayed MA. Universal scaling of plasmon coupling in metal nanostructures: extension from particle pairs to nanoshells. Nano letters 2007;7:2854-8.

[28] Jain PK, El-Sayed MA. Universal Scaling of Plasmon Coupling in Metal Nanostructures: Extension from Particle Pairs to Nanoshells. Nano letters 2007;7:2854-8.

[29] Choudhary A, Singh G, Biradar AM. Advances in gold nanoparticle-liquid crystal composites. Nanoscale 2014;6:7743-56.

[30] Jain PK, Huang X, El-Sayed IH, El-Sayed MA. Noble metals on the nanoscale: optical and photothermal properties and some applications in imaging, sensing, biology, and medicine. Accounts of chemical research 2008;41:1578-86.

[31] McQuillan AJ. The discovery of surface-enhanced Raman scattering. Notes and Records of the Royal Society 2009;63:105-9.

[32] Gellner M, Niebling S, Kuchelmeister HY, Schmuck C, Schlucker S. Plasmonically active micron-sized beads for integrated solid-phase synthesis and label-free SERS analysis. Chemical communications 2011;47:12762-4.

[33] Qian X, Li J, Nie S. Stimuli-responsive SERS nanoparticles: conformational control of plasmonic coupling and surface Raman enhancement. Journal of the American Chemical Society 2009;131:7540-1.

[34] Xu H, Bjerneld E, Käll M, Börjesson L. <title>Spectroscopy of Single Hemoglobin Molecules by Surface Enhanced Raman Scattering</title>. Physical Review Letters 1999;83:4357-60.

[35] Qian XM, Nie SM. Single-molecule and single-nanoparticle SERS: from fundamental mechanisms to biomedical applications. Chemical Society reviews 2008;37:912-20.

[36] Chowdhury J, Ghosh M, Misra TN. pH-Dependent Surface-Enhanced Raman Scattering of 8-Hydroxy Quinoline Adsorbed on Silver Hydrosol. Journal of colloid and interface science 2000;228:372-8.

[37] Liu Q, Dong J, Luo Y, Wen G, Wei L, Liang A, et al. A highly sensitive SERS method for the determination of nitrogen oxide in air based on the signal amplification effect of nitrite catalyzing the bromate oxidization of a rhodamine 6G probe. RSC Advances 2014;4:10955-9.

[38] Dreaden EC, Austin LA, Mackey MA, El-Sayed MA. Size matters: gold nanoparticles in targeted cancer drug delivery. Therapeutic delivery 2012;3:457-78.

[39] Veronese FM. Peptide and protein PEGylation: a review of problems and solutions Biomaterials 2001;22:405-17.

[40] Sperling RA, Parak WJ. Surface modification, functionalization and bioconjugation of colloidal inorganic nanoparticles. Philosophical transactions Series A, Mathematical, physical, and engineering sciences 2010;368:1333-83.

[41] Colombo M, Mazzucchelli S, Collico V, Avvakumova S, Pandolfi L, Corsi F, et al. Protein-assisted one-pot synthesis and biofunctionalization of spherical gold nanoparticles for selective targeting of cancer cells. Angewandte Chemie 2012;51:9272-5.

[42] Zhou J, Rossi JJ. Cell-type-specific, Aptamer-functionalized Agents for Targeted Disease Therapy. Mol Ther Nucleic Acids 2014;3:e169.

[43] J. William Harbour LW, Duanduan Ma, Michael Cohen, T. ransducible Peptide Therapy for Uveal Melanoma and Retinoblastoma,. Archives of Ophhthalmology 2002;120:1341-6.

[44] Kumar A, Ma H, Zhang X, Huang K, Jin S, Liu J, et al. Gold nanoparticles functionalized with therapeutic and targeted peptides for cancer treatment. Biomaterials 2012;33:1180-9.

[45] Scarì G, Porta F, Fascio U, Avvakumova S, Dal Santo V, De Simone M, et al. Gold nanoparticles capped by a GC-containing peptide functionalized with an RGD motif for integrin targeting. Bioconjugate chemistry 2012;23:340-9.

[46] Elison JR CD, Claros N, Abramson DH, Lee TC, 75. Small molecule inhibition of HDM2 leads to p53-mediated cell death in retinoblastoma cells. Arch Ophthalmol 2006;124:1269-75.

[47] Koshevoy IO, Smirnova ES, Haukka M, Laguna A, Chueca JC, Pakkanen TA, et al. Synthesis, structural characterization, photophysical properties and theoretical analysis of gold(I) thiolate-phosphine complexes. Dalton transactions 2011;40:7412-22.

[48] Tiwari PM, Eroglu E, Bawage SS, Vig K, Miller ME, Pillai S, et al. Enhanced intracellular translocation and biodistribution of gold nanoparticles functionalized with a cell-penetrating peptide (VG-21) from vesicular stomatitis virus. Biomaterials 2014;35:9484-94.

[49] Manjumeena R, Elakkiya T, Duraibabu D, Feroze Ahamed A, Kalaichelvan P, Venkatesan R. 'Green' biocompatible organic-inorganic hybrid electrospun nanofibers for potential biomedical applications. Journal of biomaterials applications 2014.

[50] Sanchez C, Belleville P, Popall M, Nicole L. Applications of advanced hybrid organic-inorganic nanomaterials: from laboratory to market. Chemical Society reviews 2011;40:696-753.

[51] Scari G, Porta F, Fascio U, Avvakumova S, Dal Santo V, De Simone M, et al. Gold nanoparticles capped by a GC-containing peptide functionalized with an RGD motif for integrin targeting. Bioconjugate chemistry 2012;23:340-9.

[52] Friedman AD, Claypool SE, Liu R. The Smart Targeting of Nanoparticles. Current pharmaceutical design 2013;19:6315-29.

[53] Yu MK, Park J, Jon S. Targeting strategies for multifunctional nanoparticles in cancer imaging and therapy. Theranostics 2012;2:3-44.

[54] Matsumura Y, Maeda H. A new concept for macromolecular therapeutics in cancer chemotherapy: mechanism of tumoritropic accumulation of proteins and the antitumor agent smancs. Cancer research 1986;46:6387-92.

[55] Sirova M, Mrkvan T, Etrych T, Chytil P, Rossmann P, Ibrahimova M, et al. Preclinical evaluation of linear HPMA-doxorubicin conjugates with pH-sensitive drug release: efficacy, safety, and immunomodulating activity in murine model. Pharmaceutical research 2010;27:200-8.

[56] Porta F, Speranza G, Krpetić Ž, Dal Santo V, Francescato P, Scari G. Gold nanoparticles capped by peptides. Materials Science and Engineering: B 2007;140:187-94.

[57] Shukla S, Ablack AL, Wen AM, Lee KL, Lewis JD, Steinmetz NF. Increased tumor homing and tissue penetration of the filamentous plant viral nanoparticle Potato virus X. Molecular pharmaceutics 2013;10:33-42.

[58] Abramson DH. Retinoblastoma: diagnosis and management. CA: a cancer journal for clinicians 1982;32:130-40.

[59] Knudson AG, Jr. Mutation and cancer: statistical study of retinoblastoma. Proceedings of the National Academy of Sciences of the United States of America 1971;68:820-3.

[60] McEvoy J, Ulyanov A, Brennan R, Wu G, Pounds S, Zhang J, et al. Analysis of MDM2 and MDM4 Single Nucleotide Polymorphisms, mRNA Splicing and Protein Expression in Retinoblastoma. PLoS ONE 2012;7:e42739.

[61] Marine JC, Jochemsen AG. Mdmx and Mdm2: brothers in arms? Cell cycle (Georgetown, Tex) 2004;3:900-4.

[62] de Oliveira Reis AH, de Carvalho IN, de Sousa Damasceno PB, Ferman SE, Lucena E, Lopez-Camelo JS, et al. Influence of MDM2 and MDM4 on development and survival in hereditary retinoblastoma. Pediatric blood & cancer 2012;59:39-43.

[63] Castera L, Sabbagh A, Dehainault C, Michaux D, Mansuet-Lupo A, Patillon B, et al. MDM2 as a modifier gene in retinoblastoma. Journal of the National Cancer Institute 2010;102:1805-8.

[64] Kohen R, Nyska A. Oxidation of biological systems: oxidative stress phenomena, antioxidants, redox reactions, and methods for their quantification. Toxicologic pathology 2002;30:620-50.

[65] Murphy MP, Holmgren A, Larsson NG, Halliwell B, Chang CJ, Kalyanaraman B, et al. Unraveling the biological roles of reactive oxygen species. Cell metabolism 2011;13:361-6.

[66] Shields CL, Lally SE, Leahey AM, Jabbour PM, Caywood EH, Schwendeman R, et al. Targeted retinoblastoma management: when to use intravenous, intra-arterial,

periocular, and intravitreal chemotherapy. Current opinion in ophthalmology 2014;25:374-85.

[67] Shields CL, Shields JA. Retinoblastoma management: advances in enucleation, intravenous chemoreduction, and intra-arterial chemotherapy. Current opinion in ophthalmology 2010;21:203-12.

[68] Parul Saxenam SK, Mandeep Singh Bajaj, Neelam Pushker, Supriyo Ghose and Jasbir Kaur. Expression of p53 and Mdm2 in Human Retinoblastoma. Journal of Clinical & Experimental Ophthalmology 2012;3:1-5.

[69] Kubik T, Bogunia-Kubik K, Sugisaka M. Nanotechnology on duty in medical applications. Current pharmaceutical biotechnology 2005;6:17-33.

[70] Sandhiya S, Dkhar SA, Surendiran A. Emerging trends of nanomedicine--an overview. Fundamental & clinical pharmacology 2009;23:263-9.

[71] Liu Y, Miyoshi H, Nakamura M. Nanomedicine for drug delivery and imaging: a promising avenue for cancer therapy and diagnosis using targeted functional nanoparticles. International journal of cancer Journal international du cancer 2007;120:2527-37.

[72] Johnson CJ, Zhukovsky N, Cass AE, Nagy JM. Proteomics, nanotechnology and molecular diagnostics. Proteomics 2008;8:715-30.

[73] Dreaden EC, El-Sayed MA. Detecting and destroying cancer cells in more than one way with noble metals and different confinement properties on the nanoscale. Accounts of chemical research 2012;45:1854-65.

[74] Huo Q. A perspective on bioconjugated nanoparticles and quantum dots. Colloids Surf B Biointerfaces 2007;59:1-10.

[75] Huang RB, Mocherla S, Heslinga MJ, Charoenphol P, Eniola-Adefeso O. Dynamic and cellular interactions of nanoparticles in vascular-targeted drug delivery. Mol Membr Biol 2010;27:312-27.

[76] Liu P, Sun Y, Wang Q, Sun Y, Li H, Duan Y. Intracellular trafficking and cellular uptake mechanism of mPEG-PLGA-PLL and mPEG-PLGA-PLL-Gal nanoparticles for targeted delivery to hepatomas. Biomaterials 2014;35:760-70.

[77] Alan TR, Trial of Insulin-Coated Gold Nanoparticles Approved, Science business , November 15th, 2011. Trial of Insulin-Coated Gold Nanoparticles Approved, Science business , November 15th, 2011. 2011.

[78] Arvizo RR, Bhattacharyya S, Kudgus R, Giri K, Bhattacharya R, Mukherjee P. Intrinsic Therapeutic Applications of Noble Metal Nanoparticles: Past, Present and Future. Chemical Society Reviews 2012;41:2943-70.

[79] Namiki Y, Fuchigami T, Tada N, Kawamura R, Matsunuma S, Kitamoto Y, et al. Nanomedicine for cancer: lipid-based nanostructures for drug delivery and monitoring. Accounts of chemical research 2011;44:1080-93.

[80] Al-Jamal WT, Kostarelos K. Liposomes: from a clinically established drug delivery system to a nanoparticle platform for theranostic nanomedicine. Accounts of chemical research 2011;44:1094-104.

[81] Estella-Hermoso de Mendoza A, Campanero MA, Mollinedo F, Blanco-Prieto MJ. Lipid nanomedicines for anticancer drug therapy. Journal of biomedical nanotechnology 2009;5:323-43.

[82] Koning GA, Krijger GC. Targeted multifunctional lipid-based nanocarriers for image-guided drug delivery. Anti-cancer agents in medicinal chemistry 2007;7:425-40.

[83] Klein C VL. Targeting the p53-MDM2 interaction to treat cancer. British Journal of Cance;18:1415-9.

[84] Ma P, Mumper RJ. Paclitaxel Nano-Delivery Systems: A Comprehensive Review. Journal of nanomedicine & nanotechnology 2013;4:1000164.

[85] Tkachenko AG, Xie H, Coleman D, Glomm W, Ryan J, Anderson MF, et al. Multifunctional gold nanoparticle-peptide complexes for nuclear targeting. Journal of the American Chemical Society 2003;125:4700-1.

[86] Shibu ES, Sugino S, Ono K, Saito H, Nishioka A, Yamamura S, et al. Singlet-Oxygen-Sensitizing Near-Infrared-Fluorescent Multimodal Nanoparticles. Angewandte Chemie International Edition 2013;52:10559-63.

[87] Dickerson EB, Dreaden EC, Huang X, El-Sayed IH, Chu H, Pushpanketh S, et al. Gold nanorod assisted near-infrared plasmonic photothermal therapy (PPTT) of squamous cell carcinoma in mice. Cancer Lett 2008;269:57-66.

[88] Biju V. Chemical modifications and bioconjugate reactions of nanomaterials for sensing, imaging, drug delivery and therapy. Chemical Society reviews 2014;43:744-64.

[89] Choi WI, Kim JY, Kang C, Byeon CC, Kim YH, Tae G. Tumor regression in vivo by photothermal therapy based on gold-nanorod-loaded, functional nanocarriers. ACS Nano 2011;5:1995-2003.

[90] Son SJ, Bai X, Lee SB. Inorganic hollow nanoparticles and nanotubes in nanomedicine Part 2: Imaging, diagnostic, and therapeutic applications. Drug discovery today 2007;12:657-63.

[91] J. Kimling MM, B. Okenve,V. Kotaidis,H. Ballot, and, and A. Plech . . Turkevich Method for Gold Nanoparticle Synthesis Revisited. The Journal of Physical Chemistry B 2006 110 15700-7.

[92] Jennings T SG, Past. present, and future of gold nanoparticles. Advances in experimental medicine and biology 2007;620:34-47.

[93] Tapan k. Sau and Catherine j. Murphy. Room temperature, high-yield synthesis of multiple shapes of gold nanoparticles in aqueous solution,. J Am Chem Soc , 2004;126,:8648-9. .

[94] Kalmodia S, Harjwani J, Rajeswari R, Yang W, Barrow CJ, Ramaprabhu S, et al. Synthesis and characterization of surface-enhanced Raman-scattered gold nanoparticles. Int J Nanomedicine 2013;8:4327-38.

[95] Dong s. Ys, Tang c., . Rapid synthesis of size-controlled gold nanoparticles bycomplex intramolecular photoreduction", . Chem Res Chinese 2007; 23: 500-4,.

[96] Grzelczak M, Perez-Juste J, Mulvaney P, Liz-Marzan LM. Shape control in gold nanoparticle synthesis. Chemical Society Reviews 2008;37:1783-91.

[97] Senthil Kumar P, Pastoriza-Santos I, Rodriguez-Gonzalez B, Javier Garcia de Abajo F, Liz-Marzan LM. High-yield synthesis and optical response of gold nanostars. Nanotechnology 2008;19:015606.

[98] Khoury CG, Vo-Dinh T. Gold Nanostars For Surface-Enhanced Raman Scattering: Synthesis, Characterization and Optimization. The journal of physical chemistry C, Nanomaterials and interfaces 2008;2008:18849-59.

[99] Nehl CL, Liao H, Hafner JH. Optical properties of star-shaped gold nanoparticles. Nano Lett 2006;6:683-8.

[100] Gong T, Kong KV, Goh D, Olivo M, Yong KT. Sensitive surface enhanced Raman scattering multiplexed detection of matrix metalloproteinase 2 and 7 cancer markers. Biomedical optics express 2015;6:2076-87.

[101] Poon W, Zhang X, Bekah D, Teodoro JG, Nadeau JL. Targeting B16 tumors in vivo with peptide-conjugated gold nanoparticles. Nanotechnology 2015;26:285101.

[102] Oyelere AK, Chen PC, Huang X, El-Sayed IH, El-Sayed MA. Peptide-conjugated gold nanorods for nuclear targeting. Bioconjugate chemistry 2007;18:1490-7.

[103] Mannelli I, Marco MP. Recent advances in analytical and bioanalysis applications of noble metal nanorods. Analytical and bioanalytical chemistry 2010;398:2451-69.

[104] Rodriguez-Lorenzo L, Krpetic Z, Barbosa S, Alvarez-Puebla RA, Liz-Marzan LM, Prior IA, et al. Intracellular mapping with SERS-encoded gold nanostars. Integrative Biology 2011;3:922-6.

[105] Chithrani b. D. gaA, Chanw. c. W. Determining the size and shape dependence of gold nanoparticle uptake into mammalian cells". Nano letters 2006;6:662-8.

[106] Patra HK, Banerjee S, Chaudhuri U, Lahiri P, Dasgupta AK. Cell selective response to gold nanoparticles. Nanomedicine 2007;3:111-9.

[107] Eun chul cho QzaYx. The effect of sedimentation and diffusion on cellular uptake of gold nanoparticles,. Nature nanotechnology 2011;6:385-91.

[108] Coradeghini R, Gioria S, García CP, Nativo P, Franchini F, Gilliland D, et al. Size-dependent toxicity and cell interaction mechanisms of gold nanoparticles on mouse fibroblasts. Toxicology Letters 2013;217:205-16.

[109] Pan Y, Neuss S, Leifert A, Fischler M, Wen F, Simon U, et al. Size-dependent cytotoxicity of gold nanoparticles. Small 2007;3:1941-9.

[110] Boisselier E, Astruc D. Gold nanoparticles in nanomedicine: preparations, imaging, diagnostics, therapies and toxicity. Chemical Society reviews 2009;38:1759-82.

[111] Wan J, Wang J-H, Liu T, Xie Z, Yu X-F, Li W. Surface chemistry but not aspect ratio mediates the biological toxicity of gold nanorods in vitro and in vivo. Scientific Reports 2015;5:11398.

[112] Fang H, Zhang K, Shen G, Wooley KL, Taylor J-SA. Cationic Shell-crosslinked Knedel-like (cSCK) Nanoparticles for Highly Efficient PNA Delivery. Molecular pharmaceutics 2009;6:615-26.

[113] Elbakry A, Wurster EC, Zaky A, Liebl R, Schindler E, Bauer-Kreisel P, et al. Layer-by-layer coated gold nanoparticles: size-dependent delivery of DNA into cells. Small 2012;8:3847-56.

[114] Alkilany AM, Nagaria PK, Hexel CR, Shaw TJ, Murphy CJ, Wyatt MD. Cellular uptake and cytotoxicity of gold nanorods: molecular origin of cytotoxicity and surface effects. Small 2009;5:701-8.

[115] Weinberg H, Galyean A, Leopold M. Evaluating engineered nanoparticles in natural waters. TrAC Trends in Analytical Chemistry 2011;30:72-83.

[116] Tsai SW, Liaw JW, Kao YC, Huang MY, Lee CY, Rau LR, et al. Internalized gold nanoparticles do not affect the osteogenesis and apoptosis of MG63 osteoblast-like cells: a quantitative, in vitro study. PLoS One 2013;8:e76545.

[117] Yinghua Q, Xiaoying L. Aqueous synthesis of gold nanoparticles and their cytotoxicity in human dermal fibroblasts–fetal. Biomedical Materials 2009;4:025007.

[118] Wang C, Wang J, Liu D, Wang Z. Gold nanoparticle-based colorimetric sensor for studying the interactions of β-amyloid peptide with metallic ions. Talanta 2010;80:1626-31.

[119] Brandenberger C, Rothen-Rutishauser B, Muhlfeld C, Schmid O, Ferron GA, Maier KL, et al. Effects and uptake of gold nanoparticles deposited at the air-liquid interface of a human epithelial airway model. Toxicology and applied pharmacology 2010;242:56-65.

[120] Malugin A, Ghandehari H. Cellular uptake and toxicity of gold nanoparticles in prostate cancer cells: a comparative study of rods and spheres. Journal of applied toxicology : JAT 2010;30:212-7.

[121] Ding HL, Zhang YX, Wang S, Xu JM, Xu SC, Li GH. Fe3O4@SiO2 Core/Shell Nanoparticles: The Silica Coating Regulations with a Single Core for Different Core Sizes and Shell Thicknesses. Chemistry of Materials 2012;24:4572-80.

[122] Jiang S, Win KY, Liu S, Teng CP, Zheng Y, Han M-Y. Surface-functionalized nanoparticles for biosensing and imaging-guided therapeutics. Nanoscale 2013;5:3127-48.

[123] Sun H, Zeng X, Liu M, Elingarami S, Li G, Shen B, et al. Synthesis of size-controlled Fe3O4@SiO2 magnetic nanoparticles for nucleic acid analysis. Journal of nanoscience and nanotechnology 2012;12:267-73.

[124] Xu Y, Zhou Y, Ma W, Wang S, Li S. Functionalized magnetic core–shell Fe3O4@SiO2 nanoparticles for sensitive detection and removal of Hg2+. Journal of Nanoparticle Research 2013;15:1-9.

[125] Peng S, Wang C, Xie J, Sun S. Synthesis and Stabilization of Monodisperse Fe Nanoparticles. Journal of the American Chemical Society 2006;128:10676-7.

[126] Trewyn BG. Biological applications and transmission electron microscopy investigation of mesoporous silica nanoparticles. Retrospective Theses and Dissertations 2006.

[127] Andre nel Tx, Lutz mädler, Ning li. Toxic potential of materials at the nano level. Science 2006;311:622-7.

[128] Kunjiappan S, Chowdhury R, Bhattacharjee C. A green chemistry approach for the synthesis and characterization of bioactive gold nanoparticles using Azolla microphylla methanol extract. Front Mater Sci 2014;8:123-35.

[129] Gurunathan S, Han J, Park JH, Kim JH. A green chemistry approach for synthesizing biocompatible gold nanoparticles. Nanoscale research letters 2014;9:248.

[130] Iravani S. Green synthesis of metal nanoparticles using plants. Green Chemistry 2011;13:2638-50.

[131] Makarov VV, Love AJ, Sinitsyna OV, Makarova SS, Yaminsky IV, Taliansky ME, et al. "Green" nanotechnologies: synthesis of metal nanoparticles using plants. Acta Naturae 2014;6:35-44.

[132] Ki won lee AmbZd. Opinion: molecular targets of phytochemicals for cancer prevention. Nature reviews cancer 2011;11:211-8.

[133] Elavazhagan t Ak, Int Memecylon edule leaf extract mediated green synthesis of silver and gold nanoparticles. . j Nanomedicine 2011;6: 1265-78.

[134] Aromal sa Vv, Philip d. , Acta a mol biomol spectrosc. Green synthesis of well-dispersed gold nanoparticles using macrotyloma uniflorum. Spectrochim. 2012; 85:99-104. .

[135] Kavita katti Nc, Ravi shukla, Ajit zambre, Thilakavathi suibramanian, Rajesh r. Kulkarni, Raghuraman kannan, and Kattesh v. Kattia, . Green nanotechnology from cumin phytochemicals: generation of biocompatible gold nanoparticles, . Int j green nanotechnol biomed 2009;1: b39–b52.

[136] Shukla r. Bv, Chaudhary m., et al Biocompatibility of gold nanoparticles and their endocytotic fate inside the cellular compartment: a microscopic overview,. Langmuir 2005; 21:10644-54.

[137] Shukla R NS, Chanda N, Katti K, Mekapothula S, Kulkarni RR, Welshons WV, Kannan R, Katti KV. Soybeans as a phytochemical reservoir for the production and stabilization of biocompatible gold nanoparticles. Small 2008;4:1425-36.

[138] Nune SK CN, Shukla R, Katti K, Kulkarni RR, Thilakavathi S, Mekapothula S, Kannan R, Katti KV. Green Nanotechnology from Tea: Phytochemicals in Tea as Building Blocks for Production of Biocompatible Gold Nanoparticles. J Mater Chem 2009;19:2912-20.

[139] Xia DL, Wang YF, Bao N, He H, Li XD, Chen YP, et al. Influence of reducing agents on biosafety and biocompatibility of gold nanoparticles. Applied biochemistry and biotechnology 2014;174:2458-70.

[140] Sreenivasan S, Thirumalai K, Krishnakumar S. Expression profile of genes regulated by curcumin in Y79 retinoblastoma cells. Nutrition and cancer 2012;64:607-16.

[141] Hasima N, Aggarwal BB. Cancer-linked targets modulated by curcumin. International Journal of Biochemistry and Molecular Biology 2012;3:328-51.

[142] Kloesch B, Becker T, Dietersdorfer E, Kiener H, Steiner G. Anti-inflammatory and apoptotic effects of the polyphenol curcumin on human fibroblast-like synoviocytes. International immunopharmacology 2013;15:400-5.

[143] Bisht S, Feldmann G, Soni S, Ravi R, Karikar C, Maitra A, et al. Polymeric nanoparticle-encapsulated curcumin ("nanocurcumin"): a novel strategy for human cancer therapy. Journal of Nanobiotechnology 2007;5:3.

[144] Heo DN, Ko WK, Moon HJ, Kim HJ, Lee SJ, Lee JB, et al. Inhibition of Osteoclast Differentiation by Gold Nanoparticles Functionalized with Cyclodextrin Curcumin Complexes. ACS Nano 2014.

[145] Kakran M, Sahoo N, Tan IL, Li L. Preparation of nanoparticles of poorly water-soluble antioxidant curcumin by antisolvent precipitation methods. J Nanopart Res 2012;14:1-11.

[146] Manju S, Sreenivasan K. Gold nanoparticles generated and stabilized by water soluble curcumin-polymer conjugate: blood compatibility evaluation and targeted drug delivery onto cancer cells. J Colloid Interface Sci 2012;368:144-51.

[147] Gupta SC, Patchva S, Aggarwal BB. Therapeutic Roles of Curcumin: Lessons Learned from Clinical Trials. The AAPS Journal 2013;15:195-218.

[148] Colvin VL, Goldstein AN, Alivisatos AP. Semiconductor nanocrystals covalently bound to metal surfaces with self-assembled monolayers. Journal of the American Chemical Society 1992;114:5221-30.

[149] Gao J, Huang X, Liu H, Zan F, Ren J. Colloidal stability of gold nanoparticles modified with thiol compounds: bioconjugation and application in cancer cell imaging. Langmuir : the ACS journal of surfaces and colloids 2012;28:4464-71.

[150] Volkert AA, Subramaniam V, Ivanov MR, Goodman AM, Haes AJ. Salt-mediated self-assembly of thioctic acid on gold nanoparticles. ACS Nano 2011;5:4570-80.

[151] Xia E-Q, Deng G-F, Guo Y-J, Li H-B. Biological Activities of Polyphenols from Grapes. International Journal of Molecular Sciences 2010;11:622-46.

[152] Amarnath K, Kumar J, Reddy T, Mahesh V, Ayyappan SR, Nellore J. Synthesis and characterization of chitosan and grape polyphenols stabilized palladium nanoparticles and their antibacterial activity. Colloids Surf B Biointerfaces 2012;92:254-61.

[153] Amarnath K, Mathew N, Nellore J, Siddarth C, Kumar J. Facile synthesis of biocompatible gold nanoparticles from Vites vinefera and its cellular internalization against HBL-100 cells. Cancer Nano 2011;2:121-32.

[154] Aggarwal BB, Bhardwaj A, Aggarwal RS, Seeram NP, Shishodia S, Takada Y. Role of Resveratrol in Prevention and Therapy of Cancer: Preclinical and Clinical Studies. Anticancer Research 2004;24:2783-840.

[155] Sanna V, Pala N, Dessì G, Manconi P, Mariani A, Dedola S, et al. Single-step green synthesis and characterization of gold-conjugated polyphenol nanoparticles with antioxidant and biological activities. International journal of nanomedicine 2014;9:4935-51.

[156] Mantena SK, Baliga MS, Katiyar SK. Grape seed proanthocyanidins induce apoptosis and inhibit metastasis of highly metastatic breast carcinoma cells. Carcinogenesis 2006;27:1682-91.

[157] Shih PH, Yeh CT, Yen GC. Anthocyanins induce the activation of phase II enzymes through the antioxidant response element pathway against oxidative stress-induced apoptosis. Journal of agricultural and food chemistry 2007;55:9427-35.

[158] Fan P, Lou H. Effects of polyphenols from grape seeds on oxidative damage to cellular DNA. Mol Cell Biochem 2004;267:67-74.

[159] Faria A, Calhau C, de Freitas V, Mateus N. Procyanidins as antioxidants and tumor cell growth modulators. Journal of agricultural and food chemistry 2006;54:2392-7.

[160] Wenzel U, Kuntz S, Brendel MD, Daniel H. Dietary flavone is a potent apoptosis inducer in human colon carcinoma cells. Cancer research 2000;60:3823-31.

[161] Conti M, Tazzari V, Baccini C, Pertici G, Serino LP, De Giorgi U. Anticancer drug delivery with nanoparticles. In vivo (Athens, Greece) 2006;20:697-701.

[162] Kobayashi H, Watanabe R, Choyke PL. Improving Conventional Enhanced Permeability and Retention (EPR) Effects; What Is the Appropriate Target? Theranostics 2014;4:81-9.

[163] Sinha R, Kim GJ, Nie S, Shin DM. Nanotechnology in cancer therapeutics: bioconjugated nanoparticles for drug delivery. Molecular cancer therapeutics 2006;5:1909-17.

[164] Bamrungsap S, Zhao Z, Chen T, Wang L, Li C, Fu T, et al. Nanotechnology in therapeutics: a focus on nanoparticles as a drug delivery system. Nanomedicine (Lond) 2012;7:1253-71.

[165] Wang Z. Plasmon—resonant gold nanoparticles for cancer optical imaging. Sci China Phys Mech Astron 2013;56:506-13.

[166] Lim Z-ZJ, Li J-EJ, Ng C-T, Yung L-YL, Bay B-H. Gold nanoparticles in cancer therapy. Acta Pharmacol Sin 2011;32:983-90.

[167] Siddharth V. Patwardhan FSE, Rajiv J. Berry, Sharon E. Jones, Rajesh. R. Naik, Olivier Deschaume , Hendrik Heinz ,, and Carole C. Perry. Chemistry of Aqueous Silica

Nanoparticle Surfaces and the Mechanism of Selective Peptide Adsorption,. J Am Chem Soc , 2012;134:6244-56.

[168] Kanaras DBaAG. Preparation of Peptide-Functionalized Gold Nanoparticles Using One Pot EDC/Sulfo-NHS Coupling,. Langmuir 2011, ;27 10119-23.

[169] DeLong RK, Reynolds CM, Malcolm Y, Schaeffer A, Severs T, Wanekaya A. Functionalized gold nanoparticles for the binding, stabilization, and delivery of therapeutic DNA, RNA, and other biological macromolecules. Nanotechnology, Science and Applications 2010;3:53-63.

[170] Patra CR, Bhattacharya R, Wang E, Katarya A, Lau JS, Dutta S, et al. Targeted delivery of gemcitabine to pancreatic adenocarcinoma using cetuximab as a targeting agent. Cancer research 2008;68:1970-8.

[171] Jiang W, KimBetty YS, Rutka JT, ChanWarren CW. Nanoparticle-mediated cellular response is size-dependent. Nat Nano 2008;3:145-50.

[172] Jain S, Hirst DG, O'Sullivan JM. Gold nanoparticles as novel agents for cancer therapy. The British Journal of Radiology 2012;85:101-13.

[173] Furst DE. Mechanism of action, pharmacology, clinical efficacy and side effects of auranofin. An orally administered organic gold compound for the treatment of rheumatoid arthritis. Pharmacotherapy 1983;3:284-98.

[174] Kean WF, Kean IR. Clinical pharmacology of gold. Inflammopharmacology 2008;16:112-25.

[175] Chen Y-S, Hung Y-C, Liau I, Huang GS. Assessment of the In Vivo Toxicity of Gold Nanoparticles. Nanoscale Research Letters 2009;4:858-64.

[176] De Jong WH, Hagens WI, Krystek P, Burger MC, Sips AJ, Geertsma RE. Particle size-dependent organ distribution of gold nanoparticles after intravenous administration. Biomaterials 2008;29:1912-9.

[177] Balogh L, Nigavekar SS, Nair BM, Lesniak W, Zhang C, Sung LY, et al. Significant effect of size on the in vivo biodistribution of gold composite nanodevices in mouse tumor models. Nanomedicine 2007;3:281-96.

[178] Yi Z, Chen Y, Chen S-j, Tan X-l, Niu G, Luo J-s, et al. Preparation of nano-structured Ag solid materials and application to surface-enhanced Raman scattering. J Cent South Univ Technol 2011;18:1877-82.

[179] Chowdhury J GM, Misra TN. pH-Dependent Surface-Enhanced Raman Scattering of 8-Hydroxy Quinoline Adsorbed on Silver Hydrosol.

. J Colloid Interface Sci 2000 228:372-8.

[180] Kneipp K WY, Kneipp H , Perelman Lev T, Itzkan I, Dasari RR, Feld SM. Single molecule detection using surface enhanced raman scattering. Phys Rev Lett 1997;78:1667–70.

[181] Nie SM ES. Probing single molecules and single nanoparticles by surface-enhanced raman scattering. Science 1997;275:1102–6.

[182] Dinish US, Balasundaram G, Chang Y-T, Olivo M. Actively Targeted In Vivo Multiplex Detection of Intrinsic Cancer Biomarkers Using Biocompatible SERS Nanotags. Sci Rep 2014;4.

[183] Silva NC, Sarmento B, Pintado M. The importance of antimicrobial peptides and their potential for therapeutic use in ophthalmology. International journal of antimicrobial agents 2013;41:5-10.

[184] Albericio F, Kruger HG. Therapeutic peptides. Future medicinal chemistry 2012;4:1527-31.

[185] Thundimadathil J. Cancer treatment using peptides: current therapies and future prospects. Journal of amino acids 2012;2012:967347.

[186] Soto-Pantoja DR, Menon J, Gallagher PE, Tallant EA. Angiotensin-(1-7) inhibits tumor angiogenesis in human lung cancer xenografts with a reduction in vascular endothelial growth factor. Molecular Cancer Therapeutics 2009;8:1676-83.

[187] Joo SH. Cyclic peptides as therapeutic agents and biochemical tools. Biomolecules & therapeutics 2012;20:19-26.

[188] Zheng LH, Wang YJ, Sheng J, Wang F, Zheng Y, Lin XK, et al. Antitumor peptides from marine organisms. Marine drugs 2011;9:1840-59.

[189] Khalili P, Arakelian A, Chen G, Plunkett ML, Beck I, Parry GC, et al. A non-RGD-based integrin binding peptide (ATN-161) blocks breast cancer growth and metastasis in vivo. Mol Cancer Ther 2006;5:2271-80.

[190] Deplanque G, Madhusudan S, Jones PH, Wellmann S, Christodoulos K, Talbot DC, et al. Phase II trial of the antiangiogenic agent IM862 in metastatic renal cell carcinoma. British journal of cancer 2004;91:1645-50.

[191] Bajo AM, Schally AV, Krupa M, Hebert F, Groot K, Szepeshazi K. Bombesin antagonists inhibit growth of MDA-MB-435 estrogen-independent breast cancers and decrease the expression of the ErbB-2/HER-2 oncoprotein and c-jun and c-fos oncogenes. Proceedings of the National Academy of Sciences of the United States of America 2002;99:3836-41.

[192] Constance JE, Lim CS. Targeting malignant mitochondria with therapeutic peptides. Ther Deliv 2012;3:961-79.

[193] Zhao ZM WY, Han J, Wang KL, Yang D, Yang YH, Du Q, Song YJ, Yin XX. Self-assembled micelles of amphiphilic poly(L-phenylalanine)-b-poly(L-serine) polypeptides for tumor-targeted delivery. International Jounal of Nanomedicine 2014 9:5849—62.

[194] Danho W, Swistok J, Khan W, Chu XJ, Cheung A, Fry D, et al. Opportunities and challenges of developing peptide drugs in the pharmaceutical industry. Advances in experimental medicine and biology 2009;611:467-9.

[195] Campenni A, Pignata SA, Baldari S. Can peptide receptor radionuclide therapy (PRRT) be useful in radioiodine-refractory differentiated thyroid cancer? Endocrine 2014.

[196] Heldring N, Pike A, Andersson S, Matthews J, Cheng G, Hartman J, et al. Estrogen receptors: how do they signal and what are their targets. Physiological reviews 2007;87:905-31.

[197] Leclercq G, Gallo D, Cossy J, Laios I, Larsimont D, Laurent G, et al. Peptides targeting estrogen receptor alpha-potential applications for breast cancer treatment. Current pharmaceutical design 2011;17:2632-53.

[198] Renoir JM, Marsaud V, Lazennec G. Estrogen receptor signaling as a target for novel breast cancer therapeutics. Biochemical pharmacology 2013;85:449-65.

[199] Jr. KA. Mutation and cancer statistical study of retinoblastoma,. Proc Natl Acad SciU S A 1971,;68:820-3.

[200] Jehanne M, Brisse H, Gauthier-Villars M, Lumbroso-le Rouic L, Freneaux P, Aerts I. [Retinoblastoma: recent advances]. Bulletin du cancer 2014;101:380-7.

[201] Doz F. [Retinoblatoma: a review]. Archives de pediatrie : organe officiel de la Societe francaise de pediatrie 2006;13:1329-37.

[202] Mehta M, Sethi S, Pushker N, Kashyap S, Sen S, Bajaj MS, et al. Retinoblastoma. Singapore medical journal 2012;53:128-35; quiz 36.

[203] Grossniklaus HE. Retinoblastoma. Fifty years of progress. The LXXI Edward Jackson Memorial Lecture. American journal of ophthalmology 2014;158:875-91.

[204] Watts P. Retinoblastoma: clinical features and current concepts in management. Journal of the Indian Medical Association 2003;101:464-6, 8.

[205] Classon M, Harlow E. The retinoblastoma tumour suppressor in development and cancer. Nature reviews Cancer 2002;2:910-7.

[206] Herwig S, Strauss M. The retinoblastoma protein: a master regulator of cell cycle, differentiation and apoptosis. European journal of biochemistry / FEBS 1997;246:581-601.

[207] Classon M, Harlow E. The retinoblastoma tumour suppressor in development and cancer. Nature reviews Cancer 2002;2:910-7.

[208] Whyte P. The retinoblastoma protein and its relatives. Seminars in cancer biology 1995;6:83-90.

[209] de Andrade AF, da Hora Barbosa R, Vargas FR, Ferman S, Eisenberg AL, Fernandes L, et al. A molecular study of first and second RB1 mutational hits in retinoblastoma patients. Cancer genetics and cytogenetics 2006;167:43-6.

[210] Liu Y, Zhong X, Wan S, Zhang W, Lin J, Zhang P, et al. p16(INK4a) expression in retinoblastoma: a marker of differentiation grade. Diagnostic Pathology 2014;9:180.

[211] Toma NM, Hungerford JL, Plowman PN, Kingston JE, Doughty D. External beam radiotherapy for retinoblastoma: II. Lens sparing technique. The British journal of ophthalmology 1995;79:112-7.

[212] Hungerford JL, Toma NM, Plowman PN, Kingston JE. External beam radiotherapy for retinoblastoma: I. Whole eye technique. The British journal of ophthalmology 1995;79:109-11.

[213] Mohney BG, Robertson DM, Schomberg PJ, Hodge DO. Second nonocular tumors in survivors of heritable retinoblastoma and prior radiation therapy. American journal of ophthalmology 1998;126:269-77.

[214] Abramson DH, Frank CM. Second nonocular tumors in survivors of bilateral retinoblastoma: a possible age effect on radiation-related risk. Ophthalmology 1998;105:573-9; discussion 9-80.

[215] Deepa PR, Vandhana S, Krishnakumar S. Fatty acid synthase inhibition induces differential expression of genes involved in apoptosis and cell proliferation in ocular cancer cells. Nutrition and cancer 2013;65:311-6.

[216] Krishnakumar S, Kandalam M, Mohan A, Iyer A, Venkatesan N, Biswas J, et al. Expression of Fas ligand in retinoblastoma. Cancer 2004;101:1672-6.

[217] Shanmugam MP, Lakshmi A, Biswas J, Krishnakumar S. Prognostic significance of Fas expression in retinoblastoma. Ocular immunology and inflammation 2003;11:107-13.

[218] Martowicz A, Rainer J, Lelong J, Spizzo G, Gastl G, Untergasser G. EpCAM overexpression prolongs proliferative capacity of primary human breast epithelial cells and supports hyperplastic growth. Molecular Cancer 2013;12:56-.

[219] Beta M, Khetan V, Chatterjee N, Suganeswari G, Rishi P, Biswas J, et al. EpCAM Knockdown Alters MicroRNA Expression in Retinoblastoma- Functional Implication of EpCAM Regulated MiRNA in Tumor Progression. PloS one 2014;9:e114800.

[220] Kandalam MM, Beta M, Maheswari UK, Swaminathan S, Krishnakumar S. Oncogenic microRNA 17-92 cluster is regulated by epithelial cell adhesion molecule and could be a potential therapeutic target in retinoblastoma. Molecular vision 2012;18:2279-87.

[221] Liu TG YJ, Shang BY, Min Z, He HW, Jiang JM, Chen F, Zhen YS, Shao RG. . Silencing of hdm2 oncogene by siRNA inhibits p53-dependent human breast cancer. Cancer Gene Ther Nov 2004 11:748-56.

[222] Kluck RM B-WE, Green DR, Newmeyer DD. The release of cytochrome c from mitochondria: a primary site for Bcl-2 regulation of apoptosis. Science 1997;275:1132-6.

[223] Gembarska A LF, Fedele C, Russell EA, Dewaele M, Villar S, Zwolinska A, Haupt S, de Lange J, Yip D, Goydos J, Haigh JJ, Haupt Y, Larue L, Jochemsen A, Shi H, Moriceau G, Lo RS, Ghanem G, Shackleton M, Bernal F, Marine JC, , , . MDM4 is a key therapeutic target in cutaneous melanoma. Nat Med 2012 doi: 10.1038/nm.2863.

[224] Nagata T, Shirakawa K, Kobayashi N, Shiheido H, Tabata N, Sakuma-Yonemura Y, et al. Structural basis for inhibition of the MDM2:p53 interaction by an optimized MDM2-binding peptide selected with mRNA display. PLoS One 2014;9:e109163.

[225] Kallen J, Goepfert A, Blechschmidt A, Izaac A, Geiser M, Tavares G, et al. Crystal Structures of Human MdmX (HdmX) in Complex with p53 Peptide Analogues Reveal Surprising Conformational Changes. The Journal of biological chemistry 2009;284:8812-21.

[226] Bhavsar D, Subramanian K, Sethuraman S, Krishnan UM. Management of retinoblastoma: opportunities and challenges. Drug delivery 2015:1-9.

[227] Jo DH, Lee TG, Kim JH. Nanotechnology and nanotoxicology in retinopathy. Int J Mol Sci 2011;12:8288-301.

[228] Bakri SJ PJ, Mukherjee P, Marler RJ, Mukhopadhyay D, . Absence of histologic retinal toxicity of intravitreal nanogold in a rabbit model, . Retina 2008;28(147-9.

[229] Hahn I HP, Endl E, Eter N.Ophthalmologe. . Use of nanoparticles in ophthalomology. Langmuir 2011;27:10119–23.

[230] Kim JH KM, Jo DH, Yu YS, Lee TG, Kim JH. The inhibition of retinal neovascularization by gold nanoparticles via suppression of VEGFR-2 activation. Biomaterials 2010;2011:1865-71.

[231] Chanda N KP, Watkinson LD, Shukla R, Zambre A, Carmack TL, Engelbrecht H, Lever JR, Katti K, Fent GM, Casteel SW, Smith CJ, Miller WH, Jurisson S, Boote E, Robertson JD, Cutler C, Dobrovolskaia M, Kannan R, Katti KV Radioactive gold nanoparticles in cancer therapy: therapeutic efficacy studies of (198)AuNP-GA nanoconstruct in prostate tumor-bearing mice. . Nanomedicine (lond) 2010;6:201-9.

[232] Patricia Metthe Todebush JC, Jennifer Roden and George C. Schatz. Theoretical analysis of gold nanoparticles. J Chem 1999;7:949-55.

[233] J. Turkevich PCS, J. Hillier. A study of the nucleation and growth processes in the synthesis of colloidal gold. Discuss Faraday Soc 1951;11:55-75.

[234] Shehzad A, Wahid F, Lee YS. Curcumin in cancer chemoprevention: molecular targets, pharmacokinetics, bioavailability, and clinical trials. Archiv der Pharmazie 2010;343:489-99.

[235] Wen J, Li HZ, Ji ZG, Jin J. Human urothelial carcinoma cell response to Sunitinib malate therapy in vitro. Cancer cell international 2015;15:26.

[236] Clogston JD, Patri AK. Zeta potential measurement. Methods in molecular biology (Clifton, NJ) 2011;697:63-70.

[237] Shukla RK, Sharma V, Pandey AK, Singh S, Sultana S, Dhawan A. ROS-mediated genotoxicity induced by titanium dioxide nanoparticles in human epidermal cells. Toxicology in vitro : an international journal published in association with BIBRA 2011;25:231-41.

[238] Parameswaran S, Wang R, Hastings G. Calculation of the Vibrational Properties of Chlorophyll a in Solution. The Journal of Physical Chemistry B 2008;112:14056-62.

[239] Dreaden EC, Alkilany AM, Huang X, Murphy CJ, El-Sayed MA. The golden age: gold nanoparticles for biomedicine. Chemical Society reviews 2012;41:2740-79.

[240] Gruene P, Rayner DM, Redlich B, van der Meer AF, Lyon JT, Meijer G, et al. Structures of neutral Au7, Au19, and Au20 clusters in the gas phase. Science 2008;321:674-6.

[241] Zhang YX, Zheng J, Gao G, Kong YF, Zhi X, Wang K, et al. Biosynthesis of gold nanoparticles using chloroplasts. International journal of nanomedicine 2011;6:2899-906.

[242] Mosmann T. Rapid colorimetric assay for cellular growth and survival: application to proliferation and cytotoxicity assays. Journal of immunological methods 1983;65:55-63.

[243] Carmichael J, DeGraff WG, Gazdar AF, Minna JD, Mitchell JB. Evaluation of a tetrazolium-based semiautomated colorimetric assay: assessment of chemosensitivity testing. Cancer research 1987;47:936-42.

[244] Chanda N, Kattumuri V, Shukla R, Zambre A, Katti K, Upendran A, et al. Bombesin functionalized gold nanoparticles show in vitro and in vivo cancer receptor specificity. Proceedings of the National Academy of Sciences of the United States of America 2010;107:8760-5.

[245] Yin H. Quest for better antioxidants: a commentary on "enhanced radical-scavenging activity by antioxidant-functionalized gold nanoparticles: a novel inspiration for development of new artificial antioxidant". Free Radic Biol Med 2007;43:1229-30.

[246] Zhang YX ZJ, Gao G, Kong YF, Zhi X, Wang K, Zhang XQ, Cui DX. Biosynthesis of gold nanoparticles using chloroplasts. Internatinal journal of Nanomedicine 2011;6:2899 -906.

[247] Lepock JR, Frey HE, Hallewell RA. Contribution of conformational stability and reversibility of unfolding to the increased thermostability of human and bovine superoxide dismutase mutated at free cysteines. The Journal of biological chemistry 1990;265:21612-8.

[248] Zelko IN, Mariani TJ, Folz RJ. Superoxide dismutase multigene family: a comparison of the CuZn-SOD (SOD1), Mn-SOD (SOD2), and EC-SOD (SOD3) gene structures, evolution, and expression. Free radical biology & medicine 2002;33:337-49.

[249] Harbour JW, Worley L, Ma D, Cohen M. Transducible peptide therapy for uveal melanoma and retinoblastoma. Archives of ophthalmology 2002;120:1341-6.

[250] Kannan P AJS. Synthesis of mercaptothiadiazole-functionalized gold nanoparticles and their self-assembly on Au substrates. Nanotechnology 2008;19.

[251] Vermes I, Haanen C, Steffens-Nakken H, Reutelingsperger C. A novel assay for apoptosis. Flow cytometric detection of phosphatidylserine expression on early apoptotic cells using fluorescein labelled Annexin V. Journal of immunological methods 1995;184:39-51.

[252] Kerr JF, Wyllie AH, Currie AR. Apoptosis: a basic biological phenomenon with wide-ranging implications in tissue kinetics. British journal of cancer 1972;26:239-57.

[253] Shapiro H. Practical Flow Cytometry. . second edition ed. New York: Alan R. Liss, Inc;1988.

[254] Darzynkiewicz Z. Nucleic Acid Analysis. Current Protocols in Cytometry: New York : J Wiley & Sons, Inc; ; 1997.

[255] Burr DB, Molina SA, Banerjee D, Low DM, Takemoto DJ. Treatment with Connexin 46 siRNA Suppresses the Growth of Human Y79 Retinoblastoma Cell Xenografts in vivo. Experimental eye research 2011;92:251-9.

[256] Vongsvivut J, Heraud P, Gupta A, Puri M, McNaughton D, Barrow CJ. FTIR microspectroscopy for rapid screening and monitoring of polyunsaturated fatty acid production in commercially valuable marine yeasts and protists. The Analyst 2013;138:6016-31.

[257] Raveendran P, Fu J, Wallen SL. A simple and "green" method for the synthesis of Au, Ag, and Au-Ag alloy nanoparticles. Green Chemistry 2006;8:34-8.

[258] Andre nel, Tian xia, Lutz mädler, li N. Toxic potential of materials at the nano level. Science 2006;311:622-7.

[259] Satish K. Nune, Nripen Chanda, Ravi Shukla, Kavita Katti, Rajesh R. Kulkarni, Subramanian T, et al. Green Nanotechnology from Tea: Phytochemicals in Tea as Building Blocks for Production of Biocompatible Gold Nanoparticles. J Mater Chem 2009 19:2912-20.

[260] Elavazhagan T, Arunachalam KD. Memecylon edule leaf extract mediated green synthesis of silver and gold nanoparticles. International journal of nanomedicine 2011;6:1265-78.

[261] Lehui Lu , Atsuko Kobayashi , Keiko Tawa , Ozaki aY. Silver Nanoplates with Special Shapes: Controlled Synthesis and Their Surface Plasmon Resonance and Surface-Enhanced Raman Scattering Properties. Chem Mater 2006;18:4894–901.

[262] Willets KA, Duyne aRPV. Localized Surface Plasmon Resonance Spectroscopy and Sensing. Annual Review of Physical Chemistry 2007;58:267-97.

[263] Maiti KK, Samanta A, Vendrell M, Soh KS, Olivo M, YT. C. Multiplex cancer cell detection by SERS nanotags with cyanine and triphenylmethine Raman reporters. Chem Commun 2011;28:3514-6.

[264] Nie S, Emory SR. Probing Single Molecules and Single Nanoparticles by Surface-Enhanced Raman Scattering. Science 1997;275:1102-6.

[265] Kho KW, Fu CY, Dinish US, M. O. Clinical SERS: are we there yet? J Biophotonics 2011;4:667-84.

[266] Kneipp J, Kneipp H, McLaughlin M, Brown D KK. In vivo molecular probing of cellular compartments with gold nanoparticles and nanoaggregates. . Nano Lett 2006;6:2225-31.

[267] Lee S, Chon H, Yoon SY, Lee EK, Chang SI, Lim DW, et al. Fabrication of SERS-fluorescence dual modal nanoprobes and application to multiplex cancer cell imaging. Nanoscale 2012;4:124-9.

[268] Jokerst JV, Cole AJ, Van de Sompel D, SS. G. Gold nanorods for ovarian cancer detection with photoacoustic imaging and resection guidance via Raman imaging in living mice. ACS Nano 2012;6:10366-77.

[269] Sanda Boca, Dumitrita Rugina, Adela Pintea, Nicolae Leopold, Astilean aS. Designing Gold Nanoparticle-Ensembles as Surface Enhanced Raman Scattering Tags inside Human Retinal Cells ,. Journal of Nanotechnology 2012;doi:10.1155/2012/961216.

[270] Li JF, Huang YF, Ding Y, Yang ZL, Li SB, Zhou XS, et al. Shell-isolated nanoparticle-enhanced Raman spectroscopy. Nature 2010;464:392-5.

[271] García I, Marradi M, S P. Glyconanoparticles: multifunctional nanomaterials for biomedical applications. Nanomedicine (Lond) 2010;5:777-92.

[272] Nune SK, Chanda N, Shukla R, Katti K, Kulkarni RR, Thilakavathi S, et al. Green Nanotechnology from Tea: Phytochemicals in Tea as Building Blocks for Production of Biocompatible Gold Nanoparticles. Journal of materials chemistry 2009;19:2912-20.

[273] Marco Marradia, Fabrizio Chiodo, Isabel Garcíaa, Penadés aS. Synthesis and Biological Applications of Glycoconjugates;Glycoliposomes and Metallic Glyconanoparticles in Glycoscience Bentham Science; 2011.

[274] Mie G. Beitrage zer Optik truber Meiden speziell kolloidaler Metallosungen. Ann Phys (Leipzig) 1908;25.

[275] Eric Le Ru, Etchegoin P. Prinziples of surface-enhanced Raman spectroscopy and related plasmonic effects and related plasmonic effects: Elsevier; 2009.

[276] Neshatian M, Chung S, Yohan D, Yang C, Chithrani DB. Determining the Size Dependence of Colloidal Gold Nanoparticle Uptake in a Tumor-like Interface (Hypoxic). Colloids and Interface Science Communications 2014;1:57-61.

[277] J. C. Earnshaw MWS. The Application of Laser Light Scattering to the Study of Biological Motion: Springer US; 1983.

[278] Semmler-Behnke M, Kreyling WG, Lipka J, Fertsch S, Wenk A, Takenaka S, et al. Biodistribution of 1.4- and 18-nm Gold Particles in Rats. Small 2008;4:2108-11.

[279] Li Wang, Yujing Sun, Yuncheng Cui, Jiku Wang aZL. Synthesis of Silver Nanoplates with Fibronectin Nanofibril Template and Their SERS Applications. Bull Korean Chem Soc 2013;34:443-6.

[280] Anna Kolbe, Axel Tiessen, Henriette Schluepmann, Matthew Paul, and SU, Geigenberger P. Trehalose 6-phosphate regulates starch synthesis via posttranslational redox activation of ADP-glucose pyrophosphorylase. PNAS 2005;102:11118–23.

[281] López-Vázquez C, Orriols I, Perelló M-C, de Revel G. Determination of aldehydes as pentafluorobenzyl derivatives in grape pomace distillates by HS-SPME-GC/MS. Food Chemistry 2012;130:1127-33.

[282] Kashif Ali, Federica Maltese, Young Hae Choi, Verpoorte R. Metabolic constituents of grapevine and grape-derived products. Phytochem Rev 2010 9:357–78.

[283] Rajasekharreddy P, Usha Rani P, B S. Qualitative assessment of silver and gold nanoparticle synthesis in various plants: a photobiological approach. J Nanopart Res 2010;12:1711–21.

[284] Beattie IR, RG. H. Silver and gold nanoparticles in plants: sites for the reduction to metal. Metallomics 2011 3:628-32.

[285] Dharmadhikari, Murli. Composition of Grapes , Newsletter: Vineyard & Vintage. Publications of the Missouri State Fruit Experiment Station 1994;9:3-8. .

[286] Rajesh Vasita , Katti DS. Structural and functional characterization of proteins adsorbed on hydrophilized polylactide-co-glycolide microfibers. International Journal of Nanomedicine 2012;7 61–71.

[287] Schwartzberg AM, Grant CD, Wolcott A, Talley CE, Huser TR, Bogomolni R, et al. Unique Gold Nanoparticle Aggregates as a Highly Active SERS Substrate. J Phys Chem B 2004;108:19191-7.

[288] En-Qin Xia, Gui-Fang Deng, Ya-Jun Guo, Li aH-B. Biological Activities of Polyphenols from Grapes. Int J Mol Sci 2010;11:622-46.

[289] Chia-Wei Chang, Jiunn-Der Liao, Hsien-Chang Chang, Li-Kai Lin, Yin-Yi Lin, Weng C-C. Fabrication of nano-indented cavities on Au for the detection of chemically-adsorbed DTNB molecular probes through SERS effect Journal of Colloid and Interface Science 2011;358:384–91.

[290] Shelley a. Claridge , Huiyang W.Liang , S. Roger Basu , Fréchet JMJ, Alivisatos aAP. Isolation of discrete nanoparticle−dna conjugates for plasmonic applications. Nano letters 2008;8:1202–6.

[291] Joke De Gelder, Kris De Gussem, Peter Vandenabeele, Moens L. Reference database of Raman spectra of biological molecules. Journal of Raman Spectroscopy 2007;38:1133–47.

[292] Zuk M, Dymińska L, Kulma A, Boba A, Prescha A, Szopa J, et al. IR and Raman studies of oil and seedcake extracts from natural and genetically modified flax seeds. Spectrochimica Acta Part A: Molecular and Biomolecular Spectroscopy 2011;78:1080-9.

[293] T. Mosmann. Rapid colorimetric assay for cellular growth and survival: application to proliferation and cytotoxicity assays. J Immunol Methods 1983;16 55-63.

[294] Khlebtsov N, Dykman aL. Biodistribution and toxicity of engineered gold nanoparticles: a review of in vitro and in vivo studies. Chem Soc Rev 2011;40:1647-71.

[295] FRENS G. Controlled Nucleation for the Regulation of the Particle Size in Monodisperse Gold Suspensions. Nature physical science 1973 241:20-2

[296] Biological evaluation of medical devices Part 5: Tests for in vitro cytotoxicity. ISO 10993-5 2009.

[297] Singh DK, Jagannathan R, Khandelwal P, Abraham PM, Poddar P. In situ synthesis and surface functionalization of gold nanoparticles with curcumin and their antioxidant properties: an experimental and density functional theory investigation. Nanoscale 2013;5:1882-93.

[298] Aaboe J, Bliddal H, Messier SP, Alkjaer T, Henriksen M. Effects of an intensive weight loss program on knee joint loading in obese adults with knee osteoarthritis. Osteoarthritis and cartilage / OARS, Osteoarthritis Research Society 2011;19:822-8.

[299] Allpress JG, Sanders JV. The structure and orientation of crystals in deposits of metals on mica. Surface Science 1967;7:1-25.

[300] Zuniga FA, Ormazabal V, Gutierrez N, Aguilera V, Radojkovic C, Veas C, et al. Role of lectin-like oxidized low density lipoprotein-1 in fetoplacental vascular dysfunction in preeclampsia. BioMed research international 2014;2014:353616.

[301] E. Ya. Gren, A. K. Grinvalde, Vanag GY. IR spectra and enolization of some β-diketones. J Appl Spectrosc 1967;6:253-5.

[302] Sindhu K, Rajaram A, Sreeram KJ, Rajaram R. Curcumin conjugated gold nanoparticle synthesis and its biocompatibility. RSC Advances 2014;4:1808-18.

[303] Peng Q, Zeng C, Zhou Y, Lian S, Nie G. Rapid Determination of Turmeric Roots Quality Based on the Raman Spectrum of Curcumin. Food Anal Methods 2014:1-6.

[304] Pezzotti G. Raman piezo-spectroscopic analysis of natural and synthetic biomaterials. Analytical and bioanalytical chemistry 2005;381:577-90.

[305] Schulz H, Baranska M. Identification and quantification of valuable plant substances by IR and Raman spectroscopy. Vibrational Spectroscopy 2007;43:13-25.

[306] Refat MS. Synthesis and characterization of ligational behavior of curcumin drug towards some transition metal ions: chelation effect on their thermal stability and biological activity. Spectrochimica acta Part A, Molecular and biomolecular spectroscopy 2013;105:326-37.

[307] Kimling J, Maier M, Okenve B, Kotaidis V, Ballot H, Plech A. Turkevich Method for Gold Nanoparticle Synthesis Revisited. The Journal of Physical Chemistry B 2006;110:15700-7.

[308] Frens G. Controlled Nucleation for the Regulation of the Particle Size in Monodisperse Gold Suspensions Nature physical science 1973;241:20-2

[309] John Turkevich, Stevenson PC, Hillier aJ. A study of the nucleation and growth processes in the synthesis of colloidal gold. Discussions of the Faraday Society 1951;11:55-75.

[310] Mittemeijer EJ. Fundamentals of Materials Science: The Microstructure-Property Relationship Using Metals as Model Systems (Graduate Texts in Physicsna) [Hardcover]. 2011 ed: Springer; 2011.

[311] Goh LP, Razak KA, Ridhuan NS, Cheong KY, Ooi PC, KC. A. Direct formation of gold nanoparticles on substrates using a novel ZnO sacrificial templated-growth hydrothermal approach and their properties in organic memory device. Nanoscale Res Lett 2012 7:563.

[312] Visioli FL, C. A. D. L. Andres-Lacueva, C. Aviram, M. Calhau, C. Cassano, A. D'Archivio, M. Faria, A. Favé, G. Fogliano, V. Llorach, R. Vitaglione, P. Zoratti, M. Edeas, M. Polyphenols and Human Health: A Prospectus Critical Reviews. Food Science and Nutrition 2011;51:524-46.

[313] Maria russo Cs, Idolo tedescoand Gian luigi russo. Phytochemicals in cancer prevention and therapy: truth or dare? Toxins 2010;2:517-51.

[314] Jacob A, Wu R, Zhou M, Wang P. Mechanism of the Anti-inflammatory Effect of Curcumin: PPAR-gamma Activation. PPAR research 2007;2007:89369.

[315] Rath KS, McCann GA, Cohn DE, Rivera BK, Kuppusamy P, Selvendiran K. Safe and targeted anticancer therapy for ovarian cancer using a novel class of curcumin analogs. Journal of Ovarian Research 2013;6:35-.

[316] Chiodo F, Marradi M, Tefsen B, Snippe H, van Die I, Penades S. High sensitive detection of carbohydrate binding proteins in an ELISA-solid phase assay based on multivalent glyconanoparticles. PLoS One 2013;8:e73027.

[317] Marin MJ, Schofield CL, Field RA, Russell DA. Glyconanoparticles for colorimetric bioassays. The Analyst 2014;140:59-70.

[318] Arnida M, Alexander Ghandehari, Hamidreza. Cellular uptake and toxicity of gold nanoparticles in prostate cancer cells: a comparative study of rods and spheres. Journal of Applied Toxicology 2010;30:212-7.

[319] Fent GM, Casteel SW, Kim DY, Kannan R, Katti K, Chanda N, et al. Biodistribution of maltose and gum arabic hybrid gold nanoparticles after intravenous injection in juvenile swine. Nanomedicine 2009;5:128-35.

[320] Cooke MS, Evans MD, Dizdaroglu M, Lunec J. Oxidative DNA damage: mechanisms, mutation, and disease. FASEB journal : official publication of the Federation of American Societies for Experimental Biology 2003;17:1195-214.

[321] Conklin KA. Cancer chemotherapy and antioxidants. The Journal of nutrition 2004;134:3201s-4s.

[322] Rybak LP. Mechanisms of cisplatin ototoxicity and progress in otoprotection. Current opinion in otolaryngology & head and neck surgery 2007;15:364-9.

[323] Conklin KA. Dietary antioxidants during cancer chemotherapy: impact on chemotherapeutic effectiveness and development of side effects. Nutrition and cancer 2000;37:1-18.

[324] Franceschi CM, Tochetto T, Silveira AF, Fantinel MR, Algarve TD. Cisplatin effects on guinea pigs: cochlear histology and genotoxicity. Brazilian journal of otorhinolaryngology 2011;77:728-35.

[325] Tokgoz SA, Vuralkan E, Sonbay ND, Caliskan M, Saka C, Besalti O, et al. Protective effects of vitamins E, B and C and L-carnitine in the prevention of cisplatin-induced ototoxicity in rats. The Journal of laryngology and otology 2012;126:464-9.

[326] Simsek G, Tokgoz SA, Vuralkan E, Caliskan M, Besalti O, Akin I. Protective effects of resveratrol on cisplatin-dependent inner-ear damage in rats. European archives of oto-rhino-laryngology : official journal of the European Federation of Oto-Rhino-

Laryngological Societies (EUFOS) : affiliated with the German Society for Oto-Rhino-Laryngology - Head and Neck Surgery 2013;270:1789-93.

[327] Droge W. Free radicals in the physiological control of cell function. Physiological reviews 2002;82:47-95.

[328] Finkel T. Oxidant signals and oxidative stress. Current opinion in cell biology 2003;15:247-54.

[329] Halliwell B. Oxidative stress and cancer: have we moved forward? The Biochemical journal 2007;401:1-11.

[330] Deepa PR, Nalini V, Mallikarjuna K, Vandhana S, Krishnakumar S. Oxidative stress in retinoblastoma: correlations with clinicopathologic features and tumor invasiveness. Current eye research 2009;34:1011-8.

[331] Adithi M, Nalini V, Krishnakumar S. The role of nitric oxide synthases and nitrotyrosine in retinoblastoma. Cancer 2005;103:1701-11.

[332] Mates JM. Effects of antioxidant enzymes in the molecular control of reactive oxygen species toxicology. Toxicology 2000;153:83-104.

[333] Gupta SC, Hevia D, Patchva S, Park B, Koh W, Aggarwal BB. Upsides and Downsides of Reactive Oxygen Species for Cancer: The Roles of Reactive Oxygen Species in Tumorigenesis, Prevention, and Therapy. Antioxidants & Redox Signaling 2012;16:1295-322.

[334] Zhu C, Hu W, Wu H, Hu X. No evident dose-response relationship between cellular ROS level and its cytotoxicity - a paradoxical issue in ROS-based cancer therapy. Sci Rep 2014;4.

[335] Seifried HE, McDonald SS, Anderson DE, Greenwald P, Milner JA. The antioxidant conundrum in cancer. Cancer research 2003;63:4295-8.

[336] Kohen R NA. Oxidation of biological systems: oxidative stress phenomena, antioxidants, redox reactions, and methods for their quantification. Toxicol Pathol 2002;30:620-50.

[337] Trachootham D, Alexandre J, Huang P. Targeting cancer cells by ROS-mediated mechanisms: a radical therapeutic approach? Nat Rev Drug Discov 2009;8:579-91.

[338] Sankaranarayanan K, Jaiswal AK. Nrf3 negatively regulates antioxidant-response element-mediated expression and antioxidant induction of NAD(P)H:quinone oxidoreductase1 gene. The Journal of biological chemistry 2004;279:50810-7.

[339] Miyamoto M, Murphy TH, Schnaar RL, Coyle JT. Antioxidants protect against glutamate-induced cytotoxicity in a neuronal cell line. The Journal of pharmacology and experimental therapeutics 1989;250:1132-40.

[340] Stagos D, Kazantzoglou G, Magiatis P, Mitaku S, Anagnostopoulos K, Kouretas D. Effects of plant phenolics and grape extracts from Greek varieties of Vitis vinifera on Mitomycin C and topoisomerase I-induced nicking of DNA. International journal of molecular medicine 2005;15:1013-22.

[341] Halliwell B. Free radicals and antioxidants - quo vadis? Trends in pharmacological sciences 2011;32:125-30.

[342] Lamson DW, Brignall MS. Antioxidants in cancer therapy; their actions and interactions with oncologic therapies. Altern Med Rev 1999;4:304-29.

[343] Gorrini C, Harris IS, Mak TW. Modulation of oxidative stress as an anticancer strategy. Nat Rev Drug Discov 2013;12:931-47.

[344] Trachootham D, Alexandre J, Huang P. Targeting cancer cells by ROS-mediated mechanisms: a radical therapeutic approach? Nat Rev Drug Discov 2009;8:579-91.

[345] Valko M, Leibfritz D, Moncol J, Cronin MTD, Mazur M, Telser J. Free radicals and antioxidants in normal physiological functions and human disease. The International Journal of Biochemistry & Cell Biology 2007;39:44-84.

[346] Almansour NM, Pirogova E, Coloe PJ, Cosic I, Istivan TS. Investigation of cytotoxicity of negative control peptides versus bioactive peptides on skin cancer and normal cells: a comparative study. Future Med Chem 2012;4:1553-65.

[347] Khaitan D, Dwarakanath BS. Endogenous and induced oxidative stress in multi-cellular tumour spheroids: implications for improving tumour therapy. Indian J Biochem Biophys 2009;46:16-24.

[348] Toyokuni S. Novel aspects of oxidative stress-associated carcinogenesis. Antioxid Redox Signal 2006;8:1373-7.

[349] Rahman K. Studies on free radicals, antioxidants, and co-factors. Clin Interv Aging 2007;2:219-36.

[350] Mates JM, Perez-Gomez C, Nunez de Castro I. Antioxidant enzymes and human diseases. Clin Biochem 1999;32:595-603.

[351] Shargorodsky M, Debby O, Matas Z, Zimlichman R. Effect of long-term treatment with antioxidants (vitamin C, vitamin E, coenzyme Q10 and selenium) on arterial compliance, humoral factors and inflammatory markers in patients with multiple cardiovascular risk factors. Nutr Metab (Lond) 2010;7:55.

[352] Bajaj S, Khan A. Antioxidants and diabetes. Indian J Endocrinol Metab 2012;16:S267-71.

[353] Ma H, Das T, Pereira S, Yang Z, Zhao M, Mukerji P, et al. Efficacy of dietary antioxidants combined with a chemotherapeutic agent on human colon cancer progression in a fluorescent orthotopic mouse model. Anticancer Res 2009;29:2421-6.

[354] Borek C. Dietary antioxidants and human cancer. Integr Cancer Ther 2004;3:333-41.

[355] Gu L, Zhao M, Li W, You L, Wang J, Wang H, et al. Chemical and cellular antioxidant activity of two novel peptides designed based on glutathione structure. Food Chem Toxicol 2012;50:4085-91.

[356] Park H, Tsutsumi H, Mihara H. Cell penetration and cell-selective drug delivery using alpha-helix peptides conjugated with gold nanoparticles. Biomaterials 2013;34:4872-9.

[357] Katti K, Chanda N, Shukla R, Zambre A, Suibramanian T, Kulkarni RR, et al. Green Nanotechnology from Cumin Phytochemicals: Generation of Biocompatible Gold Nanoparticles. Int J Green Nanotechnol Biomed 2009;1:B39-B52.

[358] Aromal SA, Vidhu VK, Philip D. Green synthesis of well-dispersed gold nanoparticles using Macrotyloma uniflorum. Spectrochim Acta A Mol Biomol Spectrosc 2012;85:99-104.

[359] Valko M, Rhodes CJ, Moncol J, Izakovic M, Mazur M. Free radicals, metals and antioxidants in oxidative stress-induced cancer. Chemico-Biological Interactions 2006;160:1-40.

[360] Valko M, Morris H, Cronin MTD. Metals, Toxicity and Oxidative Stress. Current Medicinal Chemistry 2005;12:1161-208.

[361] Ercal N, Gurer-Orhan H, Aykin-Burns N. Toxic metals and oxidative stress part I: mechanisms involved in metal-induced oxidative damage. Curr Top Med Chem 2001;1:529-39.

[362] Sareen D, van Ginkel PR, Takach JC, Mohiuddin A, Darjatmoko SR, Albert DM, et al. Mitochondria as the Primary Target of Resveratrol-Induced Apoptosis in Human Retinoblastoma Cells. Investigative Ophthalmology & Visual Science 2006;47:3708-16.

[363] Berendsen HJC, van der Spoel D, van Drunen R. GROMACS: A message-passing parallel molecular dynamics implementation. Computer Physics Communications 1995;91:43-56.

[364] Elias RJ, Kellerby SS, Decker EA. Antioxidant activity of proteins and peptides. Crit Rev Food Sci Nutr 2008;48:430-41.

[365] Matés JM, Pérez-Gómez C, de Castro IN, Asenjo M, Márquez J. Glutamine and its relationship with intracellular redox status, oxidative stress and cell proliferation/death. The International Journal of Biochemistry & Cell Biology 2002;34:439-58.

[366] Agyei D, Danquah MK. Industrial-scale manufacturing of pharmaceutical-grade bioactive peptides. Biotechnol Adv 2011;29:272-7.

[367] MK Danquah DA. Pharmaceutical applications of bioactive peptides. OA Biotechnology 2012;29:1-7.

[368] Ajibola CF, Fashakin JB, Fagbemi TN, Aluko RE. Effect of Peptide Size on Antioxidant Properties of African Yam Bean Seed (Sphenostylis stenocarpa) Protein Hydrolysate Fractions. Int J Mol Sci 2011;12:6685-702.

[369] Mine Y, Li-Chan E, Jiang B. Bioactive proteins and peptides as functional foods and nutraceuticals. Ames, Iowa: Wiley-Blackwell; 2010.

[370] Nie Z, Liu KJ, Zhong CJ, Wang LF, Yang Y, Tian Q, et al. Enhanced radical scavenging activity by antioxidant-functionalized gold nanoparticles: a novel inspiration for development of new artificial antioxidants. Free Radic Biol Med 2007;43:1243-54.

[371] Wu Y, Tian Q, Li L, Khan MN, Yang X, Zhang Z, et al. Inhibitory effect of antioxidant peptides derived from Pinctada fucata protein on ultraviolet-induced photoaging in mice. Journal of Functional Foods 2013;5:527-38.

[372] Khan MA, Chen HC, Wan XX, Tania M, Xu AH, Chen FZ, et al. Regulatory effects of resveratrol on antioxidant enzymes: a mechanism of growth inhibition and apoptosis induction in cancer cells. Mol Cells 2013;35:219-25.

[373] Hällbrink M, Oehlke J, Papsdorf G, Bienert M. Uptake of cell-penetrating peptides is dependent on peptide-to-cell ratio rather than on peptide concentration. Biochimica et Biophysica Acta (BBA) - Biomembranes 2004;1667:222-8.

[374] Kosuge M, Takeuchi T, Nakase I, Jones AT, Futaki S. Cellular internalization and distribution of arginine-rich peptides as a function of extracellular peptide concentration, serum, and plasma membrane associated proteoglycans. Bioconjugate chemistry 2008;19:656-64.

[375] Christianson HC, Belting M. Heparan sulfate proteoglycan as a cell-surface endocytosis receptor. Matrix Biology 2014;35:51-5.

[376] Amand HL, Rydberg HA, Fornander LH, Lincoln P, Norden B, Esbjorner EK. Cell surface binding and uptake of arginine- and lysine-rich penetratin peptides in absence and presence of proteoglycans. Biochimica et biophysica acta 2012;1818:2669-78.

[377] Guterstam P, Madani F, Hirose H, Takeuchi T, Futaki S, El Andaloussi S, et al. Elucidating cell-penetrating peptide mechanisms of action for membrane interaction,

cellular uptake, and translocation utilizing the hydrophobic counter-anion pyrenebutyrate. Biochimica et Biophysica Acta (BBA) - Biomembranes 2009;1788:2509-17.

[378] Maus L, Dick O, Bading H, Spatz JP, Fiammengo R. Conjugation of peptides to the passivation shell of gold nanoparticles for targeting of cell-surface receptors. ACS nano 2010;4:6617-28.

[379] Balaji S, Mukunthan KS, Kannan N. Bio-Nanomaterials: Structure and Assembly. Reviews in Advanced Sciences and Engineering 2014;3:250-60.

[380] Aryal S, B KCR, Dharmaraj N, Bhattarai N, Kim CH, Kim HY. Spectroscopic identification of S-Au interaction in cysteine capped gold nanoparticles. Spectrochimica acta Part A, Molecular and biomolecular spectroscopy 2006;63:160-3.

[381] Chanda N, Kattumuri V, Shukla R, Zambre A, Katti K, Upendran A, et al. Bombesin functionalized gold nanoparticles show in vitro and in vivo cancer receptor specificity. Proceedings of the National Academy of Sciences of the United States of America 2010;107:8760-5.

[382] Flora SJ, Pachauri V. Chelation in metal intoxication. International journal of environmental research and public health 2010;7:2745-88.

[383] Bei F, Hou X, Chang SLY, Simon GP, Li D. Interfacing Colloidal Graphene Oxide Sheets with Gold Nanoparticles. Chemistry – A European Journal 2011;17:5958-64.

[384] Liu Y, Shipton MK, Ryan J, Kaufman ED, Franzen S, Feldheim DL. Synthesis, Stability, and Cellular Internalization of Gold Nanoparticles Containing Mixed Peptide−Poly(ethylene glycol) Monolayers. Analytical Chemistry 2007;79:2221-9.

[385] Tiwari PM, Eroglu E, Bawage SS, Vig K, Miller ME, Pillai S, et al. Enhanced intracellular translocation and biodistribution of gold nanoparticles functionalized with a

cell-penetrating peptide (VG-21) from vesicular stomatitis virus. Biomaterials 2014;35:9484-94.

[386] Alexander A. Kamnev LAD, Petros A. Tarantilis and Moschos G. Polissiou Spectroimmunochemistry Using Colloidal Gold Bioconjugates Bioscience Reports 2002 22:541-7.

[387] Chen J, Zheng A, Chen A, Gao Y, He C, Kai X, et al. A functionalized gold nanoparticles and Rhodamine 6G based fluorescent sensor for high sensitive and selective detection of mercury(II) in environmental water samples. Anal Chim Acta 2007;599:134-42.

[388] Oishi M, Tamura A, Nakamura T, Nagasaki Y. A Smart Nanoprobe Based On Fluorescence-Quenching PEGylated Nanogels Containing Gold Nanoparticles for Monitoring the Response to Cancer Therapy. Advanced Functional Materials 2009;19:827-34.

[389] Barros LF, Kanaseki T, Sabirov R, Morishima S, Castro J, Bittner CX, et al. Apoptotic and necrotic blebs in epithelial cells display similar neck diameters but different kinase dependency. Cell death and differentiation 2003;10:687-97.

[390] Elmore S. Apoptosis: a review of programmed cell death. Toxicologic pathology 2007;35:495-516.

[391] Ou P, Tritschler HJ, Wolff SP. Thioctic (lipoic) acid: a therapeutic metal-chelating antioxidant? Biochemical pharmacology 1995;50:123-6.

[392] Szeto HH. Cell-permeable, mitochondrial-targeted, peptide antioxidants. AAPS J 2006;8:E277-83.

[393] Mendis E, Rajapakse N, Kim SK. Antioxidant properties of a radical-scavenging peptide purified from enzymatically prepared fish skin gelatin hydrolysate. J Agric Food Chem 2005;53:581-7.

[394] Olas B, Wachowicz B. Resveratrol, a phenolic antioxidant with effects on blood platelet functions. Platelets 2005;16:251-60.

[395] Apostolou A, Stagos D, Galitsiou E, Spyrou A, Haroutounian S, Portesis N, et al. Assessment of polyphenolic content, antioxidant activity, protection against ROS-induced DNA damage and anticancer activity of Vitis vinifera stem extracts. Food and chemical toxicology : an international journal published for the British Industrial Biological Research Association 2013;61:60-8.

[396] Verrax J, Taper H, Buc Calderon P. Targeting cancer cells by an oxidant-based therapy. Current molecular pharmacology 2008;1:80-92.

[397] Yang Y, Karakhanova S, Werner J, Bazhin AV. Reactive oxygen species in cancer biology and anticancer therapy. Current medicinal chemistry 2013;20:3677-92.

[398] Seifried HE, Anderson DE, Sorkin BC, Costello RB. Free radicals: the pros and cons of antioxidants. Executive summary report. The Journal of nutrition 2004;134:3143s-63s.

[399] Conklin KA. Dietary polyunsaturated fatty acids: impact on cancer chemotherapy and radiation. Alternative medicine review : a journal of clinical therapeutic 2002;7:4-21.

[400] Gina Manda MTNaT-MN. Reactive Oxygen Species, Cancer and Anti-Cancer Therapies. Current Chemical Biology 2009;3:342-66.

[401] Bresciani G, da Cruz IB, Gonzalez-Gallego J. Manganese superoxide dismutase and oxidative stress modulation. Advances in clinical chemistry 2015;68:87-130.

[402] Fahmy B, Cormier SA. Copper oxide nanoparticles induce oxidative stress and cytotoxicity in airway epithelial cells. Toxicology in vitro : an international journal published in association with BIBRA 2009;23:1365-71.

[403] Zhang H, Ji Z, Xia T, Meng H, Low-Kam C, Liu R, et al. Use of metal oxide nanoparticle band gap to develop a predictive paradigm for oxidative stress and acute pulmonary inflammation. ACS Nano 2012;6:4349-68.

[404] Zhao X, Sheng L, Wang L, Hong J, Yu X, Sang X, et al. Mechanisms of nanosized titanium dioxide-induced testicular oxidative stress and apoptosis in male mice. Particle and Fibre Toxicology 2014;11:47-.

[405] Hernandez-Escolano M, Juan-Diaz MJ, Martinez-Ibanez M, Suay J, Goni I, Gurruchaga M. Synthesis of hybrid sol-gel materials and their biological evaluation with human mesenchymal stem cells. Journal of materials science Materials in medicine 2013;24:1491-9.

[406] Hybrid Nanocomposites for Nanotechnology: Electronic, Optical, Magnetic and Biomedical Applications: Springer; 2009.

[407] Sanchez C, Julian B, Belleville P, Popall M. Applications of hybrid organic-inorganic nanocomposites. Journal of Materials Chemistry 2005;15:3559-92.

[408] Catauro M, Raucci MG, Ausanio G, Ambrosio L. Sol-gel synthesis, characterization and bioactivity of poly(ether-imide)/TiO2 hybrid materials. Journal of applied biomaterials & biomechanics : JABB 2007;5:41-8.

[409] Lee B, Luo H, Yuan CY, Lin JS, Dai S. Synthesis and characterization of organic-inorganic hybrid mesoporous silica materials with new templates. Chemical communications 2004:240-1.

[410] Kang H, Kim S-H, Yang S-M, Park J-H. Bio-inspired nanotadpoles with component-specific functionality. Journal of Materials Chemistry B 2014;2:6462-6.

[411] Manjumeena R, Elakkiya T, Duraibabu D, Feroze Ahamed A, Kalaichelvan P, Venkatesan R. 'Green' biocompatible organic–inorganic hybrid electrospun nanofibers for potential biomedical applications. Journal of Biomaterials Applications 2014.

[412] Raveendran P, Fu J, Wallen SL. Completely "green" synthesis and stabilization of metal nanoparticles. Journal of the American Chemical Society 2003;125:13940-1.

[413] da Rocha Lindner G, Khalil NM, Mainardes RM. Resveratrol-loaded polymeric nanoparticles: validation of an HPLC-PDA method to determine the drug entrapment and evaluation of its antioxidant activity. TheScientificWorldJournal 2013;2013:506083.

[414] Biewenga GP, Haenen GR, Bast A. The pharmacology of the antioxidant lipoic acid. Gen Pharmacol 1997;29:315-31.

[415] Akhtar MS, Umar, Ahmad. Biosynthesis of Nanomaterials and Their Applications. Reviews in Advanced Sciences and Engineering 2014;3:197-8.

[416] Sanchez C, Belleville P, Popall M, Nicole L. Applications of advanced hybrid organic-inorganic nanomaterials: from laboratory to market. Chemical Society Reviews 2011;40:696-753.

[417] Ooi VEC, Liu F. Immunomodulation and Anti-Cancer Activity of Polysaccharide-Protein Complexes. Current Medicinal Chemistry 2000;7:715-29.

[418] Obreza A, Gobec S. Recent Advances in Design, Synthesis and Biological Activity of Aminoalkylsulfonates and Sulfonamidopeptides. Current Medicinal Chemistry 2004;11:3263-78.

[419] Zhao Y, Alakhova DY, Kabanov AV. Can nanomedicines kill cancer stem cells? Advanced drug delivery reviews 2013;65:1763-83.

[420] Peer D, Karp JM, Hong S, Farokhzad OC, Margalit R, Langer R. Nanocarriers as an emerging platform for cancer therapy. Nat Nano 2007;2:751-60.

[421] Ghosh P, Han G, De M, Kim CK, Rotello VM. Gold nanoparticles in delivery applications. Advanced drug delivery reviews 2008;60:1307-15.

[422] Momand J, Jung D, Wilczynski S, Niland J. The MDM2 gene amplification database. Nucleic acids research 1998;26:3453-9.

[423] Laurie NA, Donovan SL, Shih CS, Zhang J, Mills N, Fuller C, et al. Inactivation of the p53 pathway in retinoblastoma. Nature 2006;444:61-6.

[424] Aarestrup J, Kyro C, Knudsen KE, Weiderpass E, Christensen J, Kristensen M, et al. Plasma enterolactone and incidence of endometrial cancer in a case-cohort study of Danish women. The British journal of nutrition 2013;109:2269-75.

[425] Momand J, Zambetti GP, Olson DC, George D, Levine AJ. The mdm-2 oncogene product forms a complex with the p53 protein and inhibits p53-mediated transactivation. Cell 1992;69:1237-45.

[426] Patel S, Player MR. Small-molecule inhibitors of the p53-HDM2 interaction for the treatment of cancer. Expert opinion on investigational drugs 2008;17:1865-82.

[427] Hu CQ, Hu YZ. Small molecule inhibitors of the p53-MDM2. Current medicinal chemistry 2008;15:1720-30.

[428] Lau LMS, Nugent JK, Zhao X, Irwin MS. HDM2 antagonist Nutlin-3 disrupts p73-HDM2 binding and enhances p73 function. Oncogene 2007;27:997-1003.

[429] Wei SJ, Joseph T, Sim AYL, Yurlova L, Zolghadr K, Lane D, et al. In Vitro Selection of Mutant HDM2 Resistant to Nutlin Inhibition. PloS one 2013;8:e62564.

[430] O'Keefe K, Li H, Zhang Y. Nucleocytoplasmic shuttling of p53 is essential for MDM2-mediated cytoplasmic degradation but not ubiquitination. Molecular and cellular biology 2003;23:6396-405.

[431] Shields CL, Shields JA. Basic understanding of current classification and management of retinoblastoma. Current opinion in ophthalmology 2006;17:228-34.

[432] Evans SC, Viswanathan M, Grier JD, Narayana M, El-Naggar AK, Lozano G. An alternatively spliced HDM2 product increases p53 activity by inhibiting HDM2. Oncogene 2001;20:4041-9.

[433] Pronk S, Pall S, Schulz R, Larsson P, Bjelkmar P, Apostolov R, et al. GROMACS 4.5: a high-throughput and highly parallel open source molecular simulation toolkit. Bioinformatics (Oxford, England) 2013;29:845-54.

[434] Ramezani F, Habibi M, Rafii-Tabar H, Amanlou M. Effect of peptide length on the conjugation to the gold nanoparticle surface: a molecular dynamic study. DARU Journal of Pharmaceutical Sciences 2015;23:9.

[435] Hirn S, Semmler-Behnke M, Schleh C, Wenk A, Lipka J, Schäffler M, et al. Particle size-dependent and surface charge-dependent biodistribution of gold nanoparticles after intravenous administration. European Journal of Pharmaceutics and Biopharmaceutics 2011;77:407-16.

[436] Sainsbury T, Ikuno T, Okawa D, Pacilé D, Fréchet JMJ, Zettl A. Self-Assembly of Gold Nanoparticles at the Surface of Amine- and Thiol-Functionalized Boron Nitride Nanotubes. The Journal of Physical Chemistry C 2007;111:12992-9.

[437] Pyshnaya IA, Razum KV, Poletaeva JE, Pyshnyi DV, Zenkova MA, Ryabchikova EI. Comparison of behaviour in different liquids and in cells of gold nanorods and spherical nanoparticles modified by linear polyethyleneimine and bovine serum albumin. BioMed research international 2014;2014:908175.

[438] Sareen D, van Ginkel PR, Takach JC, Mohiuddin A, Darjatmoko SR, Albert DM, et al. Mitochondria as the primary target of resveratrol-induced apoptosis in human retinoblastoma cells. Investigative ophthalmology & visual science 2006;47:3708-16.

[439] Fulda S. Regulation of cell death and survival by resveratrol: implications for cancer therapy. Anti-cancer agents in medicinal chemistry 2012;12:874-9.

[440] Cal C, Garban H, Jazirehi A, Yeh C, Mizutani Y, Bonavida B. Resveratrol and cancer: chemoprevention, apoptosis, and chemo-immunosensitizing activities. Current medicinal chemistry Anti-cancer agents 2003;3:77-93.

[441] Greish K. Enhanced Permeability and Retention (EPR) Effect for Anticancer Nanomedicine Drug Targeting. 2010. p. 25-37.

[442] Arnida, Malugin A, Ghandehari H. Cellular uptake and toxicity of gold nanoparticles in prostate cancer cells: a comparative study of rods and spheres. Journal of applied toxicology : JAT 2010;30:212-7.

[443] Eckelman BP, Salvesen GS, Scott FL. Human inhibitor of apoptosis proteins: why XIAP is the black sheep of the family. EMBO Reports 2006;7:988-94.

[444] Viard I, Wehrli P, Jornot L, Bullani R, Vechietti JL, Schifferli JA, et al. Clusterin gene expression mediates resistance to apoptotic cell death induced by heat shock and oxidative stress. The Journal of investigative dermatology 1999;112:290-6.

[445] Hsiao WT, Tsai MD, Jow GM, Tien LT, Lee YJ. Involvement of Smac, p53, and caspase pathways in induction of apoptosis by gossypol in human retinoblastoma cells. Molecular vision 2012;18:2033-42.

[446] Ikeguchi M, Liu J, Kaibara N. Expression of survivin mRNA and protein in gastric cancer cell line (MKN-45) during cisplatin treatment. Apoptosis : an international journal on programmed cell death 2002;7:23-9.

[447] Tan CP, Lu YY, Ji LN, Mao ZW. Metallomics insights into the programmed cell death induced by metal-based anticancer compounds. Metallomics : integrated biometal science 2014;6:978-95.

[448] Aggarwal BB, Bhardwaj A, Aggarwal RS, Seeram NP, Shishodia S, Takada Y. Role of resveratrol in prevention and therapy of cancer: preclinical and clinical studies. Anticancer research 2004;24:2783-840.

[449] Kanwar JR, Mahidhara G, Roy K, Sasidharan S, Krishnakumar S, Prasad N, et al. Fe-bLf nanoformulation targets survivin to kill colon cancer stem cells and maintains absorption of iron, calcium and zinc. Nanomedicine 2014:0.

[450] Soman NR, Baldwin SL, Hu G, Marsh JN, Lanza GM, Heuser JE, et al. Molecularly targeted nanocarriers deliver the cytolytic peptide melittin specifically to tumor cells in mice, reducing tumor growth. The Journal of Clinical Investigation 2009;119:2830-42.

[451] Ruoslahti E, Bhatia SN, Sailor MJ. Targeting of drugs and nanoparticles to tumors. The Journal of cell biology 2010;188:759-68.

[452] Wang H, Nan L, Yu D, Agrawal S, Zhang R. Antisense anti-MDM2 oligonucleotides as a novel therapeutic approach to human breast cancer: in vitro and in vivo activities and

mechanisms. Clinical cancer research : an official journal of the American Association for Cancer Research 2001;7:3613-24.

[453] Moll UM, Petrenko O. The MDM2-p53 interaction. Molecular cancer research : MCR 2003;1:1001-8.

[454] Roy AM, Baliga MS, Elmets CA, Katiyar SK. Grape Seed Proanthocyanidins Induce Apoptosis through p53, Bax, and Caspase 3 Pathways. Neoplasia (New York, NY) 2005;7:24-36.

[455] Sahpazidou D, Geromichalos GD, Stagos D, Apostolou A, Haroutounian SA, Tsatsakis AM, et al. Anticarcinogenic activity of polyphenolic extracts from grape stems against breast, colon, renal and thyroid cancer cells. Toxicology letters 2014;230:218-24.

[456] Nassiri-Asl M, Hosseinzadeh H. Review of the pharmacological effects of Vitis vinifera (Grape) and its bioactive compounds. Phytotherapy research : PTR 2009;23:1197-204.

[457] Liu T-g, Yin JQ, Shang B-y, Min Z, He H-w, Jiang J-m, et al. Silencing of hdm2 oncogene by siRNA inhibits p53-dependent human breast cancer. Cancer Gene Ther 2004;11:748-56.

[458] Shukla S, Gupta S. Apigenin-induced prostate cancer cell death is initiated by reactive oxygen species and p53 activation. Free radical biology & medicine 2008;44:1833-45.

[459] Manfredi JJ. The Mdm2–p53 relationship evolves: Mdm2 swings both ways as an oncogene and a tumor suppressor. Genes & Development 2010;24:1580-9.

[460] Gu L, Zhu N, Zhang H, Durden DL, Feng Y, Zhou M. Regulation of XIAP translation and induction by MDM2 following irradiation. Cancer cell 2009;15:363-75.

[461] Aghbali A, Hosseini SV, Delazar A, Gharavi NK, Shahneh FZ, Orangi M, et al. Induction of apoptosis by grape seed extract (Vitis vinifera) in oral squamous cell carcinoma. Bosnian journal of basic medical sciences / Udruzenje basicnih mediciniskih znanosti = Association of Basic Medical Sciences 2013;13:186-91.

[462] Pochampally R, Fodera B, Chen L, Lu W, Chen J. Activation of an MDM2-specific caspase by p53 in the absence of apoptosis. The Journal of biological chemistry 1999;274:15271-7.

[463] Fotin-Mleczek M, Welte S, Mader O, Duchardt F, Fischer R, Hufnagel H, et al. Cationic cell-penetrating peptides interfere with TNF signalling by induction of TNF receptor internalization. Journal of cell science 2005;118:3339-51.

[464] Chiu JJ, Wung BS, Shyy JYJ, Hsieh HJ, Wang DL. Reactive Oxygen Species Are Involved in Shear Stress-Induced Intercellular Adhesion Molecule-1 Expression in Endothelial Cells. Arteriosclerosis, Thrombosis, and Vascular Biology 1997;17:3570-7.

[465] Edelman GM. Cell adhesion and the molecular processes of morphogenesis. Annual review of biochemistry 1985;54:135-69.

[466] Granger DN, Korthuis RJ. Physiologic mechanisms of postischemic tissue injury. Annual review of physiology 1995;57:311-32.

[467] Weber C, Erl W, Pietsch A, Strobel M, Ziegler-Heitbrock HW, Weber PC. Antioxidants inhibit monocyte adhesion by suppressing nuclear factor-kappa B mobilization and induction of vascular cell adhesion molecule-1 in endothelial cells stimulated to generate radicals. Arteriosclerosis and thrombosis : a journal of vascular biology / American Heart Association 1994;14:1665-73.

[468] Shigematsu S, Ishida S, Hara M, Takahashi N, Yoshimatsu H, Sakata T, et al. Resveratrol, a red wine constituent polyphenol, prevents superoxide-dependent inflammatory responses induced by ischemia/reperfusion, platelet-activating factor, or oxidants. Free radical biology & medicine 2003;34:810-7.

[469] Bastus NG, Sanchez-Tillo E, Pujals S, Farrera C, Lopez C, Giralt E, et al. Homogeneous conjugation of peptides onto gold nanoparticles enhances macrophage response. ACS Nano 2009;3:1335-44.

[470] Ma Q, Kinneer K. Chemoprotection by phenolic antioxidants. Inhibition of tumor necrosis factor alpha induction in macrophages. The Journal of biological chemistry 2002;277:2477-84.

[471] Sadauskas E, Jacobsen NR, Danscher G, Stoltenberg M, Vogel U, Larsen A, et al. Biodistribution of gold nanoparticles in mouse lung following intratracheal instillation. Chemistry Central journal 2009;3:16.

[472] El-Sayed MA, Shabaka AA, El-Shabrawy OA, Yassin NA, Mahmoud SS, El-Shenawy SM, et al. Tissue distribution and efficacy of gold nanorods coupled with laser induced photoplasmonic therapy in ehrlich carcinoma solid tumor model. PloS one 2013;8:e76207.

[473] Shuming Nie, Emory SR. Probing single molecules and single nanoparticles by surfaceenhanced Raman scattering. Science 1997;275:1102-6.

[474] Allpress JGS, J. V. The structure and orientation of crystals in deposits of metals on mica. Surface Science 1967;7:1-25.

[475] AshaRani PV, Low Kah Mun G, Hande MP, S. V. Cytotoxicity and Genotoxicity of Silver Nanoparticles in Human Cells. . ACS Nano 2009;3:279-90.

[476] Ward JH. Hierarchical Grouping to optimize an objective function. Journal of American Statistical Association (1963);58:236-44.

[477] Jokerst JV TM, Kempen PJ, Sinclair R, Gambhir SS. Photoacoustic imaging of mesenchymal stem cells in living mice via silica-coated gold nanorods. ACS Nano 2012;6:5920-30.

[478] Socrates G. Infrared and Raman Characteristic Group Frequencies: Tables and Charts. 3rd ed: John Wiley & Sons, Chichester, UK; 2001.

[479] Barth A. The infrared absorption of amino acid side chains. Progress in biophysics and molecular biology 2000;74:141-73.

[480] Dong L, Sun X, Chao Z, Zhang S, Zheng J, Gurung R, et al. Evaluation of FTIR spectroscopy as diagnostic tool for colorectal cancer using spectral analysis. Spectrochimica acta Part A, Molecular and biomolecular spectroscopy 2014;122:288-94.

[481] Zhou S, Xu Z, Ling XF, Li QB, Xu YZ, Zhang L, et al. [FTIR spectroscopic characterization of freshly removed breast cancer tissues]. Zhonghua zhong liu za zhi [Chinese journal of oncology] 2006;28:512-4.

[482] Icard P, Poulain L, Lincet H. Understanding the central role of citrate in the metabolism of cancer cells. Biochimica et biophysica acta 2012;1825:111-6.

[483] Ghosh D, Saha C, Hossain M, Dey SK, Kumar GS. Biophysical studies of mutated K562 DNA (erythroleukemic cells) binding to adriamycin and daunomycin reveal that mutations induce structural changes influencing binding behavior. Journal of biomolecular structure & dynamics 2013;31:331-41.

[484] Ami D, Neri T, Natalello A, Mereghetti P, Doglia SM, Zanoni M, et al. Embryonic stem cell differentiation studied by FT-IR spectroscopy. Biochimica et Biophysica Acta (BBA) - Molecular Cell Research 2008;1783:98-106.

[485] Vogel R, Siebert F. Fourier transform IR spectroscopy study for new insights into molecular properties and activation mechanisms of visual pigment rhodopsin. Biopolymers 2003;72:133-48.

[486] Hughes C, Brown MD, Clarke NW, Flower KR, Gardner P. Investigating cellular responses to novel chemotherapeutics in renal cell carcinoma using SR-FTIR spectroscopy. The Analyst 2012;137:4720-6.

[487] Quaroni L, Zlateva T. Infrared spectromicroscopy of biochemistry in functional single cells. The Analyst 2011;136:3219-32.

[488] Tan S-T, Chen K, Ong S, Chew W. Utilization of spectral vector properties in multivariate chemometrics analysis of hyperspectral infrared imaging data for cellular studies. The Analyst 2008;133:1395-408.

APPENDIX I (LIST OF CHEMICALS)

S.N	Chemicals	Company
1	Acetone	Merck
2	Acetonitrile	Merck
3	Annexin V apoptosis kit,	BD Biosciences
4	Antibiotic antimycotic solution	HiMedia
5	Anti-HDM2 antibody	Santa cruz
6	Anti-P53 antibody	Santa cruz
7	Anti-β actin antibody	Sigma Aldrich
8	Chloroform	Merck
9	Curcumin	Sigma
10	Dicholorodihydrofluorescein fluorescence assay kit,	Cell Biolabs
11	Diethyl ether	Merck
12	Diethyl pyrocarbonate	Sigma Aldrich
13	Dimethyl sulfoxide	Sigma Aldrich
14	DMEM	Gibco
15	DTT	Sigma
16	Enhanced chemiluminescence kit	Pierce
17	Fetal bovine serum	Gibco
18	HDM2-Peptide	Sigma Aldrich

19	Isopropanol	Merck
20	MTT	Sigma Aldrich
21	Mouse anti-mouse antibody	Santa-Cruz
22	PEG-1000	
23	NaAuCl4	Sigma Aldrich
24	Peptide-A	Ana Spec
25	Ponceau S	Sigma Aldrich
26	RNAse out	Sigma Aldrich
27	Reverse Transcriptase kit	Applied Biosystem
28	SYBR green real time RT-PCR master mix	Applied Biosystem
29	Sodium Citrate	Merck
30	Triton X 100	HiMedia
31	Trizol	Sigma Aldrich
32	Trypsin	Sigma Aldrich
33	Vitis Vinifera	Local vendor

APPENDIX III (REAGENT PREPARATION)

S.N.	Chemical	Composition
1	RPMI/DMEM(Cell culture medium)	445 ml culture medium 50 ml FBS 5 ml Antibiotic-antimycotic
2	Tris-HCl Buffer (pH 8.8)	Tris-9.0gm Water-25ml Adjust the pH to 8.8 with1N HCl and made up to 50ml with Distilled water
3	Tris-HCl Buffer (pH6.8):	Tris-3.0gm Water-25ml Adjust the pH to 6.8 with 1N HCl and made up to 50ml with Distilled Water
4	10% APS	Ammonium per sulphate -10gm Distilled water -100ml
5	10% SDS	SDS -10gm Distilled water-100ml
6	10%gel	30% Acrylamide - 4ml

		Tris HCl pH 8.8 -2.5ml 10%APS -50µl TEMED -5µl 10%SDS -100µl Distilled water -3.344ml
7	4% Acrylamide	30% Acrylamide -1.33ml TrisHCl- (pH 6.8) -2.5ml 10%APS -50µl TEMED -10µl 10%SDS -100µl Distilled water -6.01ml
8	Western blotting transfer buffer	Tris -3.3g Glycine -14.4g SDS -1.0 Dissolve in 100 ml of distilled water
9	Ponseau stain	Ponseau S -0.5gm Glacial acetic acid -1ml Made up to 100ml with distilled water. Prepared just before use. Electrophoretic buffer (5x):

		Tris base -15.1gm Glycine -72.0gm SDS -5.0gm Distilled water made up to 1000ml
10	Radioimmunoprecipitation buffer (RIPA-Lysis buffer)	Tris - 50mM Nacl - 150mM SDS - 0.1% Triiton X-100 - 0.5% Dissolved in 10 ml dH2O Protease inhibitor cocktail (PIC) - 1mg/ml RIPA buffer and PIC solution -10ml HEPES+300µl PIC Sample loading Buffer (3x): 1M Tris HCl (pH 6.8) -2.4ml 20%SDS -3ml Glycerol -3ml β-Mercaptoethanol -1.6ml Bromophenol Blue -0.006gm
11	Tris buffered saline (pH:7.6) (TBS	Sodium chloride -8gm

		1M Tris HCl -20ml Tween-20 -10ml. Diluted to 1000ml with distilled water.
12	5% Skimmed milk	2.5g of skimmed milk powder was dissolved in 50ml of TBS